# JAC: Jena's Atomic Calculator

## — Manual, compendium & theoretical background —

http://www.atomic-theory.uni-jena.de/

Stephan Fritzsche

Helmholtz-Institut Jena &

Theoretisch-Physikalisches Institut, Friedrich-Schiller-Universität Jena, Fröbelstieg 3, D-07743 Jena, Germany

(Email: s.fritzsche@gsi.de, Telefon: +49-3641-947606, Raum 204)

Wednesday 6th March, 2019

# Contents

**6. Atomic properties** **105**

# 1. Overview about JAC. Structure of this Manual

## 1.1. Goals of the JAC toolbox

### Purpose of the JAC module:

- The Jena Atomic Calculator (JAC) provides tools for performing atomic (structure) calculations at various degrees of complexity and sophistication. This toolbox has been designed to calculate not only atomic level structures and properties [g-factors, hyperfine and isotope-shift parameters, etc.] or transition amplitudes between bound-state levels [dipole operator, Schiff moment, parity non-conservation, etc.] but, in particular, also (atomic) transition probabilities, Auger rates, photoionization cross sections, radiative and dielectronic recombination rates as well as cross sections and parameters for many other (elementary) processes.
- JAC also facilitates interactive computations, the simulation of atomic cascades and atomic responses, the time-evolution of statistical tensors as well as various semi-empirical estimates of atomic properties. It provides a diverse and wide-ranging, yet consistent set of methods which can be applied in different fields of atomic physics and elsewhere.
- In addition, the JAC module has been designed to readily support the display of level energies, electron and photon spectra, radial orbitals and several others entities.
- To find (the details about) individual features of the JAC program, see the index or search for keywords/phrases in this text.
- In practice, the design of JAC has been based on an analysis of typical user requirements and a hierarchical structure of the code.
- Since the theoretical background and data, implemented in JAC, have been extracted from quite many sources, we also hope to develop JAC as a repository of previous experience with electronic structure calculations of atoms in different environments, and that is to be further refined, expanded and developed here.
- The source code, an extensive documentation as well as a number of tutorials and examples are available from our Web site https://www.github.com/sfritzsche/JAC.jl.
- In order to support all these goals, several types of computation are distinguished within the JAC toolbox.

## Types of computations:

- Atomic computations, based on explicitly specified electron configurations: A typical computation, that is based on explicitly specified electron configurations, refers to the level energies, atomic states and to either one (or several) atomic properties for levels from a given multiplet or to the rates and cross sections of just one selected atomic process. For further details, see the supported amplitudes, properties and processes in Sections 5–7 below.
- Restricted active-space computations (RAS): A RAS computation refers to systematically-enlarged calculations of atomic states and level energies due to a specified (and usually restricted) active space of orbitals as well as due to the number and/or kind of virtual excitations to be included. Such RAS computations are internally performed *stepwise* in JAC by utilizing the self-consistent field (orbitals) from some prior step. This type has not yet been properly implemented so far.
- Interactive computations: In an interactive computation, the functions/methods of the JAC program are applied interactively, either directly within the REPL or by just a short JULIA script, in order to compute energies, expansion coefficients, transition matrices, rates, cross sections, etc. An interactive computation typically first prepares and generates (instances of) of different data structures of JAC, such as orbitals, (configuration-state) bases, multiplets, and later applies these computed data to obtain the desired information. More generally, all methods from JAC and its submodules can be utilized also interactively, although some specialized methods are often available and may facilitate the computations. Like for other JULIA functions, the functions and methods provided by JAC can be seen as (high-level) language elements in order to perform atomic computations at various degrees of sophistication.
- Atomic cascade computations: A cascade computation typically refers to three or more charge states of an atom, and which are connected to each other by different atomic processes, such as photoionization, dielectronic recombination, Auger decay, radiative transitions, etc. Different (cascade) approaches have been predefined in order to deal with atomic cascades. The particular atomic processes that are to be taken into account for the inidividual steps of the cascade need to be specified explicitly; these cascade computations have been only partly implemented so far.
- Atomic responses: Atomic response computations will support simulations of how atoms *respond* to an incident (beam of) light pulses and particles, such as field-induced ionization processes, high-harmonic generation and others. For these responses, the detailed atomic structure has often not been considered in much detail in the past, though it will become relevant as more elaborate and accurate measurements are carried out. These response computations have not yet been implemented so far.
- Time evolution of statistical tensors in (intense) light pusles: A time evolution of statistical tensors always proceeds within a pre-specified set of sublevels $\{\, |\alpha \mathbb{J} M\rangle \,\}$, i.e. subspace of the many-electron Hilbert space; all further (decay) processes that lead the system *out of this*

*subspace* must be treated by loss rates. Although such a time evolution can deal with pulses of different shape, strength and duration, it is assumed that they are *weak enough* not to substantially disturb the level structure and level sequence of the atoms in their neutral or ionic stage, i.e. that every sublevel can still be characterized by its (total) energy and symmetry. This time-evolution has not yet been implemented in detail so far. No attempt is made in JAC to solve the time-dependent (many-electron) Schrödinger equation explicitly.

➢ Semi-empirical estimates of atomic properties, cross sections, asymptotic behaviour, etc.: A semi-empirical 'estimate' of atomic data refers to some simple model computation or to the evaluation of fit functions in order to provide such atomic data, that cannot be generated so easily by *ab-initio* computations. These semi-empirical estimates are typically built on — more or less — sophisticated models and external parameter optimizations, although only a very few of such estimates have been implemented so far.

# 1.2. Notations

## Atomic shells & subshells:

➢ Atomic shell model: This model, in which electrons fill a (more or less) regular list of atomic shells or make transitions (quantum jumps) between different shells, is key and guidance for calculating the electronic structure of atoms, ions and molecules, and most of their properties.

➢ Electron configuration: Describes the occupation of shells within the atomic shell model, for instance, $1s^2\, 2s^2\, 2p^6\, 3s^2$. In JAC, closed-shell configurations can often be abbreviated, for instance, by [Ne] $3s^2$.

➢ Shells and subshells: Shells and subshells are the building blocks for the atomic shell model. In the relativistic theory, each non-relativistic $n\ell$-shell (apart from the $ns$-shells) splits into two relativistic subshells due to $j = \ell \pm 1/2$. In JAC, the shell and subshell notations are therefore used in order to denote the electron configurations, configuration state functions (CSF) and the orbitals of equivalent electrons. In JAC, there are special data struct's available to easily deal and communicate the (sub-) shell specification of levels and wave functions.

➢ Relativistic angular-momentum quantum number: $\kappa = \pm (j + 1/2)$ for $\ell = j \pm 1/2$ carries information about both, the total angular momentum $j$ and the parity $(-1)^\ell$ of the (single-electron) wavefunction.

## Atomic level notations:

- Bound (many-electron) levels and states: $|\alpha\mathbb{J}\rangle \;\equiv\; \left|\alpha J^P\right\rangle ; \quad |\alpha\mathbb{J}M\rangle \;\equiv\; \left|\alpha J^P M\right\rangle .$

  Here, the multi-index $\alpha$ refers to all additional quantum numbers that are needed for a unique specification of some many-electron level or state. — For instance, we shall often use below $|\alpha_i\mathbb{J}_i\rangle$ and $|\alpha_f\mathbb{J}_f\rangle$ in order to denote the initial and final-ionic bound states of some atomic amplitude and process.

- (Many-electron) resonances or scattering states with a single free electron: $|(\alpha\mathbb{J},\, \varepsilon\kappa)\; \mathbb{J}_t\rangle \;\equiv\; \left|(\alpha J^P,\, \varepsilon\kappa)\; J_t^{P_t}\right\rangle$

  describes a many-electron scattering wave with a single free electron in the partial wave $|\epsilon\kappa\rangle$ , and where $\mathbb{J}_t$ denotes the overall symmetry of the many-electron scattering state (level).

## Atomic multipoles:

- The multipole components (fields) of the radiation field occur at many different places in atomic theory due to the electron-photon interaction, though often within slightly different contexts. We here use the standard notations for the E1 (electric-dipole), M1 (magnetic-dipole), E2 (electric-quadrupole), etc. components and refer to them briefly as *multipoles* $\mathbb{M}$ of the radiation field.
- These multipoles or multipole components of the radiation field frequently occurs also in terms of *multipole transition operators* $\mathbb{O}^{(\mathbb{M})}$ and *multipole moment operators* $\mathbb{Q}^{(\mathbb{M})}$ as well as in summations $\sum_{\mathbb{M}} \ldots$ over such operators and/or the associated transition amplitudes (matrix elements).
- A multipole $\mathbb{M}$ is internally characterized by its multipolarity $L$ and its (boolean) character *electric* `(= true/false)`.

## Frequent techical terms used in the manual:

- Amplitude: Transition amplitudes are the many-electron matrix elements upon which atomic structure and collision theory is usually built on.
- Basis: In JAC, a basis refers to a many-electron basis that is specified in terms of a CSF list and the radial orbitals of all (equivalent) electrons. Each CSF is specified uniquely by a proper set of quantum numbers; here, the (so-called) seniority scheme is applied for the unique classification of the CSF and the evaluation of all matrix elements.

- ➢ Channel: Sublines of a given line that need to be distinguished due to the symmetry properties of the multipoles or partial waves in the decomposition of the many-electron levels or matrix elements.
- ➢ Grid: In JAC, all radial orbital functions are always represented on a grid. Only their grid representation is applied in the evaluation of all (single- and many-electron) matrix elements. Predefined grids refer to a 'exponential grid', suitable for bound-state computations, as well as a log-lin grid, which increases exponentially in the inner part and linearly in the outer part. The latter grid is suitable for collision processes and for dealing with the electron continuum.
- ➢ Lines and transitions: A line referts to an atomic transition that is characterized in terms of a well-defined initial and final level; it frequenty occurs in the computation of different properties, such as cross sections or rates, angular distribution parameters. Typically, a line contains various channels (sublines), for instance, due to occurance of multipoles or partial waves in the decomposition of the many-electron matrix elements
- ➢ Multiplet: Atomic levels are naturally *grouped together* into (so-called) mutiplets; most often, this term just stands for all fine-structure levels of one or several given configurations. More generally, multiplets may refer to any group of levels, for instance, to groups levels with the same total angular momentum $J$ and/or parity $P$, or fine-structure levels of closely related configurations, etc.
- ➢ Orbital: In atomic physics, an orbital typically refers to a one-electron function in an radial-spherical representation. Often, only the radial function(s) are meant. In the relativistic theory, of course, one needs to distinghuish between the large and small components of the orbital, following Dirac's theory.
- ➢ Pathway: In contrast to an (atomic) line, that is characterized by an initial- and a final-level (and the corresponding multiplets), a pathway describe a sequence of three or more levels, and which often correspond to different atomic processes. These levels are usually referred to as initial, (one or several) intermediate and final level. Pathways occur naturally in dielectronic recombination as well as in various excitation-ionization of excitation-autoioization processes.
- ➢ Settings: In JAC, the control of most, if not all, computations is made by `Settings` that are associated to particular amplitudes, properties and processes. These settings are used to specify all details about the requested computation and enable one, for instance, to select individual levels or lines as well as various physical and technical parameters, such as the multipoles, gauges, etc.

## 1.3. A quick overview about amplitudes, level properties and processes handled in JAC

### In Jac (partly) implemented amplitudes:

- Selected many-electron (reduced) amplitudes that are accessible within the JAC program. Further details about the call of these amplitudes can be found below in this manual or interactively by `?<module>.amplitude`.

| Amplitude | Call within JAC | Brief explanation |
|---|---|---|
| $\left\langle \alpha \mathbb{J} \Vert \mathbb{T}^{(1)} \Vert \beta \mathbb{J}' \right\rangle , \quad \left\langle \alpha \mathbb{J} \Vert \mathbb{T}^{(2)} \Vert \beta \mathbb{J}' \right\rangle$ | Hfs.amplitude | Amplitude for the hyperfine interaction with the magnetic-dipole and electric-quadrupole field of the nucleus. |
| $\left\langle \alpha \mathbb{J} \Vert \mathbb{N}^{(1)} \Vert \beta \mathbb{J}' \right\rangle$ | LandeZeeman.amplitude | Amplitude for the interaction with an external magnetic field. |
| $\left\langle \alpha_f \mathbb{J}_f \Vert \mathbb{O}^{(\mathbb{M},\, \text{emission})} \Vert \alpha_i \mathbb{J}_i \right\rangle$ | Radiative.amplitude | Transition amplitude for the emission of a multipole ($\mathbb{M}$) photon. |
| $\left\langle \alpha_f \mathbb{J}_f \Vert \mathbb{O}^{(\mathbb{M},\, \text{absorption})} \Vert \alpha_i \mathbb{J}_i \right\rangle$ | Radiative.amplitude | Transition amplitude for the absorption of a multipole ($\mathbb{M}$) photon. |
| $\left\langle (\alpha_f \mathbb{J}_f, \varepsilon\, \kappa)\, \mathbb{J}_t \Vert \mathbb{O}^{(\mathbb{M},\, \text{photoionization})} \Vert \alpha_i \mathbb{J}_i \right\rangle$ | PhotoIonization.amplitude | Photoionization amplitude for the absorption of a multipole ($\mathbb{M}$) photon and the release of an electron into the partial wave $\left\vert \varepsilon\, \kappa \right\rangle$ . |
| $\left\langle \alpha_f \mathbb{J}_f \Vert \mathbb{O}^{(\mathbb{M},\, \text{recombination})} \Vert (\alpha_i \mathbb{J}_i, \varepsilon \kappa) \mathbb{J}_t \right\rangle$ | PhotoRecombination.amplitude | Photorecombination amplitude for the emission of a multipole ($\mathbb{M}$) photon and the capture of an electron that comes *in* the partial wave $\left\vert \varepsilon\, \kappa \right\rangle$ . |
| $\left\langle (\alpha_f \mathbb{J}_f,\, \varepsilon\, \kappa)\, \mathbb{J}_t \Vert \mathbb{V}^{(\text{Auger})} \Vert \alpha_i\, \mathbb{J}_i \right\rangle$ | Auger.amplitude | Auger transition amplitude due to the electron-electron interaction and the release of an electron into the partial wave $\left\vert \varepsilon\, \kappa \right\rangle$ . |
| $\langle \alpha_f \mathbb{J}_f \Vert \sum\, \exp i\, \mathbf{q} \cdot \mathbf{r}_i \Vert \alpha_i \mathbb{J}_i \rangle$ | FormFactor.amplitude | Amplitude for a momentrum transfer $\mathbf{q}$ with an external particle of photon field. |
| $\left\langle \alpha_f \mathbb{J}_f \Vert \mathbb{H}^{(\text{weak}-\text{charge})} \Vert \alpha_i \mathbb{J}_i \right\rangle$ | PNC.weakChargeAmplitude | Amplitude for the nuclear-spin independent Hamiltonian of the ($P$-odd, $T$-even) internaction. |
| $\left\langle \alpha_f \mathbb{J}_f \Vert \mathbb{H}^{(\text{Schiff}-\text{moment})} \Vert \alpha_i \mathbb{J}_i \right\rangle$ | PNC.schiffMomentAmplitude | Amplitude for the nuclear Schiff moment of the ($P$-odd, $T$-odd) internaction. |
| $\left\langle \alpha_f \mathbb{J}_f \Vert \mathbb{H}^{(\text{scalar}-\text{pseudo}-\text{scalar})} \Vert \alpha_i \mathbb{J}_i \right\rangle$ | PNC.scalarPseudoScalarAmplitude | Amplitude for the scalar-pseudo-scalar ($P$-odd, $T$-odd) internaction. |

## In Jac (partly) implemented atomic level properties:

➢ In JAC implemented or partly-implememted atomic properties. For these properties, different parameters (observables) can generally be obtained by performing an `Atomic.Computation(..., properties=[id`$_1$`, id`$_2$`, ...])`, if one or more of the given identifiers are specified. For each of these properties, moreover, the corresponding (default) `Settings` can be overwritten by the user in order to control the detailed computations.

| Property | id | Brief explanation. |
|---|---|---|
| $\|\alpha\mathbb{J}\rangle \;\longrightarrow\; \|\alpha(J)\,\mathbb{F}\rangle$ | HFS | Hyperfine splitting of an atomic level into hyperfine (sub-) levels with total angular momentum $F = \|I - J\|$, ..., $I + J - 1,\, I + J$ ; hyperfine $A$ and $B$ coefficients; hyperfine energies and interaction constants; representation of atomic hyperfine levels in a $IJF$ -coupled basis. |
| $\|\alpha\mathbb{J}\rangle \;\longrightarrow\; \|\alpha\,\mathbb{J}M\rangle$ | LandeJ | Zeeman splitting of an atomic level into Zeeman (sub-) levels; Lande $g_J \equiv g(\alpha\mathbb{J})$ and $g_F \equiv g(\alpha\mathbb{F})$ factors for the atomic and hyperfine levels. |
| $K^{\,(\mathrm{MS})},\; F$ | Isotope | Isotope shift of an atomic level for two isotopes with mass numbers $A,\, A'$: $\Delta\, E^{\,AA'} = E(\alpha\mathbb{J};\, A) - E(\alpha\mathbb{J};\, A')$; mass-shift parameter $K^{\,(\mathrm{MS})}$ and field-shift parameter $F$. |
| $\alpha$-variations | AlphaX | Differential sensitivity of an atomic level $\|\beta\mathbb{J}\rangle$ with regard to variation of the fine-structure constant; $\Delta\, E(\delta\alpha;\, \beta\mathbb{J}),\; \Delta q(\delta\alpha;\, \beta\mathbb{J}),\; K(\beta\mathbb{J})$ . |
| $F(q;\, \alpha\,\mathbb{J})$ | FormF | Standard and modified atomic form factor of an atomic level $\|\alpha\mathbb{J}\rangle$ with a spherical-symmetric charge distribution. |
| $\omega(\alpha\mathbb{J}) + a(\alpha\mathbb{J}) = 1$ | Yields | Fluorescence & Auger decay yields of an atomic level, or averaged over an electron configuration. |
| $\alpha^{\,(\mathbb{M})}(\omega)$ | | Static and dynamic (ac, multipolar) polarizibilities. |
| $E(\alpha\mathbb{J};\,\text{plasma model})$ | Plasma | Plasma shift of an atomic level as obtained for different but still rather simple plasma models. |
| $\|\alpha_i\mathbb{J}_i\rangle \;\longrightarrow\; \|\alpha_f\mathbb{J}_f\rangle + \hbar\omega$ | EinsteinX[a] | Photon emission from an atom or ion; Einstein $A$ and $B$ coefficients and oscillator strength between levels $\|\alpha_i\mathbb{J}_i\rangle \rightarrow \|\alpha_f\mathbb{J}_f\rangle$ that belong to a single multiplet (representation). |

[a] Although the Einstein coefficients are not the property of a single level, we here still support a quick computation of these coefficients by means of the `Einstein` module for pairs of levels that are represented within a single CSF basis.

## In Jac (partly) implemented atomic processes:

- In Jac implemented or partly-implememted atomic processes. For *one* process at a time, different parameters (observables) can generally be obtained by performing an `Atomic.Computation(..., process=id)`, if the corresponding identifier is specified. For this selected property, moreover, the corresponding (default) `Settings` can be overwritten by the user in order to control the detailed computations.

| Process | id | Brief explanation |
|---|---|---|
| $A^* \longrightarrow A^{(*)} + \hbar\omega$ | RadiativeX | Photon emission from an atom or ion; transition probabilities; oscillator strengths; angular distributions. |
| $A + \hbar\omega \longrightarrow A^*$ | PhotoExc | Photoexcitation of an atom or ion; alignment parameters; statistical tensors. |
| $A + \hbar\omega \longrightarrow A^{+*} + e_p^-$ | PhotoIon | Photoionization of an atom or ion; cross sections; angular parameters; statistical tensors. |
| $A^{q+} + e^- \longrightarrow A^{(q-1)+} + \hbar\omega$ | Rec | Photorecombination of an atom or ion; recombination cross sections; angular parameters. |
| $A^{q+*} \longrightarrow A^{(q+1)+(*)} + e_a^-$ | AugerX | Auger emission (autoionization) of an atom or ion; rates; angular and polarization parameters. |
| $A^{q+} + e^- \rightarrow A^{(q-1)+*} \rightarrow A^{(q-1)+(*)} + \hbar\omega$ | Dierec | Dielectronic recombination (DR) of an atom or ion; resonance strengths. |
| $A + \hbar\omega_i \longrightarrow A^* \longrightarrow A^{(*)} + \hbar\omega_f$ | PhotoExcFluor | Photoexcitation of an atom or ion with subsequent fluorescence emission. |
| $A + \hbar\omega \longrightarrow A^* \longrightarrow A^{(*)} + e_a^-$ | PhotoExcAuto | Photoexcitation & autoionization of an atom or ion. |
| $A + \hbar\omega_i \longrightarrow A^{(*)} + \hbar\omega_f$ | Compton | Rayleigh or Compton scattering of photons at an atom or ion; angle-differential and total cross sections. |
| $A + n\,\hbar\omega \longrightarrow A^*$ or<br>$A^* \longrightarrow A^* + n\,\hbar\omega$ | MultiPhoton | Multi-photon (de-) excitation of an atom or ion, including two-photon decay, etc. |
| $A + Z_p \longrightarrow A^* + Z_p$ | CoulExc | Coulomb excitation of an atom or ion by fast, heavy ions; energy-differential, partial and total Coulomb excitation cross sections. |
| $A + \hbar\omega \rightarrow A^* + e_p^- \rightarrow A^{(*)} + e_p^- + \hbar\omega'$ | PhotoIonFluor | Photoionization of an atom or ion with subsequent fluoescence emission. |
| $A + \hbar\omega \rightarrow A^* + e_p^- \rightarrow A^{(*)} + e_p^- + e_a^-$ | PhotoIonAuto | Photoionization of an atom or ion with subsequent autoionization. |
| $A^{q+} + e^- \rightarrow A^{(q-1)+*} \rightarrow A^{(q-1)+(*)} + \hbar\omega$<br>$\rightarrow A^{(q-1)+} + \hbar\omega + \hbar\omega'$ | DierecFluor | Dielectronic recombination of an atom or ion with subsequent fluorescence. |

| Process | id | Brief explanation |
|---|---|---|
| $e_s^- \,+\, A \,\longrightarrow\, A^* \,+\, e_s^{-\prime}$ | Eimex | Electron-impact excitation of an atom or ion; collision strength. |
| $A \,+\, e_s^- \,\to\, A^* \,+\, e_s^{-\prime} \,\to\, A^{+(*)} \,+\, e_s^{-\prime} \,+\, e_a^-$ | EimexAuto | Electron-impact excitation and subsequent autoionization of an atom or ion. |
| $A^{q+*} \,\longrightarrow\, A^{(q+1)+(*)} \,+\, (e_a^- \,+\, \hbar\omega)$ | RadAuger | Radiative-Auger (autoionization) of an atom or ion. |
| $A \,+\, n\,\hbar\omega \,\longrightarrow\, A^{(*)} \,+\, e_p^-$ | MultiIon | Multi-photon ionization of an atom or ion. |
| $A \,+\, n\,\hbar\omega \,\longrightarrow\, A^{(*)} \,+\, e_{p_1}^- \,+\, e_{p_1}^-$ | MultiDoubleIon | Multi-photon double ionization of an atom or ion. |
| $A^{q+}[\text{nucleus}^*] \,\longrightarrow\, A^{(q+1)+*} \,+\, e_c^-$ | Conversion | Internal conversion, i.e. electron emission due to nuclear de-excitation. |

## 1.4. Short comparison of JAC with other existing codes

We here compile some (incomplete) information about other existing atomic structure codes for the computation of level energies, transition rates, cross sections, etc. We remind to some of their special features and briefly summarize how these codes differ from the implementation of the JAC toolbox.

### CATS (Cowan: 'Theory of Atomic Spectra', 1980):

- CATS relies on a semi-relativistic self-consistent potential and by using either a nonlocal Hartree-Fock (HF) or local Hartree-Fock-Slater (HFS) approach in order to deal with the exchange interaction.
- Level energies & ASF: Since the late 1960s, Cowan's HFX code has set some standard for many experimentalists and has, together with his well-known textbook, helped many (atomic) physicist to understand and make use of atomic structure theory. While these earlier developments are highly appreciated (and are still utilized for various applications), CATS has several severe limitations in the layout and implementation of the code, which are hard to *overcome*. The same applies also for the computation of various atomic properties, such at transition probabilities, photo-excitation and ionization cross sections and Auger rates.
- Cowan's code has been found a mature tool for identifying new lines, especially if additional information is available from experimental observations to support empirical adjustments.

- ➢ Display of data & spectra: Several tools and facility-programs have been developed for CATS in order to display the computed data and to compare them with each other and with experiment. The success of some of these tools has or will motivate us for developing some graphical interfaces for the display of (radial) orbitals, line spectra, etc. also for thte JAC toolbox.
- ➢ Selected advantages of JAC: JAC provides methods to display, for instance, radial functions and line spectra; cf. `JAC.display().`

## GRASP (Grant *et al.*, 1980; Jönsson *et al.*, 2013; Fischer *et al.*, 2018):

- ➢ Level energies & ASF: GRASP has originally been devoloped since the late 1960s in order to provide level energies and eigenvectors for quite general open-shell atoms. Much emphasize during the last two decades was placed upon the systematic improvement of these energies and representations. While we also provide such level energies and atomic state functions by the JAC toolbox, we *do not* intent to facilitate such extensive wave function expansions. Instead, approximate level energies and ASF are mainly considered as the *technical preposition* for describing further atomic properties and processes. With the restricted-active space (RAS) computations, however, we shall provide in JAC useful features for a (more or less) systematic improvement of such *ab-initio* computations.
- ➢ Transition probabilities & oscillator strength: Apart from the level energies, GRASP has been extensively applied in order to compute and tabulate transition probabilities for many atoms, ions and isoeletronic sequences throughout the periodic table of elements. With JAC, we provide analogue or even simpler tools for such computations. Moreover, (the many-electron amplitudes that arise from) the coupling of the radiation field provides the natural *building blocks* for a large number of other atomic processes, cf. section 7 on atomic processes below.
- ➢ Selected advantages of JAC:
  - JAC supports larger flexibility in handling the output data and, in particular, does not know practically-relevant limitations with regard to the length of filenames (in contrast, for instance, to 24 letters in grasp2K).
  - SCF fields can be generated in JAC at different levels of complexity, including several (local) mean-field potentials as well as, in the future, the average-level and extended average-level schemes.
  - JAC enables one to handle a much larger number of atomic properties and processes as well as atomic cascades and several other types of computation.
  - The use of the JULIA language clearly facilitates the coding and maintenance of the JAC code, when compared to previous Fortran codes.

## RATIP (Fritzsche, 2001, 2012):

- Relativistic CI (RELCI): While RATIP has always used the SCF computations and orbitals from the GRASP code, it also supports relativistic CI computations. For several years, it helped define a new standard for performing the angular intergration (angular coefficients; cf. Gaigalas *et al.*, 2002). These angular coefficients are also utilized in JAC by an interface to the Fortran modules of RATIP.
- Atomic properties and processes: RATIP was (one of) the first codes that made use of GRASP's systematically improved wave functions in order to compute a good number of atomic properties and processes, such as relaxed-orbital transition probabilities (REOS; Fritzsche and Froese Fischer 1999), Auger rates, photoionization cross sections and angular parameters, radiative and dielectronic recombination rates, electron-impact excitation cross sections, and several others. The experience with RATIP has been found central for the development of JAC and has find its continuation here.

## HULLAC (Bar-Shalom *et al.*, 2001):

- HULLAC has been developed as an integrated code for calculating atomic structure and cross sections for collisional and radiative atomic processes, based on the relativistic configuration interaction method.
- All collisional cross sections are calculated in the distorted wave approximation with special emphasis on efficiency.
- A parametric potential method is applied for the generation of both, the bound and free orbitals, while a (so-called) factorization-interpolation method is utilized in order to derive all collisional rates.

## LADW (Bar-Shalom *et al.*, 2001):

- LADW, the Los Alamos Distorted-Wave code, has been developed by Sampson and co-workers; it has been further utilized and partly incorporated into the LASER code.

## GEANT4 (Amako *et al.*, 2005):

- GEANT4 is an object-oriented toolkit for analyzing and simulating the passage of particeles through matter that provides a variety of semi-empirical models to describe the underlying electromagnetic and hadronic interactions. GEANT4 combines theorical models with experimental data or parameterizations of such data.

- ➢ GEANT4 is especially based on a number of separate packages to deal with the electromagnetic interactions of (either) electrons, muons, positrons, photons, hadrons and ions as well as for specific energy range of the processes considered.
- ➢ Implemented processes: The electromagnetic packages of this code include: multiple scattering, ionization, Bremsstrahlung, positron annihilation, photoelectric effect, Compton and Rayleigh scattering, pair production, synchrotron and transition radiation, Cherenkov effect, refraction, reflection, absorption, scintillation, fluorescence as well as Auger electron emission (Amako *et al.*, 2005). Less attention has been placed however on the electronic structure of atoms and ions.

## FAC (Gu 2008):

- ➢ FAC is a well-known relativistic atomic structure code based on the fit of free parameters in order to define the atomic potentials and is mainly based on the (standard) Dirac-Fock-Slater method.
- ➢ Level energies & wave functions: The simplified and more object-oriented treatment of wave functions in the FAC code, when compared with GRASP, has stimulated the development of the JAC program. While JAC will enable the user to perform also systematic improvements on the underlying computational models, the support of rather simple approximations is crucial and need to be supported, for example, for dealing with cascades and time-evolutions.

## AUTOSTRUCTURE (Badnell, 2011):

- ➢ AUTOSTRUCTURE is a rather general atomic code for the description of free-bound electron and photon collision processes, based on the original SUPERSTRUCTURE code bei Eissner and coworkers.
- ➢ AUTOSTRUCTURE supports efficient computations of dielectronic recombination cross sections and rates, especially if large numbers of highly-excited states are involed in the radiative stabilization of an atom or ion.
- ➢ The code applies the Breit-Pauli distorted wave method for the electron-impact excitation of atomic ions in order to support problems that are impractical or even impossible for more sophisticated methods.
- ➢ AUTOSTRUCTURE mainly computes (Maxwell-averaged) effective collision strengths at temperatures of broad ionic abundance, rather then the detailed collision strength at all the energies.

## LASER (Fontes *et al.*, 2015):

- Laser, i.e. the Los Alamos suite of relativistic atomic physics code, comprises various codes for fundamental atomic structure calculations as well as for various processes, such as photoexcitation, electron-impact excitation and ionization, photoionization and autoionization, within a consistent framework. It may help develop atomic physics models in either configuration- average and fine-structure modes, and by including a proper self-consistency. This suite has been developed for more than 20 years.
- Applications of the code: The Laser code has been applied to the collisional-radiative modeling of of plasmas, for line identifications in plasma spectroscopy and for testing relativistic atomic and quantum electro-dynamics (QED) theories. The code has been applied also for feasibility studies of the collisional-radiative modeling of non-LTE (optically thin) gold plasmas for and to questions from inertial confinement fusion.
- Approximations: Laser mainly employs the semi-relativistic theory, similar and often by directly applying Cowan's atomic structure code (Cats). The bound-electron wavefunctions are obtained from the semi-relativistic approach in Cats, while the continuum-electron wavefuctions are obtained as solutions of the Schrödinger equation from some specialized routines. Typically, the bound and continuum radial wave functions are single-component type wavefunctions associated with the Schrdinger equation, rather than the four-component spinors associated with the Dirac equation.
- Features: Cross sections and other properties can be calculated for five fundamental processes: photo-excitation, photo-ionization, electron-impact excitation and ionization and autoionization. The code supports the Ipcress (Independent of Platform and Can be Read by Existing Software Subroutines) random-access binary file format that is used to store large amounts of data, and which can be ported to any platform.

## QEDMOD (Shabaev *et al.*, 2015):

- Self energy, $\mathbb{h}^{(\mathrm{QED})}$: Computes a model QED operator $\mathbb{h}^{(\mathrm{QED})}$ that accounts for the Lamb shift in accurate atomic-structure calculations. However, there are various difficulties with QedMod which make a direct application of the code and its combination with Grasp or Jac rather cumbersome.
- Effective QED Hamiltonian: The QedMod code provides one-electron matrix elements that, in principle could be directly added to any CI matrix and, hence, to the computation of level energies and multiplets. For the vacuum polarization, it includes automatically both, the Uehling and Wichmann-Kroll terms.
- Selected advantages of Jac: A simlified version of the effective QED Hamiltonian from QedMod has been implemented also in Jac.

## 1.5. To-do's, next steps & desired features of the JAC program

### Encouragement for external users and developers:

- While we (will further) develop JAC for those applications, which are requested frequently by the users, here I shall compile a number of desired features which will make JAC even more powerful and/or easy to use. For these *additional features*, I wish to encourage collaboration with external developers. We welcome in particular all help from outside if the overall style of the program is maintained, and if some prior consensus exist how to add and implement additional features.
- New code developments may concern incremental improvements or also multiple approaches for algorithms and modules in order to provide well-defined alternatives, for instance, if some particular approach does not work properly.
- Emphasis will be placed first usually on those applications that receive enough attention by the community.

### 1.5.a. To-do lists

### Urgent to-do's:

- Bring JAC up to the (public) Github.
- Establish the travis-ci system in order to support regular tests on the overall JAC package.
- Visualize a (given) continuum orbital and its normalization as obtained at sufficiently large $r$-values.
- Use of JAC on remote clusters: Work out some prototype example how 'job scripts' (similar to those from examples) can be exportet and handled at remote cluster computers and how to re-import the results later on.
- Documenter.jl: How to establish a documentation of JAC.
- Github: Which license is useful and recommended (MIT) for such a large project ??

## Short-term to-do's:

- ➢ Implement ... `Jac.modify("level energies: interactive", multiplet::Multiplet)`
- ➢ Implement ... `Jac.display("level energies: HFS", multiplets::HFSMultiplet[..])`
- ➢ Implement ... `Jac.display("level energies", multiplets::Multiplet[..])`
- ➢ Implement ... `Jac.display("configuration list: from basis", basis::Basis)`

## Medium-term to-do's:

- ➢ Implement ... `Jac.apply("restrictions: CSF list", csfs::CsfR[..], basis::Basis)` ... to apply a number of restrictions interactively to a list of CSF. The procedure proceeds in three steps: (i) by taking and applying a restriction to a given CSF list; (ii) showing the number of CSF to be deleted from the given list; (iii) making this restrictions explicit. The user is requested to enter one restriction after the other, and until the reduction process is terminated by the user. A csfList::CsfR[] is returned; ...... Here we might adopt the form of restrictions from the RATIP program.
- ➢ Implement ... `Jac.apply("biorthogonal transformation", mplta::Multiplet, mpltb::Multiplet, grid::Radial.Grid)`
- ➢ Atoms in plasma environments: Implement 2-3 plasma models in order to deal with atoms in a few (averaged but) different plasma environments. This usually works via some effective `Jac.InteractionStrength.XL_BreitXL_plasma_ionSphere(L::Int64, a::Orbital, b::Orbital, c::Orbital, d::Orbital, lambda::Float64)` that depends on some particular model and plasma parameters; cf. Saha and Fritzsche, PRE (2004). This will likely require also the set-up of a corresponding Hamiltonian matrix: `Jac.compute("matrix: plasma, ion-sphere model", settings::Plama.Settings, basis::Basis)`.
- ➢ Interpolation: We might need (from time to time) a proper interpolation of functions from one grid to another, for instance, for using GRASP-type orbitals that have been generated on a different grid. Implement some function `Jac.interpolate("function: for new radial grid, trapez rule", from::Tuple(rOld::Float64[..],gridOld::Jac.Radial.Grid), to::Tuple(rNew::Float64[..],gridNew::Jac.Radial.Grid) )`.

### 1.5.b. Discussion about (further) implementations

## Issues that need to be discussed:

- Further documentation of the code: How can the internal *doc-strings* be readily combined with the JAC websites ??
- Parallelization and performance of the code: How can one make the code parallel without that the user need to know and provide much information about the cluster that is used for the computations.
- Modern input forms in scientific computing: Which modern formats do exist ?? Which simple graphical (applet) features exist ? tomel.jl ??

### 1.5.c. Desired medium- and long-term features of the JAC program

## Plotting and visualization:

- Implement ... `Jac.plot("radial orbitals", orbitals::Orbital[..])`
- Implement ... `Jac.plot("spectrum: oscillator strength over energy, emission", lines::RadiativeLine[..]; widths=value::Float64)` and `Jac.plot("spectrum: oscillator strength over energy, absorption", lines::RadiativeLine[..]; widths=value::Float64)`
- Implement ... `Jac.plot("spectrum: transition rates over energy, Gaussian", lines::RadiativeLine[..]; widths=value::Float64)` and `Jac.plot("spectrum: transition rates over energy, Lorentzian", lines::RadiativeLine[..]; widths=value::Float64)`
- Visualize the convergence of energies or other results as function of the size of the computation and/or model space.
- Visualize the level structure of a given multiplet, for instance, by displaying the level energies in different colors for different (leading) configurations or groups of such configurations.
- Visualize the level structure of a given multiplet together with further level or transition properties, such as lifetimes, HFS parameters, isotope parameters, etc.

## Excitation and decay cascades:

- Analyze (and report) the fine-structure level population following the decay of an inner-shell hole state.
- Compute and extract the Fano parameters and line-shapes for a given set of autoionizing resonances.
- For a given cascade (data), evaluate the ion yields, electron spectra, (fine-structure) level population, fluorescence spectra, etc.

## More physics in Jac ?

- Atomic spectra: Evaluate and display the photoabsorption spectra from calculated photoexcitation and photoionization cross sections.
- Computation of approximate single-electron properties:
  - Subshell-dependent differential and total photoionization cross sections; cf. Eichler and Meyerhof (1995, Eqs. 9.34 and 9.47).
  - Nonrelativistic total K-shell or subshell radiative recombination cross sections by using the Stobbe cross section; cf. Eichler & Meyerhof (1995, Eqs. 9.49, 9.50)
  - Dirac energy (subshell); Dirac $r^k$ expectation values; Dirac-matrices; `Dirac.Omega(subshell,theta,phi)`.
  - Coulomb-Greens functions for some given hydrogenic orbital.
- Collisional-radiative models: Such collisonal-radiative models have been frequently applied to describe the evolution of plasma and to derive information for plasma diagnostics. JAC provides many, if not all, the rates and cross sections to built-up such models for selected (plasma) environments.
- Electron-momentum distributions: Provide the expectation values $\left\langle p^k \right\rangle, \quad k = -2, ..., 4$ of the single-electron radial momentals, i.e. the radial orbitals in momentum space. These expectation values are frequently applied in crystallography and in studying Compton profiles; cf. Koga and Thakkar (1996), Eq. (10-11). In the first instance, these expectation values could be readily provided as semi-empirical values by following the work above.

## 1.6. Remarks on the implementation of JAC

### Why Julia ?

- Here, we just recall a few remarks from the literature as well as some own experience why Julia have been found helpful for developing the Jac program. Some of these arguments are directly taken from the work of Bezanson *et al.* (2017, 2018).
- Julia is a language for scientific computing that offers many of the features of productivity languages, namely rapid development cycles; exploratory programming without having to worry about types or memory management; reflective and meta-programming; and language extensibility via multiple dispatch (Bezanson *et al.*, 2018).
- Productivity *vs.* performance: Julia is often said to stand for the combination of productivity and performance through a careful language design and carefully chosen technologies; it never forces the user to resort to C or Fortran for fast computations. — Julia's design allows for gradual learning of modern concepts in scientific computing; from a manner familiar to many users and towards well-structured and high-performance code.
- Julia's productivity features include: dynamic typing, automatic memory management, rich type annotations, and multiple dispatch. Julia also supports some control of the memory layout and just-in-time compilation in order to eliminate much of the overhead of these features above (Bezanson *et al.*, 2018).
- Julia promises scientific programmers the ease of a productivity language at the speed of a performance language (Bezanson *et al.*, 2018).
- High-level languages: Most traditional high-level languages are hampered by the overhead from the interpretor, and which typically results into more run-time processing of what is strictly necessary. One of these hindrances is (missing) type information, and which then results in the request for supporting vectorization. Julia is a 'verb'-based language in contrast to most object-oriented 'noun'-based language, in which the generic functions play a more important role than the datatypes.
- Language design: Julia includes a number of (modern) features that are common to many productivity languages, namely dynamic types, optional type annotations, reflection, dynamic code loading, and garbage collection (Bezanson *et al.*, 2018).
- Multiple dispatch: This concept refers to the dynamically selected implementation and to running the right code at the right time. This is achieved by overloading by means of multiple-argument function, a very powerful abstraction. Multiple dispatch makes it easier to structure the programs close to the underlying science.
- Multiple dispatch is perhaps the most prominent feature of Julia's design and is crucial for the performance of the language and its ability to inline code efficiently. Another promise of multiple dispatch is that it can be used to extend existing behavior with new features.

- Multiple dispatch: At run-time, a function call is dispatched to the most specific method applicable to the types of its arguments. JULIAs type annotations can also be attached to datatype declarations so that they can be checked whenever typed fields are assigned to. Multiple dispatch also help the programmers to extend the core languages functionalities to their particular needs.
- Multiple dispatch also reduces the needs for argument checking at the begin of a function. The overloading of functions by multiple dispatch is also called ad-hoc polymophism. Instead of encapsulating methods inside classes, JULIA's multiple dispatch is a paradigm in wich methods are defined on combinations of data types (classes). JULIA shows that this is remarkably well-suited for numerical computing.
- JULIA's type system: JULIA's expressive type system allows optional type annotations; this type system supports an agressive code specializiation against run-time types. To a large extent, however, JULIA code can be used without any mentioning of types (in contrast to C and Fortran); this is achieved by data-flow interference. — User's own types are also first class in JULIA, that is there is no meaningful distinction between built-in and user-defined types. There are mutable and (default: immutable) composite types.
- Optimization in JULIA: The JULIA compiler is built on three strategies that are performed on a high-level intermediate representation, while all native code generation is later delegated to the LLVM compiler infrastructure. These optimization strategies are: (1) method inlining which devirtualizes multi-dispatched calls and inline the call target; (2) object unboxing to avoid heap allocation; and (3) method specialization where code is special cased to its actual argument types (Bezanson *et al.*, 2018).
- Performance: There are helpful macros, such as `@timing function_call(parameters)` or `@benchmark function_call(parameters)` to analyze the performance of the program and to find (and resolve) bottlenecks.
- Data types: JULIA distinguishes between concrete data types, that can be instantiated, and abstract types, that can (only) be extended by subtypes to built up an hierarchy of such types.
- In JULIA, users are always encouraged to make their programs, whenever possible, type stable. Much of the efficiency of a JULIA code relies on being type stable and on devirtualization and inlining.
- LAPACK: All of LAPACK is available in JULIA, not just the most common functions. LAPACK wrappers are fully implemented by `ccall` and can be called directly from the Julia promt.

## Requests in building large software packages:

- These and further requests have been summarized by Post and Kendall (2004).
- Physical models: In general, better physics is more important than better computer science. It is recommended to use modern but well-proven computer-science techniques, and a 'physics code' should not be a computer-science research project. Instead, one should use best

engineering practices to improve quality rather than processes. Emphasis should be given to improvements of the physics capabilities. Do not use the latest computer-science features; let the new ideas mature first. Better physics is the most important product of the code.

- Code development and evolution: The scale of code-development can become truly immense; a good overview/quantitative database about (previously) successful software projects in some given field is typically required for good estimation for resources and schedules. It is easy to loose motivation on a project that last years and which has few incremental deliveries. Continues replacement of code modules is recommended as better tools and techniques are developed. Every code development typically proceeds in steps: First develop a core capability (with a small team) and let this small core be tested by users and, if successful, add further capabilities (so-called incremental delivery).
- Success criteria: One of the important success criteria is the costumer focus. — What do the user really need ?
- Code specification: Some flexibility in the requirement specification phase is essential because it is difficult to predict when (or if) a new algorithm/approach will be available. There is a need to pursue multiple approaches for algorithms and modules near to the critical path. If one approach is not feasible, another one can be used.
- External users and developers: The validation of physics models is a critical issue for all extended software packages and need to be done with regard to authoritative reference data.
- Documentation should be intended to cover all needs of the beginner through to the expert user who wishes to expand the capabilities of JAC.

# 2. Dirac's hydrogenic atom

## 2.1. Energies and wave functions

### Notations & application in Jac:

- In JAC, non-relativistic hydrogenic orbitals can be easily generated by a call to `JAC.HydrogenicIon.radialOrbital()`.
- JAC also provides approximate radial (relativistic bound-state) orbitals by just applying the kinetic-balance condition to the corresponding non-relativistic radial orbital and by re-normalizing it afterwards.

### Dirac's (one-electron) energies:

- Relativistic bound-state energy spectrum: For electrons with principal quantum number $n$ and angular-momentum quantum number $\kappa$, the relativistic bound-state energy spectrum is given by

  $$\varepsilon_{n\kappa} \;=\; mc^2\, W_{n\kappa} \;=\; \frac{mc^2}{\left[1 \,+\, \left(\tfrac{\alpha Z}{n' + s}\right)\right]}$$

  where $\alpha$ is the fine-structure constant, $n' \,=\, n - |\kappa| \,=\, 0,\, 1,\, 2,\, ...$ is the number of nodes, and $s \,=\, \sqrt{\kappa^2 \,-\, (\alpha Z)^2}$, respectively.
- Since $W_{n\kappa} \,<\, 1$, it can be expanded in terms of $(\alpha Z)$ and written as

  $$W_{n\kappa} \;=\; 1 \,-\, \frac{1}{2}\,\frac{(\alpha Z)^2}{n^2} \,-\, \frac{1}{2}\,\frac{(\alpha Z)^4}{n^3}\,\left(\frac{1}{j + 1/2} \,-\, \frac{3}{4\,n}\right) \,-\, ...$$

  where the second term, multiplied with $mc^2$, represents the nonrelativistic binding energy of a hydrogenic atom.

- For a given (principal) shell $n$, the eigenvalues are the same for equal values of $j$ but are different for equal values of $\ell$. For a given value of $\ell$, the spin-orbit splitting between states with $j = \ell + 1/2$ and $j = \ell - 1/2$ gives rise to the fine-structure in the spectrum of hydrogen-like atoms. The equation above shows that the relativistic corrections to the one-electron energies decreases rapidly with $n$. The relativistic correction to the non-relativistic energy is therefore important, especially for highly-charged ions with rather large $Z$.

## Non-relativistic radial orbitals:

- The (radial) function $P(r)$ in the non-relativistic orbital $\psi(r, \vartheta, \varphi) = \frac{P(r)}{r} Y_{\ell m}(\vartheta, \varphi)$ is known to obey the *radial* Schrödinger equation and belongs to either the discrete part of the spectrum with the (negative) energies $E_n = -\frac{Z^2}{2n^2}$ a.u. $< 0$ (bound states), or to the contineous part for all energies $E > 0$ (the so-called *free-electron* or *continuum* states).
- An analytic solution of the radial functions $P(r)$ in terms of the confluent hypergeometric function $F(\alpha, \beta; x)$ are known for both, the bound-states

$$P_{n\ell}(r) \;=\; r^{l+1} \frac{1}{(2\ell+1)!} \sqrt{\frac{(n+\ell)!}{(n-\ell-1)!\, 2n}} \left(\frac{2Z}{n}\right)^{3/2+\ell} e^{\left(-\frac{Zr}{n}\right)} F\left(-(n-\ell-1),\, 2\ell+2;\, \frac{2Zr}{n}\right)$$

as well as for the *continuum* $(E > 0)$ with $k = \sqrt{2E}$ and $n' = Z/k$

$$P_{E\ell}(r) \;=\; \frac{2\sqrt{Z}}{\sqrt{1-e^{-2\pi n'}}} \left[\prod_{s=1}^{\ell} \sqrt{s^2 + n'^2}\right] \frac{(2kr)^{l}}{(2\ell+1)!}\, e^{-ikr}\, F(in' + \ell + 1,\, 2\ell+2,\, 2ikr).$$

## Relativistic radial orbitals:

- Analogue to the non-relativistic case, the solution $\psi(\mathbf{r})$ of the Dirac equation can be separated for a spherical potential into a radial and angular part

$$\psi_{\kappa m}(r, \vartheta, \varphi) \;=\; \frac{1}{r} \begin{pmatrix} P(r)\, \Omega_{\kappa m}(\vartheta, \varphi) \\ i\, Q(r)\, \Omega_{-\kappa m}(\vartheta, \varphi) \end{pmatrix},$$

where $\Omega_{\kappa m}(\vartheta, \varphi)$ denotes a standard Dirac spin-orbital function, and where $\kappa = \pm\, (j + 1/2\,)$ for $\ell = j \pm 1/2$ is called the *relativistic* angular-momentum quantum number.

- Owing to the definition of $\kappa = \pm 1, \pm 2, \ldots$, this relativistic quantum number carries information about both, the total angular momentum $j$ and the parity $(-1)^\ell$ of the wavefunction.
- Large & small component: The radial part of a relativistic wavefunctions is given by the two functions $P(r)$ and $Q(r)$, and which are often called the *large* and *small* components.
- Dirac spin-orbital: As usual, the Dirac spin-orbitals can be written in terms of the spin-1/2 Pauli spinors $\chi_\pm$ and the spherical harmonics by

$$\begin{aligned} \Omega_{\kappa m}(\vartheta, \varphi) &= \sum_{m_\ell} \langle \ell \, m_l, \; 1/2, m - m_\ell \,|\, jm \rangle \; Y_{\ell m_\ell}(\vartheta, \varphi) \; \chi_{m-m_\ell} \, . \\ Q(r) &= \frac{1}{2m\,c} \left( \frac{d}{dr} + \frac{\kappa}{r} \right) P(r) \end{aligned}$$

## 2.2. Coulomb-Green function

### Relativistic radial Coulomb-Greens function:

- Radial Green function of the Dirac equation: Following Yerokhin and Shabaev (1999, appendix D), the radial Green function of the Dirac equation for electrons with the angular-momentum symmetry $\kappa$ can be written in the form:

$$G_\kappa(\omega, r_1, r_2) = -\frac{1}{W_\kappa(\omega)} \left[ \boldsymbol{\phi}_\kappa^\infty(\omega, r_1) \; \boldsymbol{\phi}_\kappa^{0^T}(\omega, r_2) \, \Theta(r_1 - r_2) + \boldsymbol{\phi}_\kappa^0(\omega, r_1) \; \boldsymbol{\phi}_\kappa^{\infty^T}(\omega, r_2) \, \Theta(r_2 - r_1) \right]$$

where $\boldsymbol{\phi}_\kappa^0(\omega, r)$ and $\boldsymbol{\phi}_\kappa^\infty(\omega, r)$ are solutions of the radial Dirac equation, bounded at the origin and at the infinity, and where $W_\kappa(\omega)$ is the Wronskian.

- The functions $\boldsymbol{\phi}_\kappa^0(\omega, r)$ and $\boldsymbol{\phi}_\kappa^\infty(\omega, r)$ can be calculated in terms of the Whittaker functions of the first and second kind, although special care has to be taken.

## 2.3. Matrix elements with Dirac orbitals

### 2.3.a. Matrix elements with radial orbitals

#### Matrix elements with non-relativistic radial orbitals:

- Special non-relativistic $r^k$ expectation values: The following expectation values are displayed by Marxer (1991)

$$\left\langle r^{-1} \right\rangle = \frac{Z}{a_o\, n^2}$$

$$\left\langle r^{-6} \right\rangle = \left[ \frac{Z}{a_o} \right]^6 \frac{35n^4 - n^2\,[30\ell\,(\ell+1) - 25] + 3(\ell-1)\,\ell\,(\ell+1)\,(\ell+2)}{8n^7\,(\ell-3/2)\,(\ell-1)\,(\ell-1/2)\,\ell\,(\ell+1/2)\,(\ell+1)\,(\ell+3/2)\,(\ell+2)\,(\ell+5/2)}$$

$$\left\langle r^{-k-2} \right\rangle = \left[ \frac{Z}{a_o} \right]^{k+2} \frac{1}{n^{k+3}\,\ell^{k+1}}\,\mathcal{P}_{k,\ell}\left(\frac{n}{\ell}\right), \qquad \mathcal{P}_{k,\ell}(x) = \frac{(2\ell)^{k+1}\,(2\ell-k)!)}{(2\ell+1)!}\;{}_3F_2(-k, k+1, \ell+1-\ell\,x;\; 1, 2\ell+2;\; 1)$$

- Pasternack-Kramers rekursion relation: For $k \le 0$, the $r^{-k}$ expectation values of any $(n\ell)$ level fullfill the relation (Marxer 1991)

$$\left\langle r^{-k-2} \right\rangle = \frac{4}{(2\ell+1)^2 - k^2} \left[ \left( \frac{2k - 1}{k} \right) \frac{Z}{a_o} \left\langle r^{-k-1} \right\rangle - \left( \frac{k - 1}{k} \right) \frac{Z^2}{n^2\, a_o^2} \left\langle r^{-k} \right\rangle \right]$$

$$\left\langle r^{k} \right\rangle = \frac{(2\ell + k + 2)!}{(2\ell - k - 1)!} \left[ \frac{n\, a_o}{2Z} \right]^{2k+3} \left\langle r^{-k-3} \right\rangle$$

From this relation, explicit formulas for low principal quantum number $n$ can be computed rather easily.

#### Matrix elements with relativistic Dirac wavefunctions:

- An analytical expression of the matrix elements with operators $r^k\, e^{-sr}$ can be found (also) for Dirac's relativistic wavefunctions. In order to derive such expressions, it is typically more convenient first to re-write the standard representation of the hydrogenic functions in terms of a series expansion in $r$ as it was suggested originally by Rose (1961).

- An expression for the corresponding matrix element is given by:

$$\left\langle n\,\kappa \left| r^k \, e^{-\sigma\, r} \right| n'\,\kappa' \right\rangle \;=\; \int_0^\infty dr\; e^{-\sigma r}\; \left( P_{n\kappa}(r)\, P_{n'\kappa'}(r) + Q_{n\kappa}(r)\, Q_{n'\kappa'}(r) \right)$$

$$=\; N_{n\kappa}\, N_{n'\kappa'} \sum_{\nu=0}^{n-|\kappa|} \sum_{\nu'=0}^{n'-|\kappa'|} \left( c^{+}_{n\kappa,\nu}\, c^{+}_{n'\kappa',\nu'} \;+\; c^{-}_{n\kappa,\nu}\, c^{-}_{n'\kappa',\nu'} \right) \frac{q^{s+\nu-1}\, q'^{\,s'+\nu'-1}}{(q+q'+\sigma)^{1+\nu+\nu'+s+s'+k}}\; \Gamma(\nu+\nu'+k+s+s'+1)\,,$$

$$c^{\pm}_{n\kappa,\nu} \;=\; \left( 1 \pm \sqrt{1-q^2} \right)^{1/2} \frac{((-n+|\kappa|)_\nu\; 2^\nu)}{\nu!\; (2s+1)_\nu}\; \left[ (\nu - n + |\kappa|) \pm (\alpha Z/q - \kappa) \right]$$

with $(a)_\nu$ being the Pochhammer symbol and where the parameters $q$, $s$ and the normalization factor $N_{n\kappa}$ were defined above.

### 2.3.b. Matrix elements including the angular part of Dirac orbitals

## Matrix elements of spherical tensors:

- Matrix elements of the $\mathbb{C}^K$ tensors: Gaidamauskas *et al.* (2011) use the following definition:

$$\left\langle \kappa_a \left\| \, \mathbb{C}^{(K)} \, \right\| \kappa_b \right\rangle \;=\; (-1)^{j_a + 1/2}\; [j_a,\, j_b]^{1/2} \begin{pmatrix} j_a & K & j_b \\ 1/2 & 0 & -1/2 \end{pmatrix} \delta_{\,\ell_\mathrm{a}+\ell_\mathrm{b}+1,\,\mathrm{even}}$$

## 2.4. Frequently applied expansions and identities in atomic theory

### 2.4.a. Partial-wave expansions of free electrons

### Partial-wave expansion:

- Partial-wave components of a plane-wave electron: The computation of partial (and total) ionization cross sections often requires an integration over all possible angles $\Omega_p = (\vartheta_p, \varphi_p)$ of the photoelectrons, emitted in $4\pi$. In practice, this integration over $\Omega_p$ can be carried out rather easily by making use of the *decomposition* of the free-electron wavefunction $|\mathbf{p}\, m_s\rangle$ into *partial-wave* components.
- In practice, however, this expansion generally depends on the choice of the quantization axis.
- If the quantization axis is taken along $\mathbf{e}_z$ , this expansion is given by

$$|\mathbf{p}\, m_s\rangle \;=\; \sum_{\kappa\, m} i^{\ell}\, e^{-i\,\Delta_\kappa}\, \langle l m_\ell,\, 1/2\, m_s \,|\, jm\rangle\; Y^*_{\ell m_\ell}(\vartheta_p, \varphi_p)\; |\varepsilon\kappa m\rangle \;,$$

  and where the summation runs over all partial waves, $\kappa = \pm 1, \pm 2, \ldots$ as well as $m = -j, \ldots, j$. In this expansion, moreover, $\Delta_\kappa$ is the Coulomb phase shift, and the (nonrelativistic orbital angular momentum) quantum number $\ell$ just distinguishes the parity of the partial waves.

### 2.4.b. Expansions including spherical harmonis

### Expansions including the spherical harmonics:

- Expansion of a plane-wave in terms of spherical Bessel functions:

$$e^{i\,\mathbf{k}\cdot\mathbf{r}} \;=\; 4\pi \sum_{\ell m} i^{\ell}\, j_\ell(kr)\, Y^*_{\ell m}(\hat{k})\, Y^*_{\ell m}(\hat{r}) \;.$$

- Multipole expansion of the (transverse-gauge) plane-wave vector potential:

$$\mathbf{A}^{\,\mathrm{(transverse)}}(\mathbf{r},\omega) \;=\; 4\pi \sum_{LM\, p=0,1} i^{L-p}\, \left(\mathbf{Y}^{(p)}_{LM}(\hat{k}) \cdot \boldsymbol{\epsilon}\right)\; \mathbf{a}^{(p)}_{LM}(\mathbf{r}),$$

where the vector functions $\mathbf{a}_{LM}^{(p)}(\mathbf{r})$ are referred to as multipole potentials, and where only terms with $p = 0$ (magnetic) and $p = 1$ (electric) contribute, since $\mathbf{Y}_{LM}^{(-1)}(\hat{k})$ is orthogonal to $\boldsymbol{\epsilon}$ .

## 2.4.c. Useful idendities

### Useful idendities:

➢ Derivative of the spherical Bessel functions:

$$j_{n-1}(z) \;=\; \frac{n+1}{z}\, j_n(z) \;+\; j_n'(z), \qquad\qquad j_{n+1}(z) \;=\; \frac{n}{z}\, j_n(z) \;-\; j_n'(z)$$

## 2.5. Frequently occuring radial integrals

### Notation & applications in Jac:

- ➢ In Jac, all these radial integrals can be directly computed by a call to some function from the `RadialIntegrals` module.

### Grant's radial integrals for the coupling of the radiation field:

- ➢ Grant (1988) defines the following radial integrals that frequently occur in the coupling of the radiation field

$$
\begin{aligned}
I_L^o(q;\, ab) &= \int_0^\infty dr\; j_L(qr)\; [P_a\, Q_b] \;=\; \int_0^\infty dr\; j_L(qr)\; [P_a(r)\, Q_b(r)] \\
I_L^\pm(q;\, ab) &= \int_0^\infty dr\; j_L(qr)\; [P_a\, Q_b \;\pm\; Q_a\, P_b] \\
J_L(q;\, ab) &= \int_0^\infty dr\; j_L(qr)\; [P_a\, P_b \;+\; Q_a\, Q_b]
\end{aligned}
$$

- ➢ These integrals are useful also if the spherical Bessel function occurs in the integrant as $j_L(qr)/qr$ , and where the following recursion relations can be used:

$$
\frac{j_L(x)}{x} \;=\; \frac{1}{2L+1}\,\left[\, j_{L-1}(x) \;+\; j_{L+1}(x) \,\right].
$$

### Further radial integrals for different one-electron spherical tensor operators:

- ➢ In the treatment of the electron nucleus (hyperfine) interaction and the interaction with an external magnetic field, some radial integrals occur frequently:

$$I_L^{[r]}(ab) \;\equiv\; [r^L]_{ab} \;=\; \int_0^\infty dr\, r^L \;[P_a\, Q_b \;+\; Q_a\, P_b]$$

$$J_L^{<r>}(ab) \;=\; \langle r^L \rangle_{ab} \;\equiv\; \int_0^\infty dr\, r^L \;[P_a\, P_b \;+\; Q_a\, Q_b]$$

- Vinti-Integral: In the treatment of the (relativistic) mass shift, the (so-called) Vinti-Integrals occur

$$R^{\,(\mathrm{Vinti})}(a,b) \;=\; \int_0^\infty dr\, P_a \left[\frac{d}{dr} \;-\; \frac{\kappa_a(\kappa_a+1) \;-\; \kappa_b(\kappa_b+1)}{2r}\right] P_b \;\;+\;\; \int_0^\infty dr\, Q_a \left[\frac{d}{dr} \;-\; \frac{-\kappa_a(-\kappa_a+1) \;+\; \kappa_b(-\kappa_b+1)}{2r}\right] Q_b \,.$$

## 2.6. B-splines

### Properties of B-splines:

- A B-spline (basis spline) is a spline function with a minimal support and which can be used to express all spline function of any given as a finite linear combination.
- In physics, B-splines are often utilized for curve-fitting and in order to fit derivatives to experimental data.
- Knot sequence: A sequence of (radial) grid points $\{t_1,\, t_2,\, ...,\, t_m\}$ with $t_1 \;\le\; t_2 \;\le\; ... \;\le\; t_m$ .
- Set of B-splines: Set of piecewise polynomial functions of order $k$, the so-called B-splines:

$$\left\{ B_1^{(k)}(x),\, B_2^{(k)}(x),\, ...,\, B_n^{(k)}(x) \right\}, \qquad\qquad B_i^{(1)}(x) \;=\; \begin{cases} 1 & \text{for } t_i \;\le\; x \;\le\; t_{i+1} \\ 0 & \text{otherwise,} \end{cases} \qquad\qquad i \;=\; 1, 2,\, ...,\, m-1\,.$$

- Recursion relation for the generation of B-splines:

$$B_i^{(k)}(x) \;=\; \frac{x \;-\; t_i}{t_{i+k-1} \;-\; t_i}\, B_i^{(k-1)}(x) \;+\; \frac{t_{i+k} \;-\; x}{t_{i+k} \;-\; t_{i+1}}\, B_{i+1}^{(k-1)}(x) \qquad\qquad i \;=\; 1, 2,\, ...,\, m-k$$

The number of B-splines $n = m - k$ $(k < m)$ is determined by the order $k$ and the number of knots $m$. For B-splines of a given order, it is therefore sufficient to use the notation $B_i^{(k)}(x)$

- Each B-spline is non-negative and is non-zero only for: $B_i(x) > 0$ for $t_i < x < t_{i+k}$ and $B_i(x) = 0$ for $x < t_i,\ x > t_{i+k}$. — Essentially, the B-spline $B_i(x)$ starts at $t_i$ and ends at $t_{i+k}$ with only positive values in between.

## 2.7. Generation of continuum orbitals

### Simple approximations in Jac:

- For a first estimate of continuum processes, we have implemented a number of (rather) simple approximations/methods for the continuum orbitals that occur frequently at various places in the program. In JAC, the particular method can be selected by (re-) defining the global variable `JAC_CONT_SOLUTION` by a proper call to `Jac.define("method: continuum; ...)`.
- In particular, the following four methods have been implemented: (a) spherical Bessel functions; (b) non-relativistic Coulomb waves for the large component of the continuum orbital, together with the kinetic-balance condition to obtain a small component; (c) asymptotically correct, relativistic Coulomb orbital; (d) Galerkin method to solve for continuum orbitals within a B-spline basis and for a given atomic potential.
- In JAC, spherical Bessel orbitals are generated if the global constant `JAC_CONT_SOLUTION = ContBessel`; cf. `JAC.define()`.
- In JAC, a free nonrelativstic Coulomb orbitals are generated if the global constant is `JAC_CONT_SOLUTION = NonrelativisticCoulomb`; cf. `JAC.define()`.
- In JAC, asymptotically-correct relativistic Coulomb orbitals are generated for a potential with a Coulombic tail, if the global constant `JAC_CONT_SOLUTION = AsymptoticCoulomb`; cf. `JAC.define()` and section 2.7.c.
- In JAC, a B-spline representation of the relativistic orbital $\varepsilon\kappa$ in a given local potential are generated if the global constant `JAC_CONT_SOLUTION = BsplineGalerkin`; cf. `JAC.define()` and section 2.7.d.
- In JAC, different normalization methods can be selected for all continuum orbitals; a pure-sine normalization for `JAC_CONT_NORMALIZATION = PureSine`, an asymptotic Coulomb normalization for `JAC_CONT_NORMALIZATION = CoulombSine`, or a WKB-type normalization for multiply and highly-charged ions for `JAC_CONT_NORMALIZATION = OngRussek`; cf. `JAC.define()`.
- At present, no attempt has yet been made to incorporate the exchange interaction of the continuum and bound-state orbitals.

## 2.7.a. Spherical Bessel orbitals

### Implementation and numerical details:

- Generating equation and solutions: The spherical Bessel functions $j_\ell(|\mathbf{k}|\, r)$ obey the *free* radial Schrödinger equation for the one-electron energy $\varepsilon$ and the corresponding wave number $k = \sqrt{2\,\varepsilon}$, $\rho = kr$

$$R_{\varepsilon\ell}(r) \;=\; \frac{P_{\varepsilon\ell}}{r} \;=\; N\, j_\ell(|\mathbf{k}|\, r) \;=\; N\, j_\ell(\sqrt{2\,\varepsilon}\; r) \qquad \Longleftrightarrow \qquad j''_\ell(\rho) \,+\, 2\,\frac{j'_\ell(\rho)}{\rho} \,+\, \left(1 \,-\, \frac{\ell(\ell+1)}{\rho^2}\right) j_\ell(\rho) \;=\; 0\,.$$

- While the large component of such a continuum (Bessel) orbital $|\varepsilon\kappa\rangle$ are represented by the Bessel function $P \;=\; N\,r\;\; j_\ell(|\mathbf{k}|\, r)$ above, the small components are here obtained from the kinetic-balance condition.

## 2.7.b. Non-relativistic Coulomb orbitals

### Implementation and numerical details:

- The non-relativstic Coulomb orbitals $|\varepsilon\ell\rangle$ are known analytically for $\varepsilon \;>\; 0$ and can be utilized to represent the large components of a relativistic orbital with this (given kinetic) energy, while the small components are here obtained again from the kinetic-balance condition.
- See section 2.1 for a representation of a non-relativistic Coulomb orbital with positive energy $\varepsilon \;>\; 0$.

## 2.7.c. Asymptotically-correct relativistic Coulomb orbitals

### Implementation and numerical details:

- Relativistic free Coulomb waves: The free solutions to the radial Dirac equation in a spherical potential with Coulombinc tail satisfy the boundary conditions (Åberg and Howat, 1982; Eqs. (19.29-30))

$$P_{\varepsilon\ell}(0) \;=\; Q_{\varepsilon\ell}(0) \;=\; 0$$

$$P_{\varepsilon\kappa}(r \rightarrow \infty) \;\simeq\; \sqrt{\frac{\varepsilon \,+\, 2c^2}{\pi\, c^2\, k}}\; \cos\,[\theta_\kappa(\varepsilon) \,+\, \delta_\kappa(\varepsilon)]\,, \qquad Q_{\varepsilon\ell}(r \rightarrow \infty) \;\simeq\; -\sqrt{\frac{\varepsilon}{\pi\, c^2\, k}}\; \sin\,[\theta_\kappa(\varepsilon) \,+\, \delta_\kappa(\varepsilon)]$$

$$\theta_\kappa(\varepsilon) \;=\; k\,r \,+\, y\,\ln(2k\,r) \,-\, \arg\Gamma(\bar{\gamma} \,+\, i\,y) \,-\, \frac{1}{2}\,\pi\,\bar{\gamma} \,+\, \eta, \qquad k^2 \;=\; 2\,\varepsilon \,+\, \frac{\varepsilon}{c^2}$$

$$\bar{\gamma} \;=\; +\left(\kappa^2 \,-\, \frac{\bar{Z}^2}{c^2}\right)^{1/2}, \qquad y \;=\; \frac{\bar{Z}\,(\varepsilon \,+\, c^2)}{c^2\, k} \qquad \exp(2i\,\eta) \;=\; -\,\frac{\kappa \,-\, i\,y\,/\,(\varepsilon \,+\, c^2)}{\bar{\gamma} \,+\, i\,y}\,.$$

- The phase-shift $\delta_\ell$ is the non-Coulombic phase shift and is set to $\delta_\ell \;=\; 0$ for a pure Coulombic potential.

## 2.7.d. Continuum orbitals in an atomic potential: Galerkin method

### Implementation and numerical details:

- One advantages of using B-splines is that solutions of the Schrödinger or Dirac equation can be found for any energy $\varepsilon \,>\, 0$ by properly adopting $r_{\rm max}$ .
- While the Schrödinger and Dirac equations have formally a solution for every positive energy $\varepsilon$, a diagonalization in a B-spline representation only provides a discrete set of solutions due to the boundary condition $P(r_{\rm max}) \;=\; Q(r_{\rm max}) \;=\; 0$ , and where $r_{\rm max}$ here denotes the size of the *numerical box*.
- Galerkin method: This method determines an approximate solution of the generalized eigenvalue equations

$$\sum_i \,\langle B_i\,|\,(\mathbb{H} \,-\, \varepsilon)\,|\,B_j\rangle\; c_j \;=\; \sum_i\, A_{ij}\, c_j \;=\; 0, \qquad A_{ij} \;=\; \langle B_i\,|\,(\mathbb{H} \,-\, \varepsilon)\,|\,B_j\rangle \;=\; H_{ij} \,-\, \varepsilon\, S_{ij}.$$

- A possible approximation is to compute the smallest eigenvalue of $\mathbf{A} \cdot \mathbf{c} \;=\; \lambda\,\mathbf{c}$ , a more accurate solution follows from a minimization of $|\,A\,\psi\,|^2$ under the contraint $|\,\psi\,|^2 \;=\; 1$ . This variational problem is equivalent to find the smallest eigenvalue of the matrix $A^+\,A$ : $\mathbf{A}^+\,\mathbf{A} \cdot \mathbf{c} \;=\; a\,\mathbf{c}$ . — The eigenvector of the smallest eigenvalue $a_i \;>\; 0$ is then requested (approximate) solution.

## 2.7.e. Normalization and phase of continuum orbitals

### Pure sine behaviour at large $r$:

- An asymptotic pure sine behaviour $\sim \sin(kr + \varphi)$ occurs just for the free radial Schrödinger equation without an external potential, while a pure sine behaviour $\sim \sin(kr - \ell\,\pi/2 + \varphi)$ applies for the standard radial Schödinger equation with just a centrifugal potential (but $Z(r) = 0$ otherwise).
- For this normalization, the large component is assumed to be given with $k = \sqrt{2\,\varepsilon}$ by

$$P(r \approx r_{\rm max}) \;=\; \sqrt{\frac{2}{\pi\,k}} \begin{cases} \sin\left(kr + \varphi\right) & \text{for} \quad \ell = 0 \\ \sin\left(kr - \frac{\ell\pi}{2} + \varphi\right) & \text{for} \quad \ell > 0\,. \end{cases}$$

With this behaviour, the normalization constant $N$ and phase $\varphi$ can be obtained by means of the logarithmic derivative $P/P'$ .

### Asymptotic Coulomb behaviour at large $r$:

- For this normalization, the large and small components are assumed to be described for all $r$-values by the asymptotic behaviour as shown in subsection 2.7.c. With this assumption, the normalization constant $N$ and phase $\varphi$ can again be obtained by means of the logarithmic derivative $P'/P$ .
- Instead of the logarithmic derivative $P'/P$ , one can of course also apply the ratio $Q/P$ ; this option is currently hard-coded in JAC but need to be further tested.

### Normalization for multiply-charged ions due to Ong and Russek (1973):

- This normalization scheme has not yet been implemented and tested so far.

## 2.8. Nuclear potentials

### Nuclear charge distributions:

- Fermi model: For a nucleus with *root-mean-square* (rms) radius $R = \sqrt{\langle r^2 \rangle}$

  $$\rho(r, R) = \frac{N}{1 + \exp[(r - c)/a]}, \qquad \int dr\, r^2\, \rho(r, R) = 1$$

  where the thickness parameter $a$ is often chosen as $a = 2.3/4 \ln 3$.

- With high accuracy, the parameters $N$ and $c$ can be obtained from the analytical formulas

  $$N = \frac{3}{4\pi\, c^3} \left( 1 + \frac{\pi^2\, a^2}{c^2} \right)^{-1}, \qquad c = \sqrt{\frac{5}{3}\, \langle r^2 \rangle - \frac{7}{3}\, \pi^2\, a^2}\,.$$

### Nuclear potential:

- Potential of extended nucleus:

  $$\mathbb{V}^{(\mathrm{nuc})}(r; R) = -4\pi\, \alpha\, Z \int_0^\infty dr'\, r'^2\, \frac{\rho(r', R)}{r_>} = -\frac{4\pi\, \alpha\, Z}{r} \int_0^r dr'\, r'^2\, \rho(r', R) - 4\pi\, \alpha\, Z \int_r^\infty dr'\, r'\, \rho(r', R), \qquad r_> = \max(r, r').$$

# 3. Many-electron atomic interactions, state functions, density operators and statistical tensors

## 3.1. Electron-electron interaction

### Motivation:

- In the (non-relativistic) limit of a rather slow motion of the electrons, each electron pair just interact by the instantaneous Coulomb repulsion

  $$\frac{1}{r_{12}} \equiv \frac{1}{|\mathbf{r}_1 - \mathbf{r}_2|}.$$

  Already this quite simple (interaction) operator results mathematically in various complications and is generally the major source of electron-electron correlations in all many-electron computations.

- For moving charges, Maxwell's theory also predicts both, current-current and retarded interactions, to which we briefly refer as Breit interactions in atomic physics. — These relativistic contributions to the electron-electron interactions must be added to the electro-static Coulomb repulsion.

- An effective (relativistic) operator for the electron-electron interaction can be formally derived from QED in perturbation theory with regard to the number of virtually exchanged photons (Sapirstein 1987, Grant und Quiney 1988), while the same expressions can be obtained also from heuristic arguments as given, for example, by Bethe and Salpeter (1957) und Johnson (1995).

- In practice, the computation of the electron-electron interaction usually requires the largest effort in all electronic-structure codes and, therefore, deserves special consideration. In atomic physics, a considerable simplification is usually achieved if all electron-electron interaction operators are represented as spherical tensors.

- For two electrons in orbitals $a$, $b$ and with energies $\varepsilon_a, \varepsilon_b$, the interaction energy can be written as difference of a direct and exchange matrix element of the potential

$$\mathbb{V}^{(\mathrm{tr})} = -\frac{1}{2\pi} \int \frac{d^3k}{k^2 - \omega^2} \, e^{i\,\mathbf{k}\cdot(\mathbf{r}_1 - \mathbf{r}_2)} \sum_{i,j=1}^{3} \left[ \delta_{ij} - \frac{k_i\,k_j}{k^2} \right] \alpha_{1i}\,\alpha_{2j}$$

where $\alpha_{1i}$ is the $i$-th component of the $\boldsymbol{\alpha}$ matrix (vector) of the electron at position $\mathbf{r}_1$ and

$$\omega = \begin{cases} 0 & \text{direct matrix element} \\ \frac{|\epsilon_a - \epsilon_b|}{c} & \text{exchange matrix element} \end{cases}$$

refers to the momentum of the exchanged photon.

- The exchange matrix elements of the potential $\mathbb{V}^{(\mathrm{tr})}$ is generally complex; while the *real* part describes an energy shift due to this transverse interaction, the *imaginary* part represents a rate for the decay $a \to b$ for $\epsilon_a > \epsilon_b$ or $b \to a$ *vice versa.*
- Frequency-independent Breit interaction: For $\omega \to 0$, the transversal Breit interaction gives rise to the frequency-independent Breit interaction

$$b_{12}^{o} = -\frac{1}{2\,r_{12}} \left[ \boldsymbol{\alpha}_1 \cdot \boldsymbol{\alpha}_2 + \frac{(\boldsymbol{\alpha}_1 \cdot \mathbf{r}_{12})\,(\boldsymbol{\alpha}_2 \cdot \mathbf{r}_{12})}{r_{12}^2} \right],$$

which neglects all contributions $\sim \alpha^4 Z^3$ (as well as of higher order in $\alpha Z$).

- Typically, the explicit energy-dependence of the transverse interaction [upon the energy difference of the two electrons] gives rather tiny corrections, so that, in practice, often no difference is made between the transversal and zero-frequency Breit interaction.
- Gaunt interaction: The first term of the zero-frequency Breit interaction (operator) is known also as Gaunt interaction (Gaunt 1929). This term describes the current-current interaction due to the motion of the electrons and contributes about 90 % of the total Breit interaction for closed-shell atoms.
- For many elements of the periodic table, the corrections due to the Breit interaction are usually small, when compared with the dominant Coulomb repulsion. This applies especially for the Breit contributions to the electron-electron correlation.
- For describing most processes, it is sufficient, if at all, to include the Breit interaction perturbatively in lowest order. Formally, however, both terms

$$v_{12} = \frac{1}{r_{12}} + b_{12} \qquad \Longleftrightarrow \qquad \mathbb{V}^{(\mathrm{e-e})} = \mathbb{V}^{(\mathrm{Coulomb})} + \mathbb{V}^{(\mathrm{Breit})}$$

are equivalent, and they should be treated simply together for all (super-) heavy elements.

- In Jac, only the frequency-independent Breit interaction is currently implemented.

## Effective interaction strength $X^{(L)}(abcd)$ of scalar electron-electron interactions:

- All operators of the (scalar) electron-electron interaction can be generally represented as spherical tensors in the form:

$$g_{12} \;\equiv\; g(\mathbf{r}_1, \mathbf{r}_2) \;=\; \sum_L g_L(r_1, r_2)\; \left(\mathbb{T}^{(L)}(\vartheta_1, \varphi_1) \cdot \mathbb{T}^{(L)}(\vartheta_2, \varphi_2)\right)$$

$$\langle n_a\kappa_a m_a\,(1)\; n_b\kappa_b m_b\,(2)\,|\; \mathfrak{g}_{12}\;|\, n_c\kappa_c m_c\,(1)\; n_d\kappa_d m_d\,(2)\rangle \;=\; \sum_{L\,M} (-1)^{L-M+j_a-m_a+j_b-m_b} \begin{pmatrix} j_a & L & j_c \\ -m_a & M & m_c \end{pmatrix} \begin{pmatrix} j_b & L & j_d \\ -m_b & -M & m_d \end{pmatrix} X^{(L)}(abcd),$$

leading to a simple factorization of the two-electron matrix elements, and where the magnetic quantum numbers (i.e. the angular dependence) of the matrix elements only occurs in the phase and the Wigner $3-j$ symbols.

- Effective interaction strength $X^{(L)}(abcd)$ of order $L$: The strengths $X^{(L)}(abcd)$ describe the physical interaction and are specific for every operator. They are often used as the building blocks in order to handle the electron-electron interactions efficiently in electronic structure computations.

## Effective interaction strength $X^{(L,\,\mathrm{Coulomb})}(abcd)$ of the Coulomb repulsion:

- Coulomb repulsion: The decomposition of the Coulomb operator is given by:

$$\frac{1}{r_{12}} \;=\; \sum_{L=0}^{\infty} U_L(r,s)\; P_L(\cos(\vartheta)) \;=\; \sum_{L=0}^{\infty} U_L(r,s)\; \left(\mathbb{C}^{(L)}(\vartheta_1, \varphi_1) \cdot \mathbb{C}^{(L)}(\vartheta_2, \varphi_2)\right), \qquad U_L(r,s) \;=\; \begin{cases} \frac{r^{\,L}}{s^{\,L+1}} & r < s \\ \frac{s^{\,L}}{r^{\,L+1}} & r > s\,. \end{cases}$$

In this expansion, $P_L(x)$ denotes a Legendre-polynomial and $\vartheta = \mathbf{r} \cdot \mathbf{s}/rs$ the angle between the two electron coordinates.

➢ Effective interaction strength of the Coulomb repulsion:

$$X^{(L,\,\text{Coulomb})}(abcd) \;=\; \delta(j_a, j_c, L)\, \delta(j_b, j_d, L)\, \Pi^{e}(\kappa_a, \kappa_c, L)\, \Pi^{e}(\kappa_b, \kappa_d, L)\, (-1)^L \left\langle \kappa_a \left\| \mathbb{C}^{(L)} \right\| \kappa_c \right\rangle \left\langle \kappa_b \left\| \mathbb{C}^{(L)} \right\| \kappa_d \right\rangle \; R^L(abcd)\,,$$

$$\delta(j_a, j_b, j_c) \;=\; \begin{cases} 1 & |j_a - j_b| \;\le\; j_c \;\le\; |j_a + j_b| \quad \text{and cyclic interchanged} \\ 0 & \text{otherwise}\,, \end{cases}$$

and where $\Pi^{e}(\kappa, \kappa', L)$ represent the angular momentum and parity selection rules.

## Effective interaction strength $X^{(L,\,\text{Breit})}(abcd)$ of the Breit interaction:

➢ Effective interaction strength of the zero-frequency Breit: For the zero-frequency interaction, we find

$$X^{(L,\,\text{Breit})}(abcd) \;=\; (-1)^L \left\langle \kappa_a \left\| \mathbb{C}^{(L)} \right\| \kappa_c \right\rangle \left\langle \kappa_b \left\| \mathbb{C}^{(L)} \right\| \kappa_d \right\rangle \Bigg[ \Pi^{o}(\kappa_a, \kappa_c, L-1)\, \Pi^{o}(\kappa_b, \kappa_d, L+1) \sum_{\mu=1}^{8} s_\mu^L(abcd)\; S_\mu^L(abcd) \;+ \\ + \sum_{\nu\,=\,L-1}^{L+1} \Pi^{o}(\kappa_a, \kappa_c, \nu)\, \Pi^{o}(\kappa_b, \kappa_d, \nu) \sum_{\mu=1}^{4} t_\mu^{\nu,L}(abcd)\; T_\mu^{\nu}(abcd) \Bigg]\,.$$

$$\Pi^{o}(\kappa_a, \kappa_b, L) \;=\; \begin{cases} 1 & \text{if} \quad l_a + l_b + L \quad \text{odd} \\ 0 & \text{otherwise.} \end{cases}$$

➢ The constant coefficients $s_\mu^L$ and $t_\mu^{\nu,L}$ just depend on the angular quantum numbers $\{\kappa_a,\, \kappa_b,\, \kappa_c,\, \kappa_d,\, \nu,\, L\}$ and are diplayed, for example, by Grant (1988; tables 3 and 4, and where we here use $t_\mu^{\nu,L} \equiv r_\mu^{\nu,L}$).

Table 3.1.: Definition of the integrales $S^{\nu}_{\mu}(abcd)$ und $T^{\nu}_{\mu}(abcd)$

| | | |
|---|---|---|
| $S^{\nu}_{1}(abcd) = S^{\nu}\,[ac\,\|\|\,bd]$ | $S^{\nu}_{2}(abcd) = S^{\nu}\,[bd\,\|\|\,ac]$ | $T^{\nu}_{1}(abcd) = T^{\nu}\,[ac\,\|\|\,bd]$ |
| $S^{\nu}_{3}(abcd) = S^{\nu}\,[ca\,\|\|\,db]$ | $S^{\nu}_{4}(abcd) = S^{\nu}\,[db\,\|\|\,ca]$ | $T^{\nu}_{2}(abcd) = T^{\nu}\,[ca\,\|\|\,db]$ |
| $S^{\nu}_{5}(abcd) = S^{\nu}\,[ac\,\|\|\,db]$ | $S^{\nu}_{6}(abcd) = S^{\nu}\,[db\,\|\|\,ac]$ | $T^{\nu}_{3}(abcd) = T^{\nu}\,[ac\,\|\|\,db]$ |
| $S^{\nu}_{7}(abcd) = S^{\nu}\,[ca\,\|\|\,bd]$ | $S^{\nu}_{8}(abcd) = S^{\nu}\,[bd\,\|\|\,ca]$ | $T^{\nu}_{4}(abcd) = T^{\nu}\,[ca\,\|\|\,bd]$ |

- The radial integrals $S^{\nu}_{\mu}(abcd)$ and $T^{\nu}_{\mu}(abcd)$ are different (linear) combinations of the two integrals [cf. table 3.1]

$$S^{\nu}\,[ac\,|\,bd] \;=\; \int_0^{\infty} dr \int_0^{\infty} ds\; P_a(r)\,Q_c(r)\,\frac{1}{2}\,[\,W_{\nu-1,\,\nu+1,\,\nu}(r,s;\,\omega_{ac}) \,+\, W_{\nu-1,\,\nu+1,\,\nu}(r,s;\,\omega_{bd})\,]\;P_b(s)\,Q_d(s)$$

$$T^{\nu}\,[ac\,|\,bd] \;=\; \int_0^{\infty} dr \int_0^{\infty} ds\; P_a(r)\,Q_c(r)\,\frac{1}{2}\,[\,V_{\nu}(r,s;\,\omega_{ac}) \,+\, V_{\nu}(r,s;\,\omega_{bd})\,]\;P_b(s)\,Q_d(s)$$

$$V_{\nu}(r,s;\,\omega) \;=\; \begin{cases} -(2\nu+1)\,j_{\nu}(\omega r)\,n_{\nu}(\omega s) & r < s \\ -(2\nu+1)\,j_{\nu}(\omega s)\,n_{\nu}(\omega r) & r > s \end{cases}$$

$$W_{\nu-1,\,\nu+1,\,\nu}(r,s;\,\omega) \;=\; \begin{cases} -(2\nu+1)\,j_{\nu-1}(\omega r)\,n_{\nu+1}(\omega s) + \left(\frac{2\nu+1}{\omega}\right)^2 \frac{r^{\nu-1}}{s^{\nu+2}} & r < s \\ -(2\nu+1)\,\omega\;j_{\nu-1}(\omega s)\,n_{\nu+1}(\omega r) & r > s \end{cases} .$$

- In these expressions, $j_{\nu}(\omega r)$ and $n_{\nu}(\omega r)$ denote the spherical Bessel functions, and $\omega_{ac} = |\,\epsilon_a - \epsilon_c\,|$ the difference of the corresponding single-particle energies.

## 3.2. Atomic potentials

### 3.2.a. In JAC implemented potentials

**Atomic potentials:**

- Core-Hartree potential:

$$V^{\,(\mathrm{core-Hartree})}(r) \;=\; \int_0^\infty dr' \, \frac{\rho_c(r')}{r_>}, \qquad\qquad r_> \;=\; \max(r, r'), \qquad\qquad \rho_c(r) \;=\; \sum_a \left(P_a^2(r) \,+\, Q_a^2(r)\right),$$

  and where the summation runs over all *core* orbitals of electron configurations. This potential is applied if just a single valence electron occurs (alkali atoms). In JAC, this potential can be obtained for a given level from `Jac.computePotentialCoreHartree(grid::Radial.Grid, level::Level)`.

- Dirac-Fock-Slater potential:

$$V^{\,(\mathrm{DFS})}(r) \;=\; \int_0^\infty dr' \, \frac{\rho_t(r')}{r_>} \;-\; \left( \frac{3}{4\pi^2 \, r^2} \, \rho_t(r) \right)^{1/3}, \qquad\qquad r_> \;=\; \max(r, r'), \qquad\qquad \rho_t(r) \;=\; \sum_a \left(P_a^2(r) \,+\, Q_a^2(r)\right),$$

  and where the summation runs over *all* orbitals (electrons). In JAC, this potential can be obtained for a given level from `Jac.computePotentialDFS(grid::Radial.Grid, level::Level)`.

- Hartree potential:

$$V^{\,(\mathrm{Hartree})}(r) \;=\; -\sum_a \, \bar{q}_a \, r \, Y^0_{aa}(r)$$

  where $\bar{q}_a$ is the generalized occupation number, and where the summation runs over all orbitals here. In JAC, this potential can be obtained for a given level from `Jac.computePotentialHartree(grid::Radial.Grid, level::Level)`.

- Hartree-Slater potential:

$$V^{\,(\mathrm{HS})}(r) \;=\; -\sum_a \, \bar{q}_a \, Y^0_{aa}(r) \;+\; \frac{3}{2} \left( \frac{3}{4\pi^2 \, r^2} \, \rho(r) \right)^{1/3} \frac{r}{2} \qquad\qquad \rho(r) \;=\; \sum_a \bar{q}_a \, \left(P_a^2(r) \,+\, Q_a^2(r)\right),$$

and where the summation runs over *all* orbitals. In JAC, this potential can be obtained for a given level from `Jac.computePotentialDFS(grid::Radial.Grid, level::Level)`.

- ➢ Kohn-Sham potential:

$$V^{\,(\mathrm{Kohn-Sham})}(r) \;=\; \int_0^\infty dr' \, \frac{\rho_t(r')}{r_>} \;-\; \frac{2}{3\,r} \left( \frac{81}{32\,\pi^2} \, r \, \rho_t(r) \right)^{1/3} , \qquad r_> \;=\; \max(r, r'), \qquad \rho_t(r) \;=\; \sum_a \left( P_a^2(r) \;+\; Q_a^2(r) \right) ,$$

and where the summation runs over *all* orbitals (electrons). In JAC, this potential can be obtained for a given level from `Jac.computePotentialKohnSham(grid::Radial.Grid, level::Level)`.

### 3.2.b. Further atomic potentials, not yet considered in JAC

## Atomic potentials:

- ➢ Tietz (1954) potential:

$$V^{\,(\mathrm{Tietz})}(r) \;=\; -\,\frac{\alpha\,Z}{r}\,\phi(x), \qquad \phi(x) \;=\; \frac{1}{\left(1 \;+\; (\pi/8)^{2/3}\,x\,\right)^2}, \qquad x \;=\; \frac{r\,Z^{1/3}}{\mu}, \qquad \mu \;=\; \left(\frac{3\pi}{4}\right)^{2/3} \;\approx\; 0.8853.$$

- ➢ Modified-Tietz potential: (Neuffer and Commins, 1977)

$$V^{\,(\mathrm{modified-Tietz})}(r) \;=\; -\,\frac{\alpha}{r} \left( 1 \;+\; \frac{(Z-1)}{(1+t\,r)^2}\, e^{-\gamma\,r} \right)$$

where $\gamma$ and $t$ are parameters adjusted to fit the low-lying spectra of the atoms under consideration. Johnson *et al.* (1985) tabulate these parameters for rhubidium, cesium, gold and thallium.

## 3.3. Multi-configuration Dirac-Hartree-Fock (MCDHF) method

### Motivation:

- ➢ The multi-configuration Dirac-Hartree-Fock (MCDHF) method has been found a versatile tool for calculating the level structure and approximate wave functions for atoms and ions of all elements across the periodic table. Not much need to be said about this method, which has been presented at several places elsewhere (Grant 1989; Parpia *et al.* 1996; Fritzsche 2002).
- ➢ Atomic state function (ASF): Similar to the well-known Hartree-Fock (HF) method from non-relativistic quantum theory, in which the state of a quantum system is approximated by a single (symmetry-adapted) Slater determinant, an atomic state function (ASF) is written in the MCDHF model as linear combination of configuration state functions (CSF) with well adapted symmetry

$$|\alpha\ \mathbb{J}M\rangle \quad\equiv\quad \psi_\alpha(\mathbb{J}M) \;=\; \sum_{r=1}^{n_c} c_r(\alpha)\ |\gamma_r\ PJM\rangle \ .$$

In this ansatz, $n_c$ is the number of CSF, $\mathbb{J} \equiv J^P$ the total angular momentum and parity of the state, and $\alpha$ refers to all (further) quantum numbers that are needed to specify the state uniquely. Moreover, $\{c_r(\alpha)\}$ denotes the representation of the atomic state in the given basis.

- ➢ In most standard computations, the set of CSF $\{|\gamma_r\ PJM\rangle\}$ are constructed as antisymmetrized products of a common set of orthonormal orbitals. In contrast to the HF method, both the radial (one-electron) functions as well as the expansion coefficients $\{c_r(\alpha),\ r=1,\ldots,n_c\}$ are optimized simultaneously on the basis of the Dirac-Coulomb Hamiltonian. All further relativistic contributions to the energies and representation of the atomic states, which arise for instance from the (relativistic) interaction among the electrons or with the radiation field, are then treated in first-order perturbation theory by diagonalizing the Dirac-Coulomb-Breit Hamiltonian matrix.
- ➢ Standard MCDHF calculations give rise to the energies and wave functions $(E_\alpha,\ |\alpha\,\mathbb{J}M\rangle)$ for one or several selected bound states. From the symmetry of atoms and ions with regard to a rotation or inversion of the coordinates it is clear, that the Hamiltonian matrix is always block-diagonal in the total parity and angular momentum quantum numbers, $\mathbb{J} \equiv J^P$ and $M$, respectively.
- ➢ Based on the (one-electron) Dirac Hamiltonian, the MCDHF method enables one to describe consistently the dominant effects of relativity and correlations within the same framework.
- ➢ Owing to the symmetry of the Hamiltonian, the computational effort of the MCDHF method can be reduced by a rather large factor $(> 10)$, if the various (total) angular momenta and parities $\mathbb{J} = J^P$ of the atomic states of interest are considered independently.

➣ The decision about the atomic Hamiltonian operator, that is utilized in a particular MCDHF computation, is often made on the basis of (1) the nuclear charge, (2) the charge state of the atom or ion, (3) its particular shell structure as well as (4) the atomic property under consideration. Further relativistic and radiative corrections to the (total energies of the) atomic levels can be added in various (effective) approximations.

➣ Steps for practical MCDHF computations: In the MCDHF method and, hence, in JAC, the atomic bound states are typically generated by a series of steps:

- Definition of the nuclear parameters and the angular structure (and extent) of the CSF basis $\{|\gamma\, PJM\rangle\}$ as used in the MCDHF ansatz above;
- Algebraic evaluation and computation of the spin-angular integrals (the so-called angular coefficients), based on standard techniques from Racah's algebra;
- Initial estimates of all radial orbital functions and self-consistent field (SCF) calculations, based on the Dirac-Coulomb Hamiltonian;
- Configuration interaction (CI) calculations in order to incorporate further relativistic contributions into the Hamiltonian matrix and/or to enlarge the CSF basis beyond the given SCF model.

Often, these four steps are repeated at several stages by systematically enlarging the one-electron (active) orbital space.

## Restricted active spaces:

➣ Romplete active space (RAS) method: To include the *correlated* motion of the bound electrons in a more systematic fashion, the RAS method has been found useful for simple shell structures and has been applied along various isoelectronic sequences. The idea of this method is to account for an excitation of the *active* electrons from the outer shells (into a number of predefined *unoccupied* orbitals), while some 'electronic core' remains usually fixed in the set-up of the RAS.

➣ For a restricted active space, it is generally supposed that all possible excitations (distributions) of the valence electrons can be taken into account among the set of active orbitals. In practice, even the concept of a *restricted* active space is often not only *unfeasible* but also *unnecessary* for predicting many atomic properties, since only those CSF with a "total excitation energy" in the same region as the reference configurations need often to be taken into account in the MCDHF expansion.

➣ The necessary CSF expansions often increases by one or even several orders of magnitude for open $d$- or $f$-shells, and especially if reference configurations with nearly half-filled shells occur. — With the JAC tools, here we aim for a new generation of atomic structure programs which enables one to compute the properties of such open $d$- and $f$-shell elements with an accuracy comparable to that of simpler shell structures.

## 3.4. Atomic self-consistent-field and configuration-interaction calculations

### Hamiltonian matrix elements:

- For a given CSF basis, the representation of an atomic state in the MCDHF ansatz above (i.e. the mixing coefficients $\mathbf{c}(\alpha) \equiv (c_1(\alpha), c_2(\alpha), \ldots, c_{n_c}(\alpha))$ is obtained by solving the secular equation

$$\det\left(\mathbf{H} - E_\alpha^{(n_c)}\,\mathbf{I}\right) = 0\,, \qquad \mathbf{H} = (H_{rs}) = \left(\langle \gamma_r\, PJM \,|\, \mathbb{H} \,|\, \gamma_s\, \bar{P}\bar{J}\bar{M}\rangle\; \delta_{P\bar{P}}\,\delta_{J\bar{J}}\,\delta_{M\bar{M}}\right)$$

  where $E_\alpha^{(n_c)}\,(PJ)$ denotes the eigenvalue.

- The Hamiltonian matrix is block-diagonal in the total parity and angular momentum of the atom, and is independent of the particular choice of the electron-electron interaction in the Hamiltonian.

- Since the Hamiltonian matrix is real and symmetric, all atomic states are orthogonal for $E_\alpha \neq E_\beta$ or can be chosen in this way for $E_\alpha = E_\beta$. In practice, an efficient decomposition of the many-electron matrix elements $H_{rs}$ in the Hamiltonian matrix above is central to every implementation of the MCDHF method.

- Spin-angular integrals: The integration over the spin-angular variables of all $N$ electrons can be performed algebraically and enables one to write the matrix elements always in the form (Grant, 1989)

$$H_{rs} = \sum_t u_{rs}(a_t b_t)\; \langle a_t \,\|\, \mathbb{h}_\mathrm{D} \,\|\, b_t\rangle + \sum_t v_{L_t;rs}(a_t b_t c_t d_t)\, X^{(L_t)}(a_t b_t c_t d_t)\,.$$

  In this expansion, $u_{rs}(ab)$ and $v_{L;rs}(abcd)$ are one- and two-particle (scalar) angular coefficients, while the $X^{(L)}(abcd)$ describe the effective interaction strengths of (formally) the four electrons $a, b, c, d$ that are involved in the interaction. As usual, we here abbreviate the one-particle quantum numbers $a = (n_a, \kappa_a)$, $b = (n_b, \kappa_b)$, $\ldots$ to have a compact notation for the subshells of equivalent electrons.

- Reduced one-electron matrix elements of the Dirac Hamiltonian: The reduced matrix element in the first term of the Hamiltonian matrix elements

$$\langle a \,\|\, \mathbb{h}_\mathrm{D} \,\|\, b\rangle = \delta_{\kappa_a \kappa_b} \int_0^\infty dr \left[ c\, Q_a \left(\frac{d}{dr} + \frac{\kappa_a}{r}\right) P_b + c\, P_a \left(-\frac{d}{dr} + \frac{\kappa_a}{r}\right) Q_b - 2\,c^2\, Q_a\, Q_b + V_\mathrm{nuc}(r)\,(P_a P_b + Q_a Q_b)\right],$$

  contains the kinetic and potential energy of an electron in subshell $a$, and can be expressed in terms of the *large* and *small* (radial) components, $P_a(r)$ and $Q_a(r)$, of the corresponding one-electron orbital functions.

# 3.5. Atomic estimates of quantum-electrodynamic (QED) corrections

## 3.5.a. QED model operators & model potentials

### Motivation & notations:

- Various proposals have been made in the literature to incorporate the (radiative) quantum-electrodynamic corrections by different model potentials into correlated many-electron methods, such as MCDHF, many-body perturbation theory or coupled-cluster approaches.
- Effective single-electron QED Hamiltonian: To a good approximation, these QED correction can be included into the (many-electron) representation $\{c_r(\alpha \mathbb{J})\}$ of the level $|\alpha \mathbb{J}\rangle$ by means of some local single-electron QED Hamiltonian. This Hamiltonian can be separated into two parts

  $$\mathbb{h}^{(\mathrm{QED})} \;=\; \mathbb{h}^{(\mathrm{SE})} + \mathbb{h}^{(\mathrm{VP})},$$

  the self-energy (SE) and vacuum-polarization (VP) Hamiltonians, and which are often written in terms of (effective) potentials.
- Vacuum-polarization: The vacuum-polarization is given by a local potential and can be further splitted into an Uehling and a Wichmann-Kroll potential; this *local* potential is rather straightforward to calculate and has already been applied in many applications in the past.
- Self-energy Hamiltonian $\mathbb{h}^{(\mathrm{SE})}$ : Such a Hamiltonian can be generally represented as sum of a local and non-local potential. These potentials are typically based on *ab initio* calculations of the diagonal and nondiagonal matrix elements of the one-loop QED operator with H-like wave functions (Shabaev *et al.*, 2013).
- Shabaev and coworkers (2013) have shown that the QED corrections can be systematically incorporated into an effective Hamiltonian that acts in the space of Slater determinants, if these determinants are built from one-electron positive-energy states only and if the total (many-electron) energies of the system are smaller than the pair-creation energy. This effective QED Hamiltonian can then be added to the Dirac-Coulomb-Breit Hamiltonian.
- Explicit calculations of radiative corrections are extremely sophisticated and time-consuming for many-electron systems, if the standard QED perturbation theory is to be applied. Until the present, such detailed QED computations can be carried out only for highly-charged, few-electron ions and, still, by using an effective screening potential (instead of the complete perturbation expansion for all electron-electron pairs).

## Vacuum polarization potentials:

- Uehling potential: This potential is the dominant part of the VP and can be obtained from the direct numerical integration of the well-known formula

$$V^{\,(\mathrm{Uehling})}(r) \;=\; -\alpha\, Z\, \frac{2\,\alpha}{3\,\pi} \int_0^\infty dr'\; 4\pi\, r'\, \rho(r') \int_1^\infty dt\; \left(1 \,+\, \frac{1}{2\,t^2}\right) \frac{\sqrt{t^2 \,-\, 1}}{t^2}\; \frac{e^{-2m\,|r-r'|\,t} \,-\, e^{-2m\,(r+r')\,t}}{4m\,r\,t},$$

  and where $Z\,\rho(r)$ denotes the density of the nuclear charge distribution, if normalized to $\int dV\, \rho(r) \,=\, 1\,$.

- Approximate Uehling potential: The Uehling potential can be calculated also by the approximate formula for a point-like nucleus (Flambaum and Ginges, 2005)

$$V^{\,(\mathrm{simplified\ Uehling})}(r) \;=\; \frac{2\,\alpha}{3\,\pi}\, V(r) \int_1^\infty dt\; \left(1 \,+\, \frac{1}{2\,t^2}\right) \frac{\sqrt{t^2 \,-\, 1}}{t^2}\; e^{-2m\,r\,t}.$$

- Wichmann-Kroll potential: A detailed evaluation of the Wichmann-Kroll potential is (much) more sophisticated but can be estimated again to good accuracy by the approximate formula for a point-like nucleus (Flambaum and Ginges, 2005)

$$V^{\,(\mathrm{simplified\ WK})} \;=\; -\,\frac{2\,\alpha}{3\,\pi}\, V(r)\, \frac{0.092\, Z^2\, \alpha^2}{1 \,+\, (1.62\, r/r_c)^4}.$$

## Local self-energy potentials:

- Shabaev *et al.* (2013) suggest a local but independent part of the self-energy potential for each symmetry block $\kappa$ of the form

$$V_\kappa^{(\mathrm{local\ SE})}(r) \;=\; A_\kappa\; \exp\left(-\,\frac{2\pi\, r}{\lambda_c}\right) \;=\; A_\kappa\; \exp\left(-\,\frac{r}{\alpha}\right)$$

where the constants $A_\kappa$ are chosen to reproduce the SE shift for the lowest (one-electron, H-like) energy of each given $\kappa$ symmetry, and where $\lambda_C = h/m\,c$ is the Compton wavelength of the electron.

- These local contributions can also be cast be into the form

$$V^{\,(\text{local SE})}(r) \;=\; \sum_{\kappa} A_\kappa\, P_\kappa\, \exp\left(-\,\frac{2\pi\, r}{\lambda_c}\right), \qquad\qquad \langle a\,|P_\kappa|\,b\rangle \;=\; \delta_{\kappa,\kappa_a}\,\delta_{\kappa,\kappa_b}\;...$$

- Following the discussion with Volotka (2019), a (single-electron) local self-energy interaction strength for the (local) potential above can be written

$$\left\langle a \left\| \mathbb{h}^{\,(\text{local SE})} \right\| b \right\rangle \;=\; \frac{\left\langle n_g\kappa \left\| \mathbb{h}^{\,(\text{local SE})} \right\| n_g\kappa \right\rangle}{\left\langle n_g\kappa \left\| \exp\left(-\,\frac{r}{\alpha}\right) \right\| n_g\kappa \right\rangle}\;\left\langle a \left\| \exp\left(-\,\frac{r}{\alpha}\right) \right\| b \right\rangle$$

where $|n_g\kappa\rangle \;=\; \{1s_{1/2},\, 2p_{1/2},\, 2p_{3/2},\, 3d_{3/2},\, ...\}$ refers to the lowest hydrogenic orbitals of symmetry $\kappa$ and nuclear charge $Z$.

- Shabaev *et al.* (2013) have tabulated values for $\left\langle n_g\kappa \left\| \mathbb{h}^{\,(\text{local SE})} \right\| n_g\kappa \right\rangle$ for selected nuclear charges, which can be readily applied to compute the self-energy interactions strengths for general many-electron atoms and ions.

## Radiative potentials:

- Flambaum and Ginges (2005) suggest an approximate expression for a (so-called) radiative potential which can be utilized in order to estimate the radiative corrections in strong Coulomb fields to the energies and electric-dipole transition amplitudes in atomic (many-electron) computation. This (alternative) potential is claimed to give good QED estimates with an accuracy of a few percent but has been mainly adopted and applied to (neutral) cesium only.
- Radiative potential: Flambaum and Ginges (2005) decompose this radiative potential into the terms

$$V^{\,(\text{total QED})} \;=\; V^{\,(\text{simplified Uehling})} \;+\; V^{\,(\text{magnetic form})} \;+\; V^{\,(\text{electric form})} \;+\; V^{\,(\text{low frequency})} \;+\; V^{\,(\text{simplified WK})}$$

and where the individual terms are explained above or below.

- Magnetic form-factor potential: For the magnetic form-factor contribution, Flambaum and Ginges (2005) give

$$V^{\,(\text{magnetic form})} \;=\; \frac{\alpha}{4\,\pi\, m}\, i\,\boldsymbol{\gamma}\cdot\boldsymbol{\nabla}\left[V(r)\left(\int_1^\infty dt\;\frac{\exp\left(-\,2m\,r\,t\right)}{t^2\,\sqrt{t^2\,-\,1}}\;-\;1\right)\right],$$

and where $\boldsymbol{\gamma} = (\gamma_1, \gamma_2, \gamma_3)$ is the vector of gamma matrices

- Low-frequency potential to the electric form-factor: Flambaum and Ginges (2005) suggest the (low-frequency) expression

$$V^{\,\text{(low frequency)}} \;=\; -\,\frac{B(Z)}{e}\, Z^4\, \alpha^5\, mc^2\, \exp\left(\frac{Z\,r}{a_{\text{Bohr}}}\right), \qquad\qquad B(Z) \;=\; 0.074 \,+\, 0.35\, Z\, \alpha,$$

and where the function $B(Z)$ has been fitted in order to reproduce the radiative energy shifts for $p$-levels of selected heavy elements. This term should be used with some care however.

- Electric form-factor potential (including high-frequency contributions): Flambaum and Ginges (2005) display a final expression for the electric form-factor contribution

$$V^{\,\text{(electric form)}} \;=\; -\,A(Z,r)\,\frac{\alpha}{\pi}\,V(r)\int_1^\infty dt\;\frac{\exp\left(-\,2m\,r\,t\right)}{\sqrt{t^2\,-\,1}}\;\left[\left(1\,-\,\frac{1}{2\,t^2}\right)\,\left[\ln(t^2\,-\,1)\,+\,4\,\ln(1/Z\alpha\,+\,0.5)\right]\,-\,\frac{3}{2}\,+\,\frac{1}{t^2}\right]\,.$$

Here, the function $A(Z,r) = (1.071 - 1.976\,x^2 - 2.128\,x^3 + 0.169\,x^4)\,m\,r\,/\,(m\,r + 0.07\,Z^2\,\alpha^2)$, and with $x = (Z - 80)\,\alpha$. The detailed form of $A(Z,r)$ was found by fitting the radiative shifts for the high Coulomb $s$ levels from the literature. This term should be used with good care again.

### 3.5.b. In JAC implemented QED estimates

## Models & applications:

- ➢ In JAC, the radiative QED corrections can be incorporated into the representation of the wave functions if `AsfSettings(..)` is initialized with `qedCI = true`. This boolean flag tells JAC to include both, the vacuum polarization and the (local) self-energy contributions directly into the Hamiltonian matrix.
- ➢ In JAC, two different models are supported for the QED estimates due to the value of the global variable `JAC_QED_MODEL = QedSydney` or `JAC_QED_MODEL = QedPetersburg`, respectively. This global variable can be redefined at any time by a call to `JAC.define()`.

## Implementation:

- ➢ QedPetersburg model: Here, we add to all matrix elements $\left\langle a \left\| \mathbb{h}^{(1-\text{particle})} \right\| b \right\rangle$ in the many-electron Hamiltonian matrix the (single-electron) matrix elements

  $$\left\langle a \left\| \mathbb{h}^{(\text{QED})} \right\| b \right\rangle \;=\; \left\langle a \left\| \mathbb{h}^{(\text{local SE})} \right\| b \right\rangle + \left\langle a \left\| \mathbb{h}^{(\text{simplified Uehling})} \right\| b \right\rangle$$

  t.
- ➢ QedSydney model: Analogues, here we add to all matrix elements $\left\langle a \left\| \mathbb{h}^{(1-\text{particle})} \right\| b \right\rangle$ in the many-electron Hamiltonian matrix the (single-electron) matrix elements

  $$\left\langle a \left\| \mathbb{h}^{(\text{QED})} \right\| b \right\rangle \;=\; \left\langle a \left\| \mathbb{h}^{(\text{magnetic form})} \right\| b \right\rangle + \left\langle a \left\| \mathbb{h}^{(\text{electric form})} \right\| b \right\rangle + \left\langle a \left\| \mathbb{h}^{(\text{low frequency})} \right\| b \right\rangle + \left\langle a \left\| \mathbb{h}^{(\text{simplified Uehling})} \right\| b \right\rangle .$$

- ➢ Effective QED operator With the definitions from above, the total QED operator for a many-electron atom includes of course a summation over all atomic electrons:

  $$\mathbb{H}^{(\text{QED})} \;=\; \mathbb{H}^{(\text{SE})} + \mathbb{H}^{(\text{VP})} \;=\; \sum_j \mathbb{h}_j^{(\text{QED})} \;=\; \sum_j \left( \mathbb{h}_j^{(\text{SE})} + \mathbb{h}_j^{(\text{VP})} \right)$$

  where the $\mathbb{h}_j^{(\text{SE})}$ and $\mathbb{h}_j^{(\text{VP})}$ refers to the one-electron operators for electron $j$.

# 3.6. Unitary $jjJ - LSJ$ transformation of atomic states

## 3.6.a. Transformation matrices from $jjJ$- to $LSJ$-coupling

### Atomic coupling schemes:

- Coupling schemes: Atomic and ionic levels are usually identified and labeled by means of quantum numbers of an appropriate coupling scheme, but which are well-conserved only for cases of pure coupling. $LSJ$- and $jjJ$coupling are nowadays the two most frequently applied coupling schemes in atomic theory.
- As usual in quantum mechanics, the transformation from one to another orthogonal basis (coupling scheme) is simply given by a unitary matrix, even if it is not always so easy to evaluate this matrix for arbitrary shell structures of atoms and ions.
- $LSJ$-notation: In atomic spectroscopy, the standard $LSJ$-notation of the levels is frequently applied for classifying the low-lying level structures of atoms or ions.
- Labeling of levels: Atomic energy levels are often labeled by the leading $LSJ$-coupled CSF in its wave function expansion. However, special care has to be taken if the same CSF occurs as largest CSF in the expansion of two levels, so that the classification is no longer unique.
- The lack of providing a proper spectroscopic notation in relativistic computations may hamper the spectroscopic level classification of medium and heavy elements as well as the interpretation and analysis of inner-shell processes.

### $jjJ - LSJ$ transformation of subshell states:

- Unique subshell order: Since each non-relativistic $n\ell$-shell (except for $ns$) is associated with two relativistic subshells with $j = \ell \pm 1/2$, the order of the subshell is relevant for the transformation of the many-electron basis and always fixed to $n\ell_{j=\ell-1/2}, n\ell_{j=\ell+1/2}$. For the $np$- and $nd$-shells, for example, we therefore use $np_{1/2}, np_{3/2}$ and $nd_{3/2}, nd_{5/2}$ in all formulas below.
- Non-relativistic subshell states: In the transformation of the non-relativistic shell states $\left| n\ell^N \, \alpha\nu \, LS \right\rangle$, we generally have the product of two (relativistic) subshell states $\left| n\overset{-}{\kappa}^{\overset{-}{N}} \, \overset{-}{\nu}\overset{-}{J},\, n\overset{+}{\kappa}^{\overset{+}{N}} \, \overset{+}{\nu}\overset{+}{J} \right\rangle$, and with $\overset{-}{N} + \overset{+}{N} = N$.

- The transformation between the (sub-) shell states in $jjJ$- and $LSJ$-coupling can be expressed with real Fourier coefficients as

$$\left| (n\overset{-}{\kappa}^{\overset{-}{N}}\, \overset{-}{\nu}\overset{-}{J},\; n\overset{+}{\kappa}^{\overset{+}{N}}\, \overset{+}{\nu}\overset{+}{J})\; J \right\rangle \;=\; \sum_{\alpha\nu\, LS} \left| n\ell^{N}\, \alpha\nu\, LSJ \right\rangle \left\langle n\ell^{N}\, \alpha\nu\, LSJ \,\middle|\, (n\overset{-}{\kappa}^{\overset{-}{N}}\, \overset{-}{\nu}\overset{-}{J},\; n\overset{+}{\kappa}^{\overset{+}{N}}\, \overset{+}{\nu}\overset{+}{J})\; J \right\rangle, \qquad N \;=\; \overset{-}{N} + \overset{+}{N}$$

$$\left\langle n\ell^{N}\, \alpha\nu\, LSJ \,\middle|\, (n\overset{-}{\kappa}^{\overset{-}{N}}\, \overset{-}{\nu}\overset{-}{J},\; n\overset{+}{\kappa}^{\overset{+}{N}}\, \overset{+}{\nu}\overset{+}{J})\; J \right\rangle \;=\; \left\langle (n\overset{-}{\kappa}^{\overset{-}{N}}\, \overset{-}{\nu}\overset{-}{J},\; n\overset{+}{\kappa}^{\overset{+}{N}}\, \overset{+}{\nu}\overset{+}{J})\; J \,\middle|\, n\ell^{N}\, \alpha\nu\, LSJ \right\rangle.$$

- The evaluation of the (unitary) transformation does generally not involve the radial (orbital) functions but depends only on the spin-angular functions.
- Although the notation of the non-relativistic and relativistic (sub-) shell states is quite similar in $LSJ$- and $jjJ$-coupling, these states generally belong to different irreducible representations of the $SO_3$ rotation group. This can be seen already from the splitting of each non-relativistic shell into two subshells as outlined above.

## Transformation of atomic states:

- $LSJ$-coupled, non-relativistic CSF:

$$\left|\gamma^{\,\rm (NR)}\, LSJ\right\rangle \;=\; \big|\big(\big(.\;\big(\big((n_1\ell_1^{N_1}\, \alpha_1\nu_1\, L_1S_1),\; (n_2\ell_2^{N_2}\, \alpha_2\nu_2\, L_2S_2)\big)\; L_{12}S_{12},\; (n_3\ell_3^{N_3}\, \alpha_3\nu_3\, L_3S_3)\big)\; L_{123}S_{123},\; ...\big)\; LS\big)\; J\,\big\rangle$$

- $jjJ$-coupled, relativistic CSF:

$$\left|\gamma^{\,\rm (R)}\, J\right\rangle \;=\; \left|\left(.\left(\left(\big((n_1\overset{-}{\kappa}_1^{\overset{-}{N}_1}\; \overset{-}{\nu}_1\overset{-}{J}_1),\; (n_1\overset{+}{\kappa}_1^{\overset{+}{N}_1}\; \overset{+}{\nu}_1\overset{+}{J}_1)\big)\; \overset{+}{X}_1,\; (n_2\overset{-}{\kappa}_2^{\overset{-}{N}_2}\; \overset{-}{\nu}_2\overset{-}{J}_2)\right)\; \overset{-}{X}_2,\; (n_2\overset{+}{\kappa}_2^{\overset{+}{N}_2}\; \overset{+}{\nu}_2\overset{+}{J}_2)\right)\; \overset{+}{X}_2,\; ...\right)\; J\; \right\rangle$$

- To determine the explicit transformation matrix for going from one to another (many-electron) basis, of course, all these quantum numbers above and their details play an important role in practice. In general, however, it is sufficient here to re-call that the $jj$-coupled CSF basis spans a (finite) part of the $N$-electron Hilbert space and that the matrix $\left(\left\langle\gamma^{\,\rm (NR)}\, LSJ \,|\, \gamma^{\,\rm (R)}\, J\right\rangle\right)$ just represent the (usual) Fourier coefficients for the expansion of an atomic state with respect to the basis $\left\{\left|\gamma^{\,\rm (NR)}\, LSJ\right\rangle\right\}$.
- Representation of atomic state functions:

$$|\psi_\alpha\rangle \;=\; \sum_r c_r^{\rm (R)}(\alpha)\, \left|\gamma_r^{\rm (R)}\, JP\right\rangle \;=\; \sum_t c_t^{\rm (NR)}(\alpha)\, \left|\gamma_t^{\rm (NR)}(L_tS_t)\, JP\right\rangle$$

- Formal construction of the $jjJ \;\to\; LSJ$ transformation matrix: If the $|\text{standard} - \text{jjJ}\rangle$ and $|\text{standard} - \text{LSJ}\rangle$ refer to the basis states of the (standard) product basis of the (subshell) states in $jjJ$- and $LSJ$-coupling, the transformation of a relativistic CSF can be formally written as

$$
\begin{aligned}
\left|\gamma_r^{(\mathrm{R})}\ \mathbb{J}\right\rangle \;&=\; \sum_{\text{standard}-\text{jj}} |\text{standard} - \text{jjJ}\rangle\ \langle \text{standard} - \text{jjJ}\,|\,\gamma_r\ JP\rangle \\
&=\; \sum_{\substack{\text{standard}-\text{jjJ}\\ \text{standard}-\text{LSJ}\\ \text{atomic}-\text{LSJ}}} \left|\gamma_t^{(\mathrm{NR})}(L_t,\, S_t)\ JP\right\rangle\ \left\langle\gamma_t^{(\mathrm{NR})}(L_t,\, S_t)\ JP\,|\,\text{standard} - \text{LSJ}\right\rangle \langle \text{standard} - \text{LSJ}\,|\,\text{standard} - \text{jjJ}\rangle\ \left\langle \text{standard} - \text{jjJ}\,|\,\gamma_r^{(\mathrm{R})}\ JP\right\rangle \\
&=\; \sum_{Q_p, Q_r} \left|\gamma_t^{(\mathrm{NR})}(L_t,\, S_t)\ \mathbb{J}\right\rangle\ \times\ [\text{LSJ} - \text{recoupling}]\ \times\ [\text{product of LSJ} - \text{jjJ matrix elements}]\ \times\ [\text{jjJ} - \text{recoupling}]
\end{aligned}
$$

In the last line, the summation runs over the (product basis) quantum numbers $Q_p \;=\; [(\alpha_1\nu_1\, L_1 S_1),\, (\alpha_2\nu_2\, L_2 S_2),\, ...]$ as well as over the (re-coupling) quantum numbers as defined by the [LSJ-recoupling] and [jjJ-recoupling] recoupling coefficients $Q_p \;=\; [J_1, J_2, J_{12},\, J_3, J_{123},\, ...,\, T_1, T_2, T_{12},\, T_3, T_{123},\, ...]$ with $\delta_{J_1,T_1}\ \delta_{J_2,T_2}\ \delta_{J_{12},T_{12}}\ ...\ .$

- Re-coupling from the $LSJ$-product to the $(L_t, S_t)J$-coupled basis:

$$
\begin{aligned}
&\left\langle\gamma_t^{(\mathrm{NR})}(L_t S_t)\ JP\,|\,\text{standard} - \text{LS}\right\rangle \;=\; [\text{LSJ} - \text{recoupling}] \\
&=\; \langle(.\,(.((L_1, L_2)\, L_{12},\, L_3)\, L_{123},\, ...)\ L_t,\, (.((S_1, S_2)\, S_{12},\, S_3)\, S_{123},\, ...)\ S_t\,)\ J\,|\,(.\,((\,(L_1, S_1)\, T_1,\, (L_2, S_2)\, T_2)\, T_{12},\, (L_3, S_3)\, T_3\,)\ T_{123},\, ...)\ J\rangle
\end{aligned}
$$

- Re-coupling from the $jjJ$-product to the $jXJ$-coupled basis:

$$
\begin{aligned}
&\left\langle \text{standard} - \text{jj}\,|\,\gamma_r^{(\mathrm{R})}\ JP\right\rangle \;=\; [\text{jjJ} - \text{recoupling}] \\
&=\; \left\langle\left(.\left(\left((\overset{-}{J}_1, \overset{+}{J}_1)\, J_1,\, (\overset{-}{J}_2, \overset{+}{J}_2)\, J_2\right)\ J_{12},\, (\overset{-}{J}_3, \overset{+}{J}_3)\, J_3\right),\, J_{123},\, ...\right)\ J\,|\,\left(.\left(\left(((\overset{-}{J}_1, \overset{+}{J}_1)\, \overset{+}{X}_1,\, \overset{-}{J}_2)\, \overset{-}{X}_2,\, \overset{+}{J}_2\right)\, \overset{+}{X}_2,\, \overset{-}{J}_3\right)\, \overset{-}{X}_3,\, ...\right)\ J\right\rangle
\end{aligned}
$$

## 3.6.b. Re-coupling coefficients

### Single open shell:

- Re-coupling from the $LSJ$-product to the $(L_t, S_t)J$-coupled basis:

$$[\mathrm{LSJ-recoupling}] \;=\; \langle (L_1, S_1)\, J \,|\, (L_1, S_1)\, J \rangle \;=\; 1$$

- Re-coupling from the $jjJ$-product to the $jXJ$-coupled basis:

$$[\mathrm{jjJ-recoupling}] \;=\; \left\langle (\overset{-}{J}_1, \overset{+}{J}_1)\, J \,|\, (\overset{-}{J}_1, \overset{+}{J}_1)\, J \right\rangle \;=\; 1$$

### Two open shells:

- Re-coupling from the $LSJ$-product to the $(L_t, S_t)J$-coupled basis:

$$[\mathrm{LSJ-recoupling}] \;=\; \langle ((L_1, L_2)\, L_t,\, (S_1, S_2)\, S_t)\, J \,|\, ((L_1, S_1)\, T_1,\, (L_2, S_2)\, T_2)\, J \rangle\,, \qquad Q_r \;=\; [T_1, T_2]$$

- Re-coupling from the $jjJ$-product to the $jXJ$-coupled basis:

$$[\mathrm{jjJ-recoupling}] \;=\; \left\langle \left( (\overset{-}{J}_1, \overset{+}{J}_1)\, J_1,\, (\overset{-}{J}_2, \overset{+}{J}_2)\, J_2 \right) J \,|\, \left( ((\overset{-}{J}_1, \overset{+}{J}_1)\, \overset{+}{X}_1,\, \overset{-}{J}_2),\, \overset{-}{X}_2,\, \overset{+}{J}_2 \right) J \right\rangle, \qquad Q_r \;=\; [J_1, J_2]$$

## 3.6.c. In JAC implemented $jjJ - LSJ$ transformation

### Transformation, notations & application:

- Representation $c_s^{(\mathrm{NR})}(\alpha)$ of atomic states.

$$|\psi_\alpha\rangle \;=\; \sum_t c_t^{(\mathrm{NR})}(\alpha) \left| \gamma_t^{(\mathrm{NR})} LS\, J \right\rangle \;=\; \sum_r c_r^{(\mathrm{R})}(\alpha) \left| \gamma_r^{(\mathrm{R})}\, J \right\rangle$$

- Unique label: $\left( \ldots \left( (n_1\ell_1)^{N_1}\;\; {}^{2S_1+1}L_1;\; (n_2\ell_2)^{N_2}\;\; {}^{2S_2+1}L_2 \right)\; {}^{2S_{12}+1}L_{12},\; (n_3\ell_3)^{N_3}\;\; {}^{2S_3+1}L_3 \ldots \right)\; {}^{2S+1}L_J$
  Such a label is assigned to each selected level, for instance, ...
- At present, no $jjJ - LSJ$ transformation has been implemented yet.
- A proper $LSJ$ spectroscopic notation has been found useful also in order to explain the excitation and decay properties of individual levels, at least qualitatively.
- In JAC, the $jj - LS$ transformation is performed for all selected levels if `calcLS = true` is set in `AsfSettings()`.
- In JAC, a proper $LSJ$-coupled label is printed by default whenever the (many-electron) Hamiltonian matrix has been (re-) diagonalized before.

## Implementation of $jjJ - LSJ$ transformation:

- Internally, a $jj - LS$ transformation of selected levels from a given mutliplet is carried out by the following steps:

1 Generate all non-relativistic configurations that contribute to the given multiplet.

2 Generate a unique non-relativistic shell sequence; terminate with an error message if the relativistic subshells of the given multiplet are ordered in *non-standard order*, for example, ..., $2p_{3/2}$, $2p_{1/2}$, ... or similar.

3 Calculate either the complete or some proper parts of the $jjJ - LSJ$ transformation matrix.

4 Calculate for each transformation matrix element the recoupling coefficients; at present, only a number of rather simple recoupling coefficients are implemented explicitly.

```
"""
`struct  LS_jj_qn`  ... defines a struct for the generalized quantum numbers (qn) of a LS_jj matrix element.
    + NN           ::Int32    ... occupation w = NN
    + QQ           ::Int32    ... subshell total quasispin 2*Q = nu
    + LL           ::Int32    ... subshell total angular momentum 2*L
    + SS           ::Int32    ... subshell total angular momentum 2*S
    + JJ           ::Int32    ... subshell total angular momentum 2*J
```

```
      + Nm          ::Int32    ... subshell Nm
      + Qm          ::Int32    ... subshell quantum number 2*Qm = nu^-
      + Jm          ::Int32    ... subshell quantum number 2*Jm
      + Qp          ::Int32    ... subshell quantum number 2*Qp = nu^+
      + Jp          ::Int32    ... subshell quantum number 2*Jp
  """
```

# 3.7. Atomic interaction amplitudes

## Concept of interaction amplitudes:

- Hamiltonian matrix: The (scalar) Hamiltonian matrix elements in section **??** below describe the interaction energy between two ASF $|\alpha \mathbb{J} M\rangle$ and $|\alpha' \mathbb{J}' M'\rangle$ , and these Hamiltonian matrix elements are perhaps the most simplest (many-electron) interaction amplitudes in atomic structure theory: $\langle \psi_\alpha \,|\, \mathbb{H} \,|\, \psi_{\alpha'} \rangle = \langle \alpha\, \mathbb{J} M \,\|\, \mathbb{H} \,\|\, \alpha' \mathbb{J}' M' \rangle = \sum_{rs} c^*_r(\alpha)\, H_{rs}\, c_s(\alpha')\, \delta_{JJ'}\, \delta_{MM'}\, \delta_{PP'}$ .

- In relativistic atomic structure theory, in particular, $E_\alpha = \left\langle \alpha\, \mathbb{J} \right\| \mathbb{H}^{(\mathrm{DCB})} \left\| \alpha \mathbb{J} \right\rangle \approx \left\langle \alpha\, \mathbb{J} \right\| \mathbb{H}^{(\mathrm{DC})} \left\| \alpha \mathbb{J} \right\rangle$ is the total energy of a given level $|\alpha \mathbb{J}\rangle$ .

- Many-electron interaction amplitudes: Using time-dependent perturbation theory and Fermi's Golden rule, most atomic level and transition properties can be expressed rather similarly as matrix elements of a (so-called) transition or *interaction* operator $\mathbb{T}$ :

$$\langle \psi_\alpha \,|\, \mathbb{T} \,|\, \psi_\beta \rangle \;=\; \sum_{rs} c^*_r(\alpha)\, T_{rs}\, c_s(\beta)\,.$$

- Reduced matrix elements: More often than not, the transition operator $\mathbb{T}$ can be expressed in terms of spherical tensor operators of rank $K$, and, perhaps, with magnetic projections $Q = -K, -K+1, ..., K$, respectively. These spherical tensor operators transform under rotations like the spherical harmonics $Y_{KQ}(\vartheta, \varphi)$: $\mathbb{T} = \sum_{KQ} a(K,Q)\, \mathbb{T}^{(K)}_Q$. – Instead of the complete matrix elements, that include the magnetic projections $M$ of the given atomic or configuration states as well as of the tensor operators, one often makes then use of the reduced matrix elements by applying the Wigner-Eckart theorem:

$$T^{(K)}_{Q,\,rs} \;\equiv\; \left\langle \alpha_r\, \mathbb{J}_r M_r \,\middle|\, \mathbb{T}^{(K)}_Q \,\middle|\, \alpha_s\, \mathbb{J}_s M_s \right\rangle \;=\; \langle J_r M_r,\, KQ \,|\, J_s M_s \rangle \;\left\langle \alpha_r\, \mathbb{J}_r \right\| \mathbb{T}^{(K)} \left\| \alpha_s\, \mathbb{J}_s \right\rangle\,.$$

- Although these reduced transition amplitudes are frequently utilized in the literature, for instance in order to discuss and analyze various atomic processes, not many codes make explicit use of these amplitudes as the *natural* building blocks for describing the level structure and properties of (open-shell) atoms and ions. – More often than not, a prior decomposition of these transition amplitudes into various types of one- and two-particle (reduced) matrix elements or even directly into radial integrals is made well before any implementation or coding is considered. This prior decompositon has seriously hampered the modelling of complex processes and is still the reason, why most atomic structure codes support the computation of just a few properties, cross sections and rates.

- Indeed, the different techniques, which are employed in the decomposition of the many-electron amplitudes, as well as the large number of definitions (and notations) of angular- or radial-type integrals in the literature has hampered not only the comparison of different codes during the last decades but made it difficult also to (re-) use these entities for other properties than those considered by the original program developers.
- In JAC, we attempt to overcome this situation and to make consequent use of the many-electron amplitudes $\left\langle \alpha_r \, \mathbb{J}_r M_r \left| \mathbb{T}^{(K)}_Q \right| \alpha_s \, \mathbb{J}_s M_s \right\rangle$ and/or $\left\langle \alpha_r \, \mathbb{J}_r \left\| \mathbb{T}^{(K)} \right\| \alpha_s \, \mathbb{J}_s \right\rangle$ as the central building blocks for describing the interaction among the electrons as well as with external particles and fields.
- The concept of these interaction amplitudes has helped to simplify and maintain the code. — Moreover, it (will hopefully) enable us to exploit the many-electron interaction and transition amplitudes also in second- and higher-order processes, once an appropriate (intermediate) basis $\{\psi_\nu(PJM) \equiv |\alpha_\nu \, \mathbb{J}_\nu M_\nu\rangle \,, \;\; \nu = 1, ..., n_\nu\}$ has been constructed for modelling some given process.

## Reduced matrix elements of spherical tensor operators for two CSF:

- For two CSF of well-defined symmetry, the reduced matrix elements of spherical tensor operators take always the form

$$\left\langle \gamma_r P_r J_r \left\| \, \mathbb{T}^{(K)} \right\| \gamma_s P_s J_s \right\rangle \;=\; \sum_t u(a_t b_t; K) \, X(a_t b_t; K), \qquad \mathbb{T}^{(K)} \;=\; \sum_j \mathbb{t}^{(K)}(j; \, ...) \qquad \text{... one part. operators}$$

$$\left\langle \gamma_r P_r J_r \left\| \, \mathbb{T}^{(K)} \right\| \gamma_s P_s J_s \right\rangle \;=\; \sum_t v(L_t; \; a_t b_t c_t d_t; K) \, X^{L_t}(a_t b_t c_t d_t; K), \qquad \mathbb{T}^{(K)} \;=\; \sum_{i<j} \mathbb{T}^{(K)}(i, j; \, ...) \qquad \text{... symmetric two part. operators,}$$

  and where $X(a_t b_t; K)$ and $X^{L_t}(a_t b_t c_t d_t; K)$ are one- and two-particle (effective) interaction strengths, cf. section 3.1. These interaction strengths are specific to the particular transition or interaction operator under consideration, and special care has to be taken that the same phase convention applies, if different interaction amplitudes are to be combined with each other.
- In practice, there are two steps in the computation of the transition amplitudes above for any pair of CSF, which need to be performed separately: The (pure) angular coefficients are usually calculated by means of some proper program, for instance ANCO (Gaigalas *et al.*,

2001), for either a pair or a whole set of CSF, and all the non-vanishing coefficients are then returned together to the calling routine. For these coefficients, the associated one- or two-particle interaction strengths are evaluated and summed up to form the requested matrix element $T_{rs}$ of the transition matrix.

- To decrease the computational effort, these (one- and two-particle) interaction strength are often also *stored* and *re-utilized* in various applications, a feature which has not yet been considered in JAC.
- A similar decomposition of the many-electron matrix elements (amplitudes) as for the Hamiltonian matrix elements into a sum of *angular coefficient* × *interaction strength* can be made for every physically relevant (interaction) amplitude, independent of the particular rank of the corresponding interaction operator. Since most atomic processes can be traced back to just a (very) few of such interaction or transition amplitudes, we made use of them as the *building blocks* in the design and implementation of the JAC tools.

## Electron-electron interaction:

- The interaction among the electrons is described by the scalar operator that occurs in the Dirac-Coulomb-Breit Hamiltonian; cf. section 3.1

$$\mathbb{V}^{\,(\mathrm{e-e})} \;=\; \mathbb{V}^{\,(\mathrm{Coulomb})} + \mathbb{V}^{\,(\mathrm{Breit})} \;=\; \sum_{i<j} \left( \frac{1}{r_{ij}} + b_{ij} \right) .$$

- The Dirac-Coulomb-Breit Hamiltonian gives rise to the (reduced) interaction amplitudes

$$\left\langle \gamma_r P_r J_r \left\| \mathbb{V}^{\,(\mathrm{e-e})} \right\| \gamma_s P_s J_s \right\rangle \;=\; \left\langle \gamma_r P_r J_r \left\| \mathbb{V}^{\,(\mathrm{Coulomb})} \right\| \gamma_s P_s J_s \right\rangle \;+\; \left\langle \gamma_r P_r J_r \left\| \mathbb{V}^{\,(\mathrm{Breit})} \right\| \gamma_s P_s J_s \right\rangle .$$

For scalar operators, the full and reduced matrix elements coincide with each other and need not to be distinguished, since the Clebsch-Gordan coefficient in the Wigner-Eckert theorem then simply evaluates to $\langle J_r M_r, 00 \,|\, J_s M_s \rangle \;=\; \delta_{J_r J_s}\, \delta_{M_r M_s}$ for $K = Q = 0$.

- Since the Coulomb and Breit interaction operators are both scalar operators and since they contribute *additively* to the total electron-electron interaction, the same (pure) angular coefficients $v(L_t;\, a_t b_t\; c_t d_t; K = 0)$ occur in the decompsition of the amplitudes above, although different angular and parity selection rules apply for the various interaction strengths themselve, cf. section 3.1. In the computation of these amplitudes, the Breit interaction can therefore be added quite easily to the (usual) instantaneous Coulomb repulsion, if this appears appropriate for some particular process:

$$X^{(L)}(abcd) \;=\; X^{\,(\mathrm{L,\,Coulomb})}(abcd) \;+\; X^{\,(\mathrm{L,\,Breit})}(abcd)\,.$$

- The electron-electron interaction amplitudes above are indeed utilized (and calculated) in many components of the JAC tools.

## Electron-photon interaction:

- The (relativistic) interaction of an electron with the radiation field is central for describing all photo-excition, ionization, emission and capture processes.
- The electron-photon interaction is described by the one-particle operator: $\mathcal{R}_\lambda(\mathbf{k}) = \sum_i \boldsymbol{\alpha}_i \cdot \mathcal{A}_{\lambda,i}(\mathbf{k})$ ; cf. chapter 4 below.

## Electron-nucleus (hyperfine) interactions:

- For a nuclear spin $I > 0$, the hyperfine interaction describes the interplay of each atomic electron with the electric and magnetic (multipole) fields of the nucleus, apart from the dominant (electric-monopole) field of the nuclues due to its nuclear charge $Ze$.
- The two dominant contributions to the hyperfine interaction arise from the nuclear magnetic-dipole field $\mathbf{A} = \frac{\boldsymbol{\mu} \times \mathbf{r}}{r^3}$ and the electric-quadrupole field $\Phi(r) = \sum_{ij} \frac{r_i\, r_j}{2r^5} Q_{ij}$, while all higher magnetic and electric multipole fields, that may in principle occur for nuclei with spin $I > 1$, are typically negligible.

## 3.8. Atomic density operators

### Motivation

- Density matrix formalism: In this formalism, the state of a physical system is characterized by means of statistical operators $\rho$ which describe a single system or an ensemble of equally prepared collision systems in either a pure quantum state or in a mixture of different states with any given degree of coherence.
- The great benefit of using the (atomic) density matrix theory is that it enables one to “accompany” such an ensemble through one or several steps of excitation, decay and/or collision process, and without loss of quantum-mechanical information.
- Transition operators $R$ of the density-matrix elements If one starts from a well-specified initial state of the system, as described by the operator $\rho_i$, all information about the atomic interactions, that govern the process, simply resides in the (so-called) *transition operators* $R$, and the final state operator just follows from the well-known relation: $\rho_f \;=\; R\,\rho_i\,R^+$.
- Building blocks: The electron-photon, electron-electron interaction and electron-nucleus interaction amplitudes from above are the building blocks to form the (scattering or) transition matrix for all atomic processes of interest and, hence, the density matrices of the system at the various steps of some particular excitation or decay process.
- For scattering states with a single electron in the continuum, these interaction amplitudes can be readily calculated by means of the JAC tools.
- Apart from the efficient computation of these building blocks, one also requires a simple book-keeping of these amplitudes in order to set-up the (atomic) density matrices at the various steps. To facilitate this handling and the book-keeping of these amplitudes, they are typically provided in JAC by some (amplitude) array, and together with all quantum numbers that are needed for their unique classification.
- The prior computation of the many-electron amplitudes enables one to start directly from the amplitudes (for one or several elementary processes) and to combine them into an appropriate form, in order to support the prediction of different atomic properties and parameters.
- Set-up of the density matrix: In practice, the computation of all interaction amplitudes is performed within three steps: (i) the generation of all necessary bound-state wave functions, (ii) the evaluation of the transition amplitudes between bound states and scattering states in the continuum, and (iii) the set-up and handling of the density matrices, i.e. by applying the formulas from chapter 7.

## Density operator of an atom in level $|\alpha \mathbb{J}\rangle$ :

- Mixed states of a level $|\alpha \mathbb{J}\rangle$ : For an atom in a well-defined and isolated level $(\alpha \mathbb{J})$ , a general mixed state with regard to its magnetic subspace (i.e. its projections $M$) can always be written as

$$\hat{\rho} \;=\; \sum_{MM'} c_{MM'} \; |\alpha\, \mathbb{J} M\rangle \, \langle \alpha\, \mathbb{J} M'| \, .$$

- Statistical tensor: Often, it is most convenient to represent the intermediate state of the ions in terms of its so-called statistical tensors

$$\rho_{kq}(\alpha \mathbb{J}) \;=\; \sum_{MM'} (-1)^{J-M'} \; \langle JM,\, J\,(-M') \,|\, kq\rangle \; \langle \alpha\, JM \,|\, \rho \,|\, \alpha\, \mathbb{J} M'\rangle \; .$$

  and which are non-zero only for $0 \;\leq\; k \;\leq\; 2\,J$ and $-k \;\leq\; q \;\leq\; k$. These statistical tensors transform like the spherical harmonics.

- Although both, the (reduced, mixed) density matrix and the statistical tensors of some level $(\alpha \mathbb{J})$ are mathematically equivalent, the latter form can be transformed more easily and analogue to the spherical harmonics of rank $k$ under a rotation of the coordinates.

- (Initial) polarization state of an atom: The polarization state of the initial atom can be characterized by the statistical tensors $\rho_{kq}^{\mathbf{n}_t}(\alpha_i \mathbb{J}_i)$ , if defined with regard to the axis of the (target) polarization $\mathbf{n}_t \;=\; (\vartheta_t, \varphi_t)$ . While the odd-rank tensors $k \;=\; 1,\, 3,\, ...$ are known to characterize the orientation of the target atom, the even-rank tensors $k \;=\; 2,\, 4,\, ...$ describe its alignment. The maximal rank of these tensors is limited by the condition $k \;\leq\; 2\,J$.

# 3.9. Parity- and time-violating atomic interactions

## 3.9.a. Interactions beyond the standard model

## Standard electro-weak model:

- The success of the standard electro-weak model of elementary particles is indeed extraordinary. It has been tested by many physical processes that cover more than ten orders of magnitude in momentum transfer. The standard model also correctly predicted the existence of new particles, such as the neutral $Z$ boson.

- The standard model is sometimes understood also as a low-energy manifestation of a more complete theory that, perhaps, unifies the four forces. Many well-motivated extensions to the standard model have been proposed, such as supersymmetric, technicolour and left-right symmetric models, and they often predictr physical phenomena quite different from those of the standard model.
- CP symmetry: This symmetry refers to the combined symmetry of charge conjugation C and parity P.
- Violation of CP symmetry: The violation of CP symmetry was first discovered in 1964 in decays of the neutral K mesons, and this violation is taken into account by the standard electro-weak model by just a single complex phase in the quark-mixing matrix (the so-called Kobayashi-Maskawa mechanism).
- Various extensions of the standard model, such as supersymmetry, predict considerably larger EDM of the particles. Any observation of these EDM would therefore lead unambiguously to a hint of *new physics*.
- In addition, the standard model of particle physics is sometimes said to violate time-reversal (T) invariance, but again only through just a single phase in the Cabibbo-Kobayashi-Maskawa matrix, that mixes the quark flavors.
- For a rather long time, K mesons remained the only system in which CP-violation wwere observed explicitly. In 2001, however, the BaBar and Belle collaborations detected CP violation also for neutral B mesons, although this is still consistent with the predictions of the standard model.
- CPT symmetry: The (mathematical) structure of most gauge theories suggest that the combined symmetry of charge conjugation $C$, parity change $P$ and time-reversal violation $T$ has to be conserved.
- If CPT is *conserved*, as suggested by gauge theories, then CP-violation must be strictly accompanied by T (time-reversal) violation. Until the present, however, there has been no (undisputed) direct observation of T violation and its detection is of fundamental interest by itself. A direct detection of T-violation may shed further light also on the origin of CP-violation.
- Permanent electric dipole moment (EDM) The measurement of a per of neutrons, atoms, or molecule would show explicit evidence of T-violation.
- New physics: theories in physics beyond the standard model predict new sources of T-violation and these sources may lead to EDM that are many orders of magnitude larger than those from the standard model. This may allow EDM measurements by means of current experiments. Already the parameter space of quite popular extensions of the standard model, such as such as supersymmetry, multi-Higgs models, and left-right symmetric models, are strongly restricted by current measurements.
- Schiff theorem: If an external electric field acts upon a neutral atom, that consists out of non-relativistic point-like charged particles with some EDM and that only interact via electrostatic forces with each other, the field is screened exactly at each particle. This screening

arises due to the polarization of the atomic electrons by the external field. Therefore, an external electric field cannot induce an atomic EDM. As shown by Schiff, however, this schielding is incomplete if magnetic or finite-size effects are taken into account, and this may give rise in principle to an atomic EDM.

## High-precision measurements on fundamental symmetries of atoms:

- ➢ Atomic high-precision experiments: High-precision measurements on the (violation of fundamental) symmetries in atoms are suitable to test the standard model of elementary particles and to search for new physics beyond it. Such precision experiments in atomic physics complement measurements in high-energy physics.
- ➢ Indeed, atomic experiments have played an important role in the verification of the standard model for more than 30 years ago already. While the first evidence for neutral-weak currents, i.e. the existence of the neutral Z boson, was discovered in neutrino scattering, a parity violation was first established in atomic experiments, and before it was later observed also in high-energy electron scattering.
- ➢ Today, atomic physics plays a major role in the search for *new* physics beyond the standard model.
- ➢ PNC measurements for cesium: For example, the cesium measurement on parity non-conservation in atomic physics have been found in excellent agreement with the standard model.

### 3.9.b. Parity-violating (P-odd, T-even) interactions

## Motivation:

- ➢ Parity non-conservation (PNC) effects: These effects arise in atoms largely due to the exchange of $Z^0$-bosons between the atomic electrons and the nucleus.
- ➢ The exchange of $Z^0$ bosons is formally described by the Weinberg-Salam theory and leads to (observable) phenomena, such as circular dichroism and optical rotation, and which have been investigated in order to detect P-violation in cesium, thallium, bismut and plumbum.
- ➢ There is also another contribution to atomic parity violation due to the exchange of $Z^0$ bosons between each pair of electrons; however, this effect is negligibly small for heavy atoms and well suppressed by a factor $10^{-3} \dots 10^{-4}$. This contribution is usually neglected in most PNC studies.
- ➢ PNC effects in atoms can be caused also by nuclear moments, i.e. by parity-violating electromagnetic form factors that occur in addition to the usual nuclear magnetic-dipole and electric-quadrupole moments (form factors).

- Rare-earth atoms: Several PNC experiments in rare-earth atoms have been suggested for close-lying levels of opposite parity in order to enhance the PNC effects. Moreover, rare-earth often have various stable isotopes and, hence, the dependence on atomic theory can be removed by taking ratios of the measured PNC contributions for different isotopes.

## Nuclear-spin independent P-odd electron-nucleus interactions:

- Nuclear-spin independent Hamiltonian: For non-relativistic nucleons, the nuclear-spin independent Hamiltonian for the P-odd electron-nucleus interaction is given by the effective single-electron operator

$$\mathbb{H}^{(\text{weak}-\text{charge})} \;=\; -\frac{G}{\sqrt{2}}\,\gamma_5\,\left[Z\,C_{1p}\,\rho_p(r)\;+\;N\,C_{1n}\,\rho_n(r)\right]\,,$$

where $Z$ and $N$ are the number of protons and neutrons, and where the proton and neutron densities are normalized to unity, $\int dr\;\rho_p(r) \;=\; 1 \;=\; \int dr\;\rho_n(r)$.

- If the proton and neutron densities coincide, $\rho_p \;=\; \rho_n \;\equiv\; \rho$, the nuclear-spin independent Hamiltonian simplifies and can be described in terms of a nuclear weak-charge $Q_W$,

$$\mathbb{H}^{(\text{weak}-\text{charge})} \;=\; -\frac{G}{2\sqrt{2}}\,\gamma_5\,Q_W\,\rho\,.$$

- Nuclear weak charge $Q_W$: This charge is very close to the neutron number and is in lowest order in the electro-weak interaction given by

$$Q_W \;=\; -N + Z\,(1 - 4\sin^2\theta_W) \;\approx\; -N\,.$$

This value for $Q_W$ is modified however by radiative corrections.

- The nuclear-spin independent electron-neutron interaction is a scalar that mixes levels (states) with the same total electron angular momentum but different parity.
- For heavy atoms, the nuclear-spin independent interaction due to the nuclear weak-charge gives the dominat contribution to parity violation, when compared to other mechanisms.

## Nuclear-spin dependent P-odd electron-nucleus interactions:

- P-odd interactions that depend on the nuclear spin $I$: There are different interactions that depend on the nuclear spin $I$ due to: i) the neutral weak current; ii) hyperfine-induced neutral currents; or iii) the nuclear anapole moment.
- Interaction with the nuclear anapole: The anapole moment gives typically the dominant nuclear-spin dependent P-odd electron-nucleus interaction. The nuclear anapole moment arises from P-odd interactions inside the nucleus. These interactions manifest themselve in atoms through a slightly modified electro-magnetic interaction of the nucleus with atomic electrons.
- The anapole moment $\kappa_a$ increases with the atomic mass number, $\kappa_a \propto A^{2/3}$ and, thus, dominates in heavy atoms, when compared to other nuclear-spin dependent mechanisms listed above.

- Hamiltonian for the electron-anapole (-moment) interaction: For an external nucleon with orbital angular momentum $\ell$, the Hamiltonian is given by (Dzuba *et al.*, 2009)

$$\mathbb{H}^{(\text{anapole})} = \frac{G}{\sqrt{2}} \kappa_a \frac{K}{I(I+1)} \alpha \cdot \mathbf{I} \, \rho(r), \qquad K = (I+1/2)\,(-1)^{I+1/2-\ell}.$$

## Anapole moment:

- The notion of the anapole moment was introduced by Zel'dovich just after the discovery of parity violation.
- However, an nuclear anapole moment was unambiguously detected only 30 years later. In 1997, a group at Boulder measured a nuclear anapole moment in $^{133}$Cs to an accuracy of 14 % in an atomic experiment. This is considered as the first observation of an electromagnetic moment that violates fundamental discrete symmetries (Ginges and Flambaum, 2003).
- A P-odd, T-even anapole moment of the nucleus arises due to the presence of a parity violating weak interaction between nucleons.
- The anapole moment is directed along the nuclear spin $\mathbf{I}$: $\langle \mathbf{a} \rangle = -\pi \, \langle r^2 \, \mathbf{j} \rangle = a \, \mathbf{I}/I$ . Since the current vector $\mathbf{j}$ changes its sign under reflection of coordinates, but not the spin $\mathbf{I}$, an anapole moment need to violate parity but not time-reversal symmetry.

## 3.9.c. Time-reversal violating (P-odd, T-odd) interactions

### Motivation:

- Time-reversal symmetry: Many physical systems and processes are asymmetric under time-reversal. In classical mechanics, for example, a velocity reverses its direction under time reversal, $v \rightarrow -v$, while an acceleration does not. This time-reversal asymmetry is often associated with some energy dissipation and, hence, with the second law of thermodynamics. Without dissipation, the laws of mechanics are usually considered to be invariant with regard to time-reversal.
- In nuclei, P-odd and T-odd nuclear moments can arise due to an intrinsic EDM of the nucleons, or due to P-odd and T-odd nuclear forces. The P-odd and T-odd nuclear forces induce larger nuclear moments than a single nucleon EDM.
- Various P-odd and T-odd interactions can be considered, especially for heavy atoms and ions. These interaction include the tensor-pseudotensor electron-nucleon (e-N) interaction, the scalar-pseudoscalar (e-N) interaction, the nuclear Schiff moment and the interaction of the electron EDM with the internal nuclear magnetic field of the atom.
- An atomic EDM can be induced if the nucleus possesses P-odd and T-odd nuclear moments.

### P-odd & T-odd Hamiltonians due to electron-nucleus interactions:

- The expressions for $\mathbb{H}^{(\rm scalar-pseudoscalar)}$ and $\mathbb{H}^{(\rm weak\ charge)}$ as well as $\mathbb{H}^{(\rm I-independent)}$ are quite similar.
- These electron-nucleus interactions mixes atomic states of opposite parity and induces a static electric-dipole moments in atoms.

### P-odd & T-odd nuclear moments:

- The operators $\mathbb{H}^{(\rm scalar-pseudoscalar)}$ and $\mathbb{H}^{(\rm tensor)}$ have both electronic and nuclear components. While these Hamiltonians are overall scalar, the electronic and nuclear operators can be of any (equal) rank. To obtain any non-zero matrix element, therefore, the triangle rule for coupling of angular momenta imposes restrictions on the angular momenta of the electron and nuclear states.
- Nuclear moments that violate parity and time-reversal invariance: electric dipole, magnetic quadrupole, electric octupole. For an nuclear electric-dipole moment, the Hamiltonian must be of the form $\mathbb{H}^{(\rm Schiff\ moment)}$ in order to mix electron states of opposite parity.
- Nuclear electric-dipole (Schiff) moments: If $\mathbf{S}$ is nuclear Schiff moment, the associated P-odd and T-odd Hamiltonian is given by

$$\mathbb{H}^{(\rm Schiff-moment)} \;=\; -e\,\phi^{(\rm Schiff-moment)} \;=\; -4\pi e\,\mathbf{S}\cdot\nabla\,\delta(r).$$

Here $\phi^{(\rm Schiff-moment)}$ is the electrostatic potential of the nucleus that corresponds to a P-odd and T-odd charge distribution.

- Nuclear magnetic-quadrupole moments (MQM): A general expression for the nuclear MQM can be constructed in terms of the total angular momentum of the system $I$,

$$M_{ij} \;=\; -e\,\frac{3}{2}\,\frac{M}{I(2I-1)}\,\left[I_i I_j + I_j I_i - \frac{2}{3}\,I(I+1)\delta_{ij}\right].$$

  The quantity $M$ is conventionally referred to as the nuclear MQM and is defined as the maximum projection of $M_{ij}$ upon the nuclear axis, $M = M_{zz}$. The magnetic quadrupole moment violates parity and time-reversal invariance.

## 3.9.d. Time-reversal violating atomic electric-dipole moments

### Motivation:

- A non-zero electric-dipole moment (EDM) of atoms require P-odd and T-odd interactions, either among the nucleons or the electrons and the nucleus.
- Therefore, the null measurements of EDM in atoms place severe restrictions upon new sources of CP-violation that often arise in models beyond the standard model, such as supersymmetry.
- The nuclear EDM exceeds the EDM of single nucleons by one to two orders of magnitude. P-odd and T-odd nuclear forces generate all P-odd and T-odd nuclear moments, such as the Schiff and MQM moments. These nuclear moments can be 10-to-100 times larger than those generated by the presence of a nucleon EDM.
- In the standard model, an atomic EDM is suppressed by many orders when compared to predictions from (so-called) *new* theories. Therefore, the detection of an EDM would be unambiguous evidence of new physics, even if it contributes only weakly to a very small signal in atomic parity violation.
- An atomic EDM can arise from various P-odd and T-odd mechanisms (Ginges and Flambaum, 2004): i) an intrinsic EDM of an electron; (ii) a P-odd and T-odd electron-nucleon interaction; (iii) an intrinsic EDM of an external nucleon; (iv) a P-odd and T-odd nucleon-nucleon interaction.
- Until the present, no permanent EDMs in neutrons, atoms or molecules have been detected.
- The best limits on the electron electric dipole moment is presently derived from measurements of atomic EDM.

## Physics of the atomic EDM:

- An atomic EDM is associated with an atomic level $|\alpha \mathbb{J}\rangle$ and arises due to the admixture of levels (states) $|\nu \mathbb{J}_\nu\rangle$ with opposite-parity wave functions. This atomic EDM has the form

  $$\mathbb{d}^{\,\text{(atomic EDM)}} \;=\; 2 \sum_\nu \frac{\langle \alpha \mathbb{J} \,|\mathbb{D}|\, \nu \mathbb{J}_\nu \rangle \, \left\langle \nu \mathbb{J}_\nu \left| \mathbb{H}^{\,\text{(PT)}} \right| \alpha \mathbb{J} \right\rangle}{E_\alpha \,-\, E_\nu} \;=\; d^{\,\text{(atomic EDM)}} \, \frac{\mathbf{F}}{F}\,,$$

  where $\mathbb{D}$ is the electric dipole operator, $\mathbb{H}^{\,\text{(PT)}}$ the P-odd and T-odd operator that mixes $|\alpha \mathbb{J}\rangle$ with the set of wave functions $|\alpha_\nu \mathbb{J}_\nu\rangle$ , and $F$ is the total angular momentum of the atom corresponding to the state $|\alpha \mathbb{J}\rangle$ .
- A typical EDM experiment is performed in parallel electric and magnetic fields and can be described by the Hamiltonian

  $$\mathbb{H}^{\,\text{(em field)}} \;=\; -\mu \cdot \mathbf{B} \,-\, \mathbf{d} \cdot \mathbf{E}.$$

- A linear Stark shift is measured by observing the change in frequency when the electric field is reversed, since it is sensitive to the P-odd and T-odd term $\mathbf{E} \cdot \mathbf{B}$.
- Measurements of EDMs in paramagnetic atoms, i.e. for a total electron angular momentum $J \neq 0$ , are most sensitive to leptonic sources of P- and T-violation, and especially the electron EDM.
- In contrast, measurements of EDM in diamagnetic systems with zero total electron angular momentum are most sensitive to P-odd and T-odd mechanisms in the hadronic sector.

# 4. Atomic interactions with the radiation field

## 4.1. Wave equations & optical fields

### 4.1.a. Homogeneous wave equation

**General solutions:**

- Monochromatic plane-wave light: Monochromatic plane-wave light is uniquely determined by either the electric ($\mathbf{E}$) or magnetic ($\mathbf{B}$) field. Without restriction, we here consider a plane-wave along $\mathbf{k} \,||\, \mathbf{e}_z$ .
- Waves that propagate along the wave vector $\pm\mathbf{k}$ : We consider the homogenous wave equation (for $\psi = \{\mathbf{E},\, \mathbf{B},\, \Phi,\, \mathbf{A},\, ...\}$ ) with the known solution (proof by substitution and by means of the chain rule), whose wave fronts propagate along $\pm\mathbf{k}$

$$\Box\, \psi(\mathbf{r}, t) \;=\; 0 \qquad\qquad \psi(\mathbf{r}, t) \;=\; \psi_+(\mathbf{k}\cdot\mathbf{r} + \omega t) \;+\; \psi_- \underbrace{(\mathbf{k}\cdot\mathbf{r} - \omega t)}_{\textbf{phase}}$$

for arbitary functions $\psi_\pm(\mathbf{k}\cdot\mathbf{r} \pm \omega t)$ , and if they fullfill the dispersion relation $\omega \;=\; (\pm)\, c\, k$ .

- (Complex) monochromatic plane waves: If we restrict ourselves to periodic (harmonic) solutions, two obvious solutions are

$$\psi(\mathbf{r}, t) \;=\; A_-\, e^{i\,(\mathbf{k}\cdot\mathbf{r} - \omega t)} \qquad \text{or} \qquad \psi(\mathbf{r}, t) \;=\; A_+\, e^{i\,(\mathbf{k}\cdot\mathbf{r} + \omega t)}$$

$$\psi \;=\; \text{const.} \quad \text{for} \quad t = t_o \qquad \Longleftrightarrow \qquad \mathbf{k}\cdot\mathbf{r} \;=\; \text{const.}$$

Here, the vector $\mathbf{k}$ is called the wave or propagation vector and $\omega$ the frequency of the plane waves.

## 4.1.b. Plane-wave radiation

### Plane-wave solutions:

- Plane waves: Plane waves always propagate into the direction of the wave vector and can be written as

$$\mathbf{E}(\mathbf{r},t) \;=\; \mathbf{E}_o\, e^{i\,(\mathbf{k}\cdot\mathbf{r}\,-\,\omega t)}, \qquad\qquad \mathbf{B}(\mathbf{r},t) \;=\; \mathbf{B}_o\, e^{i\,(\tilde{\mathbf{k}}\cdot\mathbf{r}\,-\,\tilde{\omega} t)}$$

However, since the em field must satisfy not only the homogenous wave equation $\Box\,\psi \;=\; 0$ but also Maxwell's equations for the coupling of the $\mathbf{E}$ - und $\mathbf{B}$ fields

$$\textbf{rot}\;\mathbf{E} \;=\; -\,\frac{\partial\,\mathbf{B}}{\partial t} \qquad \Longleftrightarrow \qquad i\,(\mathbf{k}\times\mathbf{E}_o\,)\,e^{i\,(\mathbf{k}\cdot\mathbf{r}\,-\,\omega t)} \;=\; i\,\tilde{\omega}\,\mathbf{B}_o\,e^{i\,(\tilde{\mathbf{k}}\cdot\mathbf{r}\,-\,\tilde{\omega} t)}, \qquad \omega \;=\; \tilde{\omega}\,; \qquad \mathbf{k} \;=\; \tilde{\mathbf{k}}\,; \qquad \mathbf{k}\times\mathbf{E}_o \;=\; \omega\,\mathbf{B}_o\,.$$

Of course, this Maxwell equation need to be fulfilled for all times and places.

- If we use of the three other Maxwell equations, we furthermore obtain:

$$\textbf{div}\;\mathbf{E} \;=\; 0 \qquad \Longrightarrow \qquad \mathbf{k}\cdot\mathbf{E}_o \;=\; 0$$

$$\textbf{div}\;\mathbf{B} \;=\; 0 \qquad \Longrightarrow \qquad \mathbf{k}\cdot\mathbf{B}_o \;=\; 0$$

$$\textbf{rot}\;\mathbf{B} \;=\; \frac{1}{c^2}\,\frac{\partial\,\mathbf{E}}{\partial t} \qquad \Longrightarrow \qquad \mathbf{k}\times\mathbf{B}_o \;=\; -\,\frac{\omega}{c^2}\,\mathbf{E}_o \qquad \Longrightarrow \qquad (\mathbf{k}\times\mathbf{B}_o)^2 \;=\; k^2\,B_o^2 \;=\; \frac{\omega^2}{c^4}\,E_o^2 \qquad \Longrightarrow \qquad E_o^2 \;=\; c^2\,B_o^2.$$

Therefore, the three vectors $\mathbf{E}_o$, $\mathbf{B}_o$, $\mathbf{k}$ form (up to any even permutation) an orthogonal and right-handed system, i.e. the vectors $\mathbf{E}$ and $\mathbf{B}$ are perpendicular on $\mathbf{k}$ for plane waves.

- Vector potential:

$$\mathbf{A}(\mathbf{r},t) \;=\; \mathbf{A}_\pm\, e^{i\,(\mathbf{k}\cdot\mathbf{r}\,\pm\,\omega t)} \;=\; \sum_\lambda A_{o,\lambda}\,\mathbf{e}_\lambda\; e^{i\,(\mathbf{k}\cdot\mathbf{r}\,\pm\,\omega t)}$$

- Equation of a plane: For plane waves, all spatial points $\mathbf{r}$ with $\mathbf{k}\cdot\mathbf{r} \;=\;$ const. have the same value at any time $t \;=\; t_o$ .
- Wave crest: The wave crest of a plane wave is $A_\pm\, e^{i\,(\mathbf{k}\cdot\mathbf{r}\,\pm\,\omega t)}$ and propagates into the direction $\pm\,\mathbf{k}$ .

## Conserved properties of plane waves with $\mathbf{k} \,||\, \mathbf{e}_z$ :

- (Linear) momentum:

$$p_k \;=\; -i\,\partial_k, \qquad\qquad p_{x,y}\,\mathbf{A}(\mathbf{r},t) \;=\; 0, \qquad\qquad p_z\,\mathbf{A}(\mathbf{r},t) \;=\; k_z.$$

- Orbital angular momentum:

$$\ell_z \;=\; -i\,(x\,\partial_y \;-\; y\,\partial_x) \;=\; -i\,\frac{\partial}{\partial\,\varphi}, \qquad\qquad \ell_z\,\mathbf{A} \;=\; 0.$$

- Spin (of photons):

$$s_z \;=\; -i\begin{pmatrix} 0 & 1 & 0 \\ -1 & 0 & 0 \\ 0 & 0 & 0 \end{pmatrix}, \qquad\qquad s_z\,\mathbf{A} \;=\; \lambda\,\mathbf{A}.$$

- Total angular momentum:

$$j_z \;=\; \ell_z \;+\; s_z, \qquad\qquad j_z\,\mathbf{A} \;=\; \lambda\,\mathbf{A}.$$

- For plane waves, the (four) good quantum numbers refer to $\mathbf{p} \;=\; (p_x,\, p_y,\, p_z)$ and $\lambda_c$.

### 4.1.c. Polarization of plane waves in classical electrodynamics

## Polarization of plane-waves beams:

- Apart from the (well-defined) frequency of plane-wave photons, each photon has generally a spin angular momentum $\hbar$ that can be (partly) aligned in parallel or antiparallel to the direction of propagation. A full alignment of all photon spins gives then rise to a circularly-polarized light beam.

- A beam with a circularly-polarized planar wavefront has an azimuthal component of the Poynting vector that is proportional to the radial intensity gradient, even if it has no orbital angular momentum. This gives rise to a finite value, if integrated over the total cross-section of the beam.
- Polarization of the electric field: Polarization is an additional property of (em) waves that describes the orientation of their oscillations; by convention, the polarization $-1 \le p \le 1$ refers to the electric field. The polarization of light is associated with the spin-angular momentum (density) of the em wave.
- The polarisation is said to be linear if $p = 0$, and is left- or right-circular for $p = -1$ and $p = +1$, respectively. For all other values of $-1 < p < 1$, the wave is said to be elliptically polarized. Sometimes, one also refers to the chirality or handedness of the waves in order to denote the left- or right-circular polarization of the light beam.
- Vector potential of a circularly-polarized plane wave:

$$\mathbf{A}(\mathbf{r},t) = \mathbf{e}_\lambda \, e^{i\,(kz - \omega t)}; \qquad \mathbf{e}_\lambda = (\mathbf{e}_x + i\,\lambda\,\mathbf{e}_y) \qquad \begin{cases} \lambda = +1 & \text{left circular} \\ \lambda = -1 & \text{right circular} \end{cases}$$

- Spin angular momentum (SAM): The circular polarization of light is usually associated with a well-defined SAM.
- Complex spherical unit vectors $\mathbf{e}_\pm$:

$$\mathbf{e}_\pm = \frac{1}{\sqrt{2}} (\mathbf{e}_x \pm i\mathbf{e}_y) \qquad \Longleftrightarrow \qquad \begin{aligned} \mathbf{e}_x &= \tfrac{1}{\sqrt{2}} (\mathbf{e}_+ + \mathbf{e}_-) \\ \mathbf{e}_y &= \tfrac{-i}{\sqrt{2}} (\mathbf{e}_+ - \mathbf{e}_-) \,. \end{aligned}$$

- Complex electric field $\mathbf{E}^{(c)} = (E_x^{(c)},\, E_y^{(c)}, 0)$ : Although a complex notation of em fields is often very convinient, the transverse, real electric field is given by

$$\left. \begin{aligned} E_x^{(c)} &= |E_x^{(c)}|\, e^{i\,\gamma} \\ E_y^{(c)} &= |E_y^{(c)}|\, e^{i\,(\gamma+\delta)} \end{aligned} \right\} \qquad \mathbf{E}^{(c)} = \Re \left[ (E_x^{(c)}\,\mathbf{e}_x + E_y^{(c)}\,\mathbf{e}_y)\, e^{i\,(k\,z - \omega t)} \right] = E_x\,\mathbf{e}_x + E_y\,\mathbf{e}_y$$

$$E_x = |E_x^{(c)}| \cos(k\,z - \omega t + \gamma), \qquad E_y = |E_y^{(c)}| \cos(k\,z - \omega t + \gamma + \underbrace{\delta}_{!!}) \quad \text{... real.}$$

- Relative phase $\delta$ to distinguish different polarization: This relative phase $\delta$ refers to the complex field amplitudes $E_x^{(c)}$ and $E_y^{(c)}$

- Linear polarization along the angle $\alpha$: For $\delta = n\pi \quad (n \in \mathbb{N})$

$$\mathbf{E}^{(c)} = \left(|E_x^{(c)}|\,\mathbf{e}_x \pm |E_y^{(c)}|\,\mathbf{e}_y\right) \cos(k\,z - \omega t + \gamma) = |\mathbf{E}^{(c)}|\,\mathbf{e}_\alpha \cos(k\,z - \omega t + \gamma)$$

$$|\mathbf{E}^{(c)}| = \sqrt{|E_x^{(c)}|^2 + |E_y^{(c)}|^2}, \qquad \tan\alpha = \pm\frac{|E_y^{(c)}|}{|E_x^{(c)}|} \qquad \ldots \begin{cases} (+) & n = \text{gerade} \\ (-) & n = \text{ungerade} \end{cases}$$

$$\mathbf{e}_\alpha = \cos\alpha\,\mathbf{e}_x + \sin\alpha\,\mathbf{e}_y$$

  The angle $\alpha$ denotes the (polarization-) direction of $\mathbf{E}$ with regard to the $x$-axis.

- General monochromatic plane wave: Any plane wave can always be written as superposition of two components

## 4.2. Representation and parametrization of photons in atomic theory

### 4.2.a. Stokes parametrization and density matrix of a photon

#### Stokes parameters:

- Stokes parameters: These parameters provide a simple and alternative characterization for the polarization of plane waves and are given in terms of three real parameters that describe the polarization state of (transversal) electromagnetic radiation.
- Stokes parameters $P_1,\ P_2,\ P_3$ : The first two Stokes parameters quantify the *relative* asymmetries between intensities $I_\chi$ of light that is linearly polarized under different angles $\chi$ with regard to the the reaction plane: $P_1 = (I_o - I_{90})/(I_o + I_{90})$ and $P_2 = (I_{45} - I_{135}/(I_{45} + I_{135})$. The parameter $P_3$ reflects the degree of circular polarization of the emitted photons.
- The Stokes parameters were defined by George Gabriel Stokes in 1852 as a mathematically convenient alternative to the more common description of incoherent or partly polarized radiation in terms of its total intensity $I$, the degree of polarization $P$, and the orientation of the (so-called) polarization ellipse.
- Degree of polarization: The polarization state of the photon is said to be *pure* if they obey the Stokes parameters obey the restriction $\sum_{i=1}^{3} P_i^2 = 1$.

Table 4.1.: Stokes parametrization of photons for selected polarization of photons with $\mathbf{k} \,||\, \mathbf{e}_z$ .

| Selected photon polarization | $P_1$ | $P_2$ | $P_3$ |
|---|---|---|---|
| unpolarized | 0 | 0 | 0 |
| polarized along $x$-axis | 1 | 0 | 0 |
| polarized along $y$-axis | -1 | 0 | 0 |
| right-circularly polarized | 0 | 0 | 1 |
| left-circularly polarized | 0 | 0 | -1 |

- Degree of linear polarization: The parameter $P_\ell = \sqrt{P_1^2 + P_2^2}$ is called the degree of linear polarization.
- Stokes parameters $P_3 = P_c$ : Photons with $\lambda = +1$ are called right-circularly polarized photons, and photons with $\lambda = -1$ are called left-circularly polarized photons.
- Note that the notation in optics is often opposite to that used in quantum electrodynamics for historical reasons.

## Alternative representation of polarized photons:

- Instead of the Stokes parameters $P_1$ and $P_2$, it is often convenient for the analysis of different experimental situations to use the degree of linear polarization $P_\ell$ and the direction of the principal axis of the polarization ellipse $\varphi_0$.
- Polarization ellipse: If, in the chosen coordinate frame, the $x$-axis is directed along the principal axis of a polarized photon beam ($\varphi_0 = 0°$), the Stokes parameter $P_1$ takes the largest value $|P_1| = P_\ell$, while the Stokes parameter $P_2$ vanishes. This easily shows that the Stokes parameters $P_1$ and $P_2$ depend on the choice of the $x$-axis even if the $z$-axis is fixed along the beam, while the degree of linear polarization $P_\ell$ remains invariant.
- Polarization ellipse: It is often convenient to introduce the angle $\varphi_0$ by the relations

$$\cos\, 2\,\varphi_0 = \frac{P_1}{P_\ell}, \qquad\qquad \sin\, 2\,\varphi_0 = \frac{P_2}{P_\ell}$$

- Probability for measuring a linearly polarized photon along $\varphi$ in the $xy$-plane: For a density matrix with given $P_\ell$, $\varphi_0$ Balashov *et al.* (2001) shows the probability distribution

$$W(\varphi) = \frac{1}{2}(1 + P_\ell \cos 2(\varphi - \varphi_0))$$

for measuring linearly-polarized photon along $\varphi$ in the $xy$-plane.

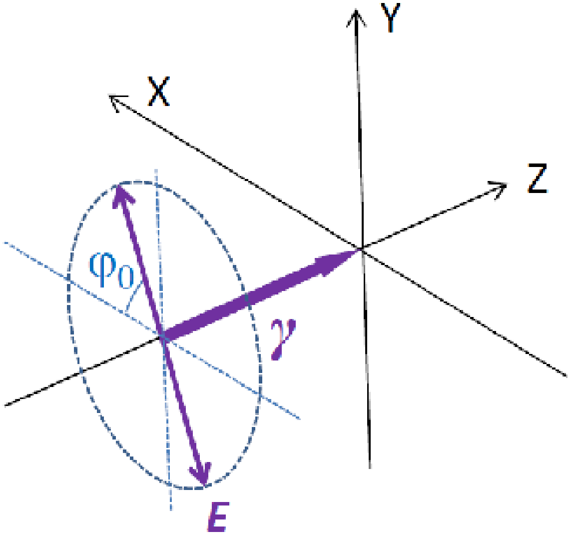

Figure 4.1.: Laboratory coordinate system.

- Angle of the polarization vector: The angle $\varphi_0$ indicates the *principal axis* of the *polarization ellipse* of the photon beam. It describes the direction of the axis (with regard to the $x$-axis) which the intensity of the transmitted photon beam is the largest, while it is lowest intensity perpendicular to this direction.

## Photon density matrix:

- Photon density matrix in helicity representation: Most naturally, the spin state of an incident photon is expressed within its helicity representation

$$\rho_\gamma \;=\; \sum_{\lambda\,\lambda'} c_{\lambda\lambda'} \, |\mathbf{k}\,\lambda\rangle \, \langle \mathbf{k}\,\lambda'| \,,$$

  where the helicity $\lambda$ is the spin projection of the photon upon the direction of its propagation, i.e. along the momemtum or wave vector $\mathbf{k}$.

- Since for a photon (with intrinsic spin $s \;\equiv\; 1$) the helicity just takes the values $\lambda = \pm 1$, only three real parameters are required to describe the spin state of the photons. These parameters in the photon density matrix are closely connected to the Stokes parameters of light (Rose, 1961)

$$(c_{\lambda\lambda'}) \;=\; \langle \mathbf{k}\,\lambda \,|\, \rho_\gamma \,|\, \mathbf{k}\,\lambda' \rangle \;=\; \frac{1}{2} \begin{pmatrix} 1 + P_3 & P_1 - iP_2 \\ P_1 + iP_2 & 1 - P_3 \end{pmatrix} .$$

  Note that this definition differs from those in Balashov *et al.* (2005) by a factor $-1$ for the $P_1$ and $P_2$ parameters because of the different convention of the spherical unit vectors $\mathbf{e}_\pm$ .

### 4.2.b. Pure polarization states of photons

## Linearly-polarized plane-wave photons with $\mathbf{k} \,||\, \mathbf{e}_z$ :

- In this section, we consider pure polarization states of an incoming photon, i.e. light with a photon density matrix $P_1^2 \,+\, P_2^2 \,+\, P_3^2 \;=\; 1$ , and which is thus equivalent to a density-matrix with $\rho^2 \;=\; \rho$ .

- With this restriction in mind, any polarized state of a transvere photon can be described by the linear combination

$$|\mathbf{e}\rangle \;=\; g_+ \, \mathbf{e}_+ \;+\; g_- \, \mathbf{e}_- \,,$$

  where $\mathbf{e}_\lambda \quad (\lambda = \pm)$ are the unit polarization vectors within the circular basis, and with $|g_+|^2 \,+\, |g_-|^2 \;=\; 1$ .

- The state of a linearly-polarized photon along some given direction $\varphi_0$ in the $x-y$ plane can be written in the form

$$|\mathbf{e}_{\varphi_0}\rangle \;=\; -\frac{1}{\sqrt{2}}\left(e^{-i\varphi_0}\,\mathbf{e}_+ \;-\; e^{i\varphi_0}\,\mathbf{e}_-\right) .$$

- Pure linearly-polarized light with $P_\ell \;=\; 1:$ $\quad |g_+| \;=\; |g_-|\,.$

## Elliptically-polarized plane-wave photons with $\mathbf{k} \,||\, \mathbf{e}_z$ :

- Photon density matrix in terms of the $g_\pm$ coefficients: With these notations, an arbitrarely polarized pure state of a (transversal) photon can be expressed in terms of the $g_\pm$ coefficients by either a $2 \times 2$ matrix or by means of the corresponding Stokes parameters:

$$\langle \mathrm{k}\lambda\,|\rho|\,\mathrm{k}\lambda'\rangle \;=\; \begin{pmatrix} |g_+|^2 & g_+\,g_-^* \\ g_+^*\,g_- & |g_-|^2 \end{pmatrix}, \qquad P_1 \;=\; -2\,\Re\left(g_+\,g_-^*\right), \qquad P_2 \;=\; 2\,\Im\left(g_+\,g_-^*\right), \qquad P_3 \;=\; |g_+|^2 \;-\; |g_-|^2 .$$

- Polarization ellipse: The linear polarization can be characterized also by $P_\ell$ and $\varphi_0$ with

$$P_\ell \;=\; 2\left|g_+\,g_-^*\right| \;=\; 2\,|g_+|\;|g_-|\cos 2\,\varphi_0 \;=\; -\frac{\Re\left(g_+\,g_-^*\right)}{|g_+\,g_-^*|}, \qquad \sin 2\varphi_0 \;=\; -\frac{\Im\left(g_+\,g_-^*\right)}{|g_+\,g_-^*|}.$$

These simple relations can be used to also find the $g_\pm$-coefficients for given paramters $P_\ell$ and $\varphi_0$ .

- Fully-polarized light with $P_\ell \;\neq\; 1:$

$$\text{for } |g_+| \;>\; |g_-|: \qquad |g_+| \;=\; \frac{1}{2}\left(\sqrt{1+P_\ell} \;+\; \sqrt{1-P_\ell}\right), \qquad |g_-| \;=\; \frac{1}{2}\left(\sqrt{1+P_\ell} - \sqrt{1-P_\ell}\right)$$

$$\text{for } |g_+| \;<\; |g_{-1}|: \qquad |g_+| \;=\; \frac{1}{2}\left(\sqrt{1+P_\ell} - \sqrt{1-P_\ell}\right), \qquad |g_-| \;=\; \frac{1}{2}\left(\sqrt{1+P_\ell} + \sqrt{1-P_\ell}\right)$$

- The relative phase of the coefficients: $g_+ \;=\; |g_+|\,e^{i\,\xi_+}$ ; $\quad g_- \;=\; |g_-|\,e^{i\,\xi_-}$ can be found from the equation: $\quad \xi_- \;-\; \xi_+ \;=\; 2\,\varphi_0 \;+\; \pi$ .
- Polarization vectors $\boldsymbol{\epsilon}_1,\,\boldsymbol{\epsilon}_2$ of elliptical-polarized plane-wave radiation: An alternative representation of the polarization vector is given by:

$$\boldsymbol{\epsilon}_j \;=\; \left(\mathbf{e}_x\,\cos\left(\frac{\xi_j}{2}\right) \;+\; i\,\mathbf{e}_y\,\sin\left(\frac{\xi_j}{2}\right)\,\exp\left(\frac{i\,\eta_j}{2}\right)\right), \qquad \boldsymbol{\epsilon}_j^* \;=\; \left(\mathbf{e}_x\,\cos\left(\frac{\xi_j}{2}\right) \;-\; i\,\mathbf{e}_y\,\sin\left(\frac{\xi_j}{2}\right)\,\exp\left(\frac{-\,i\,\eta_j}{2}\right)\right), \qquad j \;=\; 1,2.$$

- Two elliptically-polarized beams with the same angular momentum but opposite helicity: The easist way to describe such a superposition is $\xi_1 = \xi_2 = \pi/2, \quad \eta_1 = \eta_2 = 0$, and this leads to

$$\boldsymbol{\epsilon}_1 = \boldsymbol{\epsilon}_2 \equiv \boldsymbol{\epsilon}, \qquad \boldsymbol{\epsilon}_1^* = \boldsymbol{\epsilon}_2^* \equiv \boldsymbol{\epsilon}^*, \qquad \boldsymbol{\epsilon} \cdot \boldsymbol{\epsilon}^* = 1, \qquad \boldsymbol{\epsilon} \cdot \boldsymbol{\epsilon} = \boldsymbol{\epsilon}^* \cdot \boldsymbol{\epsilon}^* = 0 \,.$$

- Two elliptically-polarized beams with the same helicity and opposite angular momentum: These beams are descroibed by $\xi_1 = -\xi_2 = \pi/2, \quad \eta_1 = \eta_2 = 0$, and the two polarization vectors then fulfill

$$\boldsymbol{\epsilon}_1 = \boldsymbol{\epsilon}_2^* \equiv \boldsymbol{\epsilon}, \qquad \boldsymbol{\epsilon}_1^* = \boldsymbol{\epsilon}_2 \equiv \boldsymbol{\epsilon}^*, \qquad \boldsymbol{\epsilon} \cdot \boldsymbol{\epsilon}^* = 1, \qquad \boldsymbol{\epsilon} \cdot \boldsymbol{\epsilon} = \boldsymbol{\epsilon}^* \cdot \boldsymbol{\epsilon}^* = 0 \,.$$

## Beams of fully-polarized light with $\mathbf{k} \not\parallel \mathbf{e}_z$ :

- Sequences of completely polarized light pulses: In experiments, one often considers a sequence of (fully polarized) photon pulses, which propagate however into different directions.
- Hierarchy of angles in defining the em pulses: For such a sequence of pulses, all angles are defined with respect to a fixed laboratory frame $\Sigma = (x, y, z)$, and where we assume all coordinate systems to be properly 'right-handed'.
- In the (primed) coordinates $\Sigma'$ as associated with some given pulse, the polarization cofficients are assumed to be:

$$\begin{aligned}
g_+ &= 1, \qquad g_- = 0 \qquad && (\text{for 'helicity}: \ +1') \\
g_+ &= 0, \qquad g_- = 1 \qquad && (\text{for 'helicity}: \ -1') \\
g_+ &= -\frac{1}{\sqrt{2}}\, e^{-i\,\phi_0}, \qquad g_- = \frac{1}{\sqrt{2}}\, e^{i\,\phi_0} \qquad && (\text{for 'linear' and given } \phi_0).
\end{aligned}$$

- First pulse: The wave vector of the first pulse always defines the $z$-axis and its linear polarization $(\phi_0)$ the $x$-axis of the fixed frame $\Sigma$, i.e. the first pulse defines the $x - z$ scattering plane. For a circularly polarized pulse, the $x$-axis is defined indirectly due to the definition of subsequent pulses (see below); it need not to be defined explicitly if there is only a single, circularly-polarized pulse.

- Parameters of the first pulse:

$$\phi_1 = 0; \qquad \theta_1 = 0; \qquad (\phi_1 = 0 \qquad \text{for circularly polarized light})$$

# 4.3. Multipole decomposition of the radiation field

## 4.3.a. Elements from the theory of multipole transitions

### Transition amplitudes:

- Johnson (2008) provide a systematic decomposition of the transition amplitudes into multipole components.
- Transition amplitudes due to a transverse-gauge vector potential $\mathbf{A}^{\,\text{(transverse)}}(\mathbf{r},\omega)$ : For a single-electron atom, the transition amplitude from state $a = |n_a \kappa_a m_a\rangle \longrightarrow b = |n_b \kappa_b m_b\rangle$ due to the interaction with a plane-wave radiation field with the transverse-gauge vector potential $\mathbf{A}^{\,\text{(transverse)}}(\mathbf{r},\omega) = \boldsymbol{\epsilon}\, e^{i\,\mathbf{k}\cdot\mathbf{r}}$, with $\boldsymbol{\epsilon} \cdot \mathbf{e}_z = 0$ is

$$T_{ba} = \int d^3\mathbf{r} \;\; \psi_b^* \, \boldsymbol{\alpha} \cdot \mathbf{A}^{\,\text{(transverse)}}(\mathbf{r},\omega) \; \psi_a .$$

### Multipole potentials:

- Plane-wave multipole potentials $\mathbf{a}_{LM}^{(p)}(\mathbf{r})$ : In the multipole expansion of the plane-wave vector potential, the multipole potentials satisfy both, the Helmholtz equation and transversality condition

$$\nabla^2 \, \mathbf{a}_{LM}^{(p)} + k^2 \, \mathbf{a}_{LM}^{(p)} = 0, \qquad \nabla \cdot \mathbf{a}_{LM}^{(p)} = 0 \qquad p = 0, 1 .$$

- The multipole potentials $\mathbf{a}_{LM}^{(p)}$ with $p=0$ are the magnetic multipole potentials and with $p=1$ the electric multipole potentials.

- Electron-multipole interaction operator: The interaction operator $\boldsymbol{\alpha}\cdot\mathbf{a}^{(p)}_{LM}$ is an irreducible tensor operator of rank $L$ and parity $(-1)^{L+1-p}$.
- The multipole expansion of the (transverse-gauge) plane-wave vector potential still contains all information about the polarization and propagation direction of the photons.
- Representation of the multipole potentials: Using the well-known idendities of the spherical Bessel functions, the multipole potentials $\mathbf{a}^{(p)}_{LM}$ can be expressed as (Johnson, 2007)

$$\mathbf{a}^{(0)}_{LM}(\mathbf{r}) \;=\; j_L(kr)\,\mathbf{Y}^{(0)}_{LM}(\mathbf{r}), \qquad \mathbf{a}^{(1)}_{LM}(\mathbf{r}) \;=\; \left[ j'_L(kr) + \frac{j_L(kr)}{kr} \right] \mathbf{Y}^{(1)}_{LM}(\mathbf{r}) \;+\; \sqrt{L(L+1)}\,\frac{j_L(kr)}{kr}\,\mathbf{Y}^{(-1)}_{LM}(\mathbf{r}).$$

## 4.3.b. Single-electron (reduced) multipole-transition matrix elements

### Johnson's single-electron reduced multipole-transition matrix elements:

- Transverse (velocity) gauge: Johnson (2007, section 6.3) derives the reduced multipole-transition matrix elements for $\mathbb{M} = (L, p)$ and $q = \omega / c$ as:

$$\left\langle a \left\| \mathbb{t}^{(\mathbb{M},\,\text{magnetic})}(\omega) \right\| b \right\rangle \;=\; \left\langle -\kappa_a \left\| \mathbb{C}^{(L)} \right\| \kappa_b \right\rangle \int_0^\infty dr\; \frac{\kappa_a + \kappa_b}{L+1}\; j_L(qr)\; \left[ P_a\,Q_b + Q_a\,P_b \right]$$

$$\left\langle a \left\| \mathbb{t}^{(\mathbb{M},\,\text{electric})}(\omega) \right\| b \right\rangle \;=\; \left\langle \kappa_a \left\| \mathbb{C}^{(L)} \right\| \kappa_b \right\rangle \int_0^\infty dr\; \left\{ -\frac{\kappa_a - \kappa_b}{L+1} \left[ j'_L(qr) + \frac{j_L(qr)}{qr} \right] \left[ P_a\,Q_b + Q_a\,P_b \right] \;+\; L\,\frac{j_L(qr)}{qr}\, \left[ P_a\,Q_b - Q_a\,P_b \right] \right\}.$$

- Length gauge: While the reduced multipole-transition matrix elements are the same in length gauge, Johnson (2007, section 6.3) derives the reduced multipole-transition matrix elements in length gauge as:

$$\begin{aligned} &\left\langle a \left\| \mathbb{t}^{(\mathbb{M},\,\text{electric})}(\omega) \right\| b \right\rangle \\ &\quad = \left\langle \kappa_a \left\| \mathbb{C}^{(L)} \right\| \kappa_b \right\rangle \int_0^\infty dr\; \left\{ j_L(qr)\; \left[ P_a\,P_b + Q_a\,Q_b \right] \;+\; j_{L+1}(qr)\; \left[ \frac{\kappa_a - \kappa_b}{L+1}\, \left[ P_a\,Q_b + Q_a\,P_b \right] + \left[ P_a\,Q_b - Q_a\,P_b \right] \right] \right\}. \end{aligned}$$

## Johnson's frequency-dependent multipole-moment operators:

- ➢ Multipole-moment matrix elements: Following Johnson (2007), the reduced multipole-moment matrix elements can be calculate for the reduced multipole-transition matrix elements

$$\left\langle a \left\| \mathbb{q}^{(\mathbb{M})}(\omega) \right\| b \right\rangle \;=\; \frac{(2L+1)!!}{q^L} \; \left\langle a \left\| \mathbb{t}^{(\mathbb{M})}(\omega) \right\| b \right\rangle .$$

### 4.3.c. Many-electron (reduced) multipole emission and absorption amplitudes

## Jac's (standard) multipole amplitudes for photon absorption and emission:

- ➢ Mutipole (absorption) amplitude $|\alpha_i \mathbb{J}_i\rangle \; + \; \hbar\,\omega(\mathbb{M}, \lambda) \; to \; |\alpha_f \mathbb{J}_f\rangle :$ For the absorption of a photon with energy $\omega$, well-defined multipolarity (angular momentum) $L$ and helicity $\lambda = \pm 1$, we always use the notation

$$\left\langle \alpha_f \mathbb{J}_f \left\| \mathbb{O}^{(\mathbb{M},\,\text{absorption})}(\omega) \right\| \alpha_i \mathbb{J}_i \right\rangle .$$

- ➢ Photon emission: from an atom or ion $|\alpha_i \mathbb{J}_i\rangle \quad \longrightarrow \quad |\alpha_f \mathbb{J}_f\rangle \; + \; \hbar\omega(\mathbb{M})$.
- ➢ Care has to be taken about the many-electron multipole amplitudes which appear in many expressions. While we need formally to distinguish between the absorption $a_L^{\lambda}$ and emission operators $a_L^{\lambda\,+}$ operators, all (one- and many-electron) multipole-transition matrix elements are always evaluated *in absorption.*
- ➢ For any photon emission process, this would then require to 'interchange' the sequence *final-state* — *operator* — *initial-state* explicitly. This is a (very) high price however in such a large software project, since such an interchange affects the intuitive description of many processes in terms of initial-intermediate-final levels as well as still possibly other subsequent (final) states/levels.

# 4.4. Electromagnetic light pulses

## 4.4.a. High-intensity pulses

### Matter in intense fields:

- ➢ The exposure of atoms and matter to high-intensity laser fields is known to give rise to high-harmonic generation, above-threshold ionization and well as laser-induced dissociation and plasma formation, and which are all fundamentally different from processes in the weak-field regime.
- ➢ These phenomena are often outside of what is described by (standard) atomic-structure methods since the external field, that acts upon the electrons in typical strong-field experiments, is then comparable to the Coulomb potential of the nucleus.
- ➢ Pump-probe experiments: In these experiments, two short pulses are typically required. While the pump pulse starts the reaction, the probe pulse investigates the state of the system after a defined time delay. These measurements is repeated several times with increasing time delays in order to finally obtain a molecular movie.
- ➢ If the level structure of the atoms is not affected by the (moderately intense) laser pulses, the time-dependent density matrix may allow to model the (time-dependent) level occupation and coherences of an atoms and, eventually, all the photoexcitation and ionization processes.

## 4.4.b. Pulse shapes and optical cycles

### Pulse shaping in physics and science:

- ➢ Pulse shaping is frequently used in physics, science and technology. Pulse shaping generally refers to the the process of changing the waveform of a (transmitted) pulse, for instance, in order to make a transmitted signal better suited for a particular communication channel. In telecommunication, for example, pulse shaping is essential in order to ensure that the signal fit to a given frequency band.
- ➢ In femtosecond physics and chemistry, pulse shaping describes a technology for generating nearly arbitrary pulses with user defined, ultrafast optical waveforms, and by controlling its phase, amplitude, and polarization. Here, the most widely applied technique is Fourier transform pulse shaping.

## Frequently applied pulse shapes for time-dependent atomic computations:

- In pump- and/or pump-probe experiments, all (symmetric) light pulses are typically defined in terms of a central frequency $\omega$ and a (delay) time $T_d$ for the arrival of the pulse center with regard to same reference time $t_0 = 0$. Moreover, the shape function is always normalized to $\max[f_s(t)] = \max[f(t)/f_o] = 1$ and, hence, the intensity of the em field must be captured properly by the constant $f_o$.
- In JAC, the following (symmetric) shapes of the em pulses have been pre-defined: `"sin^2"`, `"sin^2: plateau"`, `"sin^2: cycles"` and `"gaussian"` facilitate the description of experimentally specified pulses. Further pulses shapes might be added if the need arises from the side of experiment.
- It is important to ensure that the pulse-shape function $f_s(t)$ (envelope) just contains an integer number of optical cycles. Therefore, one often starts with an $\sin^2$ envelope. For example, an envelope function $\sin^2$ 10T pulse refers to a pulse with 10 optical cycles.

### 4.4.c. Maximum pulse intensity

## Vector potential:

- Amplitude of the vector potential: This amplitude need to be derived from the (maximum) intensity of a laser pulses that is typically given in W/cm$^2$. In general, this relation between intensity and amplitude is non-trivial since the relationship between intensity and the electric field depends also slightly on the polarization of the pulse. A simple relation only occurs for a linearly-polarized laser beam.
- Average intensity of a pulse: If only the average intensity is given, the conversion factor depends also on the particular pulse-shape function. In practice, however, experimentalists rarely know the intensity accurately and, hence, a simplified normalization procedure can normally be used.

## Intensity and pulse geometry:

- The atomic unit of electric field is $m_e^2 \, e^5 / \hbar^4 = 5.1422 \cdot 10^9$ V/cm. From this we have: $E_0 \, [a.u.] = 5.34 \cdot 10^{-9} \, \sqrt{I \; [W/cm^2]}$.

### 4.4.d. Bichromatic laser fields

## Bichromatic laser fields:

- ➢ Bichromatic laser fields: Of some special interests in light-atom interaction studies are fields with two components of commensurate frequencies; for instance, the fundamental component $\omega$ and one of its low harmonics $2\,\omega$ or $3\,\omega$. Moreover, these two components are in general out of phase by some angle $\phi$.
- ➢ Linearly-polarized bichromatic fields: For such a field, the electric field can be written in a quite general form as

$$E(t) \;=\; F(t)\,\left[\cos\left(\omega\,t \,+\, \phi_1^{(\mathrm{cep})}\right) \,+\, \eta\,\cos\left(2\,\omega\,t \,+\, \phi_2^{(\mathrm{cep})}\right)\right]$$

with frequencies $\omega$ of the fundamental radiation and $2\,\omega$ due to the second harmonic. Here, the same envelope function $F(t)$ is applied for both, the fundamental and the second harmonic, while the ratio of the corresponding amplitudes is specified by the real parameter $\eta\;(\eta\,>\,0)$. The carrier-envelope phases (CEP) are here denoted by $\phi_1^{(\mathrm{cep})}$ and $\phi_2^{(\mathrm{cep})}$, respectively.

# 5. Atomic amplitudes

## 5.1. In JAC implemented amplitudes

### 5.1.a. Dipole amplitudes (`MultipoleMoment`)

**Amplitude, notations & application:**

- Formal quantum notation: $\langle \alpha_f \mathbb{J}_f \, \| \, \mathbb{D} \, \| \, \alpha_i \mathbb{J}_i \rangle \; = \; \langle \alpha_f \mathbb{J}_f \, \| \, \sum_i \, \mathbf{r}_i \, \| \, \alpha_i \mathbb{J}_i \rangle \quad \text{for} \quad P_f \, \neq \, P_i$
- Note that the full dipole operator is often defined by: $\mathbb{D}' \; = \; - \, |e| \, \mathbb{D} \, .$
- Using JAC: Call `MultipoleMoment.dipoleAmplitude(level`$_f$`::Level, level`$_i$`::Level)` or `(level`$_f$`::Level, level`$_i$`::Level; display=true)`, if the value of the amplitude needs to be printed to screen.

### 5.1.b. Electro-magnetic multipole transition amplitudes (`MultipoleMoment, Radiative`)

**Amplitude, notations & application:**

- Formal quantum notation:

$$\left\langle \alpha_f \mathbb{J}_f \left\| \mathbb{O}^{\,(\mathbb{M},\,\mathrm{emission})} \, (\omega) \, \right\| \alpha_i \mathbb{J}_i \right\rangle \;\; = \;\; \left\langle \alpha_i \mathbb{J}_i \left\| \, \sum_{k=1}^{N} \boldsymbol{\alpha}_k \, a^{p}_{k,\,L} \, \right\| \alpha_f \mathbb{J}_f \right\rangle^{*} \;\; \equiv \;\; \left\langle \alpha_i \mathbb{J}_i \left\| \mathbb{O}^{\,(\mathbb{M},\,\mathit{absorption})} (\omega) \, \right\| \alpha_f \mathbb{J}_f \right\rangle^{*}$$

$$\left\langle \alpha_f \mathbb{J}_f \left\| \mathbb{T}^{\,(\mathbb{M},\,\mathrm{absorption})} \, (\omega) \, \right\| \alpha_i \mathbb{J}_i \right\rangle$$

which retains the right order of the initial and final levels with regard to absorption or emission and which and can be obtained from `Jac.Radiative.amplitude()`; cf. section 4.3.c.

- Using JAC: Call `Radiative.amplitude("absorption", Mp::Multipole, gauge::EmGauge, omega::Float64, level`$_f$`::Level, level`$_i$`::Level)` or `("absorption", Mp::Multipole, gauge::EmGauge, omega::Float64, level`$_f$`::Level, level`$_i$`::Level; display=true)`, if the value of the amplitude needs to be printed to screen.
- Using JAC: Call `MultipoleMoment.transitionAmplitude(Mp::Multipole, gauge::EmGauge, omega::Float64, level`$_f$`::Level, level`$_i$`::Level)` or `(Mp::Multipole, gauge::EmGauge, omega::Float64, level`$_f$`::Level, level`$_i$`::Level; display=true)`, if the value of the amplitude needs to be printed to screen.

## Further remarks:

- A multipole $\mathbb{M} \equiv (L, p) \equiv (L, \text{electric/magnetic}) =$ E1, M1, E2, ... hereby contains all information about its multipolarity (angular momentum) $L$ and type *magnetic* $(p = 0)$ or *electric* $(p = 1)$, respectively.
- In the module `Radiative`, the multipole-transition amplitudes can be calculated in one of the gauge = {`Coulomb, Babushkin, Magnetic`} as appropriate for electric- and magnetic-multipole transitions.
- Johnson's multipole-transition operators: Following Johnson (2007), the electron-photon interaction with the multipole fields $(\mathbb{M})$ can be expressed in terms of a dimensionless multipole-transition operator $\mathbb{T}^{(\mathbb{M})}_M(\omega) = \sum_j \mathbb{t}^{(\mathbb{M})}_M(\mathbf{r}_j; \omega)$, an irreducible tensor operator, whose reduced (single-electron) matrix elements are given in Section 4.3.b. The amplitudes to these operators always describe the absorption of a photon with a given multipolarity.
- Johnson's (2007) multipole-transition amplitudes can be calculated in one of the gauge = {`Velocity, Length, Magnetic`} as appropriate for electric- and magnetic-multipole transitions.

### 5.1.c. Electro-magnetic multipole-moment amplitudes (`MultipoleMoment`)

## Amplitude, notations & application:

- Formal quantum notation:

$$\left\langle \alpha_f \mathbb{J}_f \left\| \mathbb{Q}^{(\mathbb{M})}(\omega) \right\| \alpha_i \mathbb{J}_i \right\rangle$$

- Using JAC: Call `MultipoleMoment.amplitude(Mp::Multipole, gauge::EmGauge, omega::Float64, level`$_f$`::Level, level`$_i$`::Level)` or `(Mp::Multipole, gauge::EmGauge, omega::Float64, level`$_f$`::Level, level`$_i$`::Level; display=true)`, if the value of the amplitude needs to be printed to screen.

## Further remarks:

- Johnson's multipole-moment operator: Johnson (2007) also defines a frequency-dependent (irreducible tensor) multipole-moment operator

$$\mathbb{Q}_M^{(\mathbb{M})}(\omega) \;=\; \sum_j \mathbb{q}_M^{(\mathbb{M})}(\mathbf{r}_j;\,\omega) \;\equiv\; \frac{(2L+1)!!}{(\omega/c)^L} \;\sum_j \mathbb{t}_M^{(\mathbb{M})}(\mathbf{r}_j;\,\omega)$$

- These amplitudes are calculated by a call to (Johnson's) multipole-transition amplitudes from above [cf. section 5.1.b] but by taking the frequency-dependence into account.
- Electric multipole-moment amplitudes can be calculated in one of the gauge = {`Velocity, Length, Magnetic`} as appropriate for electric- and magnetic-multipole transitions.

### 5.1.d. Momentum transfer amplitudes (`FormFactor`)

## Amplitude, notations & application:

- Formal quantum notation: $\left\langle \alpha_f \mathbb{J}_f \left\| \sum_j \exp\left(i\, \mathbf{q} \cdot \mathbf{r}_j\right) \right\| \alpha_i \mathbb{J}_i \right\rangle \;=\;$ selection rules
- Using JAC: Call `FormFactor.amplitude(level`$_f$`::Level, level`$_i$`::Level, ...)` or `(level`$_f$`::Level, level`$_i$`::Level, ...; display=true)`, if the value of the amplitude needs to be printed to screen.

## Further remarks:

- The (single-electron) momentum transfer amplitude help describe inelastic scattering processs and is closely related also to the (so-called) generalized oscillator strength.

- The (one-electron) momentum-transfer operator $\mathbb{T}^{(1)}(\mathbf{q}) = \sum_{j=1}^{N} \exp(i\,\mathbf{q}\cdot\mathbf{r}_j)$ can be utilized in order to express the standard form factor for an atom in a given sublevel $|\alpha\,\mathbb{J}M\rangle$ in terms of an (many-electron) expectation value; cf. 6.1.d.

## 5.2. In JAC partly-implemented amplitudes

### 5.2.a. Parity non-conservation amplitudes (`ParityNonConservation`)

### Amplitude, notations & application:

- Formal quantum notation: $\left\langle \alpha_f \mathbb{J}_f \left\| \mathbb{H}^{(\text{weak}-\text{charge})} \right\| \alpha_i \mathbb{J}_i \right\rangle$
- Using JAC: Call `ParityNonConservation.weakChargeAmplitude(level`$_f$`::Level, level`$_i$`::Level, model::Nuclear.Model)` or `(level`$_f$`::Level, level`$_i$`::Level, model::Nuclear.Model; display=true)`, if the value of the amplitude needs to be printed to screen.

### Further remarks:

- Parity non-conservation (PNC) effects arises in atoms mainly because of the exchange of $Z^0$-bosons between atomic electrons and the nucleus. Various observables due to this parity non-conserving interactions can be described in terms of a nuclear-spin independent Hamiltonian $\mathbb{H}^{(\text{weak}-\text{charge})}$, an effective single-electron operator, if non-relativistic nucleons can be assumed, cf. section 3.9.b.
- Especially, if the proton and neutron densities coincide, $\rho_p = \rho_n = \rho$, the general nuclear-spin independent Hamiltonian simplifies and can be described in terms of a single nuclear- weak charge $Q_W$,

$$\mathbb{H}^{(\text{weak}-\text{charge})} \;=\; -\frac{G}{2\sqrt{2}}\, Q_W \sum_j \gamma_{5,j}\, \rho(r_j)\,,$$

  where $G = 2.22{\cdot}10^{-14}$ a.u. is the Fermi constant, $\rho(r)$ is the normalized nuclear density with $\int dV\,\rho(\mathbf{r}) = 1$, and $Q_W \approx -N + Z\,(1 - 4\,\sin^2\,\theta_W)$ is the nuclear weak charge with $\theta_W$ being the Weinberg angle.

### 5.2.b. Schiff-moment amplitudes (`ParityNonConservation`)

## Amplitude, notations & application:

- Formal quantum notation: $\left\langle \alpha_f \mathbb{J}_f \left\| \mathbb{H}^{\,(\mathrm{Schiff-moment})} \right\| \alpha_i \mathbb{J}_i \right\rangle \;=\; \left\langle \alpha_f \mathbb{J}_f \left\| \mathbb{H}^{\,(\mathrm{Schiff-moment})} \right\| \alpha_i \mathbb{J}_i \right\rangle \, \delta_{J_f, J_i} \quad P_f \,\neq\, P_i$
- Using JAC: Call `ParityNonConservation.schiffMomentAmplitude(level`$_f$`::Level, level`$_i$`::Level, model::Nuclear.Model)` or `(level`$_f$`::Level, level`$_i$`::Level, model::Nuclear.Model; display=true)`, if the value of the amplitude needs to be printed to screen.

## Further remarks:

- Nuclear electric-dipole (Schiff) moments: If $\mathbf{S}$ is the P-odd and T-odd nuclear Schiff moment, the associated P-odd and T-odd Hamiltonian is given by (Dzuba *et al.*, 2009)

$$\mathbb{H}^{\,(\mathrm{Schiff-moment})} \;=\; -e\,\phi^{\,(\mathrm{Schiff-moment})} \;=\; -4\pi e\,\mathbf{S}\cdot\nabla\,\delta(r) \;=\; -\,\frac{3\,S^{\,(\mathrm{SM})}\,(\mathbf{I}/I)\cdot\mathbf{r}}{R}\,\rho(r)$$

  where $S^{\,(\mathrm{SM})}\;(\mathbf{I}/I)$ is the Schiff-moment vector, i.e. the product of the coupling constant $S^{(\mathrm{SM})}$ and the nuclear spin $\mathbf{I}$, and $R = \int_0^\infty dr\, r^4\, \rho(r)$. Moreover, $\phi^{\,(\mathrm{Schiff-moment})}$ is the electrostatic potential of the nucleus corresponding to a P-odd and T-odd charge distribution; cf. section 3.9.c.

# 5.3. Further amplitudes, not yet considered in JAC

### 5.3.a. Anapole-moment amplitudes (`ParityNonConservation`)

## Amplitude, notations & application:

- Formal quantum notation: $\left\langle \alpha_f \mathbb{J}_f \left\| \mathbb{H}^{\,(\mathrm{anapole-moment})} \right\| \alpha_i \mathbb{J}_i \right\rangle$

## Further remarks:

- A P-odd, T-even anapole moment of the nucleus was first introduced by Zel'dovich and arises due to the presence of a parity-violating weak interaction between nucleons, cf. section 3.9.b. The anapole moment is directed along the nuclear spin **I**, gives typically the dominant nuclear-spin dependent electron-nucleus interaction and manifests itself in terms of a slightly modified electro-magnetic interaction between the nucleus and the atomic electrons.
- Hamiltonian for the interaction of the electrons with the nuclear anapole moment: This Hamiltonian has the form (Dzuba *et al.*, 2009)

$$\mathbb{H}^{\,(\mathrm{anapole-moment})} \;=\; \frac{G}{\sqrt{2}}\,(I+1/2)\,(-1)^{I+1/2-\ell_N}\;\kappa_{\mathrm{AM}}\sum_j \frac{\mathbf{I}\cdot\boldsymbol{\alpha}_j}{I(I+1)}\;\rho(r_j),$$

  where $G = 2.22\cdot 10^{-14}$ a.u. is the Fermi constant, $I$ is the nuclear spin, $\ell_N$ the orbital angular momentum of the outermost nucleon and $\kappa_{\mathrm{AM}}$ is a dimensionless coupling constants for ...

## 5.3.b. Scalar-pseudo-scalar amplitudes

## Amplitude, notations & application:

- Formal quantum notation: $\left\langle \alpha_f \mathbb{J}_f \left\| \, \mathbb{H}^{\,(\mathrm{scalar-pseudo-scalar})} \, \right\| \alpha_i \mathbb{J}_i \right\rangle$

## Further remarks:

- Hamiltonian for the P-odd, T-odd scalar-pseudo-scalar interaction: In coordinate represetation, this Hamiltonian can be written as (Dzuba *et al.*, 2009)

$$\mathbb{H}^{\,(\mathrm{scalar-pseudo-scalar})} \;=\; -\,\frac{G}{\sqrt{2}}\;\frac{1}{2m_p\,c}\;C_s\sum_j \left[\gamma_0\,\frac{d\,\rho(r)}{dr}\right]_j$$

  where $G$ is the Fermi constant, $m_p$ is the nucleon mass, $C_s$ is a (isotope and) nuclear-state dependent constant, and where $\left[\gamma_0\,\frac{d\,\rho(r)}{dr}\right]$ is a scalar term that arises from the scalar product of the $\nabla$-vector with an particularly averaged spin-vector of the nucleus.

## 5.3.c. Tensor-pseudo-tensor amplitudes

### Amplitude, notations & application:

- Formal quantum notation: $\left\langle \alpha_f \mathbb{J}_f \left\| \, \mathbb{H}^{\,(\mathrm{tensor-pseudo-tensor})} \, \right\| \alpha_i \mathbb{J}_i \right\rangle$

### Further remarks:

- Hamiltonian for the P-odd, T-odd tensor-pseudo-tensor interaction: In coordinate representation, this Hamiltonian can be written as (Dzuba *et al.*, 2009)

$$\mathbb{H}^{\,(\mathrm{tensor-pseudo-tensor})} \;=\; i\,\sqrt{2}\,G\,C_t\,\sum_j \left[\gamma\,\rho(r)\right]_j$$

  where $G$ is the Fermi constant, $C_t$ is a (isotope and) nuclear-state dependent constant, and where $[\gamma\,\rho(r)]$ is a scalar term that arises from the scalar product of the $\gamma$-vector with an averaged spin-vector of the nucleus.
- Total P-odd, T-odd electron-nucleus interaction Hamiltonian: $\mathbb{H}^{\,(\mathrm{P-odd,\ T-odd\ electron-nucleus})} = \mathbb{H}^{\,(\mathrm{tensor-pseudo-tensor})} + \mathbb{H}^{\,(\mathrm{tensor-pseudo-tensor})}$

## 5.3.d. Nuclear magnetic-quadrupole-moment amplitudes due to internal $B$-field

### Amplitude, notations & application:

- Formal quantum notation: $\left\langle \alpha_f \mathbb{J}_f \left\| \, \mathbb{H}^{\,(\mathrm{nuclear-MQM})} \, \right\| \alpha_i \mathbb{J}_i \right\rangle$

### Further remarks:

- This interaction (Hamiltonian) arise from the interaction of the electron EDM $d_e$ with the electro-magnetic fields of the nucleus as seen by the electron. If the treatment is restricted to second order, only the interaction of the electron EDM with the magnetic field $\mathbf{B}$, which is created by the nuclear magnetic-dipole moment, need to be taken into account.

- ➢ Nuclear-MQM Hamiltonian: In coordinate representation, this Hamiltonian can be written as (Dzuba *et al.*, 2009)

$$\mathbb{H}^{(\mathrm{nuclear-MQM})} \;=\; -\,i\,d_e\,\boldsymbol{\gamma}\cdot\boldsymbol{B} \;=\; -\,i\,d_e\sum_j \boldsymbol{\gamma}_j\cdot\left[\boldsymbol{\nabla}_j\times\frac{\mathbf{M}\times\mathbf{r}_j}{r^3_{>,j}} \;+\; ...\right]$$

## 5.4. Composed many-electron amplitudes, not yet considered in JAC

### 5.4.a. Parity-violating (non-diagonal, second-order) amplitudes

### Amplitude, notations & application:

- ➢ Parity violation: The (effective) parity-violating interaction is caused by the exchange of $Z_o$ bosons between the atomic electrons and the nucleus. The parity-violating interaction typically results in non-vanishing off-diagonal electric-dipole matrix element between two atomic states of the same parity; cf. section 3.9.b.

### 5.4.b. Charge-parity-violating (diagonal, second-order) amplitudes

### Amplitude, notations & application:

- ➢ Charge-parity violation: An intrinsic electron electric dipole moment $d_e$ leads to CP-violation in atoms and also induces an atomic electric dipole moment. cf. section 3.9.d.

### 5.4.c. Electric-dipole moment enhancement factor

### Amplitude, notations & application:

- ➢ An intrinsic electric-dipole moment (EDM) of the electron can enhanced the EDM of the atom. In heavy atoms, in particular, an induced atomic EDM can be strongly enhanced, when compared to the electron EDM itself.
- ➢ A typical goal is to find the atomic EDM $d_{\rm atom} = |\mathbf{d}_{\rm atom}| \equiv d_{\rm atom} \, |\mathbf{F}/F|$ , where $\mathbf{F} = \mathbf{I} + \mathbf{J}$ is the total angular momentum of an atomic (hyperfine) level.
- ➢ The value of the atomic EDM, compared to the electron EDM, is expressed by means of an enhancement factor $K = d_{\rm atom}/d_e$ , and which increases with nuclear charge $Z$ faster than $Z^3$.

# 6. Atomic properties

## 6.1. In JAC implemented level properties

### 6.1.a. Transition probabilities for a single multiplet (`Einstein`)

**Properties, notations & application:**

- Photon emission: from an atom or ion $A^* \longrightarrow A^{(*)} + \hbar\omega$
- Formal quantum notation: $|\alpha_i \mathbb{J}_i\rangle \longrightarrow |\alpha_f \mathbb{J}_f\rangle + \hbar\omega$
- Using JAC: Perform an `Atomic.Computation(.., properties=[EinsteinX, ..], configs=[..], einsteinSettings= Einstein.Settings(..), ..)` or call directly functions from the module `Einstein`.
- In the JAC program, the transition probabilities, oscillator strength (in emission) and radiative lifetimes are calculated and tabulated by default for all selected transitions from a given single multiplet (i.e. list of configurations). Apart from the multipoles, the user can also specify an overall shift in the photon energies as well as a minimum and maximum transition energy, for which transitions are taken into account.
- In the `Einstein` module, the emission (transition) amplitudes $\left\langle \alpha_f \mathbb{J}_f \left\| \mathbb{O}^{\,(\mathbb{M},\,\mathrm{emission})} \right\| \alpha_i \mathbb{J}_i \right\rangle$ or absorption amplitudes $\left\langle \alpha_f \mathbb{J}_f \left\| \mathbb{O}^{\,(\mathbb{M},\,\mathrm{absorption})} \right\| \alpha_i \mathbb{J}_i \right\rangle$ can be obtained directly by call of the function `Jac.Einstein.amplitude()`.

**Further remarks:**

- Einstein $A$ and $B$ coefficients and oscillator strength for levels $|\alpha \mathbb{J}\rangle$ from a single multiplet are frequently needed for various applications and in different contexts.

- Although these coefficients are *no* (single) level property, the `Einstein` module still supports the computation of these coefficients for levels from a single multiplet, and which is generated by a single CSF basis.
- Although the `Einstein` module does not allow to include relaxation effects, this module helps obtain either a quick estimate of the Einstein coefficients between levels from just a few configurations or to deal with cascade computations.
- JAC's standard multipole amplitudes for photon emission: Although all (one- and many-electron) matrix elements are always evaluated *in absorption* within the JAC toolbox, we keep the intuitive description of the matrix elements as *final-state* – *operator* – *initial-state*, cf. section 4.3.c.

### 6.1.b. Hyperfine parameters and hyperfine representations (`Hfs`)

## Properties, notations & application:

- Hyperfine splitting of an atomic level into hyperfine (sub-) levels: $|\alpha \mathbb{J}\rangle \quad \longrightarrow \quad |\alpha (J)\, \mathbb{F}\rangle\,, \qquad F \;=\; |I-J|, \,..., I+J-1,\, I+J \;\;.$
- Formal quantum notation: $|\alpha \mathbb{J}\rangle \quad \longrightarrow \quad |\alpha\, \mathbb{F}\rangle \;\equiv\; |(I,\, \alpha' \mathbb{J})\, \mathbb{F}\rangle \;\equiv\; |\alpha (I \mathbb{J})\, \mathbb{F}\rangle \;\equiv\; |\alpha (IJP)\, \mathbb{F}\rangle$ or $|\alpha \mathbb{J} M_J\rangle \quad \longrightarrow \quad |\alpha\, \mathbb{F} M\rangle \;\equiv\; |(I,\, \alpha' \mathbb{J})\, \mathbb{F} M\rangle \;\equiv\; |\alpha (I \mathbb{J})\, \mathbb{F} M\rangle \;\equiv\; |\alpha (IJP)\, \mathbb{F} M\rangle \;\;.$
- Using JAC: Perform an `Atomic.Computation(.., properties=[HFS, ..], configs=[..], hfsSettings=Hfs.Settings(..), ..)` or call directly functions from the module `Hfs`. The Boolean values `calcT1` and `calcT2` in `Hfs.Settings` determine which parts of the hyperfine Hamiltonian are taken into account into the computations.
- In the JAC program, the hyperfine $A$ and $B$ coefficients as well as the (electric) hyperfine amplitudes $\left\langle \alpha \mathbb{J} \left\| \mathbb{T}^{(1)} \right\| \alpha \mathbb{J} \right\rangle,\, \left\langle \alpha \mathbb{J} \left\| \mathbb{T}^{(2)} \right\| \alpha \mathbb{J} \right\rangle$ are calculated and tabulated by default for all selected levels together with the energy shifts $\Delta\, E_F$ of the hyperfine levels with regard to the (electronic) level energy $E_{\alpha\, \mathbb{J}}$ .
- In JAC, the hyperfine amplitudes $\left\langle \beta_r \mathbb{J}_r \left\| \mathbb{T}^{(1)} \right\| \beta_s \mathbb{J}_s \right\rangle$ and $\left\langle \beta_r \mathbb{J}_r \left\| \mathbb{T}^{(2)} \right\| \beta_s \mathbb{J}_s \right\rangle$ can be obtained from the function `Jac.Hfs.amplitude()`.
- In JAC, moreover, an explicit representation of a hyperfine multiplet is obtained by diagonalizing the Hamiltonian $\mathbb{H} \;=\; \mathbb{H}^{\rm (DCB)} \;+\; \mathbb{H}^{\rm (hfs)}$ within the atomic hyperfine $IJF$ -coupled basis if `calcIJFexpansion=true` is set in `Hfs.Settings`.
- In JAC, all the (hyperfine) level energies $E_{\alpha\, \mathbb{F}}$ and the energies relative to the lowest (hyperfine) level are tabulated if `printDeltaEF=true` in `Hfs.Settings`.

- In JAC, all (diagonal and nondiagonal) hyperfine amplitudes are calculated and tabulated explicitly if `calcNondiagonal=true` in `Hfs.Settings`.

## Further remarks:

- For a nucleus with *non-zero* spin $I > 0$, a hyperfine splitting of (all) atomic levels generally occurs since each atomic electron also interacts with the electric and magnetic (multipole) fields of the nucleus. This is sometimes described also as the interaction of the magnetic moments of the electrons and nucleus.
- In atomic physics, this interaction is better known as 'hyperfine interaction' whose two dominant contributions arise from the nuclear magnetic-dipole field $\mathbf{A} = \frac{\boldsymbol{\mu} \times \mathbf{r}}{r^3}$ and the electric-quadrupole field $\Phi(r) = \sum_{ij} \frac{r_i \, r_j}{2 \, r^5} \, Q_{ij}$, respectively. In these expressions, $\boldsymbol{\mu}$ is the nuclear magnetic moment operator and $Q_{ij}, \; i, j = 1..3$ are the Cartesian components of the nuclear quadrupole operator.
- Apart from the hyperfine parameters $A(\alpha \, \mathbb{J})$ and $B(\alpha \, \mathbb{J})$, we also provide in JAC a representation of the atomic hyperfine levels that can be utilized, for instance, to compute hyperfine quenched transitions probabilities.

## Hyperfine interaction Hamiltonian:

- Relativistic hyperfine interaction Hamiltonian: For many-electron systems, this Hamiltonian can be written as

$$H^{\,(\mathrm{hfs})} = \sum_K \mathbb{W}^{\,(K)} \cdot \mathbb{T}^{\,(K)}$$

  where $\mathbb{W}^{\,(K)}$ and $\mathbb{T}^{\,(K)}$ represent the spherical tensor operators of rank $K$ that occur in the nucleonic and electronic sectors, respectively.

- Reduced nuclear matrix elements: These matrix elements are determined geometrically by

$$\langle I \, \| \, \mathbb{W}^{\,(1)} \| \, I \rangle = \mu_I \sqrt{\frac{I+1}{I}}, \qquad \qquad \langle I \, \| \, \mathbb{W}^{\,(2)} \| \, I \rangle = \frac{Q}{2} \sqrt{\frac{(I+1)\,(2I+3)}{I\,(2I-1)}},$$

  while, in contrast, the corresponding electronic amplitudes require detailed atomic structure calculations.

- Values of nuclear magnetic dipole and electric quadrupole moments can be found in the compilation by Stone (2005).

- Electronic tensor operators: For an $N$-electron atom or ion, these tensor operators are given by (Andersson and Jönsson, 2008)

$$\mathbb{T}^{(1)} = \sum_j^N \mathbb{t}^{(1)}(j) = \sum_j^N -i\sqrt{2}\,\alpha\,\frac{(\boldsymbol{\alpha}_j\,\mathbb{C}^{(1)}(j))^{(1)}}{r_j^2} \qquad \text{interaction with the magnetic} - \text{dipole field}$$

$$\mathbb{T}^{(2)} = \sum_j^N \mathbb{t}^{(2)}(j) = \sum_j^N -\frac{\mathbb{C}^{(2)}(j)}{r_j^3} \qquad \text{interaction with the electric} - \text{quadrupole field,}$$

and where $\alpha$ is the fine-structure constant, $\boldsymbol{\alpha}_j$ the vector of Dirac matrices of the $j$-th electron, and the $\mathbb{C}^{(K)}$ are (normalized) spherical tensors as before.

## Atomic (hyperfine) $IJF$-coupled basis:

- This (geometrically fixed) basis is obtained by the standard coupling of the nuclear states $|IM_I\rangle$ and the ASF $|\alpha\,\mathbb{J}M_J\rangle$

$$|\alpha(I,J)\,\mathbb{F}M\rangle \equiv |(I,\,\alpha'\,\mathbb{J})\,\mathbb{F}M\rangle = \sum_{M_I\,M_J} |IM_I\rangle\,|\alpha'\,\mathbb{J}M_J\rangle\,\langle IM_I,\,JM_J\,|\,FM\rangle\,.$$

- The atomic (hyperfine) $IJF$-coupled basis, also called the $IJF$-coupled ASF basis, is applied internally to represent all hyperfine levels, see below.

## Atomic hyperfine amplitudes and levels:

- Atomic hyperfine levels: For the combined system 'nucleus+electrons', the atomic hyperfine states (magnetic sub-levels) can be formed as linear combination

$$|\alpha\,\mathbb{F}M\rangle = \sum_{r=1} \tilde{c}_r(\alpha)\;|(I,\,\beta_r\,\mathbb{J}_r)\,\mathbb{F}M\rangle$$

of hyperfine (basis) states $|(I,\,\beta_r\mathbb{J}_r)\,\mathbb{F}M\rangle$ of the same total angular momentum $F$ and (the same electronic) parity $P$, and where $\{\tilde{c}_r(\alpha)\}$ denotes the representation of these states in the atomic hyperfine-coupled basis (Johnson, 2010).

- Analogue as for the ASF $|\alpha \mathbb{J}\rangle$ in the standard MCDF ansatz, the representation $\{\tilde{c}_r(\alpha)\}$ of an atomic hyperfine state is obtained by diagonalizing the Hamiltonian $\mathbb{H} = \mathbb{H}^{\,(\mathrm{DFB})} + \mathbb{H}^{\,(\mathrm{hfs})}$ of the combined system 'nucleus+electrons' in either the $IJF$-coupled CSF or ASF basis.
- In the $IJF$-coupled ASF basis, we can make use of $\mathbb{H}^{\,(\mathrm{DFB})} \, |(I,\, \beta_r\, \mathbb{J}_r)\, \mathbb{F} M\rangle \;=\; E(\beta_r\, \mathbb{J}_r)\; |(I,\, \beta_r\, \mathbb{J}_r)\, \mathbb{F} M\rangle \;\equiv\; E_{\beta_r\, \mathbb{J}_r}\; |(I,\, \beta_r\, \mathbb{J}_r)\, \mathbb{F} M\rangle\,.$
- For the hyperfine part of the Hamiltonian, the (reduced) matrix elements can be written after some standard angular momentum algebra as

$$\begin{aligned}
\left\langle (I,\, \beta_r \mathbb{J}_r)\, \mathbb{F} M \,\middle|\, H^{\,(\mathrm{hfs})} \,\middle|\, (I,\, \beta_s \mathbb{J}_s)\, \mathbb{F}' M' \right\rangle \;&=\; \delta_{MM'}\;\; \left\langle (I,\, \beta_r \mathbb{J}_r)\, \mathbb{F} \,\middle|\, H^{\,(\mathrm{hfs})} \,\middle|\, (I,\, \beta_s \mathbb{J}_s)\, \mathbb{F}' \right\rangle \\
&=\; \delta_{MM'}\;\; \delta_{\mathbb{F}\mathbb{F}'}\;\; (-1)^{I + J_r + F} \sum_K \begin{Bmatrix} I & J_r & F \\ J_s & I & K \end{Bmatrix} \left\langle \beta_r \mathbb{J}_r \left\| \mathbb{T}^{\,(K)} \right\| \beta_s \mathbb{J}_s \right\rangle \left\langle I \left\| \mathbb{W}^{\,(K)} \right\| I \right\rangle\,,
\end{aligned}$$

  with $\delta_{\mathbb{F}\mathbb{F}'} \;=\; \delta_{PP'}\, \delta_{FF'}$ , and if all nuclear excitations are ignored right from the beginning.
- Hyperfine amplitudes: These amplitudes refer to the (reduced) electronic matrix elements $\left\langle \beta_r \mathbb{J}_r \left\| \mathbb{T}^{\,(K)} \right\| \beta_s \mathbb{J}_s \right\rangle$. In the JAC program, we compute the hyperfine amplitudes for both, the magnetic-dipole and the electric-quadrupole operators of the electron-nucleus interaction.
- These hyperfine amplitudes are utilized to set-up and diagonalize the Hamiltonian matrix within the atomic $IJF$-coupled basis for $\mathbb{H} = \mathbb{H}^{\,(\mathrm{DCB})} + \mathbb{H}^{\,(\mathrm{hfs})}$ in order to determine the representation $\{\tilde{c}_r(\alpha)\}$ of the atomic hyperfine states.

## Hyperfine energies and interaction constants:

- Hyperfine interaction constants: Usually the hyperfine splitting is considered independently for each atomic level $|\alpha \mathbb{J}\rangle$ and without the need to specify all the hyperfine level energies $E_{\alpha \mathbb{F}}$ explicitly. Instead, the energy splitting of an atomic level $|\alpha \mathbb{J}\rangle$ into hyperfine levels $|\alpha \mathbb{F}\rangle$ can be expressed conveniently in terms of the (hyperfine interaction) constants

$$A(\alpha\, \mathbb{J}) \;=\; \frac{\mu_I}{I}\, \frac{1}{\sqrt{J(J+1)}} \left\langle \alpha\, \mathbb{J} \left\| \mathbb{T}^{\,(1)} \right\| \alpha\, \mathbb{J} \right\rangle, \qquad\qquad B(\alpha\, \mathbb{J}) \;=\; 2Q \sqrt{\frac{J(2J-1)}{(J+1)(2J+3)}} \left\langle \alpha\, \mathbb{J} \left\| \mathbb{T}^{\,(2)} \right\| \alpha\, \mathbb{J} \right\rangle$$

- Hyperfine energy splitting: With these constants, the hyperfine energy shifts with regard to the electronic level energy $E(\alpha \mathbb{J})$ is given by

$$\Delta\, E_F \;=\; \frac{A(\alpha\, \mathbb{J})\, C}{2} \;+\; B(\alpha\, \mathbb{J})\; \frac{3/4\, C(C+1) \;-\; I(I+1)\, J(J+1)}{2I\, (2I-1)\, J\, (2J-1)}, \qquad\qquad C \;=\; F(F+1) \;-\; J(J+1) \;-\; I(I+1).$$

## 6.1.c. Isotope-shift parameters (`IsotopeShift`)

### Properties, notations & application:

- Isotope shift of an atomic level for two isotopes $A,\ A'$ with nuclear masses $M \,<\, M'$: $\quad E(\alpha\mathbb{J}; A) \quad \longrightarrow \quad E(\alpha\mathbb{J}; A')\,.$
- Formal quantum notation: $\quad \Delta\, E(\alpha\mathbb{J}; A, A')\,/\,h \;=\; \frac{M'-M}{M\,M'}\, K^{\,(\mathrm{MS})} \;+\; F\,\delta\,\langle r^2 \rangle\,.$
- Using JAC: Perform an `Atomic.Computation(.., properties=[Isotope, ..], configs=[..], isotopeSettings= IsotopeShift.Settings(..), ..)` with `calcNMS=true`, `calcNMS=true` or `calcF=true` and/or call directly functions from the module `IsotopeShift` in order to include the various contribution of the recoil Hamiltonian.
- In JAC, we calculate and tabulate by default the (relativistic) mass-shift parameters $K^{\,(\mathrm{MS})}$, $K^{\,(\mathrm{NMS})}$, $K^{\,(\mathrm{SMS})}$ and the field-shift parameter $F$ for all selected levels.

### Further remarks

- Owing to the conservation of the total momentum, the (total non-relativistic) mass shift is a sum of two parts, the (so-called) normal mass shift (NMS) and the specific mass shift (SMS):

  $$\mathbb{H}^{\,(\mathrm{MS,\,nr})} \;=\; \mathbb{H}^{\,(\mathrm{NMS,\,nr})} \,+\, \mathbb{H}^{\,(\mathrm{SMS,\,nr})} \;=\; \frac{1}{2\,M} \sum_j \mathbf{p}_j^2 \quad+\quad \frac{1}{2\,M} \sum_{i \neq j} \mathbf{p}_i \cdot \mathbf{p}_j$$

  While the normal mass shift operator is obviously a one-particle operator, the specific mass shift is a two-particle operator. The sum of these two parts is known also as the total recoil operator within the nonrelativistic theory.

### Relativistic recoil (Hamilton) operator:

- Recoil Hamiltonian: Within the lowest-order relativistic approximation $(\sim v^2/c^2)$ and in first order of $m/M$ for a nucleus with mass $M$, the recoil corrections are given by means of the (recoil) Hamiltonian (Tupitsyn *et al.*, 2003):

$$\mathbb{H}^{\,(\mathrm{recoil})}(M) \;=\; \frac{1}{2\,M} \sum_{ij} \left[ \mathbf{p}_i \cdot \mathbf{p}_j \;-\; \frac{\alpha\,Z}{r_i} \left( \boldsymbol{\alpha}_i \;+\; \frac{(\boldsymbol{\alpha}_i \cdot \mathbf{r}_i)\, \mathbf{r}_i}{r_i^2} \right) \cdot \mathbf{p}_j \right]$$

- The expectation value of $\mathbb{H}^{\,(\mathrm{recoil})}(M)$ with regard to the relativistic wave function from $\mathbb{H}^{\,(\mathrm{DCB})}$ gives the recoil correction to the energy of the atomic energy $|\alpha \mathbb{J}\rangle$ in first order of $m/M$ .

- Decomposition of the relativistic recoil Hamiltonian: Similar as in the non-relativistic theory, the (relativistic) recoil operator above can be written as (Tupitsyn *et al.*, 2003; Gaidamauskas *et al.*, 2011)

$$\begin{aligned}
\mathbb{H}^{\,(\mathrm{recoil})}(M) \;&=\; \mathbb{H}^{\,(\mathrm{NMS,\,relativistic})} \;+\; \mathbb{H}^{\,(\mathrm{SMS,\,relativistic})} \\
&=\; \frac{1}{2\,M} \sum_{i} \left[ \mathbf{p}_i^2 \;-\; \frac{\alpha\,Z}{r_i} \left( \boldsymbol{\alpha}_i \;+\; \frac{(\boldsymbol{\alpha}_i \cdot \mathbf{r}_i)\, \mathbf{r}_i}{r_i^2} \right) \cdot \mathbf{p}_i \right] \;+\; \frac{1}{2\,M} \sum_{i \neq j} \left[ \mathbf{p}_i \cdot \mathbf{p}_j \;-\; \frac{\alpha\,Z}{r_i} \left( \boldsymbol{\alpha}_i \;+\; \frac{(\boldsymbol{\alpha}_i \cdot \mathbf{r}_i)\, \mathbf{r}_i}{r_i^2} \right) \cdot \mathbf{p}_j \right] \\
&=\; \frac{1}{2\,M} \sum_{i} \left[ \mathbf{p}_i^2 \;-\; \frac{\alpha\,Z}{r_i}\, \boldsymbol{\alpha}_i \cdot \mathbf{p}_i \;-\; \frac{\alpha\,Z}{r_i}\, (\boldsymbol{\alpha}_i \cdot \mathbb{C}_i^{(1)})\, \mathbb{C}_i^{(1)} \cdot \mathbf{p}_i \right] \;+\; \frac{1}{2\,M} \sum_{i \neq j} \left[ \mathbf{p}_i \cdot \mathbf{p}_j \;-\; \frac{\alpha\,Z}{r_i}\, \boldsymbol{\alpha}_i \cdot \mathbf{p}_j \;-\; \frac{\alpha\,Z}{r_i}\, (\boldsymbol{\alpha}_i \cdot \mathbb{C}_i^{(1)})\, \mathbb{C}_i^{(1)} \cdot \mathbf{p}_j \right] \\
&=\; \mathbb{H}^{\,(\mathrm{NMS})} \;+\; \mathbb{H}^{\,(\mathrm{SMS,\,A})} \;+\; \mathbb{H}^{\,(\mathrm{SMS,\,B})} \;+\; \mathbb{H}^{\,(\mathrm{SMS,\,C})}
\end{aligned}$$

- The relativistic correction to the recoil effect is typically strongly overestimated if the nonrelativistic recoil operator is applied just together with relativistic wave functions.

- The full relativistic theory of the nuclear recoil effect can be formulated only within the framework of quantum electrodynamics. Such a theory was first formulated by Shabaev (1985), where the complete $\alpha\,Z$ -dependence of the recoil corrections to an energy level $|\alpha\,\mathbb{J}\rangle$ was derived in first order of $m/M$ .

## Reduced one-electron matrix elements of the recoil (Hamilton) operator:

- Recoil Hamiltonian: While the normal mass-shift Hamiltonian is a one-particle operator, the specific mass-sift is a (symmetric) two-particle operator

$$\mathbb{H}^{(\mathrm{NMS})} = \sum_j \mathbb{h}^{(\mathrm{NMS})}(\mathbf{r}_j), \qquad \mathbb{H}^{(\mathrm{SMS,\,k})} = \sum_{i\neq j} \mathbb{h}^{(\mathrm{SMS,\,k})}(\mathbf{r}_i, \mathbf{r}_j) = \sum_{i\neq j} g(r_i, k)\, g(r_j, k) \left( \mathbb{T}_i^{(1)} \cdot \mathbb{T}_j^{(1)} \right), \qquad k = A, B, C$$

  The particular tensorial structure of the two-particle specific mass-shift Hamiltonian ensures that the reduced (one-electron) matrix elements can be expressed in terms of the first-rank effective interaction strength $X^{(1;\,\mathrm{SMS,\,k})}$ that are specified below for $k = A, B, C$.

- Reduced one-electron matrix element for the normal mass-shift: With the definition of the angular coefficients in Grasp, this one-electron matrix element is given with $P' = \frac{\partial P}{\partial r}$ (Gaidamauskas *et al.*, 2011)

$$\left\langle a \left\| \mathbb{h}^{(\mathrm{NMS})} \right\| b \right\rangle = \delta_{\kappa_a, \kappa_b} \frac{1}{2M} \int_0^\infty dr \left( \frac{P_a' P_b' + Q_a' Q_b' + \ell_b (\ell_b + 1) P_a P_b + (2j_b - 1)\, 2j_b\, Q_a Q_b}{r^2} \right.$$

$$\left. - (2\alpha Z) \frac{Q_a P_b' + Q_b P_a'}{r} - (\alpha Z) \left( \frac{\kappa_b - 1}{r^2} \right) (Q_a P_b + Q_b P_a) \right)$$

## Parametrization of the isotope shift:

- Mass shift of two isotopes: Within lowest order of $m/M$, the (isotope) mass shift for an atomic level $|\alpha\, \mathbb{J}\rangle$ is determined by the difference of the expectation values of $\mathbb{H}^{(\mathrm{recoil})}(M)$ for two different isotopes:

$$\Delta E^{(\mathrm{MS})}(M, M') = \left\langle \alpha\, \mathbb{J} \left| \mathbb{H}^{(\mathrm{recoil})}(M) - \mathbb{H}^{(\mathrm{recoil})}(M') \right| \alpha\, \mathbb{J} \right\rangle = \frac{M' - M}{M\, M'} K^{(\mathrm{MS})}$$

$$\frac{K^{(\mathrm{MS})}}{M} = \left\langle \alpha\, \mathbb{J} \left| \mathbb{H}^{(\mathrm{recoil})}(M) \right| \alpha\, \mathbb{J} \right\rangle = \left\langle \alpha\, \mathbb{J} \left\| \mathbb{H}^{(\mathrm{recoil})}(M) \right\| \alpha\, \mathbb{J} \right\rangle,$$

  and where the Wigner-Eckardt theorem is used here in a special form that is consistent with Grasp and that is utilized for the implementation of corresponding angular coefficients.

- The conversion factor between the mass-shift parameters $K^{(\mathrm{MS})}$ in the frequently applied units is:
  $K^{(\mathrm{MS})}/[\mathrm{GHz\,u}] = 3609.4824\, K^{(\mathrm{MS})}/[\mathrm{a.u.}]$.

- Field shift of two isotopes: is caused by their different nuclear charge distributions and can be parametrized by:

$$\Delta E^{(\mathrm{FS})}(M, M') = - \left\langle \alpha \, \mathbb{J} \left| \sum_{j=1}^{N} \left( \mathbb{V}^{(\mathrm{nuc})}(r_j; R') - \mathbb{V}^{(\mathrm{nuc})}(r_j; R) \right) \right| \alpha \, \mathbb{J} \right\rangle = \left\langle \alpha \mathbb{J} \left\| \sum_{j=1}^{N} \delta \, \mathbb{V}^{(\mathrm{nuc})}(r_j; \, R', R) \right\| \right\rangle = -F \, \delta \left\langle r^2 \right\rangle$$

$$F = \frac{\left\langle \alpha \, \mathbb{J} \left| \sum_j \left( \mathbb{V}^{(\mathrm{nuc})}(r_j; R') - \mathbb{V}^{(\mathrm{nuc})}(r_j; R) \right) \right| \alpha \, \mathbb{J} \right\rangle}{R' - R}$$

where $\delta \left\langle r^2 \right\rangle = R' - R$ is the difference of the *root-mean-square* (rms) charge radii of the two isotopes with masses $M', \; M$ .

### 6.1.d. Atomic form & scattering factors and scattering functions (`FormFactor`)

## Properties, notations & application:

- Form factor $F(q; \, \alpha \, \mathbb{J})$ of an atomic level with spherical-symmetric charge distribution:.
- Formal quantum notation: $F^{\,(\mathrm{standard})}(q; \, \alpha \, \mathbb{J}), \; F^{\,(\mathrm{modified})}(q; \, \alpha \, \mathbb{J})$ .
- Using JAC: Perform an `Atomic.Computation(.., properties=[FormF, ..], configs=[..], formSettings= FormFactor.Settings(..), ..)` or call directly functions from the module `FormFactor`.
- In JAC, the standard and the modified form factors are calculated and tabulated for all selected levels and for all the specified $q$-values [in a.u.] in `FormFactor.Settings`; the default values are $q = 0.1, \, 1., \, 10.$

## Further remarks:

- Atomic form factor (known also as atomic scattering factor): These form factors are often taken as a measure of the (scattering) amplitude for the scattering of some incident quantum wave by an isolated and spherical symmetric atom.
- In practice, therefore, the atomic form factor depends on the type of scattering, being elastic or inelastic, as well as on the incident radiation, such as photons, electrons or neutrons. As usual, we here restrict ourselves to the atomic form factor for photon (x-ray) scattering.

- The atomic form factor is often written as function of the momentum transfer $q \;=\; |\mathbf{q}|$ , and this momentum transfer is directly related to the scattering angle by: $\hbar\, q \;=\; 2k\, \sin(\vartheta/2) \;=\; \frac{2}{\lambda}\, \sin(\vartheta/2)$ .
- Momentum-transfer variable: Instead of the momentum transfer $q$, many tabulations for x-ray scattering make use of the (so-called) momentum-transfer variable $x \;=\; [\sin(\vartheta/2)] \,/\, \lambda\,[\mathrm{A}]$ with $\lambda\,[\mathrm{A}] \;=\; 12.398520/E\,[\mathrm{keV}]$.
- Elastic scattering of photons by atoms, ions or molecules has been found important in many fields of physics, such as crystallography, plasma physics and astrophysics. For high-photon energies (well above the K-shell threshold energy of the atom or ion), the form factor (FF) or modified form factor (MFF) approximations are widely used and were found moderately succesful in estimating the scattering cross sections. However, both form factor approximations fail at smaller photon energies.

## Definition of atomic form factors:

- Standard atomic form factor: For an atom in the level $|\alpha\, \mathbb{J}\rangle$ with a spherically-symmetric charge distribution $\rho(r)$ , the standard atomic form factor is given by

  $$F^{\,(\mathrm{standard})}(q;\, \alpha\, \mathbb{J}) \;=\; 4\pi \int dr\; r^2\; \rho(r)\; \frac{\sin(qr)}{q\,r} \;=\; \left\langle \alpha\, \mathbb{J} M \,\middle|\, \mathbb{T}^{(1)}(\mathbf{q}) \,\middle|\, \alpha\, \mathbb{J} M \right\rangle$$

  is just equal to the Fourier transform of the charge density $\rho(r)$ , if this density is normalized by $4\pi \int dr\; r^2 \rho(r) \;=\; N$ to the number of bound electrons.
- This standard form factor can be expressed also as (many-electron) expectation value of the (one-electron) momentum-transfer operator $\mathbb{T}^{(1)}(\mathbf{q}) \;=\; \sum_{j=1}^{N}\, \exp(i\, \mathbf{q} \cdot \mathbf{r}_j\,)$ for a given sublevel $|\alpha\, \mathbb{J} M\rangle$ , see above.
- Modified atomic form factor: For an atom or ion with a spherically-symmetric charge distribution, a modified atomic form factor can be defined via the charge distributions of the individual (sub-) shells or elements

  $$F^{\,(\mathrm{modified})}(q; \alpha\, \mathbb{J}) \;=\; 4\pi \sum_{i=1}^{N} \int dr\; r^2\; \rho_i(r)\; \frac{\sin(qr)}{q\,r}\; \frac{mc^2}{\varepsilon_i' \,-\, V(r)}$$

  where $\rho_i(r)$ is the charge density of the $i$-th electron, $\varepsilon_i' \;=\; \varepsilon_i \,+\, mc^2$ its energy (including the rest mass), and $V(r)$ the potential of the electron at position $r$ . Here, the summation is taken over all electrons, and the charge distribution must fullfill again the constraint that $4\pi\, \sum_i \int dr\; r^2 \rho_i(r) \;=\; N$ is equal to the number of bound electrons.

- Generalized atomic form factor: A generalized form factor can be defined for any pair of states, often take for the ground state $|\alpha_o\, \mathbb{J}_o M_o\rangle$ and some excited state $|\alpha_e\, \mathbb{J}_e M_e\rangle$

  $$F^{\,\mathrm{(generalized)}}(q;\; \alpha_e\, \mathbb{J}_e M_e; \alpha_o\, \mathbb{J}_o M_o) \;=\; \left\langle \alpha_e \mathbb{J}_e M_e \left| \, \mathbb{T}^{(1)}(\mathbf{q}) \, \right| \alpha_o\, \mathbb{J}_o M_o \right\rangle \,.$$

  This generalized atomic form factor help describe inelastic scattering processs and is closely related also to the generalized oscillator strength, cf. Section 7.3.f

## Anomalous scattering factors $g',\, g''$ :

- Anomalous scattering factor: The real $g'(\omega)$ and imaginary $g''(\omega)$ anomalous scattering factors are frequently employed in order to express the coherent (Rayleigh) scattering factor $G(\omega)$ , for incident photons with energy $\hbar\omega$ .
- Rayleigh scattering factor: For the photon energy $\hbar\omega$ , the coherent (Rayleigh) scattering factor in forward direction can be written fas (Zhou *et al.*, 1990)

  $$G(\omega) \;=\; F(0) \;+\; g'(\omega) \;+\; i\, g''(\omega)$$

  where $F(0) \;=\; N$ is the atomic form factor. Therefore, the (Rayleigh) scattering factors/amplitude can be expressed also in terms of the standard (atomic) form factor (FF) or with regard to the modified form factor (MFF).

## Incoherent scattering function $S(\mathbf{q})$ :

- Incoherent scattering function: This scattering function can be expressed by means of the generalized atomic form factor

  $$S(\mathbf{q}; \alpha_o \mathbb{J}_o M_o) \;=\; \sum_{e \,\neq\, o} |F^{\,\mathrm{(generalized)}}\,(q;\; \alpha_e \mathbb{J}_e M_e; \alpha_o \mathbb{J}_o M_o)|^2 \;=\; \left\langle \alpha_o \mathbb{J}_o \left| \, \mathbb{T}^{(2)}(\mathbf{q}) \, \right| \alpha_o \mathbb{J}_o \right\rangle \;-\; |F^{\,\mathrm{(standard)}}(q; \alpha_o \mathbb{J}_o)|^2 \,.$$

  Here, the sum over $e$ includes a summation over all discrete levels and the integration over the continuum. In the second expression, the two-electron momentum-transfer operator $\mathbb{T}^{(2)}(\mathbf{q}) \;=\; \sum_{m,n=1}^{N} \,\exp[i\, \mathbf{q} \cdot (\mathbf{r}_m \;-\; \mathbf{r}_n)]$ need to be applied, although then only matrix elements are necessary with regard to the ground state $|\alpha_o \mathbb{J}_o M_o\rangle$ .

## 6.2. In JAC partly-implemented level properties

### 6.2.a. Energy shifts in plasma environments (`PlasmaShift`)

### Properties, notations & application:

- Plasma shift of an atomic level: $E(\alpha\mathbb{J}) \quad \longrightarrow \quad E(\alpha\mathbb{J};\, \text{plasma model and parameters})\ .$
- Formal quantum notation: $\Delta\, E^{\,(\text{plasma})}(\alpha\mathbb{J}) \;=\; E(\alpha\mathbb{J};\, \text{plasma model and parameters}) \;-\; E(\alpha\mathbb{J};\, \text{unperturbed})\,.$
- Using JAC: Perform an `Atomic.Computation(.., properties=[Plasma, ..], configs=[..], plasmaSettings= PlasmaShift.Settings(..), ..)` or call directly functions from the module `PlasmaShift`.
- In JAC, the plasma (energy) shifts are calculated and tabulated by default for a Debye-Hückel plasma model with screening parameter $\lambda = 1$. Hereby, the Debye-Hückel interaction is incorporated only in first-order perturbation theory within the CI matrix.

### Further remarks:

- Spectral line shifts: The interaction between the plasma and the bound electrons of an ion embedded into the plasma alters the ionic structure and transition properties. Therefore, a plasma environment generally results in spectral line shifts, line broadening and changes in the line shapes, when compared with the free ion.
- For realistic plasma conditions, the number of bound states of the ions often becomes finite and the electrons less tightly bound by the nucleus, if the plasma coupling parameter increases.

### High-density plasma:

- Relativistic corrections to the plasma screening may become necessary for a detailed analysis of atomic spectra, especially if lines of multiply-charged ions are used in some spectral analysis.
- Collisional-radiative model: The effects of the plasma-environment can be further taken into account also by kinetic *or* collisional-radiative models, and where the energy shifts are often introduced by semi-empirically formul, such as the formula by Stewart and Pyatt.

- Application of simple plasma models: Apart from plasma diagnostics, a proper treatment of a screening potential has been found useful also in other areas of physics, such as nuclear and elementary particle physics, solid state physics, or even the design of nanostructures.
- Strongly-coupled plasma: For a strongly-coupled *dense* plasma the (averaged) electrostatic energy between neighbouring particles in the plasma exceeds their thermal energy. The coupling parameter $\Gamma = q^2/4\pi\epsilon_0 R_0\, kT > 1$ is used in order to characterize such a strongly-coupled plasma. This coupling parameter $\Gamma$ simply describes the ratio of the electrostatic and the thermal energy of the plasma particles.
- Strongly-coupled plasma obeys classical statistics and has been observed for a large number of experimental and astrophysical conditions. In the laboratory, for instance, laser-induced plasma with $\Gamma \gg 1$ has been investigated in high-compression fusion experiments. Such a laser-produced plasma provides a very typical example of a high-density, strongly-coupled plasma with electronic densities well beyond $10^{24}$ cm$^{-3}$.
- Theoretical (plasma) models for hot and dense plasma are necessary to simulate its properties, such as the equations of state, radiative transfer coefficients or the conduction coefficients in plasma. These properties are relevant for inertial confinement fusion and astrophysics.

## Frequently applied plasma models in atomic structure calculations:

- Debye-Hückel model: This model has been commonly used in order to incorporate plasma effects into atomic structure calculations. However, the validity of this model is rather questionable because it is valid only when the *correlation* time of the ion is much longer than the lifetime of excited atomic states. Therefore, this perturbative approach is at best valid for weakly-coupled plasmas and should not be applied for modeling of high-density plasmas.
- Coulomb interaction in the Debye-Hückel model: In this model, the (pairwise) Coulomb interaction among the charged particles is modified (screened) for an ion with nuclear charge $Z$ to

  $$V^{\,\rm (DH)}(r,\,\lambda) \;=\; -\sum_i^N \frac{Ze^{-\lambda\, r_i}}{r_i} + \sum_{i>j}^N \frac{e^{-\lambda\, r_{ij}}}{r_{ij}} \;=\; \sum_i^N V^{\,\rm (e-n,\, DH)}(r_i,\,\lambda) \,+\, \sum_{i>j}^N V^{\,\rm (e-e,\, DH)}(r_{ij},\,\lambda).$$

  Here, $N$ is the number of bound electrons in the ion, $r_i$ is the distance of the $i$-th electron from the nucleus, and $r_{ij}$ the distance between the electrons $i$ and $j$.
- Plasma screening parameter $\lambda$: This parameter is the inverse of the Debye shielding length for a certain plasma environment and can be

readily expressed in terms of the electron density $n_e$ and the temperature $T_e$ of the plasma:

$$\lambda \;=\; \left[\frac{4\pi\, n_e}{k\, T_e}\right]^{\frac{1}{2}} .$$

- Debye-Hückel model: To obtain the modified two-particle integrals due the plasma screening, we can write

$$V^{\,(\mathrm{e-e,\,DH})}(r_{ij}, \lambda) \;=\; -\lambda \sum_{l=0}^{\infty} (2l+1)\; j_l(i\lambda\, r_<)\; h_l^1(i\lambda\, r_>)\; P_l(cos\theta)$$

  in terms of the *larger* ($r_> = \max(r_i, r_j)$) and *smaller* radii ($r_< = \min(r_i, r_j)$) of the one-particle radii $r_i$ and $r_j$, respectively, and where $j_l$ denotes a spherical Bessel function and $h_l^1$ a Hankel function of the first kind.

- Debye-Hückel model: While the Debye-Hückel screening in the 'electron-nucleus' interaction usually destabilizes the binding of the electron, the screening of the electron-electron repulsion counteracts this trend.

- Ion-sphere model: In this model, the ion is typically enclosed in a spherically symmetric cell that contains the exact number of electrons in order to ensure neutrality. In the ion-sphere model, one needs to define an electron-density distribution that either obeys self-consistency equations or need to make some simple hypothesis, such as an uniform density within the cell.

- In practice, the ion-sphere model has been extensively used only in its simplest form, in which the free-electron density exactly cancels the ion densities outside of the Wigner-Seitz sphere, i.e. beyond the ion-sphere radius.

## Free-electron distributions in plasma:

- In a plasma, the free-electron (radial) density $n_e(r)$ can follow different distributions:

- Maxwell-Boltzmann distribution: The Maxwell-Boltzmann statistics has been often applied to describe the free-electron distribution but is not well justified for high plasma densities or low plasma temperatures.

- Fermi-Dirac distribution: This distribution is preferable if the free electrons are degenerate

$$n_e(r) \;=\; \frac{4}{\sqrt{\pi}} \int_{r_o}^{\infty} dr\, \frac{\sqrt{r}}{e^{r\,-\,r_o\,-\,\mu/k\,T_e} + 1} \;=\; 2\,\lambda_{\mathrm{th}}^{-3}\, \mathcal{F}_{1/2}\left(-\frac{V(r)}{k\,T_e} + \frac{\mu}{k\,T_e};\, -\frac{V(r)}{k\,T_e}\right) .$$

  Here $\mu$ is the chemical potential of the plasma, $\mathcal{F}_{1/2}(x,y)$ the incomplete Fermi-Dirac integral and $\lambda_{\mathrm{th}} = \sqrt{2\pi\,/\,k\,T_e}$ the thermal de-Broglie thermal wavelength.

- Uniform electron-gas distribution: This distribution considers a sphere of radius $\mathbf{R}_0$ around the ion with $N_b$ bound electrons, in which the ionic charge is completely neutralized by the additional $N_f = Z - N_b$ *free* electrons. Although all electrons inside of the sphere will strongly interact with the embedded ion, the free electrons are here assumed to be distributed uniformly. With this assumption in mind, the electrostatic potential for the $i$-th bound electron with radial coordinate $r_i$ is given by

$$V^{\,\rm (IS)}(\mathbf{r}_i; \mathbf{R}_0) \;=\; \begin{cases} -\frac{Z}{\mathbf{r}_i} + \frac{Z-N_b}{2R_0}\left[3 - \left(\frac{\mathbf{r}_i}{\mathbf{R}_0}\right)^2\right] & \text{for} \quad \mathbf{r}_i \le \mathbf{R}_0 \\ 0 & \text{for} \quad \mathbf{r}_i > \mathbf{R}_0\,. \end{cases}$$

  In this potential above, the first term describes the interaction of the bound electron with the nucleus, while the second (repulsive) term arises from the plasma background and always causes a shift of all the level energies towards the continuum.

## Gordon-Kim theory:

- In the Gordon-Kim theory (1972), the total energy of the system consists out of the direct Coulomb potential energy, the exchange Coulomb potential energy, the kinetic energy as well as the correlation energy. The direct Coulomb potential energy is calculated by integrating the Coulomb potential for the (approximated) electron density, while the other contributions to the total energy were calculated by using a temperature-dependent local density functional (LDA) approach.

### 6.2.b. Lande $g_J$ factors and Zeeman splitting of fine-structure levels (`LandeZeeman`)

## Properties, notations & application (not yet fully implemented):

- Zeeman splitting of an atomic level into Zeeman (sub-) levels: $|\alpha \mathbb{J}\rangle \quad \longrightarrow \quad |\alpha\, \mathbb{J} M\rangle\,, \qquad M \;=\; -J, ..., J-1, +J$ .
- Formal quantum notation: $|\alpha \mathbb{J} M\rangle$ .
- Using JAC: Perform an `Atomic.Computation(.., properties=[LandeJ, ..], configs=[..], zeemanSettings= LandeZeeman.Settings(..), ..)` with `calcLandeJ=true` or call directly functions from the module `LandeZeeman`.
- In JAC, we calculate and tabulate by default the Lande $g_J \equiv g(\alpha\mathbb{J})$ factors for the selected fine-structure levels.

- In the JAC program, the Zeeman amplitudes $\langle \beta_r \mathbb{J}_r \| \mathbb{N}^{(1)} \| \beta_s \mathbb{J}_s \rangle$ and $\langle \beta_r \mathbb{J}_r \| \Delta\, \mathbb{N}^{(1)} \| \beta_s \mathbb{J}_s \rangle$ can be obtained from the function `Jac.LandeZeeman.amplitude()`.

## Further remarks:

- The Zeeman effect describes the (level) splitting of an atomic level $|\alpha \mathbb{J}\rangle$ into its sub-levels $|\alpha \mathbb{J} M\rangle$ in the presence of a static magnetic field.
- The various components $|\alpha\, \mathbb{J} M\rangle$ of a Zeeman-splitted line usually have different intensities, and with some of them possibly even forbidden within the dipole approximation.
- The energy splitting of the Zeeman sub-levels depends of course on the magnetic field strength. — Therefore, the Zeeman effect has be applied for measuring magnetic field strengths, e.g. in astrophysics at the surface of the Sun or in laboratory plasmas.

## Zeeman Hamiltonian $\mathbb{H}^{(\mathrm{mag})}$:

- If the $z$-axis is chosen along the magnetic field $\mathbf{B} \,||\, \mathbf{e}_z$ and if we neglect diamagnetic contributions, the magnetic (Zeeman) Hamiltonian can be written in terms of spherical tensors (Andersson and Jönsson, 2008)

$$\mathbb{H}^{(\mathrm{mag})} = \left( \mathbb{N}_0^{(1)} + \Delta\, \mathbb{N}_0^{(1,\,\mathrm{QED})} \right) B$$

$$\mathbb{N}^{(1)} = \sum_j^N \mathbb{n}^{(1)}(j) = \sum_j^N -i\, \frac{\sqrt{2}}{2\,\alpha}\, r_j \;\; \left( \boldsymbol{\alpha}_j\, \mathbb{C}^{(1)}(j) \right)^{(1)}$$

$$\Delta\, \mathbb{N}^{(1)} = \sum_j^N \Delta\, \mathbb{n}^{(1)}(j) = \sum_j^N \frac{g_s - 2}{2}\, \beta_j\, \boldsymbol{\Sigma}_j, \qquad\qquad \boldsymbol{\Sigma} = \begin{pmatrix} \boldsymbol{\sigma} & 0 \\ 0 & \boldsymbol{\sigma} \end{pmatrix},$$

and where the second term in the magnetic Hamiltonian above is (so-called) Schwinger's QED correction. Here, $g_s = 2.00232$ is the $g$-factor of the electron, including some leading QED corrections.

## Lande factor $g_J \;\equiv\; g(\alpha\mathbb{J})$ and Zeeman splitting of an electronic level $|\alpha\,\mathbb{J}\rangle$ :

- Zeeman splitting of an atomic level $|\alpha\mathbb{J}\rangle$ : If the energy splitting due to the magnetic field is small, when compared with the fine-structure splitting, it can be expressed in first-order perturbation theory by

$$\begin{aligned}
\Delta\, E^{\,(\mathrm{mag})}\,(\alpha\mathbb{J}M) \;&=\; E(\alpha\mathbb{J}M) \;-\; E(\alpha\mathbb{J},\, M=0) \\
&=\; \left\langle \alpha\, \mathbb{J}M \,\middle|\, \mathbb{N}_0^{(1)} \;+\; \Delta\, \mathbb{N}_0^{(1,\,\mathrm{QED})} \,\middle|\, \alpha\, \mathbb{J}M \right\rangle \;=\; (-1)^{J\,-\,M} \begin{pmatrix} J & 1 & J \\ -M & 0 & M \end{pmatrix} \sqrt{2J+1}\; \left\langle \alpha\, \mathbb{J} \,\middle\|\, \mathbb{N}^{(1)} \;+\; \Delta\, \mathbb{N}^{(1,\,\mathrm{QED})} \,\middle\|\, \alpha\, \mathbb{J} \right\rangle \; B \\
&=\; \frac{M}{\sqrt{J\,(J+1)}}\; \left\langle \alpha\, \mathbb{J} \,\middle\|\, \mathbb{N}^{\,(1)} \;+\; \Delta\, \mathbb{N}^{\,(1,\,\mathrm{QED})} \,\middle\|\, \alpha\, \mathbb{J} \right\rangle \; B
\end{aligned}$$

and with regard to the unperturbed energy $E(\alpha\mathbb{J},\, M=0) \;=\; E(\alpha\mathbb{J},\, B=0)$ .

- Lande $g_J$ factor of an atomic level $|\alpha\mathbb{J}\rangle$ : Usually, the dependence on the $M$ quantum number is factored out and the energy splitting is expressed for a single level $|\alpha\mathbb{J}\rangle$ in terms of its Lande factor $g_J \;\equiv\; g(\alpha\mathbb{J})$

$$\Delta\, E^{\,(\mathrm{mag})}\,(\alpha\mathbb{J}M) \;=\; g(\alpha\mathbb{J})\; M\, \frac{B}{2}, \qquad\qquad g(\alpha\mathbb{J}) \;\equiv\; g_{\mathbb{J}} \;=\; 2\; \frac{\left\langle \alpha\, \mathbb{J} \,\middle\|\, \mathbb{N}^{\,(1)} \;+\; \Delta\, \mathbb{N}^{\,(1,\,\mathrm{QED})} \,\middle\|\, \alpha\, \mathbb{J} \right\rangle}{\sqrt{J\,(J+1)}}$$

### 6.2.c. Lande $g_F$ factors and Zeeman splitting of hyperfine levels (`LandeZeeman`)

## Properties, notations & application (not yet fully implemented):

- Zeeman splitting of an atomic hyperfine level into Zeeman (sub-) levels: $|\alpha(J)\mathbb{F}\rangle \;\longrightarrow\; |\alpha\,(J)\mathbb{F}M\rangle\,, \qquad M \;=\; -F,\, ...,\, F-1,\, +F$ .
- Formal quantum notation: $|\alpha(J)\mathbb{F}M\rangle$ .

- Using JAC: Perform an `Atomic.Computation(.., properties=[LandeJ, ..], configs=[..], zeemanSettings= LandeZeeman.Settings(..), ..)` with `calcLandeF=true` or call directly functions from the module `LandeZeeman`.
- In JAC, we calculate and tabulate by default the Lande $g_F \equiv g(\alpha\mathbb{F})$ factors for the selected hyperfine-structure levels.

## Further remarks:

- The Lande $g$-factor (also kown as $g$ value or dimensionless magnetic moment) is a dimensionless entity that characterizes the gyromagnetic ratio of an atomic or hyperfine level. The Lande $g$-factor is basically a proportionality constant how efficient a particle, spin or quantum state with given total angular momentum $s$ contributes to the splitting in an external magnetic fiel $B$.

## Lande factor $g_F \equiv g(\alpha\mathbb{F})$ of an hyperfine level $|\alpha\,\mathbb{F}\rangle$ :

- Zeeman splitting of an hyperfine level $|\alpha\mathbb{F}\rangle$ : If the energy splitting due to the magnetic field is small, when compared with the hyperfine-splitting, it can be expressed in first-order perturbation theory in terms of the reduced electronic Zeeman amplitudes by

$$\begin{aligned}
\Delta\, E^{\,(\mathrm{mag})}\,(\alpha\mathbb{F}M) &= E(\alpha\mathbb{F}M) \;-\; E(\alpha\mathbb{F},\, M=0) \\
&= \left\langle (I,\,\alpha\,\mathbb{J})\,FM \,\middle|\, \mathbb{N}_0^{(1)} \;+\; \Delta\,\mathbb{N}_0^{(1,\,\mathrm{QED})} \,\middle|\, (I,\,\alpha\,\mathbb{J})\,FM \right\rangle \\
&= M\;\frac{F(F+1)\;+\;J(J+1)\;-\;I(I+1)}{2\,F(F+1)}\;\frac{\left\langle \alpha\,\mathbb{J} \left\| \mathbb{N}_0^{(1)} \;+\; \Delta\,\mathbb{N}_0^{(1,\,\mathrm{QED})} \right\| \alpha\,\mathbb{J} \right\rangle}{\sqrt{J(J+1)}} \\
&= M\;\frac{F(F+1)\;+\;J(J+1)\;-\;I(I+1)}{2\,F(F+1)}\;g(\alpha\mathbb{J})\;\frac{B}{2}\,,
\end{aligned}$$

  and expressed with regard to the unperturbed hyperfine energy $E(\alpha\mathbb{F},\, M=0) \;=\; E(\alpha\mathbb{F},\, B=0)$ .

- Lande factor $g_F \equiv g(\alpha\mathbb{F})$ and Zeeman energy splitting of an hyperfine level $|\alpha\mathbb{F}\rangle$ :

$$g(\alpha\mathbb{F}) \;=\; \frac{F(F+1)\;+\;J(J+1)\;-\;I(I+1)}{2\,F(F+1)}\;g(\alpha\mathbb{J}) \qquad\Longrightarrow\qquad \Delta\,E^{\,(\mathrm{mag})}\,(\alpha\mathbb{F}M) \;=\; g(\alpha\mathbb{F})\;M\;\frac{B}{2}$$

### 6.2.d. Sensitivity of level energies with regard to variations of $\alpha$ (`AlphaVariation`)

## Properties, notations & application (not yet fully implemented):

- Differential sensitivity parameter $\Delta\, q\, (\delta\alpha;\; \beta \mathbb{J})$ of an atomic level: For an atomic level $|\beta \mathbb{J}\rangle$ , the level energy depends of course on the fine-structure constant $\alpha$ . Therefore, an energy shift arises for any variation $\delta\alpha \;=\; \alpha - \alpha_o$ of the fine-structure constant and for a non-zero differential sensitivity parameter $\Delta\, q\, (\delta\alpha;\; \beta \mathbb{J})$ :

  $$\Delta\, E(\delta\alpha;\; \beta \mathbb{J}) \quad = \quad \Delta\, q\, (\delta\alpha;\; \beta \mathbb{J}) \left[ \left( \frac{\alpha}{\alpha_o} \right)^2 \;-\; 1 \right],$$

  and where $\alpha_o$ is the (current) reference value of the fine-structure constant.

- Formal quantum notation: $\Delta\, E(\delta\alpha;\; \beta \mathbb{J}), \quad \Delta\, q\, (\delta\alpha;\; \beta \mathbb{J}), \quad K(\beta \mathbb{J})$ .

- Using JAC: Perform an `Atomic.Computation(.., properties=[AlphaVar, ..], configs=[..], alphaSettings= AlphaVariation.Settings(..), ..)` or call directly functions from the module `AlphaVariation`.
- In JAC, we calculate and tabulate by default the differential sensitivity parameter $\Delta\, q\, (\delta\alpha;\; \beta \mathbb{J})$ and the enhancement factor $K(\beta \mathbb{J})$ for all selected levels.

## Further remarks:

- Fine-structure constant $\alpha$: The dimensionless constant $\alpha$ becomes dynamical, i.e. explicitly time-dependent, in a number of (quantum-field) theories that go beyond the standard model and general relativity.
- Search for variations of fundamental constants: This search is closely related to several, so-far still unexplained phenomena of the Universe, such as the nature of dark matter.
- From the individual level-dependent sensitivity parameters $\Delta\, q\, (\delta\alpha;\; \beta \mathbb{J})$ and enhancement factors $K(\beta \mathbb{J})$ , the analogue values for any atomic transition can be simply obtained by taking the sum of the corresponding level parameters.

- Experimentally, a variation of $\alpha$ are currently measured by monitoring for two ions the ratio of (two) clock frequencies with quite different values of $K$ .

## Enhancement and sensitivity of atomic levels with regard to variations of $\delta\alpha$ :

- Enhancement of energy shifts due to $\delta\alpha$ variations: The sensitivy of an atomic level energy $E(\beta\mathbb{J};\, \alpha)$ on $\delta\alpha$ can be re-written also in terms of the dimensionless enhancement factor $K \;=\; 2\,\Delta q / \,\Delta E$ as:

$$\frac{E(\beta\mathbb{J};\, \alpha) \;-\; E(\beta\mathbb{J};\, \alpha_o)}{E(\beta\mathbb{J};\, \alpha_o)} \;=\; K\, \frac{\alpha \;-\; \alpha_o}{\alpha_o} \;=\; K\, \frac{\delta\alpha}{\alpha_o}$$

- The reasons for $\delta\alpha$ variations can be of different type, such as temporal, spatial, slow drift, or of oscillatory nature, and it can depend on the gravity-potential or others reasons. The theoretical reasoning about such changes is typically outside of atomic theory.

### 6.2.e. Level-dependent fluorescence and Auger yields (`DecayYield`)

## Properties, notations & application (not yet fully implemented):

- Fluorescence *versus* Auger decay of an (excited) atomic level: $A^{q+*} \quad\longrightarrow\quad \left[ \begin{array}{l} A^{q+(*)} \;+\; \hbar\omega \\ A^{(q+1)+(*)} \;+\; e^-_a \\ \ldots \end{array} \right]$ .

  The corresponding level or configuration-averaged fluorescence and Auger yields just describe the fraction of atoms in a particular level or configuration that decay by fluorescence or Auger electron emission.

- Formal quantum notation: $|\alpha\mathbb{J}\rangle \quad\longrightarrow\quad \left[ \begin{array}{l} \{\; |\alpha_r \mathbb{J}_r\rangle \;+\; \hbar\omega\, (\{\mathbb{M}\}) \;\} \\ \{\; |\alpha_a \mathbb{J}_a\rangle \;+\; |\varepsilon\, \kappa\rangle \;\} \\ \ldots \end{array} \right]$ .

- Using JAC: Perform an `Atomic.Computation(.., properties=[Yields, ..], configs=[..], yieldSettings= DecayYield.Settings(..), ..)` or call directly functions from the module `DecayYield`.

- In JAC, we calculate and tabulate by default the fluorescence yields $\omega(\alpha\mathbb{J})$ and the Auger yields $a(\alpha\mathbb{J})$ for all selected levels.

## Further remarks:

- Fluorescence yields $\omega(\alpha\mathbb{J})$ : This yield typically represents the probability of an inner-shell (core) hole to be filled by some radiative decay process, in contrast and in competition with other nonradiative processes.
- Auger yields $a(\alpha\mathbb{J})$ : This yield desribes the (complementary) probability for an inner-shell hole level to decay by an non-radiative process, hence: $\omega(\alpha\mathbb{J}) + a(\alpha\mathbb{J}) = 1$ . The Auger yield is sometimes further partioned into an Auger and Coster-Kronig yield: $a(\alpha\mathbb{J}) = a^{(\mathrm{Auger})}(\alpha\mathbb{J}) + a^{(\mathrm{Coster-Kronig})}(\alpha\mathbb{J})$.
- In JAC, all computations of fluorescence and Auger yields are always based on single-step cascade computations within the configuration-average model, and where only the Coulomb interaction $\mathbb{V}^{(\mathrm{Coulomb})}$ is included into the evaluation of the Auger transition amplitudes and rates.
- More often than not, the fluorescence and Auger yields are determined for either $K$ - and $L$ -shell states (holes), and for which usually no distinction need to be made for different fine-structure levels $(\alpha\mathbb{J})$.
- Typically, it is completely sufficient to include only electric-dipole decay channels, although other multipoles can be defined explicitly in the computations.

## 6.3. Further properties, not yet considered in JAC

### 6.3.a. Approximate many-electron Green function for atomic levels (`GreenFunction`)

### Properties & notations:

- Green function of an atomic level: .

### 6.3.b. Multipole polarizibilities (`MultipolePolarizibility`)

### Properties & notations:

- General multipole polarizibility of an atomic level: .
- Dynamic polarizibility of an atomic level: .

### Multipole polarizibilities:

- Frequency-dependent (multipole) polarizibilities are important in various fields of physics.
- The ac Stark shift of a clock transition, for example, is determined by the frequency-dependent electric-dipole polarizibilities of the clock states. The (so-called) magic wavelengths of a clock transition can be determined by finding the frequencies where the ac electric-dipole polarizabilities of the two clocks states are the same.
- Dynamic multipole (ac $2^L$-pole) polarizibility: of a level $|0\,\rangle$ is (Porsev *et al.*, 2018)

$$\alpha^{\,(\mathbb{M})}(\omega,\; \beta_o \mathbb{J}_o) \quad = \quad \frac{L+1}{L}\, \frac{2L+1}{[(2L+1)!!]^2}\, (\alpha\,\omega)^{\,2L-2} \; \sum_\nu \frac{(E_\nu - E_o)\quad \left| \left\langle \alpha_\nu \mathbb{J}_\nu \,\middle|\, \mathbb{T}^{\,(\mathbb{M})} \,\middle|\, \beta_o \mathbb{J}_o \right\rangle \right|^2}{(E_\nu - E_o)^2 \;-\; \omega^2}$$

where $\mathbb{T}^{\,(\mathbb{M})}$ is the corresponding multipole operator for E1, M1, ... transitions.

## Dynamic electric-dipole polarizibility:

- ➢ The (dynamic) electric-dipole polarizibility is defined as (Derivianko *et al.*, 1999)

$$\alpha^{(\mathrm{E1})}(i\,\omega,\; \beta_o \mathbb{J}_o) \;=\; \frac{2}{3} \sum_{\nu} \frac{E_\nu \,-\, E_o}{(E_\nu \,-\, E_o)^2 \,+\, \omega^2} \;\; \left| \langle \alpha\_\nu \mathbb{J}_\nu \,|\, \mathbf{R} \,|\, \beta_o \mathbb{J}_o \rangle \right|^2$$

and which includes for $\alpha^{(\mathrm{E1})}(\omega \,\equiv\, 0)$ the static electric-dipole polarizibility.

## Scalar and tensor polarizibility:

- ➢ The scalar polarizability of a level $\alpha\mathbb{J}$ in a light field at frequency $\omega$ can be expressed as the sum over intermediate states that are allowed by the electric-dipole selection rules (Safronova *et al.*, 2018)

$$\alpha_0(\omega) \;=\; \frac{2}{3\,(2J+1)} \sum_{k} \frac{(E_\nu \,-\, E_o)\;\; \langle \alpha_\nu \mathbb{J}_\nu \,\|\mathbb{D}\|\, \beta_o \mathbb{J}_o \rangle}{(E_\nu \,-\, E_o)^2 \,-\, \omega^2}\,,$$

and where the frequency $\omega$ of the incident light is assumed to be off resonance by at least several linewidths with regard to any of the intermediate levels $\{|\alpha_\nu \mathbb{J}_\nu\rangle\}$ .

- ➢ The expression for the tensor polarizability has a similar structure.

### 6.3.c. Dispersion coefficients

## Remarks & notations:

- ➢ Lennard-Jones model: This model refers to a mathematically simple potential for describing the interaction between a pair of neutral atoms or molecules. It was proposed first in 1924 by John Lennard-Jones.
- ➢ The long-range interactions between atoms and molecules play a prominent role especially in the low-energy and low-temperature collision experiments.

- Dispersion coefficients $C_n$: The interaction of atoms at large interatomic distances, for instance for cold gases in a cold traps, is usually described in terms of dispersion (van der Waals) coefficients $C_n$ .
- Alkaline-earth dimers: For two alkaline-earth atoms in their ground state, the long-range potential as function of the internuclear distance $R$ can be written as (Porsev and Derivianko, 2006)

$$V(R) \;=\; -\,\frac{C_6}{R^6} - \frac{C_8}{R^8} - \frac{C_{10}}{R^{10}} - \,....$$

## Atomic computation of dispersion coefficients:

- Atom-wall coefficient, $C_3$: For an atom in a spherically-symmetric ground state $|\psi_o\rangle \;=\; |\beta_o\, \mathbb{J}_o M_o\rangle$ , the dispersion coefficient $C_3$ of the Lennar-Jones interaction between an atom and a perfectly conducting wall is given by (Derivianko *et al.*, 1999)

$$C_3 \;=\; \frac{1}{4\pi} \int_0^\infty d\omega \;\; \alpha^{(\mathrm{E1})}(i\,\omega;\; \beta_o \mathbb{J}_o M_o) \;=\; \frac{1}{12}\, \langle \beta_o \mathbb{J}_o M_o \,|\, \mathbf{R}\cdot\mathbf{R} \,|\, \beta_o \mathbb{J}_o M_o \rangle\,, \qquad\qquad \mathbf{R} \;=\; \sum_{i=1}^{N} \mathbf{r}_i\,.$$

- Van-der-Waals coefficient, $C_6$: For an atom in a spherically-symmetric ground state $|\psi_o\rangle \;\equiv\; |\beta_o\, \mathbb{J}_o M_o\rangle$ , the dispersion coefficient $C_6$ of the Lennar-Jones interaction can be expressed as integral over the dynamic electric-dipole polarizibility (Derivianko *et al.*, 1999)

$$C_6 \;=\; \frac{3}{\pi} \int_0^\infty d\omega\, [\alpha^{(\mathrm{E1})}(i\,\omega;\; \beta_o \mathbb{J}_o M_o)]^2\,.$$

- Since the van-der-Waals coefficients $C_6$ contains the dipole matrix element to the fourth power, these dipole amplitudes must usually be calculated with high accuracy.
- Long-range interaction of two atoms: For two atoms $a$ and $b$ in spherical-symmetric ground states, $|\psi_a\rangle \;=\; |\beta_a\, \mathbb{J}_a M_a\rangle$ and $|\psi_b\rangle \;=\; |\beta_b\, \mathbb{J}_b M_b\rangle$ , the long-range interaction can be written as (Porsev and Derivianko, 2006)

$$V(R) \;=\; -\sum_{n=3} \frac{C_{2n}^{ab}}{R^{2n}}, \qquad\qquad C_{2n}^{ab} \;=\; \frac{(2n\,-\,2)!}{2\pi} \sum_{k=1}^{n-2} \frac{1}{(2k)!\,(2k')!} \int_0^\infty d\,\omega\; \alpha_k^{(\mathrm{E1})}(i\omega;\; \psi_a)\; \alpha_{k'}^{(\mathrm{E1})}(i\omega;\; \psi_b), \qquad\qquad k' \;=\; n\,-\,k\,-\,1,$$

and where $\alpha_k^{(\mathrm{E1})}(i\omega;\; \psi_c)$ is the $2^k$ -pole dynamic (electric-dipole) polarizibility of each atom $c$ in its given state $|\alpha_c\, \mathbb{J}_c M_c\rangle$ .

## 6.3.d. Stark shifts and ionization rates in static electric fields

### Remarks & notations:

- LoSurdo-Stark effect: refers to the shifting and broadening of atomic and molecular states under the influence of an external electric field. (Dynamic) Stark shift: The dynamic Stark shift is caused by the interaction of an atom with the electro-magnetic field.
- Such a dynamic (time-dependent) Stark shift can be induced by a laser pulses but also by a single-photon wave packet.
- Keldish adiabacity parameter $\gamma_K$ : Different strong-field ionization mechanisms can be distinguished for different laser frequencies $\omega_L$ , (electric) field strength $E_o = |\mathbf{E}_o|$ as well as atomic ionization potentials $I_p$ . They are often distinguished by the Keldish adiabacity parameter, $\gamma_K = \omega \sqrt{2 I_p} / E_o$ .
- Multiphoton regime, $\gamma_K \gg 1$ : This regime is realized at high frequency and low or moderate field strength and gives rise to a a power law for the ionization rate, $\Gamma \propto E_o^n$ .
- Tunnel regime, $\gamma_K \ll 1$ : This regime occurs at low laser frequency and high-field strength and gives rise to an exponential dependence of $\Gamma$ on $E_o$ . In the tunnel regime, the ionization is often considered as a quasi-static process due to the low frequency, and the total ionization yield is obtained as integral over the time-dependent field strength:

$$A = 1 - \exp \left[ 1 - \int_{-\infty}^{\infty} dt \, \Gamma \left( E_o(t) \right) \right] .$$

- In the tunnel regime, atomic structure computation can provide reliable predictions for both, the Stark shifts in an (quasi-static) electric field as well as for the ionization rates.
- Ammosov-Delone-Krainov (ADK) formula: This formula for the ionization rate has often been used for many-electron atoms and has been extended also towards molecules.
- Quasi-static regime: For $\gamma_K \ll 1$ , one often further distinghuishes between the (tunnel ionization and the above-barrier ionization due to the (semi-classical) field strength $E^{\,(\rm above-barrier)} = I_p^2/4$ . From a simplified classical viewpoint, the electron can leave the atom without tunneling for $E_o > E^{\,(\rm above-barrier)}$ due to the suppression of the (atomic) Coulomb potential. In practice, however, this *barrier* is not sharp since an outgoing (scattered) electron is still partly reflected even for a classical suppressed barrier.
- (Quasi-) Static ionization rates: Within the tunneling regime, a variety of semiempirical expressions exist for the static ionization rates $\Gamma(E_o)$ . Many of them are based on Landau's seminal formula for the ionization rate of the hydrogen atom in its ground state, such as the ADK rule.

### 6.3.e. Dressed atomic (Floquet) states and quasi-energies in slowly varying laser fields

## Remarks & notations:

- Dressed atomic states: In a laser pulse of moderately varying intensity, the dressed states follow adiabatically the temporal evolution of the intensity during the passage of the pulse. The slow variation of the intensity then results into fairly slow changes in the (coefficients of the) superposition of the dressed states when compared with the optical period of the laser.
- Quasi-stationary wave function of dressed states: For sufficiently slow variations of the laser intensity, each dressed state can be written in the Floquet form, i.e. by means of a space-independent complex exponential *multiplied* by a time-harmonic function that oscillates with the same (optical) period as the incident field.
- Floquet equations: If the incident field is expanded in terms of a Fourier series, the time-dependent Schrödinger equation can be decomposed and re-written as a system of time-independent equations, the (so-called) Floquet equations. For multiphoton ionization, this system should be solved together with the radiation (Siegert) boundary conditions.
- The Floquet ansatz generally enables one to adopt the (time-independent) dressed-state approach to pulses with a sufficiently slowly varying field intensity, and where the time-dependence in captured by slow changes in the coefficients of the superposition.
- The (complex) eigenvalues of the Floquet equations provide both, the quasienergies of the dressed states and the resonance poles of the scattering amplitudes for laser-assisted scattering.
- The Floquet approximation is typically adequate for infrared laser pulses as well as for atoms in either the ground or some Rydberg level. It has been found inappropriate for UV laser frequencies and for low-lying excited levels because of avoided crossings between the dressed levels and large non-ponderomotive ac Stark shifts at suchhigh frequencies.
- The computation of the widths of quasi-energies often requires to go beyond first-order perturbation theory.
- Quasi-dressed states of atoms in a constant dc-field of constant intensity and frequency:quad The dressed states of atoms in a field of constant intensity and frequency refer to particular quasi-stationary solutions of the time-dependent Schrödinger equation.
- In atomic physics and if the laser pulses are neither ultra-intense nor ultra-short, these pulses can be modeled as a rapidly oscillating electric field but with a well-defined and slowly varying envelope (field amplitude). For such quasi-constant dc-fields, the behaviour of atoms can be described in terms of superpositions of dressed bound states that decay under the emission of photoelectrons.

## Neutral atoms in direct-current (dc) fields:

- Complex-eigenvalue Schrödinger equation: The system ”neutral atom + dc field” defines a rather complicated many-electron problem. Because of the (additional) time-dependent field, the discrete spectrum of the atom changes into a resonance spectrum whose states are obtained as solutions of a complex-eigenvalue Schrödinger equation

$$(H - z_o)\psi = 0, \qquad H = H^{(\mathrm{atom})} + \sum_i \mathbf{F} \cdot \mathbf{r}_i, \qquad z_o = E_o + \Delta(F) - \frac{i}{2}\,\Gamma(F)\,.$$

- Solution of the complex eigenvalue equation: This equation can be solved in terms of square-integrable function spaces, if the transformation $\rho = r\, e^{i\,\theta}$ is applied.
- This coordinate rotation for $\rho$ has been applied to the Hamiltonian operators for the computation of the LoSurdo-Stark ground-state resonance of hydrogen atoms, and the solution was achieved by direct diagonalization of the non-Hermitian Hamiltonian on a large square-integrable basis set. However, such a direct diagonalization of the the non-Hermitian Hamiltonian matrix is quite unrealistic for the decaying states of many-electron atoms and molecules.

### 6.3.f. Fano profiles of continuum-embedded resonances

## Remarks & notations:

- In physics, a Fano resonance generally refers to a resonant scattering process (phenomenon), and which gives rise to an asymmetric line-shape due to the interference between a constant background and a resonant scattering amplitude. Fano-type resonances can be found across many areas of physics and engineering because resonant scattering is a general wave phenomenon.
- In atomic physics, the background amplitude often arise from the direct (ionization) amplitude to the continuum, while the resonant amplitude arise from the (indirect) coupling of the atom to a discrete, localized state that is embedded into the continuum.

### 6.3.g. Light shifts of atomic levels

#### Remarks & notations:

- ➢ Light shifts for clock levels: The frequency of an atomic clock can be affected by (i) the thermal bath of blackbody radiation (BBR), (ii) the electric-quadrupole coupling of the ions to the trapping field and with other residual electro-magnetic fields, (iii) by ambient magnetic fields as well as (iv) through various Stark shifts (Yudin *et al.*, 2014).
- ➢ In highly-charged ions, the gross energy intervals nominally grow $\propto \tilde{Z}^2 \equiv (Z-N)^2$ as $\tilde{Z}$ increases. This leads to a substantial suppression of the ac-Stark and BBR shifts that are $\propto 1/\tilde{Z}^4$. Moreover, the quadrupolar moments of the bound-state electronic density scale with $1/\tilde{Z}^2$ and, this also reduces the quadrupolar shifts.

### 6.3.h. Frequency-dependent ac Stark shifts of atomic levels

#### Perturbative treatment of ac-Stark shifts $E_n(\omega)$:

- ➢ Atoms and ions in intense laser field: A perturbative description of the ac Stark shift of atoms in fields with intensity $I > 10^{13}$ W/cm$^2$ ) has been a subject of continuing concern.
- ➢ Although, perturbation theory is often considered inadequate for the analysis of multiphoton ionization experiments with atoms and ions, little is known about the breakdown of perturbation theoryt (Pan *et al.*, 1988). Nevertheless, a perturbative treatment of the many-electron atom in intense fields is still of interest for various scenarios and intensities.

### 6.3.i. Black-body radiation shifts

#### Remarks & notations:

- ➢ From radiation studies it is known that object emit radiation whose wavelength depends on its temperature.
- ➢ Black-body radiation shifts: More generally, the interaction with an environment at non-zero absolute temperature causes a level shift in the atom.

### 6.3.j. Hyperpolarizibility

## Remarks & notations:

- The hyperpolarizability of atoms refers to a nonlinear-optical property of matter and is closely related to the second-order electric susceptibility (per unit volume).
- Any accurate calculation of static hyperpolarizabilities is still a great challenge for atomic theory, and this even applies to simple atoms, such as lithium with only three electrons. As reported in the literature, both the choice of the basis set (grid) as well as the electronic correlations can have a large effects upon the (accuracy of the) computed hyperpolarizabilities
- Hyperpolarizibility of closed-shell atoms: For a neutral, closed-shell atom in its ground state $|\beta\, ^1S_0\rangle$ , the energy (level) shift in the presence of a homogeneous static electric field of strength $F$ is given by (Kassimi and Thakkar, 1994)

  $$E(F;\, \beta \mathbb{J}) \,-\, E_o \;=\; -\,\alpha\, \frac{F^2}{2!} \,-\, \gamma_2\, \frac{F^4}{4!} \,-\, \gamma_4\, \frac{F^6}{6!} \,-\, \gamma_6\, \frac{F^8}{8!} \,-\, ....,$$

  where $\alpha$ is the (static) dipole polarizibility and $\gamma_k,\;\; k \;=\; 2, 4, ...$ the hyperpolarizibility parameters of the atom.
- Induced dipole moment $\mu$: In the same field static field $F$, the dipole moment is then given by

  $$\mu(F;\, \beta \mathbb{J}) \;=\; \alpha\, F \,+\, \gamma_2\, \frac{F^3}{3!} \,+\, \gamma_4\, \frac{F^5}{5!} \,+\, \ldots .$$
- Finite-field procedure: In the computational procedure, the polarizabilities and hyperpolarizabilities are obtained from energy and/or dipole moment calculations of the atom in the presence of an electric fields of various strengths, and by using truncations of the given expansion above.

## 6.4. Other topics, related to atomic properties

### 6.4.a. Laser cooling, precision spectroscopy and quantum control

#### Quantum logic spectroscopy:

- ➢ Quantum logic spectroscopy: Quantum logic is typically implemented by the laser-induced coupling of the internal and external degrees of freedom of two ions, namely the spectroscopy and the logic ion. By making use of appropriate laser pulses, the information about the internal state of the spectroscopic ion can then be transferred from the spectroscopic to the logic ion.
- ➢ Such a quantum-logical transfer scheme can be realized with two ions in a linear Paul trap.
- ➢ Quantum-logic techniques: Many limitations of precision spectroscopy can be overcome if simple quantum-logic techniques are used and if the spectroscopic and logic ion is controlled together. In this technique, especially, the readily-controllable logic ion provides sympathetic cooling, internal state preparation and detection of the ion with an interesting spectroscopic transition.
- ➢ Simply speaking, the logic ion can be viewed as both, a remote control and a sensitive quantum sensor for the internal and external state of the spectroscopy ion.
- ➢ Quantum logic can also be used to laser-cool molecules to near their rotational and vibrational ground state by avoiding spontaneous emission of photons from the molecule.

#### Laser cooling and precision spectroscopy:

- ➢ Laser-cooling techniques: The recent development of laser-cooling techniques made cold and ultra-cold atomic samples available for optical spectroscopy. This development nowadays allowed for long interrogation times and significantly reduced Doppler shifts and gave eventually rise to an unprecedented uncertainty in atomic clocks, exceeding one part in $10^{-15}$ .
- ➢ In 1995, a controlled-NOT (CNOT) gate between a trapped atomic ion and its motional mode in the trap was first experimentally realized. Since then, the coherent control over the internal and external degrees of freedom in an atomic system has been demonstrated.
- ➢ In quantum information processing with trapped ions, precision spectroscopy has lead to new applications, such as teleportation, error-correction as well as the implementation of the Deutsch-Jozsa and semi-classical Fourier transformation algorithms.
- ➢ Internal *vs.* motional degrees of freedom: Laser spectroscopy helped develop methods to simultaneously control both, the internal electronic and motional degrees of freedom of individual atoms, molecules and singly-charged ions in traps with high accuracy.

- Most laser spectroscopy with clouds of trapped ions have explored a rather small class of atoms and atomic ions, including hydrogen, the alkali and alkaline-earth atoms and ions as well as few other species (Schmöger *et al.*, 2015). These atoms and ions have electronic transitions that are suited for laser cooling and that help localize the atoms for precision spectroscopy.
- Coulomb crystals: A signature for trapped and well-localized ions is the formation of Coulomb crystals, i.e. spatially ordered ensembles of mutually repelling ions that are confined in a common external trapping potential.
- Coulomb crystals form when the thermal kinetic energy becomes (much) smaller than the ion-ion electrostatic energy.
- Sympathetic cooling: If atoms and ions do not have a direct cooling transition, sympathetic cooling by use of co-trapped ions has been found a successful strategy in the past for singly and doubly charged atoms and molecules.

### 6.4.b. Atomic clocks

#### Search and application of atomic clocks:

- An atomic clock is typically based on an electron transition of either microwave, optical or ultraviolet frequency, and which serves as frequency standard for its time-keeping element.
- Atomic clocks are the most accurate time and frequency standards; they are frequnetly applid as primary standards for international time distribution services, to control the wave frequency of television broadcasts as well as the global navigation satellite systems such as GPS.
- While earlier atomic clocks were based on masers at room temperature, modern clocks are operated near to absolute zero temperature by probing an atomic fountains in a microwave-filled cavity. The NIST-F1 atomic clock, for example, one of the national primary time and frequency standards of the United States.
- Recent developments in the set-up and control of optical atomic clocks has improved their precision by a factor of 1000 in less than two decades.
- One particular goal in developing atomic clocks is to establish a clock with a high sensitivity to the variation of the fundamental fine-structure constant $\alpha$ .
- Applications of atomic clocks: Various applications of atomic clocks are now in reach or have already been realized by the improved precision and the high stability of thse clocks. These applications include: (1) the study of many-body physics and quantum simulations; (2) relativistic geodesy; (3) very long baseline interferometry; (4) searches for the variation of the fundamental constants; (5) searches for dark matter candidates; (6) tests of the Lorentz invariance and several others.

- These and further ideas and applications, such as the use of atomic clocks for gravitational wave detection, will require even more precise clocks in the future.

## Types of optical atomic clocks:

- There are currently two types of optical atomic clocks under development: (i) based on neutral atoms in optical lattices or (ii) based on a single trapped ion. For both types, a similar uncertainty have been reached, namely: $2.1 \times 10^{18}$ for a Sr neutral atom clock (Nicholson *et al.*, 2015) and $3.2 \times 10^{18}$ for a $Yb^+$ trapped ion clock (Huntemann *et al.*, 2016), that have been operated on a particular electric-octupole (E3) transition.
- Proposals for a Yb atomic clock: The $4f^{14}\,6s^2\;\; {}^1S_0 - 4f^{14}\,6s\,6p\;\; {}^3P_0$ transition in neutral Yb can be induced by hyperfine mixing in isotopes with nuclear spin $I \neq 0$ and has served already as some frequency standard. However, neutral Yb has still another and very interesting $4f^{14}\,6s\,6p\;\; {}^3P_0 - 4f^{13}\,6s^2\,5d\;\; (J = 2)$ electric-quadrupole (E2) transition at an easily accessible wavelength of 1695 nm, which might be suitable as well for the development of another frequency standard in this atom (Safronova *et al.*, 2018).
- ${}^{229m}$ Th clock: Thorium has one exceptional nuclear state that is known for the last 40 years and that has a very low energy of presumably below 10 eV. The currently assumed excitation energy of this isomeric state is $7.8 \pm 0.5$ eV, or correspondingly $159 \pm 11$ nm or $\sim 1900$ THz. This isomeric state conceptually allows for a direct laser excitation of the nucleus by using solid-state laser technology. This state has therefore been proposed for the development of a nuclear clock of extremely high stability owing to the expected high resilience against external influences and its radiative lifetime in the range of minutes to hours (von der Wense *et al.*, 2017).

### 6.4.c. Atomic partition functions

## Motivation:

- The atomic partition function $U(T)$ includes a summation over all bound levels of the atom and is defined as

$$U(T) \;=\; \sum_j g_j \, \exp\left( - \frac{E_i}{kt} \right) .$$

### 6.4.d. Atom-atom and atom-ion interaction potentials

## Motivation:

- Interatomic forces and potentials: Accurate interatomic potentials are of fundamental importance for understanding and modelling the static and dynamic properties of gases, liquids or even solids.
- In particular, a good knowledge of the interatomic forces in (closed-shell) molecules has been found a key for understanding the behavior of various systems, such as the geometry and stability of molecular solids, the properties of liquids and their phase transitions as well as collisions between molecules in gases or in molecular beams.
- While the theory of interatomic forces has been developed over the last four decades, fast and reasonably reliable predictions are still often not easily available, especially if a whole range of intermolecular separations need to be considered.
- While the scattering of charged particles has already a rather long history, collisions of ions and neutral particles at ultracold temperatures has emerged only recently as an exciting (new) field in AMO physics.
- Ion-atom interactions at cold temperatures: At cold temperatures of just a few Kelvin or even lower, ion-atom interactions are often affected by (i) rapid energy variations in the potentials as induced by long-range polarization contributions, (ii) the generally large number of contributing partial waves and (iii) a rather sensitive dependence of the interatomic interactions upon the details of the short-range potential. Further difficulties may arise from (iv) other weak interactions, such as hyperfine interactions and other.
- The standard numerical methods for dealing with intermolecular forces are often not only inefficient in addressing these difficulties but they sometimes even miss important physics, such as extremely narrow resonances.
- Ion transport coefficients in a gaseous environment: These coefficients can often be derived from the ion-neutral interaction potentials and such computations are now routine for atomic ion-atom systems.
- The (attractive) interatomic interaction is dominated by correlation or dispersion effects at large internuclear distances $R$, where perturbation theory gives rise to a series expansion $R^{-2n}$, $n \geq 3$. However, this perturbation series is known to be asymptotically divergent and is best truncated at its smallest term, following the work of Dalgarno and Lewis.
- Because of these difficulties, many accurate interatomic potentials have been determined experimentally by combining data from beam scattering experiments, virial and transport coefficient measurements as well as liquid and solid state properties. In practise, however, the interatomic potentials are still best probed in the intermediate regions.

## Gordon-Kim (1972) theory for atom-atom interactions:

- Gordon and Kim (1972) developed a model to calculate the interactions between closed-shell atoms, ions and molecules. In this model, the electron density of the system is taken as the sum of the two separate densities, and the non-Coulombic part of the interaction potential is calculated from this density by using energy expressions from the free-electron gas.
- Assumptions of the Gordon-Kim theory: Three basic assumptions were made by Gordon and Kim (1972):

  i) No rearrangement or distortion of the separate atomic densities occurs when the two atoms are brought together and, hence, the total electron density is just the sum of the two (spherically symmetric) atomic densities. This assumption neglects of course the rearrangement of the electron density and therefore restricts the theory to systems with a strong chemical bond, including covalent chemical bonds and to interatomic distances that are smaller than about half of the equilibrium separation.

  ii) The interatomic interaction can be evaluated from the combined atomic density, including the Coulomb interactions between all charges.

  iii) Gordon and Kim applied originally Hartree-Fock wave-functions in order to obtain the electron densities of the separate atoms, although other, and perhaps more accurate, wave functions should work as well.
- Total interaction of the two (atomic) charge distributions: The total energy includes the contributions from the kinetic, exchange and correlation energies as well as the (direct) Coulomb interactions energy. Below, we briefly summarize how these contributions can be calculated by juar using atomic wave functions.
- Apart from the Coulomb interaction of the two (atomic) charge distributions, the kinetic, exchange and correlation energy contributions to the total interaction energy are obtained from the electron density and the free-electron gas approximation.
- The regions around the nuclei (in which the density varies rather rapidly) do overall not contribute much to the interaction energy, even if they strongly affect the total energy. These contributions to the total energy cancel out if the atomic energies are substracted. Only the outer regions of the atoms, in which the atomic densities overlap, contribute significantly to the interaction energy. For these reasons, the uniform electron gas model should be reasonably accurate (Gordon and Kim, 1972).
- The rather simple Gordon-Kim potential have been used, for example, in the treatment of ionic compounds such as alkali-halide and alkaline-earth-dihalide molecules in order to predict (surprisingly) accurate molecular properties (Kim and Gordon, 1974). In this work, Gordon and Kim made the following two basic assumptions in addition to those assumptions already made for their pair potentials: (a) the systems are made of free ions; (b) the interactions of ions are pairwise additive, i.e. the total interaction is the sum of all the pair interactions, neglecting the many-body interactions.

## Perturbative methods:

- ➢ Different regions of the molecular potential curves have been investigated by different theoretical methods. Perturbation theory has been applied, in particular, to describe the long-range attraction, and where the first- and second-order perturbation energies are often approximated by just the first few terms in a multipole-series expansion of the Coulomb interaction between the molecules.
- ➢ Failure of perturbation theory: However, the perturbation method fails to desribe the potential at short and intermediate distances since it: (i) does not include exchange interactions between the electrons, (ii) diverges for strong interatomic interactions, and (iii) because a multipole expansion generally fails when the electron distributions overlap each other.
- ➢ At intermediate distances, i.e. in the region of the minimum of the intermolecular potential, only SCF computations typically predict the potentials reasonably well if the molecule does not form strong chemical bonds.

### 6.4.e. Dispersive interactions in liquid and solids

## Dispersive interactions in molecular-dynamics and Monte-Carlo simulations:

- ➢ Dispersive interactions: Dispersive forces and interactions in media often refer to contributions to the intermolecular interactions that arise from the polarization of one the atoms in the (fluctuating) instantaneous multipole field of other atoms. Therefore, dispersive interactions exist between each pair, triple, etc. of atoms or ions.
- ➢ Application of dispersive interactions: Apart from inert-gas or crystallized solids of various organic molecules, the dispersive interactions are small, though not negligible. Reasonable estimates of the magnitude of the dispersion interaction are therefore necessary for many solid-state studies, such as the cohesion of matter, the behaviour of ionic crystals, for molecular liquids, the adsorption on surfaces or in porous media (Pellenq and Nicholson, 1998).
- ➢ In Monte-Carlo and molecular-dynamics simulations, for example, a reasonable accurate potential energy function is required and need to be based on quantum-mechanical estimates, even if the dynamics of the particles is described classically.
- ➢ For dense-phase and solid-state systems, full quantum mechanical calculations of the interaction energy are generally not feasible and, hence, require to describe the interactions by means of inter-molecular or inter-ionic potentials; cf. section 6.4.d.

- Expressions for the dispersion coefficients can be derived from perturbation theory; however, the theory of inter-molecular interaction also shows clearly that the dispersive interactions in media are generally not pair-additive. Apart from the two-particle interactions, the three-body terms are known to play a significant role in the thermodynamics of condensed phases.

## Two-body dispersive interactions:

- Long-range dispersive interactions: If we consider two interacting neutral atoms, time-dependent perturbation theory gives rise to a long-range dispersive interaction due to charge fluctuations of the interacting species.
- Multipole expansion: For two spherically symmetric atoms or molecules $A$ and $B$, that are separated by a distance $R$, a multipole expansion is given by (Pellenq and Nicholson, 1998)

$$V^{\,(\mathrm{dispersion,\,AB})}(R) \;=\; -\left[\frac{C_6}{R_6} + \frac{C_8}{R_8} + \frac{C_{10}}{R_{10}} + \ldots\right].$$

- In this expansion, the dispersion coefficient $C_6$ describes the interaction between two instantaneous dipoles, $C_8$ the interaction between a quadrupole and a dipole and $C_{10}$ both, the interaction between an octopole and a dipole as well as between two quadrupoles.

## Three-body dispersive interactions:

- In the multipole expansion, the terms with triplets of species $A$, $B$ and $C$ are obtained from perturbation theory at the third and fourth orders. For such a triplet, the total dispersion energy is however non-additive:

$$V^{\,(\mathrm{dispersion})} \;=\; V^{\,(\mathrm{dispersion,\,AB})} + V^{\,(\mathrm{dispersion,\,BC})} + V^{\,(\mathrm{dispersion,\,CA})} + V^{\,(\mathrm{dispersion,\,ABC})} + \ldots$$

where $V^{\,(\mathrm{dispersion,\,ABC})}$ represents a sum of several terms describing the three-body interaction.

## 6.4.f. Transport coefficients for ion mobility and diffusion in gases

### Transport coefficients in gases:

- Ion-mobility spectrometry (IMS): The IMS is an analytical technique that is used to separate and identify ionized molecules in the gas phase, based on their mobility within a carrier buffer gas.
- IMS has been heavily employed for military or security purposes, such as detecting drugs and explosives, but also for the analysis of both small and large biomolecules.
- Ion mobility $K$: The ion mobility is defined as the proportionality factor between the drift velocity $v_d$ of the ions and the applied electric field $E$ : $v_d = K\, E$ . These ion mobilities are usually reported as reduced (ion) mobilities for a standard gas density $n_0$ , i.e. for standard temperature $T = 273$ K and pressure $p_o = 1013$ hPa.
- Ion mobilities also help in analysis of collision broadening in ion cyclotron resonance, the study of ion-molecule reactions as a function of electric field strength in flow-drift tubes, and especially the use of mobility data to test or determine ion-neutral interaction potentials.
- Since the reduced ion mobility just refers to the standard density, it is still temperature dependent $K_o = K \frac{n}{n_o} == K \frac{T_o}{T} \frac{p}{p_o}$ .
- Kinetic theory of ion mobility in neutral gases: Viehland and Mason (1978) present the first rigorous kinetic theory of ion mobility in neutral gases which is valid for electric fields of arbitrary strength and without restriction to the ion-neutral mass ratio or interaction potential. The results have proved useful in a number of applications: the calculation of low-field ion mobilities in high-temperature gases, if measurements as function of electric field strength were made before in low-temperature gases.

## 6.4.g. Polarizibility and optical absorbance of nanoparticles

### Optical properties of nanoparticles:

- Noble-metal nanoparticles with a size, that is comparable to the wavelength of the incident light, show characteristic colors owing to the strong absorption and scattering of light in the visible region.
- Localized surface plasmon resonance (LSPR). The LSPR are often explained as collective oscillation of free electrons in the nanoparticle that are induced by the electro-magnetic waves. Therefore, the color of the absorbed light can be tuned by the size, shape, materials as well as the surrounding environment of the nanoparticles, and with applications in chemistry, physics and biomedical fields.
- Nanoparticles with a size below 10 nm have an extremely high surface-to-volume ratios and, thus, substantially different optical properties when compared to large nanoparticles or the bulk material. These optical properties also depend on the atomistic structure.

### Methods for calculating the polarizibility of nanoparticles:

- The polarizability of a discretized medium is in general proportional to its volume.
- Polarizability of the i-th atom $\alpha_i$ : In a given nanoparticle, the polarizability of the i-th atom $\alpha_i$ can be approximated by multiplying the polarizability of the free atom $\alpha^{(\text{free})}$ with the relative volume (ratio), i.e. by dividing the effective volume $V^{(\text{eff})}$ by the volume of the free atom $V^{(\text{free})}$,

  $$\alpha_i = \frac{V^{(\text{eff})}}{V^{(\text{free})}} \alpha^{(\text{free})} = \frac{V^{(\text{eff})}}{V^{(\text{free})}} \frac{e^2}{m} \sum_n \frac{f_n}{\omega_n^2 - \omega^2 - i\,\omega\,\delta}$$

  where $\omega_n$ is the n-th absorption frequency, $f_n$ its oscillator strength and where the frequency shift $\delta$ depends on the coordination factor within the nanoparticle.
- Optical absorbance of nanoparticles: The optical absorbance of the nanoparticle is obtained from the total polarizability by

  $$\sigma^{(\text{absorption})} = \frac{4\pi\,\omega}{c} \Im\{\alpha^{(\text{total})}(\omega)\} = \frac{4\pi\,\omega}{c} \Im\left\{\sum_i^N \alpha_i^{(\text{SCF})}(\omega)\right\}$$

### 6.4.h. Laser-produced plasma

## Properties & applications of laser-produced plasma (LPP):

- Laser-produced plasmas (LPP) have attracted recent interest because of their use in developing laboratory ion sources and pulsed light sources at short wavelengths.
- In LPP, hot electrons can subsequently ionize the much cooler atoms, forming an x-ray-emitting, high-temperature plasma spark at the surface of the solid (Murnane *et al.*, 1991).
- The emitted x-rays from such a laser-produced plasma are generally incoherent but have a high brightness because of the small size, short lifetime and the high temperature of the radiating plasma.
- LPP have been proposed as source of both, x-rays and multiply-charged ions. Whereas x-ray sources aim for a high radiation loss from the plasma due to the generation of highly stripped atoms, such higher charge states of ions are mainly produced by a high plasma temperature and a low radiation level (loss).
- To determine the properties of a LPP, such as temperature, density or its radiation emission, one needs a proper model for the coupling of the laser light with the heavy element (solid-state) target.
- LPP will find applications in extreme ultraviolet (EUV) lithography, EUV metrology as well as in the modification of surfaces.
- LPP sources have been developed for x-rays in the water window, though with limited conversion efficiency and/or brightness so far. These plasmas can be used for novel microscope designs as well as for cell tomography.
- Scaling laws for LPP: Scaling laws predict that brighter and more efficient x-ray sources will be obtained if (more) intense laser pulses are employed. These sources can then be used for time-resolved x-ray scattering studies and for the development of x-ray lasers.
- Scaling laws for LPP: Simple arguments can be used to derive scaling laws predict the response of the LPP if the laser parameters are varied. If any hydrodynamic expansion is neglected during the interaction with the laser pulse, we can equate the incident heating flux to the cooling flux that occurs due to classical thermal conduction.
- Scaling laws can be used also to predict the radiation output from a LPP. For a short pulse of about 100 fs, the heat can penetrate for about 50 nm, and the hot radiating region can be considered as optically thin (Murnane *et al.*, 1991). Therefore, the Planck mean-free path $X$ of the radiation is much longer than the characteristic length $L$, and the plasma radiates as a diluted black body with power $P_r \;=\; A\,\sigma\,T^4\,L\,/\,\lambda$, and where $\sigma$ is the Stefan-Boltzmann constant and $A$ the radiating area.

## Ultrafast x-ray pulses from laser-produced plasma:

- A high-temperature plasma is created when an intense laser pulse is focused onto the surface of a solid (Murnane *et al.*, 1991). From such a plasma, an ultrafast pulse of x-ray radiation is emitted when the laser pulse length is less than about a picosecond.
- X-ray pulses with a duration of a picosecond or less have been observed, more than an order of magnitude shorter than those produced by any other x-ray source.
- A direct comparison of fast x-ray pulses from LPP with other x-ray sources is difficult; in general, however, LPP yield x-rays with much higher peak power but lower average power than synchrotrons and other high-average power sources such as rotating anode tubes.

## Ionization models for LPP:

- Collisional-radiative (CR) ionization model: A CR model can be applied to LPP with temperatures above a few tens of eV. At these temperatures, the average ionization stage $A^{q+}$ of a given element is dominated by the electron plasma temperature due to electron and photon-impact excitation and ionization processes.
- Indeed, two main types of excitation and ionization processes occur in LPP: collisional and radiative processes, and where the corresponding de-excitation and recombination refer to the same types of processes. The ionization-recombination equations for both processes are:

$$A^{(q-1)+} + e^- \longleftrightarrow A^{q+} + e_1^- + e_2^-, \qquad\qquad A^{(q-1)+} + \hbar\omega \longleftrightarrow A^{q+} + e_p^-.$$

- Ionization-recombination equation: In these ionization-recombination equations, one often only considers collisions with (free) electrons since these collisions are much more efficient than those with heavier particles. Obviously, these equations also neglect autoionization and its (inverse) dielectronic recombination.

## Deflagration models for LPP:

- Deflagration from the dictionary: Deflagration refers to an explosion in which the speed of burning is lower than the speed of sound in the surroundings or, in other words, a deflagration is a fire in which a flame travels rapidly, but at subsonic speed, through a gas.
- The radiative deflagration (model) describes the rapid interaction of the incident laser radiation with a very thin layer near to the target surface. In this layer, the electron density reaches a cut-off $n^{\text{(cut-off)}} = 10^{21} / \lambda^2\,[\mu\text{m}]$. This rapid interaction also leads to a hot plasma that expands into the vacuum and which *vice versa,* results in a shock wave into the solid owing to momentum conservation.

- The properties of the hot plasma in the (thin) interaction layer can then be determined mainly from the power density in the focal zone and the wavelength of the incident radiation.

## 6.4.i. Plasma diagnostics

### Interpretation of line spectra:

- More often than not, any detailed interpretation of the line spectra from laboratory plasmas and astrophysical sources has been found a great challenge since it requires one to go often beyond a local thermodynamical equilibrium (LTE) approach. If no equlibrium is reached, the spatially-dependent photon emission and absorption need to be taken into account in the solution of the rate equations throughout the emitting medium.
- Laboratory *versus* astrophysical plasma: Laboratory plasmas can differ from astrophysical sources in various ways:
    - Laboratory plasmas can be short-lived so that they do not reach statistical equilibrium.
    - Even if often much larger densities occur in laboratory plasma, when compared to typical astrophysical sources, still not all lines are optically thick and, in partiular, the re-bound and free-free transitions (continuum radiation) are usually optically thin.
    - In laboratory plasma, most atomic levels are often collisionally rather than radiatively dominated.
    - The (large) density of laboratory plasma can dramatically affect the line profiles, and this should be taken into account in the radiative-transfer calculations.
- However, in order to determine the relevant physical parameters that describe both, the astrophysical and laboratory plasmas, i.e. its electron temperature, density distribution, ion and element abundances, etc., we need to compare the observed data to a theoretical model spectra.
- In general, any collision between particles cause energy exchange and changes in the state distribution changes.
- Non-local thermodynamic equilibrium (NLTE): NLTE exists in a wide variety of astrophysical and laboratory-created plasmas. Examples of NLTE astronomical plasmas are the stellar corona, interstellar nebulae and some other low-density ionized plasmas. In the laboratory, NLTE exists in laser-produced plasmas, tokamaks and Z-pinch based experiments.
- X-ray satellites, such as CHANDRA and XMM-NEWTON have provided large amounts of high-resolution spectra from astronomical objects, and with many of them in NLTE.

## Diagnostics of astrophysical plasma:

- Hot plasmas are present in the universe in a variety of astrophysical objects, from stellar coronae to the birth of stars and up to the intergalactic medium in clusters of galaxies. The high-quality data, that have been obtained during the last few decades from space observatories, like EINSTEIN, ROSAT, ASCA, and SAX, eneabled one to study in great detail the physical condition of several astrophysical plasmas.
- Solar corona plasma: The solar corona plasma is low-density plasma and is believed to be dominated by the spontaneous decay and radiative recombination. For these two processes, the corresponding decay rates are much higher than the collisional decay and three-body recombination and, hence, the plasma is not in a local thermodynamic equilibrium and cannot be described by Saha or Boltzmann equations.
- Static stellar atmospheres: In the standard models of static stellar atmospheres, the atomic (or ionic) populations, the radiation field, the temperature and density are calculated self-consistently by means of rate equations and radiative transfer equations but owing to certain constraints, such as statistical equilibrium, radiative equilibrium or a hydrostatic equilibrium.

## Diagnostics of laboratory plasma:

- For ITER, various concepts have been developed to reduce the peak heat at the plasma-facing components of the tokamak. Indeed, much of the current experimental and theoretical work in fusion research focus on the question of how the heat from the plasma need to be transferred to the walls of the main and divertor chambers.
- Heat transfer process: To analyse this heat transfer and to enroll the relative importance of the primary atomic processes, simple quasi-analytic models and refined rate coefficients and cross sections have been utilized. Important heat transfer processes refer to the radiation losses through bremsstrahlung, impurity radiation losses from the plasma edge, the charge exchange and radiation losses from hydrogen in outer layer as well as to radiation losses due to impurities in the divertor plasma.
- In large fusion devices such as ITER, most of the heating power strikes the divertor plate and results in a high peak-heat loads of all plasma-facing components.
- The ITER divertor has been designed in order to enhance the charge exchange processes, hydrogen and impurity line radiation, ionization, or elastic collisions between the recycling gas and the plasma in the diverted plasma and, hence, to spread out the heat and momentum transfer over the device.

## Diagnostics of tungsten plasma:

- ➢ Atomic physics has been crucial for understanding the plasma-energy balance and for diagnostic development. In particular, tungsten is nowadays very frequently used on present-day tokamaks in preparation for ITER.
- ➢ Tungsten has become of high importance since it will be a major constituent of ITER plasmas. Tungsten will be applied as plasma-facing component that is able to withstand high heat loads and with a lower tritium retention than other possible materials.
- ➢ ITER Core Imaging x-ray Spectrometer (CIXS): The CIXS has been designed to measure the ion temperature and the motion of ITERs plasma core, based especially on the x-ray emission of neon-like $W^{64+}$ ions (Beiersdorfer *et al.*, 2015). The emission from tungsten will be measured by extreme ultraviolet (EUV) and optical spectrometers in order to determine its concentration in the plasma and to the assess power loss and the sputtering rate of tungsten.

## Diagnostics of lanthanide ions:

- ➢ The radiative properties of the lanthanide ions have numerous applications in solid-state laser materials, photonics and the lighting industry. Radiative transitions of lanthanide ions were observed in doped crystals and in solution with small shifts relative to those of the free ions.
- ➢ Suzuki *et al.* (2018) have systematically observed extreme ultraviolet (EUV) spectra from the highly-charged ions of nine lanthanide elements with nuclear change $Z = 60 .. 70$ in optically thin plasmas as produced in the Large Helical Device (LHD). The wavelengths of the main peaks in the quasi-continuum features were found to agree well previously measured singlet transitions of Pd-like ions as well as with the discrete spectral lines from Cu-like and Ag-like ions.
- ➢ The bright emission spectra from highly-charged ions of lanthanide elements $(Z = 57 - 71)$ are known to appear in the extreme ultraviolet (EUV) or soft x-ray wavelength range due to $n = 4 - 4$ transitions of lanthanide ions in the wavelength range of 5-12 nm. These emission spectra are typically strongly affected by relativistic effects and multi-electron correlations. Likely, these emission spectra will play an important role in application to the next generation light sources for EUV lithography.
- ➢ Observationos with the Hubble Space Telescope: In astrophysics, observationos with the Hubble Space Telescope of spectra of chemically peculiar stars have proven the presence of lanthanide ions up to doubly-charged stages. More recently, the shortly delayed observation of gravitational waves and the emission of electromagnetic waves during a neutron-star merger have renewed the interest for radiative properties of higher-charged lanthanide ions.

## 6.4.j. Radial distribution functions for plasma and liquid models

### General remarks:

- Distribution functions for plasma: The radial distribution function for a plasma is often required and need to be calculated. In these computations, quantum effects have to be taken into account for small inter-particle separations, either by using a modified path-integral technique or, equivalently, by a summation over states, together with the assumption that the charged particles interact via a shielded Coulomb potential.
- General expressions for the radial distribution function in an electron-ion plasma outside of an thermal equilibrium have been obtained in the literature in first-order of the plasma parameters.
- Distribution functions for fluids: Tadial distribution function and static structure factors have been computed at several places in the literature. The radial distribution function can be utilized to characterize a fluid, for instance in terms of the pronounced maxima at some inter-particle distance, and followed by successive minima and maxima with reduced amplitudes.

### Quantal hypernetted-chain approximation:

- Hypernetted-chain equation: In statistical mechanics, the hypernetted-chain equation arises as a closure relation in order to solve the Ornstein-Zernike equation, i.e. a relation between the direct and total correlation functions. The hypernetted-chain equation is commonly applied in fluid theory in order to obtain, e.g. expressions for the radial distribution function.
- The hypernetted-chain approximation is an integral-equation method from statistical physics that arises from the theory of liquids.
- A quantal version of the hypernetted-chain equation (QHNC) was derived in the literature by using the density-functional method, and extended to treat a liquid metal and a plasma as an ion-electron mixture.

## 6.4.k. Average-atom model for warm-dense matter

### Warm-dense matter:

- Warm-dense matter (WDM): This term generally refers to some state of matter under plasma conditions, and which can range from condensed matter to weakly-coupled plasmas with typical temperatures from a few to a few hundred eV as well as with densities from a few hundredths to about a hundred times of the solid density.

- In modeling WDM, great challenges arise from the partial ionization of the plasma, the degeneracy of the electron states, the bound-state level shifts, the pressure ionization in plasma as well as the strong coupling of the ion-ion pairs that must be taken into account self-consistently.
- Equation of state: A good understanding of the properties and behaviour of WDM, such as the equation of state, its radiation opacity, or transport properties, has been found important, for modeling for example astrophysical objects or inertial confinement fusion experiments (Hou *et al.*, 2015).
- Electronic structure of impurities: Studies on the electronic structure of impurities within an electron gas have been performed in the literature as function of their density and temperature. For these investigations, one need to know the dependence of screening effects on the plasma parameters.
- Friedel oscillations: At low temperatures and metallic densities, especially, the electron density often exhibits Friedel oscillations as known also from solid-state physics.
- Hou *et al.* (2015) combined the average-atom model with the hypernetted chain approximation (to a so-called AAHNC approximation) in order to describe the electronic and ionic structure in the WDM regime.

## Average-atom model:

- Average-atom (AA) model: This model divides the plasma into separate neutral Wigner-Seitz cells with a nucleus of charge $Z$ and $Z$ free electrons. Various versions of the AA model have been implemented in plasma physics for describing warm- and hot-dense plasma.
- In the AA model, each ion or atom is described within a finite (ion) sphere and by using a central-field approximation for the bound electrons. For heavy atoms and ions, a (radial) Dirac equation can be applied but where the potential $V(r)$ need again to be calculated self-consistently.
- Electron density in the AA model: For an isolated atom or ion, the electron density is calculated in the AA model in order to include the level broadening of the energy levels within a plasma environment. This density is applied also for studying the temperature and density effects upon the electron distributions within a statistical way.
- Radial potential in the AA model: (Hou *et al.*, 2015)

$$V(r) = -\frac{Z}{r} + \int d^3r' \, \frac{\rho_b(r')}{|\mathbf{r} - \mathbf{r}'|} + V_{\rm xc}[\rho_b(r) + \rho_{e,0}] - V_{\rm xc}(\rho_{e,0}) - \frac{\rho_{e,0}}{\beta} \int d^3r' \, C_{ee}(|\mathbf{r} - \mathbf{r}'|) \, h_{ie}(r') - \frac{\rho_{i,0}}{\beta} \int d^3r' \, C_{ie}(|\mathbf{r} - \mathbf{r}'|) \, h_{ii}(r')$$

where the first four terms constitute the contributions from a single ion: electron-nucleus interaction, the electro-static repulsion with the other bound electrons as well as the exchange and correlation potential, which are often evaluated by using some local density approximation. The last two terms in this expression represent the interaction of the ion with the surrounding free electrons and with the other ions. Here, $\rho_{e,0} = \rho(r_b)$ is the uniform electron density.

## Spectral emission from plasma in a non-local thermodynamic equilibirum (NLTE):

- In a non-local thermodynamic equilibirum (NLTE), in which the levels of each configuration are in LTE among each other, the population $N_a$ of a given configuation follows as solution of a system of rate equations

$$\frac{\partial N_a}{\partial t} = -N_a \sum_b R_{ab} + \sum_b R_{ba} N_b,$$

where $R_{ab}$ is a global transition rate that connects the configurations $a$ and $b$.

- Many collisional-radiative models, that are applied for a realistic modelling of NLTE line emission, often account for individual levels explicitly for spectroscopic reasons, while the levels of other configurations are lumped together. These superlevels have no spectroscopic meaning but are included to describe the population kinetics.

### 6.4.l. Equation-of-state relations for astro physics and condensed matter

## Equation-of-state:

- Equation-of-state relations: More often than not, the equation-of-state refers to the pressure-density or pressure-temperature relation for matter under (more or less) extreme conditions.
- When the atomic density is rather low, we can deal with isolated atoms that are in equilibrium with the surrounding free electrons, while the statistical or Thomas-Fermi-Dirac model has been found useful for a very high density.

## Liberman's self-consistent model:

- Liberman (1979) describes a model for condensed matter in which the ions surrounding a particular atom are replaced by a positive charge distribution which is constant outside of a sphere containing the atom and zero inside. This models enables one to separate the quantities that pertain to the atom from those of the electron gas (in which it is imbedded) and hence to derive the desired equation-of-state data.

- The model assumes that there are sufficient electrons in the system in order to give overall electrical neutrality together with the (required) electrical neutrality inside the sphere.
- Instead of a polyhedral cell, which are surrounded by other identical cells, a nearly equivalent spherical cell is assumed in Liberman's model, and surrounded by a uniform electron gas. The density of this electron gas is the same as the mean density of ionic charges. Therefore, the electron gas outside will not alter the charge distribution inside the cell, if its density is correctly chosen, nor will the atom affect the electron gas.

## 6.4.m. Radiation damage of DNA by electron impact

### Radiation damage of DNA:

- Radiation damage: This term often refers to the damage of biological material on rather short time scales, i.e. reactions and processes that occur within ns or even less following the interaction of a high energy quantum with a living cell. These initial events may ultimately lead to the collapse of such cells. In practice, they result in the death of the individual cells within hours or days but may affect the matter also on much longer time scales.
- Low-energy electrons (LEE) that interact with the DNA: The absorption of high-energetic photons by biological matter often leads to low-energy electrons (LEE) that interact with the DNA. These LEE can cause specific resonant processes and may lead eventually either to single- or double-strand breaks in DNA materials, to the damage of its molecular components and possibly even to biological apoptosis (Bacarelli *et al.*, 2011).
- Several theoretical and computational approaches have been developed for studying the molecular processes that occur in the various steps of the energy deposition by LEE.
- In contrast, an alteration of the genetic expression of DNA may cause the onset of some diseases.

### Electron-molecule dynamics:

- To understand the electron-impact of bio-molecules, a quite sizeable computational machinery need to be developed. The multiple inelastic scattering of these electrons will result in a re-distribution in the energy content and may lead to a fragmentation as well as the excitation of various vibrational modes.

## 6.4.n. Exotic atoms and ions

### Muonic atoms and ions:

- Muonic atom: When a muon is captured by the nucleus, it generally forms a hydrogen-like muonic ion, although it is typically still surrounded by other atomic electrons.
- Measurements of the transition energies in muonic atoms help determine nuclear parameters, such as charge radii, quadrupole moments and magnetic hyperfine constants. One of the most precise measurements of the nuclear root-mean-square radius by means of muonic atoms refer to the radius of $^{208}$Pb at the 0.2 % level.
- Muonic hydrogen: In muonic hydrogen, the electron is replaced by a muon $\mu$ with a 200 times larger mass. This large mass results orbits that are 200 times closer to the nuclues, when compared to the electron in regular hydrogen.
- Because of the finite extent of the proton, muons in their $s$-state have therefore some enhanced probability to be inside the proton, and where it sees also a slightly reduced electric charge of the proton. Therefore, the muon is less bound as larger the proton is.

# 7. Atomic processes

## 7.1. In JAC implemented processes

### 7.1.a. Photo-emission. Transition probabilities (`Radiative`)

**Process & notations:**

- Photon emission: from an atom or ion $A^* \longrightarrow A^{(*)} + \hbar\,\omega$
- Formal quantum notation: $|\alpha_i \mathbb{J}_i\rangle \longrightarrow |\alpha_f \mathbb{J}_f\rangle + \hbar\omega$
- Jac's standard multipole amplitudes for photon emission: Although all (one- and many-electron) electron-photon interaction matrix elements are always evaluated in *absorption* within Jac, we wish to retain the intuitive description of matrix elements as typically applied in quantum mechanics: $\langle \text{final} - \text{state}\,|\,\text{operator}\,|\,\text{initial} - \text{state}\rangle$ . We here therefore introduce an explicit notation for a *standard (reduced, Jac) emission as well as absorption multipole matrix element*

  $$\left\langle \alpha_f \mathbb{J}_f \left\| \mathbb{O}^{(\mathbb{M},\,\text{emission})} \right\| \alpha_i \mathbb{J}_i \right\rangle = \left\langle \alpha_i \mathbb{J}_i \left\| \sum_{k=1}^{N} \boldsymbol{\alpha}_k\, a^{p}_{k,\,L} \right\| \alpha_f \mathbb{J}_f \right\rangle^{*} \equiv \left\langle \alpha_i \mathbb{J}_i \left\| \mathbb{O}^{(\mathbb{M},\,absorption)} \right\| \alpha_f \mathbb{J}_f \right\rangle^{*}$$

  which retains the right order and can be obtained from `Jac.Radiative.amplitude()`; cf. section 4.3.c. A multipole $\mathbb{M} \equiv (L, p) =$ E1, M1, E2, ... hereby contains all information about its multipolarity (angular momentum) $L$ and type *magnetic* $(p = 0)$ or *electric* $(p = 1)$ .
- Using Jac: Perform an `Atomic.Computation(.., process=Jac.RadiativeX, processSettings=Radiative.Settings(..), ..)` or call directly functions from the module `Radiative`.

## Transition probabilities:

- ➢ With the notation of the (standard reduced, JAC) emission multipole matrix element from above, the transition probability is given by

$$W_{i \to f} \;=\; \frac{8\pi\, \alpha\, \omega}{2J_i + 1} \sum_{\mathbb{M}} \left| \left\langle \alpha_f \mathbb{J}_f \left\| \mathbb{O}^{\,(\mathbb{M},\,\text{emission})} \right\| \alpha_i \mathbb{J}_i \right\rangle \right|^2$$

  and where the sum over $\mathbb{M}$ = E1, M1, E2, ... runs over all requested multipoles for a given computation.
- ➢ In JAC, the transition probabilities and radiative lifetimes are tabulated by default for all selected transitions $i \to f$ .

## Angular distribution and anisotropy parameters of the fluorescence radiation:

- ➢ The fluorescecne (radiation) from an excited atom is characterized not only by its frequency $\hbar\omega$ but also by the angular distribution and polarization of the emitted radiation. Both of these properties of the emitted photons depend on the sublevel occupation of the excited atom or ion and, hence, on its reduced statistical tensors $\mathcal{A}_{kq}(\alpha_i \mathbb{J}_i)$ which are associated with the prior excitation process.
- ➢ Angular distribution: For initially unpolarized but aligned atoms, the angular distribution of the (characteristic) fluorescence radiation is given in perturbation theory by:

$$W(\vartheta) \;=\; \frac{W_o}{4\pi} \left( 1 + \sum_{k=2,4,..} f_k(\alpha_i \mathbb{J}_i, \alpha_f \mathbb{J}_f)\, \mathcal{A}_{k0}(\alpha_i \mathbb{J}_i)\, P_k(cos\vartheta) \right) ,$$

  where $W_o$ is the total decay rate and $\vartheta$ the angle of the photons with regard to the alignment axis (quantization axis).
- ➢ Anisotropy (structure) parameters $f_k(\alpha_i \mathbb{J}_i, \alpha_f \mathbb{J}_f)$ : In the angular distribution above, the anisotropy (or structure) parameters $f_k(\alpha_i \mathbb{J}_i, \alpha_f \mathbb{J}_f)$ are independent of the particular excitation process of the level $|\alpha_i \mathbb{J}_i\rangle$ and merely reflects the electronic structure of the ion in the two levels involved in the fluorescence

$$f_k(\alpha_i \mathbb{J}_i, \alpha_f \mathbb{J}_f) \;=\; \left[ \sum_{\mathbb{M}} \left| \left\langle \alpha_i \mathbb{J}_i \left\| \mathbb{O}^{\,(\mathbb{M},\,\text{emission})} \right\| \alpha_f \mathbb{J}_f \right\rangle \right|^2 \right]^{-1} \frac{\sqrt{2J_i + 1}}{2} \sum_{\mathbb{M}\,\mathbb{M}'} i^{L'+p'-L-p}\, (-1)^{J_f + J_i + 1 + k}\, [L, L']^{1/2}\, \langle L1,\; L'-1 \,|\, k0 \rangle$$

$$\times \left( 1 + (-1)^{L+p+L'+p'-k} \right) \begin{Bmatrix} L & L' & k \\ J_i & J_i & J_f \end{Bmatrix} \left\langle \alpha_f \mathbb{J}_f \left\| \mathbb{O}^{\,(\mathbb{M},\,\text{emission})} \right\| \alpha_i \mathbb{J}_i \right\rangle \left\langle \alpha_f \mathbb{J}_f \left\| \mathbb{O}^{\,(\mathbb{M}',\,\text{emission})} \right\| \alpha_i \mathbb{J}_i \right\rangle^{*} ,$$

- Of course, there is usually one multipole term that dominates the radiative decay (fluorescence) for any given pair of initial and final-bound states.
- In JAC, the anisotropy (structure) parameters $f_k(\alpha_i \mathbb{J}_i, \alpha_f \mathbb{J}_f)$ are calculated and tabulated if the flag `calcAnisotropy = true` is set in `Radiative.Settings`.

## Line strength:

- Conversion between $gA$ [1/s] and $S$: For wavelengths $\lambda$ [Å] (NIST Atomic Spectra Database)

$$S = 3.707342 \times 10^{-14} \lambda^3 \, g \, A \qquad \text{(M1)}$$

$$S = 8.928970 \times 10^{-19} \lambda^5 \, g \, A \qquad \text{(M1)}$$

## Semi-empirical calculations of transition probabilities:

- Semi-empirical calculations of transition probabilities are often performed by using Cowan's code and, especially, the components RCN/RCN2/RCG/RCE. In a first step, Hartree-Fock calculations of radial integrals are carried out, including relativistic corrections (HFR) to generate all required atomic orbitals and average energies of configurations. The diagonalization of the Hamiltonian matrix then leads to approximate energy values and eigenvectors of levels in intermediate coupling.
- When, in addition, also experimental energies are available, RCE is run to perform an iterative least-squares fit and to minimizing the differences between the calculated and experimental energies, where the radial integrals are applied as fitted parameters. The mean error of such a fit is defined by $\Delta E = \sqrt{\sum_i \left( E_i^{(\text{exp})} - E_i^{(\text{calc})} \right)^2 / (N_i - N_p)}$ where $N_i$ is the number of experimentally known energies and $N_p$ the number of free parameters.

## Unresolved transition arrays (UTA):

- Unresolved transition arrays: The UTA approach has become the method of choice to calculate the radiative properties of higher Z elements. Within this approach, a group of lines (i.e. a so-called array) which belongs to the same pair of electron configurations are treated globally by a Gaussian distributions whose width and position are given by analytical formulae.

- The UTA approach is computationally efficient and accurate for plasma conditions where the line broadening is such that individual line profiles merge. This approach has been further extended to a group of arrays in the so-called super-transition array method (STA) where set of arrays are treated globally.
- Resolved transition arrays (RTA): The RTA method was proposed to overcome the shortcoming of the UTA method that just a few transitions often dominate the spectral emission distribution of the array. This RTA method improves on the UTA approach by resolving the transition array into individual lines by using random lines but without performing an explicit atomic structure calculation.
- UTA method: For a group of lines with known transition energies $E_i$ and corresponding the oscillator strengths $g_i$, the UTA is obtained by calculating the first two moments for the array of $N$ transitions:

$$\mu^{(1)} = \frac{\sum_i^N g_i E_i}{\sum_i g_i}, \qquad \mu^{(2)} = \frac{\sum_i^N g_i E_i^2}{\sum_i g_i},$$

- These two moments can be utilized together with the variance $\sigma^2 = \mu^{(2)} - \left(\mu^{(1)}\right)^2$ in order to define the spectral distribution of the UTA

$$f(\mathcal{E}) = \frac{1}{\sigma \sqrt{\pi}} \exp\left[ - \frac{(\mathcal{E} - \mu^1)^2}{2 \sigma^2} \right].$$

- By avoiding the explicit calculation of the properties of each line, that belongs to a given array, the UTA method enables one to account for a large number of transitions for a rather low computational cost.

## Two-electron one-photon transitions (TEOP):

- Two-electron one-photon transitions were postulated almost 100 years ago and are well-known from the optical region.
- In the early 1970s, Wölfli *et al.*. reported results for nickel and iron for which high-energetic satellites arose due to two-electron one-photon transition, where two vacancies in the K-shell were simultaneously filled by two L-shell electrons under the emission of s single photon.
- Since the interaction with the electromagnetic field is governed by an one-electron operator, however, the contribution of two-electron one-photon (TEOP) transitions can usually be ignored in comparison to other, allowed one-electron transitions.

### 7.1.b. Photo-excitation (`PhotoExcitation`)

## Process & notations:

- Photo-excitation of an atom or ion: $A \,+\, \hbar\,\omega \quad \longrightarrow \quad A^*$
- Formal quantum notation: $|\alpha_i \mathbb{J}_i\rangle \,+\, \hbar\omega\,(\mathbf{k}, \lambda) \quad \longrightarrow \quad |\alpha_f \mathbb{J}_f\rangle\,.$
- Using JAC: Perform an `Atomic.Computation(.., process=Jac.PhotoExc, processSettings=PhotoExcitation.Settings(..), ..)` or call directly functions from the module `PhotoExcitation`.

## Photoexcitation cross sections:

- Total photoabsorption cross section: For initially unpolarized atoms and incident photons with given (photon) density matrix $\langle \mathbf{k}\lambda \,|\, \rho_\gamma \,|\, \mathbf{k}\lambda' \rangle$, the total photoabsorption cross section can be most easily defined in the limit of the *zero* linewidths as

$$\sigma(\alpha_i \mathbb{J}_i \to \alpha_f \mathbb{J}_f;\, \omega) \;=\; \frac{4\pi^2 \alpha}{\omega\,(2J_i + 1)} \sum_{M_i M_f,\, \lambda\lambda'} \langle \mathbf{k}\lambda \,|\, \rho_\gamma \,|\, \mathbf{k}\lambda' \rangle \, \left\langle \alpha_f\, \mathbb{J}_f M_f \,\middle|\, \mathbb{T}^{\,\rm (absorption)}(\mathbf{k}, \lambda) \,\middle|\, \alpha_i\, \mathbb{J}_i M_i \right\rangle$$

$$\times \left\langle \alpha_f\, \mathbb{J}_f M_f \,\middle|\, \mathbb{T}^{\,\rm (absorption)}(\mathbf{k}, \lambda') \,\middle|\, \alpha_i\, \mathbb{J}_i M_i \right\rangle^* \, \delta(\omega + E_i - E_f)\,,$$

  and where $\mathbb{T}^{\,\rm (absorption)}(\mathbf{k}, \lambda)$ formally describes the electron-photon interaction operator for absorbing a photon $\hbar\omega\,(\mathbf{k}, \lambda)\,.$

- In order to allow for a finite natural width $\Gamma_f$ of the excited level, we need to replace the $\delta(\omega + E_i - E_f)$ function in the above expression by a (Lorentzian) spectral distribution

$$\sigma(\alpha_i \mathbb{J}_i \to \alpha_f \mathbb{J}_f;\, \omega) \;=\; \frac{4\pi^2 \alpha}{\omega\,(2J_i + 1)} \sum_{M_i M_f,\, \lambda\lambda'} \langle \mathbf{k}\lambda \,|\, \rho_\gamma \,|\, \mathbf{k}\lambda' \rangle \, \left\langle \alpha_f\, \mathbb{J}_f M_f \,\middle|\, \mathbb{T}^{\,\rm (absorption)}(\mathbf{k}, \lambda) \,\middle|\, \alpha_i\, \mathbb{J}_i M_i \right\rangle$$

$$\times \left\langle \alpha_f\, \mathbb{J}_f M_f \,\middle|\, \mathbb{T}^{\,\rm (absorption)}(\mathbf{k}, \lambda') \,\middle|\, \alpha_i\, \mathbb{J}_i M_i \right\rangle^* \; \frac{1}{\pi} \, \frac{\Gamma_f / 2}{(\omega + E_i - E_f)^{\,2} + \Gamma_f^2 / 4}$$

- Photoexcitation cross sections for initially unpolarized atoms: For incident plane-wave photons with (photon) density matrix $(c_{\lambda\lambda'}) = \frac{1}{2}\begin{pmatrix} 1+P_3 & P_1 - iP_2 \\ P_1 + iP_2 & 1-P_3 \end{pmatrix}$, which are resonant to the given transition $|\alpha_i \mathbb{J}_i\rangle \to |\alpha_f \mathbb{J}_f\rangle$, the total photoexcitation cross section is

$$\sigma(\alpha_i \mathbb{J}_i \to \alpha_f \mathbb{J}_f;\, \omega) \;=\; \frac{2\pi^3\alpha}{\omega\,(2J_i+1)} \sum_{\mathbb{M},\,\lambda} c_{\lambda\lambda} \left|\left\langle \alpha_f\, \mathbb{J}_f \left\| \mathbb{O}^{(\mathbb{M},\,\text{absorption})}(\lambda) \right\| \alpha_i\, \mathbb{J}_i \right\rangle\right|^2 \times \begin{cases} \delta(E_i + \omega - E_f) \\ \frac{1}{\pi}\,\frac{\Gamma_f/2}{(E_i+\omega-E_f)^2+\Gamma_f^2/4} \end{cases}$$

- Photoexcitation cross sections for initially unpolarized atoms and linear-polarized, circularly-polarized or unpolarized photons: For resonant and unpolarized or completely linearly-polarized or circularly-polarized plane-wave photons, especially, the total photoexcitation cross section is

$$\sigma(\alpha_i \mathbb{J}_i \to \alpha_f \mathbb{J}_f;\, \omega) \;=\; \frac{8\pi^3\alpha}{\omega\,(2J_i+1)} \sum_{\mathbb{M}} \left|\left\langle \alpha_f\, \mathbb{J}_f \left\| \mathbb{O}^{(\mathbb{M},\,\text{absorption})}(\lambda) \right\| \alpha_i\, \mathbb{J}_i \right\rangle\right|^2 \times \begin{cases} \delta(E_i + \omega - E_f) \\ \frac{1}{\pi}\,\frac{\Gamma_f/2}{(E_i+\omega-E_f)^2+\Gamma_f^2/4} \end{cases}$$

- In JAC, the photoexcitation cross sections are calculated by default for resonant and completely linearly-polarized plane-wave radiation.

- In JAC, the photoexcitation cross sections are calculated also for plane-wave radiation with given Stokes parameters $(P_1, P_2, P_3)$ if the flag `calcStokes = true` are set in `PhotoExcitation.Settings` and if the Stokes parameters are given explicitly by `PhotoExcitation.Settings.stokes`.

## Final-level statistical tensors and alignment parameters:

- Statistical tensors: Instead of the (final-level) density matrix above, it is often more convenient to describe the population of the magnetic sublevels in terms of the (so-called) statistical tensors of the atom or ion

$$\rho_{kq}(\alpha_f \mathbb{J}_f) \;=\; \sum_{M_f M_f'} (-1)^{J_f - M_f'} \left\langle J_f M_f,\, J_f\,(-M_f') \,|\, kq \right\rangle \left\langle \alpha_f\, \mathbb{J}_f M_f \,|\, \rho \,|\, \alpha_f\, \mathbb{J}_f M_f' \right\rangle .$$

and which are non-zero only for $0 \le k \le 2\,J_f$ and $-k \le q \le k$.

- Reduced statistical tensors: of the excited levels or so-called alignment parameters

$$\mathcal{A}_{kq}(\alpha_f \mathbb{J}_f) \;=\; \frac{\rho_{kq}(\alpha_f \mathbb{J}_f)}{\rho_{00}(\alpha_f \mathbb{J}_f)} \,.$$

- Statistical tensors for initially unpolarized atoms and incident plane-wave radiation For incident plane-wave photons with (photon) density matrix $(c_{\lambda\,\lambda'}) \;=\; \frac{1}{2} \begin{pmatrix} 1+P_3 & P_1 - iP_2 \\ P_1 + iP_2 & 1 - P_3 \end{pmatrix}$, which are resonant to the given transition $|\alpha_i \mathbb{J}_i\rangle \rightarrow |\alpha_f \mathbb{J}_f\rangle$, the reduced statistical tensors can be written as

$$\rho_{kq}(\alpha_f \mathbb{J}_f) \;=\; \ldots$$

- Statistical tensors for initially unpolarized atoms and incident plane-wave radiation with well-defined helicity $\lambda$: For incident plane-wave photons with helicity $\lambda$, the reduced statistical tensors can be written as (Surzhykov *et al.*, 2015)

$$\rho_{kq}(\alpha_f \mathbb{J}_f) \;=\; \delta_{q0}\, C \sum_{\mathbb{M}\,\mathbb{M}'} i^{\,L+L'}\, [L,\, L]^{1/2}\, (i\,\lambda)^{p}\, (-i\,\lambda)^{p'}\, (-1)^{\,L'+J_f+J_i+k}\, \langle L\lambda,\, L'-\lambda \,|\, kq\rangle \begin{Bmatrix} L & L' & k \\ J_f & J_f & J_i \end{Bmatrix}$$

$$\times\; \left\langle \alpha_f \mathbb{J}_f \left\| \,\mathbb{O}^{\,(\mathbb{M},\,\text{absorption})}\, \right\| \alpha_i \mathbb{J}_i \right\rangle \left\langle \alpha_f \mathbb{J}_f \left\| \,\mathbb{O}^{\,(\mathbb{M}',\,\text{absorption})}\, \right\| \alpha_i \mathbb{J}_i \right\rangle^{*}$$

- In JAC, the statistical tensors $\rho_{kq}(\alpha_f \mathbb{J}_f)$ and the alignment parameters $\mathcal{A}_{kq}(\alpha_f \mathbb{J}_f)$ are calculated and tabulated for unpolarized atoms and plane-wave photons with given Stokes parameters, if the flag `calcTensors = true` is set in `PhotoExcitation.Settings` and if the Stokes parameters are given explicitly by `PhotoExcitation.Settings.stokes`.

## Photoexcitation by twisted light:

- Photoexcitation by twisted light:

$$\hbar\,\omega^{(\text{twist})} \;+\; A \quad\longrightarrow\quad A^{*}$$

- For macroscopic targets: computation of sublevel-dependent photoexcitation cross sections $\sigma_{m_f}^{(\text{twist})} \;=\; f(\vartheta_k)$ as well as the cross section ratio with regard to incoming plane-wave radiation $\sigma^{(\text{twist})}/\sigma^{(\text{plane})}$ .

- For finite, localized targets:

$$\sigma_{m_f}^{\rm (twist)} \;=\; f(\vartheta_k, \quad ..., \mathbf{b}, m), \qquad\qquad \frac{\sigma^{\rm (twist)}}{\sigma^{\rm (plane)}} \;=\; f(\mathbf{b}, \text{ target size}), \qquad\qquad \mathcal{A}_2,\; P_1 \;=\; f(\mathbf{b}, \text{ target size})$$

- The photo excitation of atoms by a Bessel beam of twisted light has been investigated for low-$Z$ hydrogen-like with emphasis on the *partial* (subshell) cross sections and the alignment of the excited states if the beam interacts with macroscopic hydrogen target (Markgraf-Scholz *et al.* 2014).

## 7.1.c. Atomic photoionization (`PhotoIonization`)

### Process & notations:

- Photo-ionization of an atom or ion: $A \,+\, \hbar\,\omega \quad\longrightarrow\quad A^{+*} \,+\, e_p^-$
- Formal quantum notation: $|\alpha_i \mathbb{J}_i\rangle \,+\, \hbar\omega\,(\mathbb{M}) \quad\longrightarrow\quad |\alpha_f \mathbb{J}_f\rangle \,+\, e_p^-(\mathbf{p},\, m_s)$ or $|\alpha_i \mathbb{J}_i\rangle \,+\, \hbar\omega\,(\mathbb{M}) \quad\longrightarrow\quad |\alpha_f \mathbb{J}_f\rangle \,+\, e_p^-(\varepsilon\,\kappa)$
- Using JAC: Perform an `Atomic.Computation(.., process=Jac.Photo, processSettings=PhotoIonization.Settings(..), ..)` or call directly functions from the module `PhotoIonization`.

### Photoionization amplitude:

- Emission of an electron with asymptotic momentum $\boldsymbol{p}$ and spin projection $m_s$: If the atom undergoes the transition $|\alpha_i\, \mathbb{J}_i M_i\rangle \rightarrow |\alpha_f\, \mathbb{J}_f M_f\rangle$, the transition amplitude for the photoionization of an atom or ion by the absorption of a photon with wave vector $\boldsymbol{k}$ and helicity $\lambda \,=\, \pm\, 1$ is given by:

$$\mathcal{M}\,(M_f, m_s, \lambda, M_i) \;=\; \left(\frac{4\pi^2\alpha}{\omega}\right)^{1/2} \left\langle \alpha_f\; \mathbb{J}_f M_f,\; \boldsymbol{p}\, m_s \left| \sum_{i=1}^{N} \boldsymbol{\alpha}_i\, \mathbf{u}_\lambda\, e^{i\,\boldsymbol{k}\cdot\boldsymbol{r}_i} \right| \alpha_i\; \mathbb{J}_i M_i \right\rangle .$$

- The population of the magnetic sublevels $|\alpha_f\; \mathbb{J}_f M_f\rangle$ of the photoion depends (of course) on the spin projection $\lambda$ of the incident photons as well as the magnetic quantum numbers $M_f$ of the final state of the photoion, while one need to average over the initial sublevel and the spin projection of the emitted electrons.

- (Reduced) photoionization amplitude for a partial-wave decomposition of the outgoing photoelectron and a multipole expansion of the electron-photon interaction: This amplitude describes the contribution of an individual multipole components of the radiation field to the formation of a scattering state $|(\alpha_f \mathbb{J}_f, \varepsilon\, \kappa)\, \mathbb{J}_t\rangle$ with well-defined total symmetry and electron energy $\varepsilon$

$$\left\langle (\alpha_f \mathbb{J}_f, \varepsilon\, \kappa)\, \mathbb{J}_t \left\| \mathbb{O}^{\,(\mathbb{M},\,\mathrm{photoionization})} \right\| \alpha_i \mathbb{J}_i \right\rangle \;=\; i^{-\ell}\; \exp(i\,\Delta_\kappa)\; \left\langle (\alpha_f \mathbb{J}_f, \varepsilon\, \kappa)\, \mathbb{J}_t \left\| \mathbb{O}^{\,(\mathbb{M},\,\mathrm{absorption})} \right\| \alpha_i \mathbb{J}_i \right\rangle$$

  Here, the photoioniozation amplitude also accounts for the proper phase (or the asymptotic boundary condition) of the outgoing electron.

- In Jac, the reduced matrix elements above are the main *building blocks* to represent and discuss most photo-ionization properties as they arise from the interaction of atoms and ions with the radiation field.

## Partial and total cross sections:

- Partial photoionization cross sections for the photoionization of an initially unpolarized atom: For the photoionization of an initially unpolarized atom from level $|\alpha_i \mathbb{J}_i\rangle \;\rightarrow\; |\alpha_f \mathbb{J}_f M_f\rangle$ by unpolarized plane-wave photons with wave vector $\mathbf{k} \,||\, \mathbf{e}_z$ (quantization axis), the partial cross sections can be expressed as:

$$\begin{aligned}
\sigma(\alpha_i \mathbb{J}_i \rightarrow \alpha_f \mathbb{J}_f M_f) \;&=\; \frac{1}{2(2J_i+1)} \sum_{M_i\,\lambda m_s} \int d\Omega_p \;\left|\mathcal{M}\,(M_f, m_s, \lambda, M_i)\right|^2 \\
&=\; \frac{4\pi^2\alpha}{2\,\omega\,(2J_i+1)} \sum_{M_i\,\lambda} \sum_{\kappa m} \sum_{J J' M} \langle J_f M_f\, jm\,|\, JM\rangle\; \langle J_f M_f\, jm\,|\, J'M\rangle \left\langle (\alpha_f \mathbb{J}_f, \varepsilon\kappa)\, \mathbb{J}M \left| \sum_{i=1}^{N} \boldsymbol{\alpha}_i\, \mathbf{u}_\lambda\, e^{i\boldsymbol{k}\cdot\boldsymbol{r}_i} \right| \alpha_i \mathbb{J}_i M_i \right\rangle \\
&\qquad \times \left\langle (\alpha_f J_f, \varepsilon\kappa)\, \mathbb{J}'M \left| \sum_{i=1}^{N} \boldsymbol{\alpha}_i\, \mathbf{u}_\lambda\, e^{i\boldsymbol{k}\cdot\boldsymbol{r}_i} \right| \alpha_i J_i M_i \right\rangle^{*} .
\end{aligned}$$

  Obviously, the integration over all the emission angles $\mathbf{n}_p \;=\; (\vartheta_p, \varphi_p)$ of the photoelectron here results into the *incoherent* summation over the partial waves of the electron with different $\kappa$'s.

- Partial photoionization cross sections for initially unpolarized atoms by unpolarized plane-wave photons: The partial cross sections from above can be simplified and expressed as

$$\begin{aligned}
\sigma(\alpha_i \mathbb{J}_i \to \alpha_f J_f M_f) \;\; = \;\; & \frac{8\pi^3\, \alpha}{2\omega\,(2J_i+1)} \sum_{t\lambda} \sum_{\kappa} \sum_{JJ'} \sum_{\mathbb{M}\mathbb{M}'} i^{L-L'}\, (i\lambda)^p\, (-i\lambda)^{p'}\, (-1)^{L+L'} \sqrt{(2L+1)(2L'+1)(2J+1)(2J'+1)} \\
& \times\, \langle L'\lambda\, J_f M_f \,|\, t, \lambda + M_f \rangle\, \langle L\lambda\, J_f M_f \,|\, t, \lambda + M_f \rangle \begin{Bmatrix} j & J' & J_f \\ J & J_i & L \\ J_f & L' & t \end{Bmatrix} \\
& \times\, \left\langle (\alpha_f \mathbb{J}_f, \varepsilon\kappa)\, \mathbb{J} \left\| \mathbb{O}^{(\mathbb{M},\, \text{photoionization})} \right\| \alpha_i \mathbb{J}_i \right\rangle \left\langle (\alpha_f \mathbb{J}_f, \varepsilon\kappa)\, \mathbb{J}' \left\| \mathbb{O}^{(\mathbb{M}',\, \text{photoionization})} \right\| \alpha_i \mathbb{J}_i \right\rangle^* .
\end{aligned}$$

- In JAC, the total photoionization cross sections are calculated and tabulated by default, while the partial cross sections are calculated if the flag `calcPartialCs = true` is set in `PhotoIonization.Settings`.

## Final-state density matrix 'photo-ion + photo-electron':

- The final-state density matrix of the overall system 'photo-ion + photo-electron' is not so useful in general and is needed only for entanglement studies and related topics. Here, we just summarize some formulas but further work is needed.
- Final-state density matrix of the 'photo-ion + photo-electron': After the absorption of the photon, we have a free electron with asymptotic linear momentum $\mathbf{p}$ and with spin projection $m_s$, while the photoion is left in a fine level $|\alpha_f \mathbb{J}_f\rangle$ . Using a basis with well-defined (angular) momenta $J_i$ and $J_f$ of the initial as well as the residual ion and the asymptotic linear momentum $\boldsymbol{p}$ and spin projection $m_s$ of the ejected electron, the final-state density matrix can be written as

$$\begin{aligned}
& \langle \alpha_f J_f M_f, \boldsymbol{p}\, m_s \,|\, \rho_f \,|\, \alpha_f J_f M_f', \boldsymbol{p}\, m_s' \rangle \\
& \quad = \sum_{M_i M_i'\, \lambda\lambda'} \left\langle \alpha_f \mathbb{J}_f M_f, \boldsymbol{p}\, m_s \left| \hat{\mathcal{R}} \right| \alpha_i \mathbb{J}_i M_i, \boldsymbol{k}\lambda \right\rangle \langle \alpha_i \mathbb{J}_i M_i, \boldsymbol{k}\lambda \,|\, \rho_i \,|\, \alpha_i \mathbb{J}_i M_i', \boldsymbol{k}\lambda' \rangle \left\langle \alpha_i \mathbb{J}_i M_i', \boldsymbol{k}\lambda' \left| \hat{\mathcal{R}}^\dagger \right| \alpha_f J_f M_f', \boldsymbol{p}\, m_s' \right\rangle \\
& \quad = \sum_{M_i M_i'\, \lambda\lambda'} c_{M_i M_i'}\;\; c_{\lambda\lambda'}\, \langle \alpha_f \mathbb{J}_f M_f, \boldsymbol{p}\, m_s \left| \boldsymbol{\alpha} \cdot \boldsymbol{u}_\lambda\, e^{i\boldsymbol{k}\cdot\boldsymbol{r}} \right| \alpha_0 J_0 M_0 \rangle\, \langle \alpha_f \mathbb{J}_f M_f', \boldsymbol{p}\, m_s' \left| \boldsymbol{\alpha} \cdot \boldsymbol{u}_{\lambda'}\, e^{i\boldsymbol{k}\cdot\boldsymbol{r}} \right| \alpha_i \mathbb{J}_i M_i' \rangle^* ,
\end{aligned}$$

where $\left\langle \alpha_f \mathbb{J}_f M_f, \boldsymbol{p}\, m_s \left| \boldsymbol{\alpha} \cdot \boldsymbol{u}_\lambda \, e^{i\boldsymbol{k}\cdot\boldsymbol{r}} \right| \alpha_i \mathbb{J}_i M_i \right\rangle$ represents the photo-ionization amplitude from above.

## Angular distribution of photoelectrons:

- ➢ If the detector is not sensitive to the spin state of the photoelectron and the residual photoion, a proper measurement (projection) operator is obtained if we sum over the electron spin projections $m_s$ as well as the magnetic quantum numbers $M_f$ of the ion. In the density matrix formalism, this projection operator for measuring the angular distribution of the emitted photoelectrons therefore is

$$P \;=\; \sum_{M_f m_s} |\alpha_f \mathbb{J}_f M_f, \, \boldsymbol{p}\, m_s\rangle \, \langle \alpha_f \mathbb{J}_f M_f, \, \boldsymbol{p}\, m_s| \,,$$

- ➢ With this operator, the well-known angular distribution of the photoelectrons is just the normal trace of the finsal-state density matrix:

$$W(\vartheta) \;=\; \mathrm{Tr}\,(P\,\rho_f) \;=\; \sum_{M_f m_s} \langle \alpha_f \mathbb{J}_f M_f, \, \boldsymbol{p}\, m_s \,|\, \rho_f \,|\, \alpha_f \mathbb{J}_f M_f, \, \boldsymbol{p}\, m_s\rangle \,.$$

## Reduced statistical tensors of the photoion:

- ➢ Statistical tensors of the photo-ion in level $|\alpha_f \mathbb{J}_f\rangle$ after photoionization of unpolarized atoms by unpolarized plane-wave photons: If the incident light propagates along the $x$-axis (quantization axis, because of its typical use in experimental discussions) and if the photoelectron remains unobserved, the statistical tensors are given by Kämpfer *et al.* (2016)

$$\rho_{kq}(\alpha_f \mathbb{J}_f) \;=\; \frac{\pi}{2J_i+1}\, \delta_{q0} \sum_{\mathbb{M}\,\mathbb{M}'} \sum_{\kappa\, J J'} \sum_{\lambda=\pm 1} i^{L+p-L'-p'}\, \lambda^{p+p'}\, [L, L', J, J']^{1/2}\, (-1)^{J+J'+J_f+J_i+j+1}\, \langle L\lambda, L'-\lambda \,|\, kq\rangle \begin{Bmatrix} J_f & j & J' \\ J & k & J_f \end{Bmatrix} \begin{Bmatrix} J' & J_i & L' \\ L & k & J \end{Bmatrix}$$

$$\times \left\langle (\alpha_f \mathbb{J}_f, \varepsilon\kappa)\mathbb{J} \left\| \mathbb{O}^{\,(\mathbb{M},\,\mathrm{photoionization})} \right\| \alpha_i \mathbb{J}_i \right\rangle \left\langle (\alpha_f \mathbb{J}_f, \varepsilon\kappa)\mathbb{J}' \left\| \mathbb{O}^{\,(\mathbb{M}',\,\mathrm{photoionization})} \right\| \alpha_i \mathbb{J}_i \right\rangle^* ,$$

- ➢ Statistical tensors of the photoion in level $|\alpha_f \mathbb{J}_f\rangle$ after photoionization of unpolarized atoms by plane-wave photons with given density matrix $(c_{\lambda\lambda'})$: If the incident plane-wave light with well-defined (photon) density matrix $(c_{\lambda\lambda'})$ propagates along the $z$-axis, the statistical tensors are given more generally by (Sharma *et al.*, 2010)

$$\begin{aligned}\rho_{kq}(\alpha_f \mathbb{J}_f) \;&=\; \frac{\pi}{2J_i+1} \sum_{\mathbb{M}\mathbb{M}'} \sum_{\kappa J J'} \sum_{\lambda\lambda'} \left[\delta_{\lambda\lambda'}(1+\lambda P_3) \,+\, (1-\delta_{\lambda\lambda'})\,(P_1 - i\lambda P_2)\right] \, i^{\,L-L'+p-p'} \, \lambda^p \, (\lambda')^{p'} \, [L, L',\, J, J']^{1/2} \\ &\quad \times (-1)^{(J+J'+J_f+J_i+j+1)} \, \langle L\lambda L' -\lambda' \,|\, kq \rangle \begin{Bmatrix} J_f & j & J' \\ J & k & J_f \end{Bmatrix} : \begin{Bmatrix} J' & J_i & L' \\ L & k & J \end{Bmatrix} \\ &\quad \times \left\langle (\alpha_f J_f,\, \varepsilon\kappa) J \left\| \mathbb{O}^{\,(\mathbb{M},\,\mathrm{photoionization})} \right\| \alpha_i J_i \right\rangle \left\langle (\alpha_f J_f,\, \varepsilon\kappa) J' \left\| \mathbb{O}^{\,(\mathbb{M}',\,\mathrm{photoionization})} \right\| \alpha_i J_i \right\rangle^* ,\end{aligned}$$

- ➢ In Jac, the statistical tensors of the photoion are calculated and tabulated for the photoionization of unpolarized atoms by plane-wave photons with given Stokes parameters, if the flag `calcTensors` is set in `PhotoRecombination.Settings` and of the Stokes parameters are given explicitly in `PhotoRecombination.Settings.stokes`.

## Photoeionization by twisted light:

- ➢ Photoionization by twisted light:

$$\hbar\,\omega^{(\mathrm{twist})} \;+\; A \quad\longrightarrow\quad A^+ \;+\; e_p$$

## Further information:

- ➢ Electron-electron correlations  Often, interesting correlation effects with regard to exchange, interchannel coupling, relaxation and polarization occurs in the vincinity of the photoionization threshold.
- ➢ Giant resonances:  The $4d$ subshells of xenon and barium are both characterized by a broad and delayed absorption peak with a widths of approximately 50 eV above of the $4d$ ionization threshold, a so-called giant resonance. Photoelectron spectroscopy measurements in this region have shown that a significant fraction of the absorption arise for xenon and barium due to satellite and multielectron ionization.
- ➢ Dichroism:  Conventionally, the dichroism in the photoelectron emission is related to a change in the polarization of the incident light if the polarization state of the target is kept fixed.

### 7.1.d. Radiative recombination (`PhotoRecombination`)

## Process & notations:

- Radiative recombination of an atom or ion: $A^{q+} \,+\, e^- \quad\longrightarrow\quad A^{(q-1)+} \,+\, \hbar\omega$
- Formal quantum notation: $|\alpha_i \mathbb{J}_i\rangle \,+\, |\varepsilon\kappa\rangle \quad\longrightarrow\quad |\alpha_f \mathbb{J}_f\rangle \,+\, \hbar\omega\,(\mathbb{M})$ or $|\alpha_i \mathbb{J}_i\rangle \,+\, |\mathbf{p}\, m_s\rangle \quad\longrightarrow\quad |\alpha_f \mathbb{J}_f\rangle \,+\, \hbar\omega\,(\mathbb{M})$
- Using JAC: Perform an `Atomic.Computation(.., process=Jac.Rec, processSettings=PhotoRecombination.Settings(..), ..)` or call directly functions from the module `PhotoRecombination`.

## Motivation

- The photorecombination of ions is known also as radiative recombination (RR) or radiative electron capture (REC) in the literature.
- The radiative recombination (RR), which can be viewed as the time-reversed photoionization, occurs frequently in stellar and laboratory plasmas as well as in ion trap and storage ring experiments.
- If a highly-charged ion circulates in a storage ring, it may capture electrons from rest-gas atoms in the ring and will then be misbent by subsequent steering magnets. Therefore, the radiative recombination or electron capture typically results in a loss of the ion from the ring, and where the lifetime is usually proportional to the inverse of the product of the capture cross section and the target pressure.
- REC is dominant especially for low-$Z$ targets in the ring. For these targets, the capture cross sections of projectile ions with low or moderate energies are proportional to $Z_p^5$ and, hence, the lifetimes fall by ten orders of magnitude if $Z_p$ increases by two orders of magnitude. At (very) high projectile energies, in contrast, the lifetimes increases linearly with $\gamma \;=\; \sqrt{1 \,-\, \beta^2}$ .
- In JAC, the total radiative recombination cross sections and angular anisotropy parameters are calculated and tabulated by default for all selected recombination lines.

## Radiative recombination amplitude

- (Photo-) recombination amplitude: In first-order perturbation theory, most radiative recombination properties can be traced back to the evaluation of the (reduced emission) matrix element

$$\left\langle \alpha_f \mathbb{J}_f \left\| \mathbb{O}^{\,(\mathbb{M},\,\text{recombination})} \right\| (\alpha_i \mathbb{J}_i, \varepsilon\kappa) \mathbb{J}_t \right\rangle \;=\; \left\langle (\alpha_i \mathbb{J}_i, \varepsilon\kappa) \mathbb{J}_t \left\| \mathbb{O}^{\,(\mathbb{M},\,\text{photoionization})} \right\| \alpha_f \mathbb{J}_f \right\rangle^*$$

which describes the capture of a free electron with energy $\varepsilon$ and angular momentum $\kappa$ under the (simultaneous) emission of a photon with multipolarity $\mathbb{M} = (L, p)$ .

- ➢ In JAC, these photorecombination amplitudes are the building blocks to obtain most of the properties below.

## Final-state density matrix 'recombined ion + photon':

- ➢ Final-state density matrix 'recombined ion + photon':

$$\left\langle \alpha_f \mathbb{J}_f M_f ,\, \mathbf{k}\lambda \,|\, \rho_f \,|\, \alpha_f \mathbb{J}_f M'_f ,\, \mathbf{k}\lambda' \right\rangle$$

$$= \frac{8\pi}{2(2J_i+1)} \sum_{\mathbb{M}\mathbb{M}'\, J\, J'} \sum_{\kappa\,\kappa'} \sum_{\nu\,\mu_1\,\mu_2\,s\,s'} D^{\nu}_{\mu_1\mu_2}(\mathbf{k}\to\mathbf{e}_z)\, i^{L'-L}\, (i\lambda')^{\pi'}\, (-i\lambda)^{\pi}\, (-1)^{1/2+J_i+J'+L+s+s'-M'_{J,f}}\, [\ell, \ell', L, L', j, j', J, J', s]^{1/2}$$

$$\times [s'] \begin{Bmatrix} j' & 1/2 & \ell' \\ \ell & s & j \end{Bmatrix} \begin{Bmatrix} j' & J_i & J' \\ J & s & j \end{Bmatrix} \begin{Bmatrix} J & L & J_f \\ \nu & s' & L' \end{Bmatrix} \begin{Bmatrix} J & J' & s \\ J_f & s & L' \end{Bmatrix} \langle \ell' 0\, \ell 0 \,|\, s0 \rangle\, \left\langle J_f M_f\, s' - M'_f \,|\, \nu\mu_1 \right\rangle$$

$$\times \left\langle s0\, s' M'_f \,|\, J_f M'_f \right\rangle\, \langle L'\lambda'\, L - \lambda \,|\, \nu\mu_2 \rangle\, \left\langle \alpha_f \mathbb{J}_f \left\| \mathbb{O}^{(\mathbb{M},\, \mathrm{recombination})} \right\| (\alpha_i \mathbb{J}_i, \varepsilon\kappa)\mathbb{J} \right\rangle\, \left\langle \alpha_f \mathbb{J}_f \left\| \mathbb{O}^{(\mathbb{M}'',\, \mathrm{recombination})} \right\| (\alpha_i \mathbb{J}_i, \varepsilon\kappa')\mathbb{J} \right\rangle^{*},$$

and if a nuclear spin $I = 0$ is assumed.

- ➢ In JAC, no attempt has been made to implement the density matrix of the overall system 'recombined ion + photon' because of its little relevance for practical computations.

## Total recombination cross sections:

- ➢ Total recombination cross section: If the density of states and the principle of detailed balance between the capture and the (photo-) ionization of an electron is taken into account, the total cross section reads as

$$\sigma(\alpha_i \mathbb{J}_i, \alpha_f \mathbb{J}_f) = \frac{8\alpha^3\, \pi^3\, \omega}{(2J_i+1)}\, \frac{1}{\beta^2\, \gamma^2} \left[ \sum_{\mathbb{M}\, J\kappa} \left| \left\langle \alpha_f \mathbb{J}_f \left\| \mathbb{O}^{(\mathbb{M},\, \mathrm{recombination})} \right\| (\alpha_i \mathbb{J}_i,\, \varepsilon\kappa)\mathbb{J} \right\rangle \right|^2 \right]$$

where $\beta = v/c$ and $\gamma = \sqrt{1-\beta^2}$ arise from the Lorentz transformation in going from the projectile into the laboratory frame.

- In JAC, the total recombination cross sections are calculated and tabulated by default for all selected photorecombination lines.

## Angular distribution of emitted photons:

- Angular distribution of emitted photons: For initially unpolarized ions and unpolarized incident electrons, the angular distribution of the emitted (RR) photons can be readily obtained from the final-state density matrix by taking the trace $\mathrm{Tr}\,(P_{\mathbf{k}}\,\rho_f)$ :

$$W(\theta) \;=\; \frac{\sigma}{4\pi} \left( 1 \,+\, \sum_{\nu=1} P_\nu(\cos\theta)\, \beta_\nu^{\rm (REC)}(\alpha_i \mathbb{J}_i, \alpha_f \mathbb{J}_f) \right) .$$

- Anisotropy parameters of the emitted photons:

$$\beta_\nu^{\rm (REC)} \;=\; -\frac{1}{2} \sum_{JJ'\kappa\kappa'} \sum_{\mathbb{M}\mathbb{M}'} i^{L+p-L'-p'}\, (-1)^{J_i-1/2-J_f}\; [L, L', \ell, \ell', j, j', J, J']^{1/2}\; \langle \ell 0,\, \ell' 0 \,|\, \nu 0 \rangle\; \langle L1,\, L'-1 \,|\, \nu 0 \rangle\; \left( 1 + (-1)^{L+p+L'+p'-\nu} \right)$$

$$\times \begin{Bmatrix} J & J' & \nu \\ L' & L & J_f \end{Bmatrix} \begin{Bmatrix} J & J' & \nu \\ j' & j & J_i \end{Bmatrix} \begin{Bmatrix} j & j' & \nu \\ \ell' & \ell & 1/2 \end{Bmatrix} \left\langle \alpha_f \mathbb{J}_f \left\| \mathbb{O}^{\,(\mathbb{M},\,\text{recombination})} \right\| (\alpha_i \mathbb{J}_i,\, \varepsilon\kappa) \mathbb{J} \right\rangle^*$$

$$\times \left\langle \alpha_f \mathbb{J}_f \left\| \mathbb{O}^{\,(\mathbb{M}',\,\text{recombination})} \right\| (\alpha_i \mathbb{J}_i,\, \varepsilon\kappa') \mathbb{J}' \right\rangle \quad \left[ \sum_{J\kappa\,\mathbb{M}} \left| \left\langle \alpha_f \mathbb{J}_f \left\| \mathbb{O}^{\,(\mathbb{M},\,\text{recombination})} \right\| (\alpha_i \mathbb{J}_i,\, \varepsilon\kappa) \mathbb{J} \right\rangle \right|^2 \right]^{-1} .$$

- In JAC, the anisotropy parameters $\beta_\nu^{\rm (REC)}$, $\nu = 1, ..., 6$ are calculated and tabulated for all selected photorecombination lines if the flag `calcAnisotropy = true` is set in `PhotoRecombination.Settings`.

## Statistical tensors of the recombined ion in the level $|\alpha_f \mathbb{J}_f \rangle$ :

- Magnetic sublevel population $|\alpha_f \mathbb{J}_f M_f \rangle$ of the recombined ion: The radiative recombination amplitude from above can be used also to describe the (magnetic) sublevel population of the recombined ion. In the framework of density matrix theory, this sublevel population of the ionic (or atomic) states is described most conviniently in terms of the *statistical tensors* $\rho_{kq}(\alpha_f \mathbb{J}_f)$ of the recombined ion in its final level $|\alpha_f \mathbb{J}_f \rangle$ .
- In practice, however, the particular expression for the statistical tensors depend on the choice of the *quantization axis* of the overall system ($z$-axis) as well as the geometry of the experiments.

- In JAC, the statistical tensors for the recombination of unpolarized ions with plane-wave unpolarized electrons are calculated and tabulated if the flag `calcTensors = true` is set in `PhotoRecombination.Settings`.

## Photorecombination of twisted electrons:

- Expressions were derived for the angular distribution and the linear polarization of photons emitted due to the capture of twisted electrons into the ground state of (hydrogen-like) ions. We show that these angular and polarization distributions are sensitive to both, the transverse momentum and the topological charge of the electron beam.
- Photorecombination with twisted electrons: For twisted electrons with well-defined values of the linear momentum $p_z$ and with topological charge $m = 0, \pm 1, \pm 2$, the projection of the OAM apon the propagation direction, the initial-state wave function is given by:

  $$\psi_i^{\rm tw} (\mathbf{r}) \quad \equiv \quad \psi_{\kappa\, m\, p_z}^{\rm tw} (\mathbf{r}) \;=\; \int \frac{{\rm d}^2 \mathbf{p}_\perp}{(2\pi)^2}\, a_{\kappa m} (\mathbf{p}_\perp)\, {\rm e}^{{\rm i}\, (\mathbf{p}_\perp \cdot \mathbf{r}_\perp \,+\, p_z\, z)}$$

  where $a_{\kappa m}(\mathbf{p}_\perp)$ refer to the Fourier coefficients that include also the transverse momentum profile of the beam.

  $$\psi_f (\mathbf{r} \,-\, \mathbf{b}_\perp) \quad = \quad e^{-i\, \mathbf{p} \cdot \mathbf{b}_\perp}\; \psi_f (\mathbf{r} \;.$$

### 7.1.e. Auger processes (`Auger`)

## Process & notations:

- ➢ Auger emission (autoionization) of an atom or ion: $A^{q+*} \quad \longrightarrow \quad A^{(q+1)+(*)} \; + \; e_a^-$
- ➢ Formal quantum notation: $|\alpha_i \mathbb{J}_i\rangle \quad \longrightarrow \quad |\alpha_f \mathbb{J}_f\rangle \; + \; |\varepsilon\kappa\rangle$
- ➢ Using JAC: Perform an `Atomic.Computation(.., process=Jac.AugerX, processSettings=Auger.Settings(..), ..)` or call directly functions from the module `Auger`.

## Motivation:

- ➢ An autoionization of an (inner-shell) excited bound state can occur (only) if the initial level is energetically embedded into the *continuum* of the next higher charge state.
- ➢ Formally, an electron emission from such an embedded resonance (level) arise due to its coupling to one or several scattering states that are degenerate with the initial state and that involve one (or more) *free* electrons.
- ➢ Reaction plane of the Auger emission: For a prior photo-absorption or particle impact, this reaction plane is usually defined by the directions of the incident photon (particle) beam and the emitted Auger electron.
- ➢ In JAC, we support the computation of nonradiative (Auger) rates, relative Auger intensities and intrinsic angular anisotropy parameters. To this end, first the (reduced) Auger amplitudes are calculated for all selected pairs of initial and final levels and, later, these amplitudes are combined into Auger rates, intrinsic anisotropic as well as (intrinsic) spin-polarization parameters.
- ➢ While the Coulomb repulsion in the Auger amplitude above is typically sufficient in order to describe the autoionization of light and medium elements, the Breit interaction has been found important for electron emission and capture processes of highly-charged ions.
- ➢ The restriction to the electron-electron interaction in the computation (evaluation) of the Auger amplitudes is quite standard in all presently available Auger codes, even if the orbital functions of the resonant state $|\alpha_t \mathbb{J}_t\rangle$ and the final-ionic state $|\alpha_i \mathbb{J}_i\rangle$ are not taken orthogonal to each other.
- ➢ Often, the number of the possible scattering states $|(\alpha_f \mathbb{J}_f, \, \varepsilon\,\kappa) \, \alpha_t \mathbb{J}_t\rangle$ of a system increases rapidly since the free electrons may couple in quite different ways to the bound-state electrons from the final (Auger) ions.

- The Auger component of the previous Ratip program (Fritzsche 2012) has been widely used for studying electron emission processes after inner-shell excitation and the ionization of atoms as well as for analyzing the coherence transfer through Auger cascades.

## Auger amplitudes:

- Following Åberg and Howat (1982), the Auger transition amplitude for the autoionization of an excited bound state $|\alpha_i \, \mathbb{J}_i M_i\rangle$ into the final scattering state $|\alpha_t \, \mathbb{J}_t M_t\rangle$ , built from an ion in the final level $|\alpha_f \, \mathbb{J}_f\rangle$ , can be expressed most generally as

$$\begin{aligned}\left\langle (\alpha_f \mathbb{J}_f, \, \varepsilon \, \kappa) \, \mathbb{J}_t M_t \left| \, \mathbb{V}^{\,(\mathrm{Auger})} \, \right| \alpha_i \, \mathbb{J}_i M_i \right\rangle \;&=\; \left\langle (\alpha_f \mathbb{J}_f, \, \varepsilon \, \kappa) \, \mathbb{J}_t \left\| \, \mathbb{V}^{\,(\mathrm{Auger})} \, \right\| \alpha_i \, \mathbb{J}_i \right\rangle \, \delta_{J_i,J_t} \, \delta_{M_i,M_t} \, \delta_{P_i,P_t} \\ &=\; \left\langle (\alpha_f \mathbb{J}_f, \, \varepsilon \, \kappa) \, \mathbb{J}_t \, \| \, \mathbb{H} \, - \, E \, \| \, \alpha_i \, \mathbb{J}_i \right\rangle \, \delta_{J_i,J_t} \, \delta_{M_i,M_t} \, \delta_{P_i,P_t} .\end{aligned}$$

This amplitude is independent of the projection $M_i$ of the initial state owing to the rotational invariance of free atoms and the scalar character of the Hamiltonian and/or interelectronic interactions.

- In an autoionization process, the final scattering states $|\alpha_t \, \mathbb{J}_t M_t\rangle \;\equiv\; |(\alpha_f \mathbb{J}_f, \, \varepsilon \, \kappa) \, \mathbb{J}_t M_t\rangle$ arise from the coupling of the final state $|\alpha_f \, \mathbb{J}_f M_f\rangle$ of the ion with well-defined symmetry with the partial-wave $|\varepsilon \, \kappa \, m_j\rangle$ of the outgoing electron with energy $\varepsilon$ and (one-electron) angular momentum $\kappa \;=\; \kappa(j,l)$ as well as magnetic projection $m_j$ .

- In Jac, as in most other tools for computing autoionization processes, a common set of *orthonormal* orbitals is often supposed for the representation of the initial $|\alpha_i \mathbb{J}_i\rangle$ and final (ionic) bound levels $|\alpha_f \mathbb{J}_f\rangle$ in the evaluation of the Auger amplitudes. In this case, the Auger transition operator $\mathbb{V}^{\,(\mathrm{Auger})} \;\equiv\; \mathbb{H} \,-\, E \;\approx\; \mathbb{V}^{\,(\mathrm{e-e})}$ simplifies to the electron-electron interaction operator and the (reduced) Auger amplitude becomes

$$\left\langle (\alpha_f \mathbb{J}_f, \, \varepsilon \, \kappa) \, \mathbb{J}_t \left\| \, \mathbb{V}^{\,(\mathrm{Auger})} \right\| \alpha_i \, \mathbb{J}_i \right\rangle \;\simeq\; \left\langle (\alpha_f \mathbb{J}_f, \, \varepsilon \, \kappa) \, \mathbb{J}_t \left\| \, \mathbb{V}^{\,(\mathrm{e-e})} \, \right\| \alpha_i \, \mathbb{J}_i \right\rangle \, \delta_{J_i,J_t} \, \delta_{M_i,M_t} \, \delta_{P_i,P_t} \, .$$

Within the framework of the Dirac-Coulomb-Breit Hamiltonian, the interelectronic interaction is the sum of the Coulomb repulsion and Breit interaction, $\mathbb{V}^{\,(\mathrm{e-e})} \;=\; \mathbb{V}^{\,(\mathrm{Coulomb})} \,+\, \mathbb{V}^{\,(\mathrm{Breit})} \;\simeq\; \mathbb{V}^{\,(\mathrm{Coulomb})}$ , although it is often approximated by just the Coulomb part.

- In Jac, the partikular kind of the Auger operator $\mathbb{V}^{\,(\mathrm{Auger})}$ can be specified by selecting `Auger.Settings.operator = ("Coulomb", "Breit", "Coulomb+Breit", ...)`.

## Auger rates:

- Auger rates: If the (continuum) interaction between the different Auger channels is neglected, the Auger rates are given by

  $$A(i \to f) \;=\; 2\pi \sum_\kappa \left| \left\langle (\alpha_f \mathbb{J}_f,\, \varepsilon\, \kappa)\, \mathbb{J}_i \left\| \mathbb{V}^{\,(\mathrm{Auger})} \right\| \alpha_i\, \mathbb{J}_i \right\rangle \right|^2 ,$$

  where the Auger interaction operator $\mathbb{V}^{\,(\mathrm{Auger})}$ still need to be specified due to the (computational) framework and additional approximations that are made in practice.
- In JAC, the Auger rates and (Auger) lifetimes are tabulated by default for all selected (Auger) transitions.

## Angular distribution of Auger electrons:

- Angular distribution of the emitted electrons: If only the Auger electrons are detected from the autoionization of an (inner-shell) excited ion in level $|\alpha_i \mathbb{J}_i\rangle$ , and which is fully characterized by its reduced statistical tensors $\mathcal{A}_{kq}(\alpha_i \mathbb{J}_i)$ , the angular distribution of the emitted electrons of a given Auger transition $|\alpha_i \mathbb{J}_i\rangle \;\to\; |\alpha_f \mathbb{J}_f\rangle$ can be written in the general form (Balashov *et al.* 2000, equation 3.10)

  $$W(\vartheta, \varphi;\, \alpha_i \mathbb{J}_i \to \alpha_f \mathbb{J}_f) \;=\; \frac{A(i \to f)}{4\pi} \left[ 1 \,+\, \sum_{k\,=\,2,\,4,\,\ldots}^{k_{\max}} \sqrt{\frac{4\pi}{2k+1}}\; \alpha_k(\alpha_i \mathbb{J}_i \to \alpha_f \mathbb{J}_f) \sum_{q\,=\,-k}^{k} \mathcal{A}_{kq}(\alpha_i \mathbb{J}_i)\; Y_{kq}(\vartheta, \varphi) \right] ,$$

  and where $\alpha_k(\alpha_i \mathbb{J}_i \to \alpha_f \mathbb{J}_f)$ are the (so-called) intrinsic anisotropy parameters of the electron emission

  $$\begin{aligned} \alpha_k(\alpha_i \mathbb{J}_i \to \alpha_f \mathbb{J}_f) \;=\; & \left[ \sum_\kappa \left\langle (\alpha_f \mathbb{J}_f,\, \varepsilon\, \kappa)\, \mathbb{J}_i \left\| \mathbb{V}^{\,(\mathrm{Auger})} \right\| \alpha_i\, \mathbb{J}_i \right\rangle \right]^{-1} (-1)^{J_i + J_f + k - 1/2} \sqrt{2J_i + 1} \sum_{\kappa\kappa'} [\ell, \ell', j, j']^{1/2} \left\langle \ell 0,\, \ell' 0 \,|\, k0 \right\rangle \\ & \times \begin{Bmatrix} J_i & j & J_f \\ j' & J_i & k \end{Bmatrix} \begin{Bmatrix} \ell & j & 1/2 \\ j' & \ell' & k \end{Bmatrix} \left\langle (\alpha_f \mathbb{J}_f,\, \varepsilon\, \kappa)\, \mathbb{J}_i \left\| \mathbb{V}^{\,(\mathrm{Auger})} \right\| \alpha_i\, \mathbb{J}_i \right\rangle \left\langle (\alpha_f \mathbb{J}_f,\, \varepsilon\, \kappa')\, \mathbb{J}_i \left\| \mathbb{V}^{\,(\mathrm{Auger})} \right\| \alpha_i\, \mathbb{J}_i \right\rangle^* \end{aligned}$$

- Here, the factor $A(i \to f)$ is the total probability of the Auger transition $|\alpha_i \mathbb{J}_i\rangle \to |\alpha_f \mathbb{J}_f\rangle$ , integrated over the ejection angles. The anisotropy parameters $\alpha_k(\alpha_i \mathbb{J}_i \to \alpha_f \mathbb{J}_f)$ contain information about the dynamics of the decay, while the tensors $\mathcal{A}_{kq}(\alpha_i \mathbb{J}_i)$ just describe the polarization properties of the initial level.

- In JAC, the intrinsic anisotropy parameters are calculated and tabulated if the flag `calcAnisotropy = true` is set in `Auger.Settings`.

## Spin polarization of Auger electrons:

- The spin polarization of Auger electrons is usually described by an polarization vector **P** . The three components of **P** can be expressed in terms of the statistical tensors of the initial level and the intrinsic anisotropy parameters of the Auger transition under consideration.
- Two coordinate systems, $S(XYZ)$ and $S'(X'Y'Z')$ are often employed in the description of the spin polarization of Auger electrons; cf. the figure below and Kabachnik *et al.* (2007).

## Two-electron single Auger emission (TESA):

- Non-resonant three-electron Auger transitions have been suggested several decades ago, though clear evidence for such TESA transition were found in Ar only with very low intensity relative to normal Auger.
- These TESA transitions usually start with the creation of a double vacancy in an inner shell, and which is filled simultaneously two outer-shell electrons, while the released energy is passed to a third emitted electron.
- Such inner-shell double vacancies are normally at energies above the minimum fourfold ionization energy and can easily be filled also by two separate successive two-electron Auger transitions involving four electrons in total.

### 7.1.f. Dielectronic recombination (`Dielectronic`)

## Process & notations:

- Dielectronic recombination (DR) of an atom or ion: $A^{q+} + e^- \longrightarrow A^{(q-1)+*} \longrightarrow A^{(q-1)+(*)} + \hbar\omega$
- Formal quantum notation: $|\alpha_i \mathbb{J}_i\rangle + |\varepsilon\, \kappa\rangle \longrightarrow |\alpha_d \mathbb{J}_d\rangle \longrightarrow |\alpha_f \mathbb{J}_f\rangle + \hbar\omega\,(\mathbb{M})$ or $|\alpha_i \mathbb{J}_i\rangle + |\mathbf{p}_i\, m_i\rangle \longrightarrow |\alpha_d \mathbb{J}_d\rangle \longrightarrow |\alpha_f \mathbb{J}_f\rangle + \hbar\omega\,(\mathbb{M})$
- Using JAC: Perform an `Atomic.Computation(.., process=Jac.Dierec, processSettings=Dielectronic.Settings(..), ..)` or call directly functions from the module `Dielectronic`.

## Motivation:

- In most computations, the dielectronic recombination of a $N$-electron target ion in the (initial) level $|\alpha_i \mathbb{J}_i\rangle$ is typically handled as a two-step process, in which first an electron is captured resonantly from the continuum into a $[(N+1)$-electron$]$ resonance level $|\alpha_d \mathbb{J}_d\rangle$, embedded into the continuum of the initial ion and with often two or more electrons in some excited (one-electron) orbital. In a second step, then, this excited level $|\alpha_d \mathbb{J}_d\rangle$ either decays radiatively by the emission of photons to some (final) level $|\alpha_f \mathbb{J}_f\rangle$, below of the ionization threshold of the ion, or it returns by autoionization back to the ionization stage of the initial target ion.
- In practice, the number of the possible scattering states $|(\alpha_i\, \mathbb{J}_i,\, \varepsilon\, \kappa),\, \mathbb{J}_d M_d\rangle$ of the recombined ion often increases very rapidly since, the free electrons may couple in many different ways to the bound-state electrons of the initial ion.
- Apart from the computation of proper Auger rates, helpful calculation of DR spectra critically depends on the simple control (and handling) of the various — radiative and non-radiative — decay branches. In JAC, these branches are treated rather equally within the `Dielectronic` module.
- In JAC, the individual resonance strength $S(i \to d \to f)$ and total resonance strengthes $S(i \to d)$ are calculated and tabulated by default for all selected pathways.
- In JAC, both the radiative as well as the Auger amplitudes and rates are finally computed by the corresponding modules `Radiative` and `Auger`.

## Resonance strength of the dielectronic recombination:

- Partial resonance strength: If the interference between the radiative and dielectronic (nonradiative) capture of the electron is negligible in the field of the target, the integrated DR cross section for an isolated resonance level $|\alpha_d \mathbb{J}_d\rangle$, the (so-called) resonance strength, can be expressed in terms of the Auger and radiative rates of this level by

$$S(i \to d \to f) \quad \equiv \quad \int_{-\infty}^{\infty} dE \;\; \sigma^{\,\rm (DR)}(E) \quad = \quad \frac{2\pi^2 \, \hbar}{k_i^2} \; \frac{A_a(i \to d) \, A_r(d \to f)}{\Gamma_d}$$

where $k_i$ denotes the wave number of the incident electron and $\Gamma_d$ the half-widths of the resonance level $|\alpha_d \mathbb{J}_d\rangle$, embedded into the continuum. Since this resonance strength refers to the area under the DR cross sections, it is usually given in units of: $[S] \; = \; {\rm cm}^2 \, {\rm eV}$.

- In the resonance strength above, $A_a(i \to d)$ is the rate for the inverse Auger capture from the initial into the (doubly-excited) resonance level $|\alpha_d \mathbb{J}_d\rangle$, while $A_r(d \to f)$ refers to the rate for the radiative stabilization to the final level $|\alpha_f \mathbb{J}_f\rangle$ of the $N+1$-electron ion.

- Total width of the resonance level $|\alpha_d \mathbb{J}_d\rangle$ The total width $\Gamma_d$ is determined by all possible decay channels of the resonance level $|\alpha_d \mathbb{J}_d\rangle$ and is given in first-order perturbation theory by

$$\Gamma_d \quad = \quad \hbar \, \left( \sum_j A_a(d \to j) \;\; + \;\; \sum_{f'} A_r(d \to f') \right)$$

by taking the sum over all the individual Auger and radiative rates (widths) of the intermediate level $|\alpha_d \mathbb{J}_d\rangle$.

- The Auger and inverse capture rates $A_a(i \to d) \; = \; g_i/g_d \;\; A_a(d \to i)$ are proportional to each other owing to the principle of kinetic balance, and with the $g$'s being the statistical factors of the initial and intermediate resonance levels.

- The use of the individual resonance strength $S(i \to d \to f)$ is appropriate especially, if the energy-dependent DR cross section has a Lorentzian profile

$$\sigma^{\,\rm (DR)}(E) \quad = \quad \frac{S}{\pi} \, \frac{\Gamma/2}{(E_r \, - \, E)^2 \, + \, \Gamma^2/4}$$

around the resonance energy $E_r \; = \; E_d - E_i$ and also a natural width less or comparable to the energy spread of the electron beam. In general, this condition is well fulfilled for most $\Delta n \, \geq \, 1$ resonances (with an excitation of a bound electron from the shell $n_i \; \to \; n_f$, for which the total widths are small in most cases), but this condition can usually be utilized also for the $\Delta n \; = \; 0$ lines if the shape of the resonances is not to be analyzed in detail.

- Owing to the energy of the incident electron [cf. the factor $1/k_i^2$ above], the resonance strength increases rapidly towards the threshold of the dielectronic recombination and makes the process sensitive to low kinetic energies of the incoming electrons.
- Total resonance strength: At storage rings, the radiative stabilization of the ions in the intermediate resonance level $|\alpha_d \mathbb{J}_d\rangle$ is often not observed explicitly and, hence, the radiative rate for the individual transition $d \rightarrow f$ in the resonance strength above has to be replaced by the total radiative rate of the (doubly-excited) resonance level $|\alpha_d \mathbb{J}_d\rangle$ :

$$A_r(d \rightarrow f) \quad \longrightarrow \quad \sum_{f'} A_r(d \rightarrow f') \qquad \Longrightarrow \qquad S(i \rightarrow d \rightarrow f) \quad \longrightarrow \quad S(i \rightarrow d) \;=\; \sum_{f'} S(i \rightarrow d \rightarrow f')$$

- In JAC, both the individual $S(i \rightarrow d \rightarrow f)$ and total resonance strengthes $S(i \rightarrow d)$ are calculated and tabulated by default for all selected pathways.

### 7.1.g. Photoexcitation & fluorescence (`PhotoExcitationFluores`)

## Process & notations:

- Photo excitation of an atom or ion with subsequent fluorescence emission: $A \,+\, \hbar\omega_i \quad \longrightarrow \quad A^* \quad \longrightarrow \quad A^{(*)} \,+\, \hbar\omega_f$
- Formal quantum notation: $|\alpha_i \mathbb{J}_i\rangle \,+\, \hbar\omega\,(\mathbf{k}\,||\,\mathbf{e}_z,\, \lambda;\, \{\mathbb{M}\}) \quad \longrightarrow \quad |\alpha_e \mathbb{J}_e\rangle \quad \longrightarrow \quad |\alpha_f \mathbb{J}_f\rangle \,+\, \hbar\omega_f\,(\Omega;\, \mathbf{P})$
- Using JAC: Perform an `Atomic.Computation(.., process=PhotoExcFluor, processSettings=PhotoExcitationFluores.Settings(..), ..)` or call directly functions from the module `PhotoExcitationFluores`.

## Motivation:

- The photoexcitation and (subsequent) fluorescence emission from atoms and ions has been investigated in good detail for both, incident plane-wave radiation as well as for twisted Bessel and Laguerre-Gaussian beams.
- Since the properties of the photo-excited atoms can be calculated by the module `PhotoExcitation` and those for the radiative emission by the module `Radiative`, here we shall focus only upon properties that are related to the overall excitation-fluorescence process, such as the angular distribution or density matrix of the fluorescence photons.

- In JAC, the statistical tensors $\rho_{kq}(\alpha_e \mathbb{J}_e)$ can be calculated and tabulated by the module `PhotoExcitation`. These tensors are also required for describing the excitation-fluorescence process; they are calculated (but not tabulated here) if the flag `calcTensors = true` is set in `PhotoExcitationFluores.Settings`.

## Density matrix of the fluorescence photon $\hbar\omega_f(\Omega)$ :

- (Reduced) density matrix of the fluorescence photons for the photoemission from an aligned or oriented atom: For photons emitted under the angle $\Omega = (\vartheta, \varphi)$ with regard to the propagation direction of the incident plane-wave radiation $\mathbf{k} \,||\, \mathbf{e}_z$ , the (reduced) density matrix can be readily expressed in terms of the statistical tensors of the excited level $\rho_{kq}(\alpha_e \mathbb{J}_e)$ as

$$\begin{aligned} \left\langle \mathbf{k}_0\, \lambda \,\middle|\, \rho_{\omega_f} \,\middle|\, \mathbf{k}_0\, \lambda' \right\rangle \;&=\; 2\pi \sum_{k,\,qq'} \sum_{\mathbb{M}\,\mathbb{M}'} D^k_{-qq'}(\varphi, \vartheta, 0)\;\; \rho_{kq}(\alpha_e \mathbb{J}_e)\;\; i^{L'+p'-L-p}\; \lambda^p\; (\lambda')^{p'}\;\; \sqrt{2L+1}\,\sqrt{2L'+1}\;\; (-1)^{J_f+J_e+k+q+1} \\ &\times\;\; \langle L\lambda,\, L'(-\lambda') \,|\, k -q' \rangle \begin{Bmatrix} L & L' & k \\ J_e & J_e & J_f \end{Bmatrix} \left\langle \alpha_f\, \mathbb{J}_f \,\middle\|\, \mathbb{O}^{(\mathbb{M},\,\mathrm{emission})}(\omega_f) \,\middle\|\, \alpha_e\, \mathbb{J}_e \right\rangle \left\langle \alpha_f\, \mathbb{J}_f \,\middle\|\, \mathbb{O}^{(\mathbb{M}',\,\mathrm{emission})}(\omega_f) \,\middle\|\, \alpha_e\, \mathbb{J}_e \right\rangle^* \end{aligned}$$

- In JAC, the reduced density matrix of a fluorescence photon can be calculated and tabulated at selected angles $\{\Omega_1 = (\vartheta_1, \varphi_1),\, \Omega_2,\, ...\}$, if the flags `calcTensors = true` and `calcPhotonDm = true` is set in `PhotoExcitationFluores.Settings` and if the solid angles are specified explicitly by `PhotoExcitationFluores.Settings.Omegas`.

## Angular distribution and Stokes parameters of the fluorescence photon $\hbar\omega_f(\Omega;\, \mathbf{P})$ :

- Angular distribution of the fluorescence light for the photoemission from a aligned or oriented atom: Most generally, the angular distribution can be obtained from the photon density matrix above by a summation over the polarization states:

$$W(\vartheta, \varphi) \;=\; \sum_{\lambda} \left\langle \mathbf{k}_0\, \lambda \,\middle|\, \rho_{\omega_f} \,\middle|\, \mathbf{k}_0\, \lambda \right\rangle .$$

- Using the expressions from above, this angular distribution could be calculated for selected angles $\{\Omega_1 = (\vartheta_1, \varphi_1),\, \Omega_2,\, ...\}$ . However, the computation of this angular distribution is currently not (yet) implemented, although this could be readily done.

- Angular distribution of the fluorescence light: For initially unpolarized atoms and unpolarized photons in the photo-excitation process, in particular, this distribution is given by the same formulas as for the photoemission (alone), if the alignment parameters $\mathcal{A}_{k0}(\alpha_e \mathbb{J}_e)$ are known for the excited level $|\alpha_e \mathbb{J}_e\rangle$ .

$$W(\vartheta) \;=\; \frac{W_o}{4\pi} \left( 1 + \sum_{k=2,4,..} f_k(\alpha_e \mathbb{J}_e, \alpha_f \mathbb{J}_f)\, \mathcal{A}_{k0}(\alpha_e \mathbb{J}_e)\, P_k(cos\vartheta) \right) .$$

- In JAC, the alignment parameters of the (intermediate) excited level $\mathcal{A}_{kq}(\alpha_e \mathbb{J}_e)$ can be calculated and tabulated by the module `PhotoExcitation`, while the structure functions $f_k(\alpha_e \mathbb{J}_e,\, \alpha_f \mathbb{J}_f)$ can be obtained by using the module `Radiative`.

### 7.1.h. Photoexcitation & autoionization (`PhotoExcitationAutoion`)

## Process & notations:

- Photo-excitation & autoionization of an atom or ion: $A \,+\, \hbar\omega \quad \longrightarrow \quad A^* \quad \longrightarrow \quad A^{(*)} \,+\, e_a^-$
- Formal quantum notation: $|\alpha_i \mathbb{J}_i\rangle \,+\, \hbar\omega\,(\mathbb{M}) \quad \longrightarrow \quad |\alpha_r \mathbb{J}_r\rangle \quad \longrightarrow \quad |\alpha_f \mathbb{J}_f\rangle \,+\, |\varepsilon\kappa\rangle$
- Using JAC: Perform an `Atomic.Computation(.., process=PhotoExcAuto, processSettings=PhotoExcitationAutoion.Settings(..), ..)` or call directly functions from the module `PhotoExcitationAutoion`.

## Motivation:

- The photoexcitation and (subsequent) autoionization of atoms and ions has been explored in good detail, either as the dominant (photo-) ionization process within the vincinity of certain (photoionization) resonances or simply as competitive process to atomic photoionization.
- Often, the photoexcitation-autoionization can be considered independently of the *direct* photoionization and then leads to partial and total photoexcitation-autoionization cross sections.
- If the direct photoionization is negligible, the photoexcitation-autoionization is the time-reversed process to the dielectronic recombination.

- In JAC, partial resonance strength $S(i \to r \to f)$ and total resonance strength $S(i \to r)$ are calculated an tabulated by default. Further implementations are required to obtain also Fano profiles, total photoioniozation cross sections, etc.

## Fano profiles in photo-ionization cross sections:

- For an isolated resonance, the total photoionization cross section can be (formally) parametrized in the vincinity of the resonant level $|\alpha_r \mathbb{J}_r\rangle$ by the energy-dependent cross section

$$\sigma(\mathcal{E}) \;=\; \sigma^{\,(\mathrm{EA})} \, \frac{(q \,+\, \mathcal{E})^2}{1 \,+\, \mathcal{E}^2} \;+\; \sigma^{\,(\mathrm{D})}$$

  where $\sigma^{(\mathrm{D})}$ is the direct photoionization cross section and $\sigma^{\,(\mathrm{EA})}$ the cross section due to the photo-excitation and autoionization of the resonance. Moreover, $\mathcal{E} \,=\, (E_\omega \,-\, E_r)/(\Gamma/2)$ indicates the departure of the incident photon energy $E_\omega$ from the resonance energy $E_r$, in units of the half-width $(\Gamma/2)$ of the resonance.

- The Fano $q$ parameter determines the overall profile of the cross section, ranging from a near-Lorentzian $(q \;\to\; \infty)$, to a window-like $(q \;\to\; 0)$, and up to a completely asymmetric resonance $(q \;\to\; \pm 1)$.

- In JAC, no attempt has (yet) been made to calculate the Fano profiles explicitly for selected resonances, although this would be possible by combining proper calls to functions from the modules `PhotoIonization`, `PhotoExcitation` as well as `Auger`.

## Total photoionization amplitudes and cross sections across the resonance level $|\alpha_r \mathbb{J}_r\rangle$ :

- The photoexcitation and (subsequent) autoionization of atoms and ions obviously contributes to the photoionization and, hence, to its amplitudes and cross sections.

- Total photoionization amplitudes across the resonance level $|\alpha_r \mathbb{J}_r\rangle$ :

$$\mathcal{M}\,(\omega;\, (\alpha_f \mathbb{J}_f,\, \varepsilon\kappa)\, \mathbb{J}_t,\, \alpha_r \mathbb{J}_r,\, \alpha_i \mathbb{J}_i)$$

$$=\; \left\langle (\alpha_f \mathbb{J}_f,\, \varepsilon\kappa)\; \mathbb{J}_t \,\middle\|\, \mathbb{O}^{\,(\mathbb{M},\,\text{photoionzation})} \middle\|\, \alpha_i \mathbb{J}_i \right\rangle \;+\; \frac{\left\langle (\alpha_f \mathbb{J}_f,\, \varepsilon\kappa)\; \mathbb{J}_t \,\middle\|\, \mathbb{O}^{\,(\text{Auger})} \,\middle\|\, \alpha_r \mathbb{J}_r \right\rangle \left\langle \alpha_r \mathbb{J}_r \,\middle\|\mathbb{O}^{\,(\mathbb{M},\,\text{absorption})}\middle\|\, \alpha_i \mathbb{J}_i \right\rangle}{E_i \,+\, \omega \,-\, E_r \,+\, i\,\Gamma_r/2}$$

  In this notation of the resonant photoionization, we assume the photoelectron to escape by means of the partial wave $|\varepsilon\,\kappa\rangle$ with kinetic energy $\varepsilon \,=\, E_i \,+\, \omega \,-\, E_f$ and with well-defined angular momentum and parity.

➢ Apart from the *direct* photoionization amplitude (first term), the total photoionization amplitude now also contains the photoexcitation-autoionization amplitudes (second term).

➢ From these amplitudes, the total photoionization cross section (intensity) is obtained as before by the summation over all the possible scattering states of the final system 'photoion + electron':

$$\sigma\,(\omega;\,\alpha_i\mathbb{J}_i,\,\alpha_f\mathbb{J}_f) \;=\; \frac{4\,\pi^2\,\alpha\,\omega}{3\,(2J_i+1)} \sum_{\alpha_r\mathbb{J}_r\,\kappa\,\mathbb{J}_t} |\,\mathcal{M}\,(\omega;\,(\alpha_f\mathbb{J}_f,\,\varepsilon\kappa)\,\mathbb{J}_t,\,\alpha_r\mathbb{J}_r,\,\alpha_i\mathbb{J}_i)\,|^2,$$

This includes both, the summation over all relevant resonances as well as the summation over the partial waves of the photoelectron and the total angular momenta and parities of the scattering levels $|\alpha_t\mathbb{J}_t\rangle$ .

➢ In JAC, no attempt has yet been made to calculate and tabulate the resonant photoionization cross sections or angular anisotropy parameters, although this would be possible since all required many-electron matrix elements are internally quite readily available.

## Angular distribution of Auger electrons:

➢ Of course, the angular distribution of the emitted Auger electrons always critically depend on the (properties of the) prior excitation process; in this `ImpactExcitationAutoIon` module, we typically assume a photoexcitation of the atoms or ions for calculating subsequent properties of Auger electrons. We also assume that the direct photoionization is negligible near to the considered resonance level $|\alpha_r\mathbb{J}_r\rangle$ .

➢ If the initial level $|\alpha_i\mathbb{J}_i\rangle$ is axially symmetric along the $z$-axis, $\mathcal{A}_{kq}(\alpha_i\mathbb{J}_i) \;\sim\; \delta_{q0}$ , the angular distribution only depends on the angle $\vartheta$ between the symmetry ($z$-) axis and the linear momentum of the ejected electron, and the angular distribution then simplifies to

$$W(\vartheta;\,\alpha_i\mathbb{J}_i \rightarrow \alpha_f\mathbb{J}_f) \;=\; \frac{A_a(i\rightarrow f)}{4\pi}\left[1+\sum_{k\,=\,2,\,4\,,\ldots}^{k_{\rm max}} \alpha_k(\alpha_i\mathbb{J}_i \rightarrow \alpha_f\mathbb{J}_f)\;\mathcal{A}_{k0}(\alpha_i\mathbb{J}_i)\;P_k(\cos\vartheta)\right] .$$

➢ In JAC, no attempt has (yet) been made to tabulate the angular distribution $W(\vartheta;\,\alpha_i\mathbb{J}_i \;\rightarrow\; \alpha_f\mathbb{J}_f)$ explicitly for selected scenarios; cf. section 7.1.e.

### 7.1.i. Rayleigh & Compton scattering of light (`RayleighCompton`)

## Process &amplitude:

- Rayleigh or Compton scattering of photons at an atom or ion: $A \,+\, \hbar\omega_i \quad \longrightarrow \quad A^{(*)} \,+\, \hbar\omega_f$ ... including $\omega_i \,=\, \omega_f$
- Formal quantum notation: $|\alpha_i \mathbb{J}_i M_i\rangle \,+\, \hbar\omega_i(\mathbf{k}_i, \lambda_i;\, \{\mathbb{M}_i\}) \quad \longrightarrow \quad |\alpha_f \mathbb{J}_f M_f\rangle \,+\, \hbar\omega_f(\mathbf{k}_f, \lambda_f;\, \{\mathbb{M}_f\})$

  $\omega_i \,=\, \omega_f$ ... for elastic Rayleigh scattering
- Using JAC: Perform an `Atomic.Computation(.., process=Compton, processSettings=RayleighCompton.Settings(..), ..)` or call directly functions from the module `RayleighCompton`.

## Motivation:

- The elastic scattering of light by the bound electrons of an atom or ion is commonly known as Rayleigh scattering and has been found a versatile tool in the past for studying the electronic structure of atoms and their (chemical) environment.
- The inelastic (Compton or Raman) scattering of light on atoms, ions or molecules is associated in contrast with an excitation of the target and has also been explored since the 1920s, both experimentally and theoretically.
- First theoretical investigations on the elastic scattering of photon by bound electrons date back to the mid-1930s. While initially rather simple approximations were applied, for instance based on atomic form factors, a more rigorous quantum-electrodynamical (QED) approach was developed later in terms of the relativistic second-order S-matrix amplitude.
- In JAC, the angular-differential cross sections for the elastic Rayleigh and inelastic Compton scattering are calculated and tabulated for all selected levels of $(i \to f)$ line.

## Second-order scattering amplitude

- Compton scattering amplitude: In second-order perturbation theory, the elastic Rayleigh and inelastic Compton process can be described in terms of the two-photon transition amplitudes for a transition from substates $|\alpha_i \mathbb{J}_i M_i\rangle \to |\alpha_f \mathbb{J}_f M_f\rangle$ owing to the absorption and emission of photons with well-defined wave vectors $\mathbf{k}_{i,f}$ and polarization vectors $\boldsymbol{\epsilon}_{i,f}$ . This amplitude is given in terms of the electron-photon interaction operator by (Jahrsetz *et al.*, 2015)

$$\mathcal{M}_{fi}^{(\text{Compton})}(\alpha_f \mathbb{J}_f M_f,\, \alpha_i \mathbb{J}_i M_i; \mathbf{k}_f, \boldsymbol{\epsilon}_f,\, \mathbf{k}_i, \boldsymbol{\epsilon}_i) \;=\; \sum_{\alpha_\nu \mathbb{J}_\nu M_\nu} \left[ \frac{\left\langle \alpha_f \mathbb{J}_f M_f \left| \hat{R}^\dagger(\boldsymbol{k}_f, \boldsymbol{\epsilon}_f) \right| \alpha_\nu \mathbb{J}_\nu M_\nu \right\rangle \left\langle \alpha_\nu \mathbb{J}_\nu M_\nu \left| \hat{R}(\boldsymbol{k}_i, \boldsymbol{\epsilon}_i) \right| \alpha_i \mathbb{J}_i M_i \right\rangle}{E_i \,+\, \omega_i \,-\, E_\nu} \right.$$

$$\left. + \frac{\left\langle \alpha_f \mathbb{J}_f M_f \left| \hat{R}(\boldsymbol{k}_i, \boldsymbol{\epsilon}_i) \right| \alpha_\nu \mathbb{J}_\nu M_\nu \right\rangle \left\langle \alpha_\nu \mathbb{J}_\nu M_\nu \left| \hat{R}^\dagger(\boldsymbol{k}_f, \boldsymbol{\epsilon}_f) \right| \alpha_i \mathbb{J}_i M_i \right\rangle}{E_i \,-\, \omega_f \,-\, E_\nu} \right] .$$

Here, the energies of the photons involved are related by $\omega_f \;=\; \omega_i \,-\, E_f \,+\, E_i$ to each other and to the energies of the initial and final states of the atoms or ions.

- Owing to the time-ordering in (time-dependent) perturbation theory, there are obviously two contributions to this second-order amplitude for the *absorption-emission* and *emission-absorption* of the two photons involved.

- Although these second-order amplitudes can be readily written down, they are less useful for practical computations as they are based on different representations of the atomic and photon state(s); we therefore first need to perform a multipole expansion of the electron-photon interaction operators and to do all neccessary simplifications.

- Compton (scattering) amplitude for the scattering of photons with well-defined helicity and multipolarity:

$$\mathcal{M}_{fi}^{(\text{Compton})}(\alpha_f \mathbb{J}_f M_f,\, \alpha_i \mathbb{J}_i M_i;\, \mathbb{M}_f, \lambda_f,\, \mathbb{M}_i, \lambda_i) \;=\; \ldots \frac{\left\langle \alpha_f \mathbb{J}_f \left\| \,\mathbb{O}^{(\mathbb{M}_f,\,\text{emission})}\, \right\| \alpha_\nu \mathbb{J}_\nu \right\rangle \left\langle \alpha_\nu \mathbb{J}_\nu \left\| \,\mathbb{O}^{(\mathbb{M}_i,\,\text{absorption})}\, \right\| \alpha_i \mathbb{J}_i \right\rangle}{E_i \,+\, \omega_f \,-\, E_\nu} \;+\; \ldots$$

## Angle-differential and total cross sections:

- Angle-differential cross section for the Compton scattering of unpolarized light by initially unpolarized atoms: For unpolarized incident plane-wave photons and if the polarization of the scattered photons as well as the magnetic sublevel population of the residual ions both remain unobserved, the angle-differential cross section is given by

$$\frac{d\sigma^{\,\rm (Compton)}}{d\Omega}\,(\vartheta;\,\omega_i)$$

$$= \frac{1}{2}\,\frac{\omega_f}{\omega_i}\,\frac{1}{2J_i+1}\,\sum_{\lambda_i\,\lambda_i'\,\lambda_f\lambda_f'}\;\sum_{M_i,\,M_f}\,c_{\lambda_i\,\lambda_i'}\;\mathcal{M}_{fi}^{\rm (Compton)}(\alpha_f\mathbb{J}_fM_f,\,\alpha_i\mathbb{J}_iM_i;\,\mathbb{M}_f,\lambda_f,\,\mathbb{M}_i,\lambda_i)\;\;\mathcal{M}_{fi}^{\rm (Compton)}(\alpha_f\mathbb{J}_fM_f,\,\alpha_i\mathbb{J}_iM_i;\,\mathbb{M}_f,\lambda_f',\,\mathbb{M}_i,\lambda_i')$$

Unfortunately, there is no simple parametrization of this angle-differential cross section $\frac{d\sigma^{\rm (Compton)}}{d\Omega}\,(\vartheta;\,\omega_i)$ .

- The angle-differential Rayleigh cross sections can be obtained from the formulas above by using $|\alpha_f\mathbb{J}_f\rangle = |\alpha_i\mathbb{J}_i\rangle$ in the two-photon amplitudes and irreducible tensors.
- In JAC, the angle-differential Rayleigh and Compton scattering cross sections are calculated by default for all selected initial levels and $(i \to f)$ lines, if a proper spectrum is specified in `RayleighCompton.Settings.spectrum`.

## Further information:

-

### 7.1.j. Multi-photon excitation and decay (`MultiPhotonDeExcitation`)

## Process & notations:

- Multi-photon excitation of an atom or ion: $A \,+\, n\,\hbar\omega \quad\longrightarrow\quad A^*$
- Multi-photon decay of an atom or ion: $A^* \quad\longrightarrow\quad A^* \,+\, n\,\hbar\omega$
- Formal quantum notation: $|\alpha_i\mathbb{J}_i\rangle \,+\, \hbar\omega_1\,(\mathbf{k}_1,\lambda_1;\,\{\mathbb{M}_1\}) \,+\, \hbar\omega_2\,(\mathbf{k}_2,\lambda_2;\,\{\mathbb{M}_2\}) \,+\, ... \,+\, \hbar\omega_n\,(\mathbf{k}_n,\lambda_n;\,\{\mathbb{M}_n\}) \quad\longrightarrow\quad |\alpha_f\mathbb{J}_f\rangle$ or

  $|\alpha_i\mathbb{J}_i\rangle \quad\longrightarrow\quad |\alpha_f\mathbb{J}_f\rangle \,+\, \hbar\omega_1\,(\mathbf{k}_1,\lambda_1;\,\{\mathbb{M}_1\}) \,+\, \hbar\omega_2\,(\mathbf{k}_2,\lambda_2;\,\{\mathbb{M}_2\}) \,+\, ... \,+\, \hbar\omega_n\,(\mathbf{k}_n,\lambda_n;\,\{\mathbb{M}_n\})$

- Using JAC: Perform an `Atomic.Computation(.., process=MultiPhoton, processSettings=MultiPhotonDeExcitation.Settings(..), ..)` or call directly functions from the module `MultiPhotonDeExcitation`.

## Motivation:

- The two-photon decay of few-electron ions $|\alpha_i\, \mathbb{J}_i\rangle \;\longrightarrow\; |\alpha_f\, \mathbb{J}_f\rangle \;+\; \hbar\omega_1 \;+\; \hbar\omega_2$ has often been considered, both experimentally and theoretically. For this two-photon decay, the total decay rate as well as the spectral (energy) distribution of the emittedvphotons have been explored.
- In JAC, only the inital and final levels are tabulated by default, together with their symmetry and total transition energy, while the proper flags must be set in `MultiPhotonDeExcitation.Settings` for all further cross section information.

## Two-photon decay amplitude and total rate:

- Two-photon amplitude for the emission of photons with well-defined helicity and multipolarity:

$$\mathcal{M}_{fi}^{(2-\mathrm{emission})}\left(\alpha_f \mathbb{J}_f M_f,\, \alpha_i \mathbb{J}_i M_i;\, \mathbb{M}_2, \lambda_2,\, \mathbb{M}_1, \lambda_1;\, \omega\right) \;=\; \frac{\left\langle \alpha_f \mathbb{J}_f \left\| \mathbb{O}^{(\mathbb{M}_2,\, \mathrm{emission})} \right\| \alpha_\nu \mathbb{J}_\nu \right\rangle \left\langle \alpha_\nu \mathbb{J}_\nu \left\| \mathbb{O}^{(\mathbb{M}_1,\, \mathrm{emission})} \right\| \alpha_i \mathbb{J}_i \right\rangle}{E_i \;-\; \omega \;-\; E_\nu}$$

- Two-photon energy-differential emission rate: For the transition of the atom from level $|\alpha_i \mathbb{J}_i\rangle \;\rightarrow\; |\alpha_f \mathbb{J}_f\rangle$ can be written as (Goldman and Drake, 1988; Surzhykov 2005)

$$\begin{aligned}
\frac{dW}{d\omega_1}(\omega_1;\, \alpha_i\, \mathbb{J}_i \rightarrow \alpha_f\, \mathbb{J}_f) \;&=\; \frac{4\pi}{2J_i \;+\; 1}\, \frac{\omega_1\, \omega_2}{(2\pi)^3\, c^2} \sum_{M_i\, M_f} \sum_{\lambda_1,\, \lambda_2} \left|\, \mathcal{M}_{fi}(\alpha_f \mathbb{J}_f M_f,\, \alpha_i \mathbb{J}_i M_i;\, \mathbb{M}_2, \lambda_2,\, \mathbb{M}_1, \lambda_1;\, \omega)\, \right|^2 d\,\Omega_1\, d\,\Omega_2 \\
&=\; \frac{(4\pi)^5}{2J_i \;+\; 1}\, \frac{\omega_1\, \omega_2}{(2\pi)^3\, c^2} \sum_{\mathbb{M}_1,\, \mathbb{M}_2} \sum_{\mathbb{J}_\nu} \left\{ \frac{1}{2J_\nu \;+\; 1} \left( |S_{\mathbb{J}_\nu}^{(2-\mathrm{emission})}(\omega_1;\, \mathbb{M}_2, \mathbb{M}_1;\, fi)|^2 \;+\; |S_{\mathbb{J}_\nu}^{(2-\mathrm{emission})}(\omega_2;\, \mathbb{M}_1, \mathbb{M}_2;\, fi)|^2 \right) \right. \\
&\qquad \left. +\; 2 \sum_{\mathbb{J}'_\nu} (-1)^{J_\nu \,+\, J'_\nu \,+\, L_1 \,+\, L_2} \begin{Bmatrix} J_f & J'_\nu & L_1 \\ J_i & J_\nu & L_2 \end{Bmatrix} S_{\mathbb{J}_\nu}^{(2-\mathrm{emission})}(\omega_2;\, \mathbb{M}_1, \mathbb{M}_2;\, fi)^*\;\; S_{\mathbb{J}_\nu}^{(2-\mathrm{emission})}(\omega_1;\, \mathbb{M}_2, \mathbb{M}_1;\, fi) \right\}
\end{aligned}$$

Here, the summations over $\mathbb{J}_\nu$ and $\mathbb{J}'_\nu$ are restricted, and their allowed values can be quite easily read-off from the standard selection rules for the multipole matrix elements.

- Reduced two-photon (emission) amplitude:

$$
\begin{aligned}
S^{(2-\text{emission})}_{\mathbb{J}_\nu}(\omega;\, \mathbb{M}_2, \mathbb{M}_1;\, \alpha_f\, \mathbb{J}_f,\, \alpha_i\, \mathbb{J}_i) \;&\equiv\; S^{(2-\text{emission})}_{\mathbb{J}_\nu}(\omega;\, \mathbb{M}_2, \mathbb{M}_1;\, fi) \\
&= \sum_{\alpha_\nu} \frac{\left\langle \alpha_f \mathbb{J}_f \left\| \mathcal{O}^{(\mathbb{M}_2,\,\text{emission})} \right\| \alpha_\nu \mathbb{J}_\nu \right\rangle \left\langle \alpha_\nu \mathbb{J}_\nu \left\| \mathcal{O}^{(\mathbb{M}_1,\,\text{emission})} \right\| \alpha_i \mathbb{J}_i \right\rangle}{E_i \,-\, \omega \,-\, E_\nu} \\
&= S^{(2-\text{absorption})}_{\mathbb{J}_\nu}(???\; \omega;\, \mathbb{M}_2, \mathbb{M}_1;\, fi\; ???) \;=\; S^{(2-\text{Compton})}_{\mathbb{J}_\nu}(???\; \omega;\, \mathbb{M}_2, \mathbb{M}_1;\, fi\; ???)
\end{aligned}
$$

- In Jac, the two-photon energy-differential emission rate are calculated and tabulated if ...

### 7.1.k. Coulomb excitation (`CoulombExcitation`)

## Process & notations:

- Coulomb excitation of an atom or ion by fast, heavy ions: $A \,+\, Z_p \quad\longrightarrow\quad A^* \,+\, Z_p$ (projectile remains unaffected)
- Formal quantum notation: $|\alpha_i \mathbb{J}_i\rangle \,+\, Z_p(\beta_p) \quad\longrightarrow\quad |\alpha_f \mathbb{J}_f\rangle\,, \qquad \beta_p \,=\, \frac{v_p}{c}$
- Using Jac: Perform an `Atomic.Computation(.., process=CoulExc, processSettings=CoulombExcitation.Settings(..), ..)` or call directly functions from the module `CoulombExcitation`.

## Motivation

- In Coulomb excitation processes, one often assumes that a single electron from a (fast-moving) projectile ion with relative velocity $\beta_p = v_p/c$ (with regard to the target) is excited by a target nucleus at rest.
- Of course, an analogue process occurs also when we consider the excitation of the target that may occur due to a fast-moving (bare) projectile ion, and in which case the role of the projectile and target need simply to be interchanged in all formulas below.

- The Coulomb excitation or ionization of the projectile (ion) will be affected, in addition, also by the target electrons (or, *vice versa,* the projectile electrons) but such rather small effects are often not considered in detail.
- The Coulomb excitation of few-electron ions in fast ion-atom collisions leads to the formation of excited ionic states. In typical ion-atom collision experiments, a *prefared* direction is hereby defined for the overall systems, both at storage rings and the EBIT, and this typically results in an *alignment* of the excited ions along this distinct direction.
- The first step in calculating energy- and angle-differential as well as total Coulomb excitation cross sections usually refers to determining the impact-parameter dependence of the excitation probability $P(b)$. The weighted $K$-shell Coulomb excitation probability $2\pi\, b\, P(b)$ is known to have a maximum in the vincinity of the $K$-shell radius. This is quite similar as for the Coulomb ionization probabilities.
- In JAC, the partial and total Coulomb excitation cross sections are calculated and tabulated by default for all selected pairs of initial and final levels.

## Coulomb excitation amplitude of few-electron projectile ions in position space

- Coulomb (excitation) amplitude for the excitation of a (single) projectile electron: If a one-electron projectile moves at a trajectory with impact parameter $b$, the amplitude for an excitation from level $i \rightarrow f$ is given by Eichler & Meyerhof (1995, Eq. 6.2)

$$\mathcal{M}_{fi}^{(\text{Coulex})}(b) \;=\; i\,\frac{\gamma\, Z_t\, e^2}{\hbar} \int dt\, \exp\left(\frac{i}{\hbar}\,(E_f - E_i)\,t\right) \int d^3r\, \psi_f^\dagger(\mathbf{r})\, \frac{(1-\beta_p\,\alpha_z)}{r'(t)}\;\; \psi_i(\mathbf{r}),$$

$$r'(t) \;=\; \sqrt{(x-b)^2 \,+\, y^2 \,+\, \gamma^2\,(z - v\,t)^2}, \qquad\qquad \beta_p \;=\; \frac{v_p}{c}\,,$$

where $\mathbf{r}$ is the coordinate of the projectile electron, $r'(t)$ its (time-dependent) distance from the target nucleus, and where $\psi_f(\mathbf{r})$ and $\psi_i(\mathbf{r})$ denote the final- and initial-state eigenfunctions of the projectile electron with energies $E_f$ and $E_i$.

- Coulomb (excitation) amplitude for the excitation of a many-electron projectile (ion): For an Coulomb excitation of a many-electron projectile from the sublevel $|\alpha_i\, \mathbb{J}_i M_i\rangle \;\rightarrow\; |\alpha_f\, \mathbb{J}_f M_f\rangle$, the excitation amplitude for given impact parameter $b$ can then be written in first-order perturbation theory and natural units ($\hbar = m_\mathrm{e} = c = 1$) as:

$$\mathcal{M}_{fi}^{(\text{Coulex})}(b;\, \alpha_f\, \mathbb{J}_f M_f,\, \alpha_i\, \mathbb{J}_i M_i) \;=\; i\,\gamma\,\alpha\, Z_t \int dt\;\; e^{i\,(E_f - E_i)t} \left\langle \alpha_f \mathbb{J}_f M_f \left| \sum_{k=1}^{N} \frac{1-\beta_p\,\hat{\alpha}_z(k)}{r'_k(t)} \right| \alpha_i \mathbb{J}_i M_i \right\rangle .$$

- From this transition amplitude, the cross section for an excitation of the projectile from (sub-) level $|\alpha_i \mathbb{J}_i\rangle \rightarrow |\alpha_f \mathbb{J}_f M_f\rangle$ can be obtained by integrating over all the impact parameters $b$ and by taking the average over the initial magnetic sublevels $M_i$.

- In JAC, we do not use the Coulomb excitation amplitude in position space but make use of a representation of this amplitude in momentum space instead, see below.

## Coulomb excitation amplitude of few-electron projectile ions in momentum space:

- Coulomb (excitation) amplitude for the excitation of a (single) projectile electron: To evaluate Coulomb excitation cross sections for one- and many-electron atoms, it is often more convinient to work in momentum space and to express all properties in terms of the Fourier transform of the Coulomb excitation amplitude in position space. If we make use of the momentum transfer $\mathbf{q} = (\mathbf{q}_b, q_z)$, the time-integration in this Coulomb (excitation) amplitude can be carried out explicitly (Eichler & Meyerhof 1995, Eq. 6.4)

$$\mathcal{M}_{fi}^{(\mathrm{Coulex})}(b) = \frac{i\,\nu_p}{\pi} \int \frac{d^2\, q_b}{q_b^2 + (1-\beta^2)\, q_0^2}\; e^{-i\,\mathbf{q}_0\cdot\mathbf{b}}\, \mathcal{K}_{fi}^{(\mathrm{Coulex})}(\mathbf{q})\,; \qquad \mathcal{K}_{fi}^{(\mathrm{Coulex})}(\mathbf{q}) = \left\langle \psi_f(\mathbf{r}) \left| (1-\beta\,\alpha_z)\, e^{i\,\mathbf{q}\cdot\mathbf{r}} \right| \psi_i(\mathbf{r}) \right\rangle .$$

  This formula removes the complicated time dependence in $r'(t)$ and replaces it instead by an explicit wave number (momentum transfer) dependence.

- Note, that in momentum space, the (momentum-space) Coulomb excitation amplitude $\mathcal{K}_{fi}^{(\mathrm{Coulex})}(\mathbf{q})$ does no longer depend on the impact parameter $b$ but now simply contains an integration over the momentum transfer $\mathbf{q}$, and which starts from the minimum momentum transfer for the excitation of the initial ion from level $|i\rangle \rightarrow |f\rangle$: $q_0 = (E_f - E_i)/v_p$.

- In momentum space, indeed, most Coulomb excitation cross sections can be expressed directly in terms of the momentum-space Coulomb excitation amplitude $\mathcal{K}_{fi}^{(\mathrm{Coulex})}(\mathbf{q})$.

- (Momentum-space) Coulomb excitation amplitude for many-electron projectiles: This amplitude can be further simplified by using the

Wigner-Eckert theorem (Surzhykov and Fritzsche, 2008)

$$
\begin{aligned}
\mathcal{K}_{fi}^{(\mathrm{Coulex})}(\mathbf{q};\, \alpha_f\, \mathbb{J}_f M_f,\, \alpha_i\, \mathbb{J}_i M_i) \;&=\; \left\langle \alpha_f\, \mathbb{J}_f M_f \left| \sum_k^N \left(1 - \beta\, \alpha_z(k)\right) e^{i\,\mathbf{q}\cdot\mathbf{r}_k} \right| \alpha_i\, \mathbb{J}_i M_i \right\rangle \\
&=\; \sum_{LM} i^L\, Y^*_{LM}(\arccos(q_0/q), 0) \left\langle \alpha_f \mathbb{J}_f M_f \left| \sum_{k=1}^N \left(1 - \beta_p\, \hat{\alpha}_z(k)\right) j_L(q\, r_k)\, Y_{LM}(\vartheta_k, \varphi_k) \right| \alpha_i \mathbb{J}_i M_i \right\rangle , \\
&=\; \sum_t \frac{1}{\sqrt{2J_f + 1}} \left\langle J_i M_i,\, t\,(M_f - M_i) \,|\, J_f M_f \right\rangle \sum_L i^L\, Y^*_{L,\, M_f - M_i}(\arccos(q_0/q), 0) \left\langle \alpha_f \mathbb{J}_f \left\| H_{tL}^{(\mathrm{Coulex})}(q) \right\| \alpha_i \mathbb{J}_i \right\rangle \\
&=\; \sum_t \frac{1}{\sqrt{2J_f + 1}} \left\langle J_i M_i,\, t\,(M_f - M_i) \,|\, J_f M_f \right\rangle \sum_L i^L\, Y^*_{L,\, M_f - M_i}(\arccos(q_0/q), 0) \\
&\qquad \times \left( \delta_{t\,L} \left\langle \alpha_f \mathbb{J}_f \left\| \mathbb{K}^{(\mathrm{L,\, Coulex,\, jY})} \right\| \alpha_i \mathbb{J}_i \right\rangle \;-\; \beta_p \left\langle LM,\, 10 \,|\, tM \right\rangle \left\langle \alpha_f \mathbb{J}_f \left\| \mathbb{K}^{(\mathrm{t,\, Coulex,\, jT})} \right\| \alpha_i \mathbb{J}_i \right\rangle \right)
\end{aligned}
$$

- In Jac, these (momentum-space) Coulomb excitation amplitudes $\mathcal{K}_{fi}^{(\mathrm{Coulex})}(\mathbf{q};\, \alpha_f\, \mathbb{J}_f M_f,\, \alpha_i\, \mathbb{J}_i M_i)$ are implemented explicitly and the integration over $q$ is typically performed by a Gauß-Legendre integration.

## Coulomb excitation operators and interaction strength:

- Coulomb excitation (interaction) strength: The (full) Coulomb excitation amplitude in momentum space above combines two kinds of reduced (many-electron) matrix elements due to the two interaction operators: $\sum_{k=1}^N\; j_L(q\, r_k) Y_L\,(\vartheta_k, \varphi_k)$ of rank $L$ as well as $\sum_{k=1}^N\; j_L(q\, r_k)\, \hat{\boldsymbol{\alpha}}(k) \cdot \mathrm{T}_{tL}(\vartheta_k, \varphi_k)$ of rank $t$, respectively. These two reduced matrix elements are the actual building blocks that are needed in order to represent and to explore the properties of the target or projectile excitation process.

- Coulomb excitation (interaction) strength: The building blocks for the computation of the Coulomb excitation and ionization amplitudes are given by the reduced matrix elements

$$\left\langle \alpha_f \mathbb{J}_f \left\| \mathbb{K}^{(\mathrm{L,\,Coulex,\,jY})} \right\| \alpha_i \mathbb{J}_i \right\rangle = \left\langle \alpha_f \mathbb{J}_f \left\| \sum_{k=1}^{N} j_L(q\, r_k)\, Y_L(\vartheta_k, \varphi_k) \right\| \alpha_i \mathbb{J}_i \right\rangle$$

$$\left\langle \alpha_f \mathbb{J}_f \left\| \mathbb{K}^{(\mathrm{t,\,Coulex,\,jT})} \right\| \alpha_i \mathbb{J}_i \right\rangle = \left\langle \alpha_f \mathbb{J}_f \left\| \sum_{k=1}^{N} j_L(q\, r_k)\, \hat{\boldsymbol{\alpha}}(k) \cdot \boldsymbol{T}_{tL}(\vartheta_k, \varphi_k) \right\| \alpha_i \mathbb{J}_i \right\rangle$$

## Energie-differential, partial and total Coulomb excitation cross sections:

- Partial Coulomb excitation cross section: If the Fourier transformation from the position to momentum coordinates is performed, the integrals over the time $t$ and the impact parameter $b$ can be evaluated *analytically*. Then, the partial (excitation) cross section for the Coulomb excitation from (sub-) levels $|\alpha_i \mathbb{J}_i\rangle \to |\alpha_f \mathbb{J}_f M_f\rangle$ can be written as (Surzhykov and Fritzsche, 2008)

$$\begin{aligned}
\sigma(\alpha_i \mathbb{J}_i \to \alpha_f \mathbb{J}_f M_f) &= \frac{2\pi}{2J_i + 1} \sum_{M_i} \int_0^\infty \mathrm{d}b\; b \left| \mathcal{M}_{fi}^{(\mathrm{Coulex})}(b;\, \alpha_f\, \mathbb{J}_f M_f,\, \alpha_i\, \mathbb{J}_i M_i) \right|^2 \\
&= 2\pi \left( \frac{8\,\pi\, Z_t\, \alpha}{\beta_p} \right)^2 \frac{1}{2J_i + 1} \sum_{M_i} \int_{q_0}^\infty dq\, \frac{q}{\left(q^2 \,-\, q_0^2 \beta_p^2\right)^2} \left| \mathcal{K}_{fi}^{(\mathrm{Coulex})}(\mathbf{q};\, \alpha_f\, \mathbb{J}_f M_f,\, \alpha_i\, \mathbb{J}_i M_i) \right|^2 .
\end{aligned}$$

## Alignment of Coulomb-excited ions:

- Alignment of Coulomb-excited ions in level $|\alpha_f \mathbb{J}_f\rangle$ : For a well-defined ion-atom collision axis, a Coulomb-excited ion in level $|\alpha_f \mathbb{J}_f\rangle$ is generally aligned; this alignment depends on the partial Coulomb cross sections $\sigma(\alpha_f\, \mathbb{J}_f M_f)$ can be described in terms of one (or several) parameters $\mathcal{A}_k(\alpha_f \mathbb{J}_f)$:

$$\mathcal{A}_k(\alpha_i \mathbb{J}_i \to \alpha_f \mathbb{J}_f) \quad = \quad \frac{\sqrt{2J_f+1}}{\sigma(\alpha_i \mathbb{J}_i \to \alpha_f \mathbb{J}_f)} \sum_{M_f} (-1)^{J_f - M_f} \left\langle J_f M_f \, J_f - M_f \,|\, k0 \right\rangle \;\; \sigma(\alpha_i \mathbb{J}_i \to \alpha_f \mathbb{J}_f M_f) \,,$$

## 7.2. In JAC partly-implemented processes

### 7.2.a. Photoionization & fluorescence `(PhotoIonizationFluores)`

**Density operator of the fluorescence photon $\hbar\omega_f(\mathbb{M})$ :**

- ➢ After the inner-shell photoionization, the photoion appears to be in an excited level $|\alpha_e \mathbb{J}_e\rangle$ that decays subsequently to some energetically lower level $|\alpha_F \mathbb{J}_f\rangle$ by the emission of a characteristic photon.
- ➢ Characteristic photon density matrix in the helicity representation: For this characteristic photon, the density matrix can be expressed in the form $\langle \mathbf{k}_0 \, \lambda \,|\, \hat{\rho}_\gamma \,|\, \mathbf{k}_0 \, \lambda' \rangle$, in which $\mathbf{k}_0 \equiv (\vartheta_0, \varphi_0)$ denotes the wave vector along the propagation direction of the fluorescence photon and $\lambda = \pm 1$ its helicity. Note that the helicity representation of this density matrix also describes the photon polarization.

**Stokes parameter of the fluorescence photon $\hbar\omega_f(\mathbb{M})$ :**

- ➢ The density matrix of the fluorescence photon $\hbar\omega_f(\mathbb{M})$ is usually parametrized in terms of the so-called Stokes parameters (Blum 1981; Balashov *et al.*, 2001)

$$\left\langle \mathbf{k}_0 \lambda \,\middle|\, \hat{\rho}_{\omega_f} \,\middle|\, \mathbf{k}_0 \lambda' \right\rangle \quad \equiv \quad c_{\lambda,\lambda'} \quad = \quad \frac{1}{2} \begin{pmatrix} 1 + P_3 & -P_1 + iP_2 \\ -P_1 - iP_2 & 1 - P_3 \end{pmatrix} ,$$

and which are utilized to characterize both the degree of linear ($P_1$ and $P_2$) and circular ($P_3$) polarization of the light.

### 7.2.b. Photoionization & autoionization (`PhotoIonizationAutoion`)

## Process & notations:

- Photo ionization of an atom or ion with subsequent autoionization: $A + \hbar\omega \longrightarrow A^{+,*} + e_p^- \longrightarrow A^{(*)} + e_p^- + e_a^-$
- Formal quantum notation: $|\alpha_i \mathbb{J}_i\rangle + \hbar\omega(\mathbb{M}) \longrightarrow |\alpha_r \mathbb{J}_r\rangle + |\varepsilon_p \kappa_p\rangle \longrightarrow |\alpha_f \mathbb{J}_f\rangle + |\varepsilon_p \kappa_p\rangle + |\varepsilon_a \kappa_a\rangle$
- Using JAC: Perform an `Atomic.Computation(..., process = Jac.xxx, processSettings = PhotoIonizationAutoion.Settings(), ...` or call directly functions from the module `PhotoIonizationAutoion`.

## Motivation:

- PhotoelectronAuger electron coincidence spectrometry has been found a versatile tool for studying the structure and dynamics of atoms, molecules and solids. In atomic physics, for example, it has been used to realize a so-called complete experiment in the photoionization of atoms as well as for exploring small effects of coherence and post-collision interactions in photo-induced Auger processes.
- For a full analysis of the photo-ionization & autoionization process, both electrons should be detected in coincidence by measuring the energy and angular distributions, i.e. the photo-electron – (Auger) electron correlation function.
- The photoionization & autoionization process differs from the direct double photoionization by the emission of the two electrons that proceeds through the formation of a (well-defined) intermediate ionic state and, thus, can usually be considered within a two-step model.

### 7.2.c. Dielectronic recombination & fluorescence (`DielectronicFluores`)

## Process & notations:

- Dielectronic recombination of an atom or ion with subsequent fluorescence:

  $A^{q+} + e_s^- \longrightarrow A^{(q-1)+*} \longrightarrow A^{(q-1)+(*)} + \hbar\omega \longrightarrow A^{(q-1)+(*)} + \hbar\omega + \hbar\omega'$
- Formal quantum notation: $|\alpha_i \mathbb{J}_i\rangle + \hbar\omega(\mathbb{M}) \longrightarrow |\alpha_r \mathbb{J}_r\rangle + |\varepsilon_p \kappa_p\rangle \longrightarrow |\alpha_f \mathbb{J}_f\rangle + |\varepsilon_p \kappa_p\rangle + |\varepsilon_a \kappa_a\rangle$

- Using JAC: Perform an `Atomic.Computation(..., process=DierecFluor, processSettings=DielectronicFluores.Settings(), ..=` or call directly functions from the module `DielectronicFluores`.

### 7.2.d. Electron-impact (de-) excitation (`ImpactExcitation`)

## Process & notations:

- Electron-impact excitation of an atom or ion: $e_s^- + A \longrightarrow A^* + e_s^{-\prime}$
- Formal quantum notation: $|\alpha_i \mathbb{J}_i\rangle + |\varepsilon_i \kappa_i\rangle \longrightarrow |\alpha_f \mathbb{J}_f\rangle + |\varepsilon_f \kappa_f\rangle$ or $|\alpha_i \mathbb{J}_i\rangle + |\mathbf{p}_i\, m_i\rangle \longrightarrow |\alpha_f \mathbb{J}_f\rangle + |\mathbf{p}_f\, m_f\rangle$
- 
- Using JAC: Perform an `Atomic.Computation(..., process = Jac.xxx, processSettings = ImpactExcitation.Settings(), ...` or call directly functions from the module `ImpactExcitation`.

## Motivation:

- The electron-impact excitation of atoms is often described in first-order Born approximation, in which one can easily distinguish individual excitation channels. This approximation neglects however the coupling of *closed channels* but which can later be incorperated perturbatively.
- We here make use of the distorted-wave Born approximation (DWBA) that accounts for the distortion of the continuum orbitals due to (local) potential of the nucleus and all remaining electrons. The DWBA typically gives better results than the pure Born or the Coulomb-Born approximation. The current implementation is similar to the codes by Zhang *et al.*(1989) as well as to the FAC code (Gu 2008).
- Electron-impact ionization cross sections are required, for example, for calculating level populations and spectral line intensities of non-local-thermodynamic-equilibrium (non-LTE) plasmas.

## Collision strength and cross sections:

- The name collision strength was first suggested by Seaton (1953). For a given transition $\alpha_i \mathbb{J}_i \to \alpha_f \mathbb{J}_f$, the collision strength is related to the cross section $Q$ by

  $$\Omega(\alpha_i \mathbb{J}_i,\, \alpha_f \mathbb{J}_f) \;=\; \frac{4\pi\, g_i}{\lambda_i^2}\, Q(\alpha_i \mathbb{J}_i,\, \alpha_f \mathbb{J}_f)$$

  The statistical weight $g_i$ of level $|\alpha_i \mathbb{J}_i\rangle$ ensures the relation $\Omega(\alpha_i \mathbb{J}_i,\, \alpha_f \mathbb{J}_f) = \Omega(\alpha_f \mathbb{J}_f,\, \alpha_i \mathbb{J}_i)$ by detailed balance.

- Collision strength:

  $$\Omega_{if} \;=\; \sum_{\kappa_i,\,\kappa_f} \sum_{\mathbb{J}_t} [J_t] \left| \left\langle (\mathbb{J}_f,\, \epsilon_f, \kappa_f)\, \mathbb{J}_t M_t \right| V^{\,\mathrm{e-e}} \left| (\mathbb{J}_i,\, \epsilon_i, \kappa_i)\, \mathbb{J}_t M_t \right\rangle \right|^2$$

  where $|\varepsilon_i, \kappa_i\rangle$ and $|\varepsilon_f, \kappa_f\rangle$ denote the partial waves of the incident and scattered electron.

- A continuum orbital is said to be normalized per unit energy if it has an asymptotic amplitude $\sqrt{k/\epsilon}$ (or, $\sqrt{2/k}$ in the non-relativistic limit) or if it fullfills, equivalently,

  $$\int dr\; \left[ P_\epsilon(r)\, P_{\epsilon'}(r) \;+\; Q_\epsilon(r)\, Q_{\epsilon'}(r) \right] \;=\; \pi\, \delta(\epsilon \,-\, \epsilon')\,.$$

- Electron-impact excitation cross section: If the continuum orbitals are normalized *per unit energy*, the electron-impact ionization cross section is obtained from the collision strength $\Omega_{if}$ by

  $$\sigma_{if} \;=\; \frac{\pi}{k_i^2\, g_i}\, \Omega_{if}$$

  where $g_i$ is the statistical weight of the initial state and $k_i$ is the wavenumber or initial momentum of the incident (scattered) electron. The wavenumber of the incident electron is related to its energy $\varepsilon_i$ by $k_i^2 \;=\; 2\,\varepsilon_i\, \left(1 \,+\, \frac{\cdot\cdot}{\cdot\cdot}\, \epsilon_i\right)$.

- In the JAC program, the standard decomposition of the electron-electron interaction matrix elements is utilized to compute the collision strength.

### 7.2.e. Electron-impact excitation & autoionization (`ImpactExcitationAutoIon`)

## Process & notations:

- ➢ Electron-impact excitation & autoionization of an atom or ion: ... $A \,+\, e_s^- \quad\longrightarrow\quad A^* \,+\, e_s^{-\prime} \quad\longrightarrow\quad A^{+(*)} \,+\, e_s^{-\prime} \,+\, e_a^-$
- ➢ Formal quantum notation: $|\alpha_i \mathbb{J}_i\rangle \,+\, |\varepsilon_i \kappa_i\rangle \quad\longrightarrow\quad |\alpha_r \mathbb{J}_r\rangle \,+\, |\varepsilon_r \kappa_r\rangle \quad\longrightarrow\quad |\alpha_f \mathbb{J}_f\rangle \,+\, |\varepsilon_r \kappa_r\rangle \,+\, |\varepsilon_a \kappa_a\rangle$
- ➢ Using JAC: Perform an `Atomic.Computation(..., process = Jac.xxx, processSettings = ImpactExcitationAutoIon.Settings(), ...` or call directly functions from the module `ImpactExcitationAutoIon`.

### 7.2.f. Radiative-Auger decay (`RadiativeAuger`)

## Process & notations:

- ➢ Radiative-Auger (autoionization) of an atom or ion: $A^{q+*} \quad\longrightarrow\quad A^{(q+1)+(*)} \,+\, (e_a^- \,+\, \hbar\omega)$
- ➢ Formal quantum notation: $|\alpha_i \mathbb{J}_i\rangle \quad\longrightarrow\quad |\alpha_f \mathbb{J}_f\rangle \,+\, \hbar\omega(\mathbb{M}) \,+\, |\varepsilon_a\, \kappa_a\rangle$
- ➢ Using JAC: Perform an `Atomic.Computation(..., process = Jac.xxx, processSettings = RadiativeAuger.Settings(), ...` or call directly functions from the module `RadiativeAuger`.

### 7.2.g. Multi-photon ionization (`MultiPhotonIonization`)

## Process & notations:

- ➢ Multi-photon ionization: of an atom or ion $A \,+\, n\,\hbar\omega \quad\longrightarrow\quad A^{(*)} \,+\, e_p^-$
- ➢ Formal quantum notation: $|\alpha_i \mathbb{J}_i\rangle \,+\, \hbar\omega_1(\mathbb{M}_1) \,+\, \hbar\omega_2(\mathbb{M}_2) \,+\, ... \,+\, \hbar\omega_n(\mathbb{M}_n) \quad\longrightarrow\quad |\alpha_f \mathbb{J}_f\rangle \,+\, |\varepsilon\,\kappa\rangle$

- Using JAC: Perform an `Atomic.Computation(..., process = Jac.xxx, processSettings = MultiPhotonIonization.Settings(), ...` or call directly functions from the module `MultiPhotonIonization`.

### Motivation:

- The standard models for multi-photon ionization are typically based on a semiclassical time-dependent description of the laser field and on scattering-theoretical arguments. In these models, the photons and electrons are thus not treated as particles of a truly closed system to which formal scattering theory would be applicable.

## 7.2.h. Multi-photon double ionization (`MultiPhotonDoubleIon`)

### Process & notations:

- Multi-photon double ionization: of an atom or ion $A \,+\, n\,\hbar\omega \quad\longrightarrow\quad A^{(*)} \,+\, e^-_{p_1} \,+\, e^-_{p_1}$
- Formal quantum notation: $|\alpha_i \mathbb{J}_i\rangle \,+\, \hbar\omega_1(\mathbb{M}_1) \,+\, \hbar\omega_2(\mathbb{M}_2) \,+\, ... \,+\, \hbar\omega_n(\mathbb{M}_n) \quad\longrightarrow\quad |\alpha_f \mathbb{J}_f\rangle \,+\, |\varepsilon_1\,\kappa_1\rangle \,+\, |\varepsilon_2\,\kappa_2\rangle$

- Using JAC: Perform an `Atomic.Computation(..., process = Jac.xxx, processSettings = MultiPhotonDoubleIon.Settings(), ...` or call directly functions from the module `MultiPhotonDoubleIon`.

## 7.2.i. Internal conversion (`InternalConversion`)

### Process & notations:

- Internal conversion of an atom or ion: $A^{q+} \,+\, \text{nucleus}^* \quad\longrightarrow\quad A^{(q+1)+*} \,+\, e^-_c$

- Formal quantum notation: $|\alpha_i \mathbb{J}_i\rangle \; + \; \text{nucleus}^* \, (\{\mathbb{M}\}, \, \mathcal{E}) \quad \longrightarrow \quad |\alpha_f \mathbb{J}_f\rangle \; + \; e_c^- \, (\mathbf{p}, \, m_s)$ or
  $|\alpha_i \mathbb{J}_i\rangle \; + \; \text{nucleus}^* \, (\{\mathbb{M}\}, \, \mathcal{E}) \quad \longrightarrow \quad |\alpha_f \mathbb{J}_f\rangle \; + \; |\varepsilon \, \kappa\rangle \, ,$ $\qquad \varepsilon \; = \; \mathcal{E} \; - \; (E_i \; - \; E - f)$
- Here, the excited nucleus decays by (several) multipoles $\{\mathbb{M}\}$ and releases the energy $\mathcal{E}$, leading to an emitted electron with kinetic energy $\varepsilon$ .
- Using JAC: Perform an `Atomic.Computation(.., process=Jac.Conversion, processSettings=InternalConversion.Settings(..), ..)` or call directly functions from the module `InternalConversion`.

## Motivation:

- Internal conversion: refers to the (decay) process in which an excited nucleus undergoes a transition to its ground or some lower-lying level and in which the excitation energy is given to an electron, leading to an ionization of the atom or ion. In general, this internal (energy) conversion, gamma-ray emission as well as electron-positron pair formation (for nucear excitation energies above 1.022 MeV) are competing processes.
- However, internal conversion does not constitute a simple photoionization process in which an emitted $\gamma$ photon leads to the emission of electrons but it refers to an alternate de-excitation pathway of excited nuclei.
- The internal conversion process (ICP) has been found a versatile tool for studying nuclear structure. The measurement and analysis of conversion electron spectra reveal possible transitions between nuclear levels. By comparing these spectra with calculated internal conversion coefficients, it is often possible to assign a unique multipolarity to the nuclear gamma radiation and, hence, a total angular momentum and parity to the excited nuclear states.
- The internal conversion coefficients can provide detailed information about the atomic nucleus, if theoretical and experimental values are compared for transitions of different multipolarity and mixing ratios. A detailed knowledge of these coefficients is needed for determining absolute transition rates and for the normalization of decay schemes, for Mössbauer spectrocopy, for nuclear reaction computations as well as for the calculation of the decay heat of the fuell cells of nuclear reactors.

## General theory:

- The internal conversion process can be described by means of the quantum theory of retarded charge interactions.
- In particular, the internal conversion is a second-order quantum electrodynamical process in which a virtual photon is exchanged between the nucleus (proton) and an electron.

- Internal conversion amplitude: The (single-electron) matrix element of the conversion transition can be written as (Listengarten ...; Band *et al.*, 2002)

$$\langle f \,|\, \mathbb{H}^{\,(\mathrm{conversion})} \,|\, i \rangle \;=\; -e \int d^3\mathbf{r}\; \psi_f^*(\mathbf{r}) \;\; [\, \Phi(\mathbf{r}) \,+\, \boldsymbol{\alpha} \cdot \mathbf{A}(\mathbf{r}) \,]\; \psi_i(\mathbf{r}),$$

where $\Phi(\mathbf{r})$ and $\mathbf{A}(\mathbf{r})$ are the time-independent parts of the scalar and vector potentials of the electromagnetic field that arise due to the nuclear transition charges and currents, and by including the retardation of these interactions.

- The retarded potentials in the internal conversion amplitude above are

$$\Phi(\mathbf{r}, t) \;=\; e^{-i\,\omega\,t}\, \Phi(\mathbf{r}), \qquad \Phi(\mathbf{r}) \;=\; \int d^3\mathbf{R}\; \frac{\rho\mathbf{R}}{|\mathbf{r} \,-\, \mathbf{R}|}\; e^{i\,k\,|\mathbf{R}\,-\,\mathbf{R}|} \;=\; \sum_{LQ} \Phi_{LQ}(\mathbf{r})$$

$$\mathbf{A}(\mathbf{r}, t) \;=\; e^{-i\,\omega\,t}\, \mathbf{A}(\mathbf{r}), \qquad \mathbf{A}(\mathbf{r}) \;=\; \frac{1}{c} \int d^3\mathbf{R}\; \frac{\mathbf{Jr}}{|\mathbf{R} \,-\, \mathbf{R}|}\; e^{i\,k\,|\mathbf{R}\,-\,\mathbf{R}|} \;=\; \sum_{LQ} \mathbf{A}_{LQ}(\mathbf{r})$$

with the wavenumber $k \;=\; \omega/c \;=\; \mathcal{E}/\hbar\, c$, and where $\mathbf{r} \;=\; (r, \vartheta, \varphi)$ and $\mathbf{R}$ are the coordinates of the electron and nucleus (proton), respectively.

- Here, we shall not go into the details for the representation of these potentials but just note that these interaction potentials can be written as sum over multipole contributions as well as in terms of the nuclear charge density $\rho\mathbf{R}$ and current density $\mathbf{Jr}$ , respectively.

## Internal conversion coefficients:

- The internal conversion coefficient is defined as the ratio of the number of electrons $N_e$ ejected from the $i$-th atomic shell to the number of gamma quanta $N_\gamma$ leaving the atom during the same time:

$$\alpha^{\,(\mathrm{conversion})}(\alpha_i \mathbb{J}_i \;\rightarrow\; \alpha_f \mathbb{J}_f) \;=\; \frac{N_e}{N_\gamma}, \qquad \alpha^{\,(\mathrm{conversion})}(\alpha_i \mathbb{J}_i) \;=\; \sum_f \alpha^{\,(\mathrm{conversion})}(\alpha_i \mathbb{J}_i \;\rightarrow\; \alpha_f \mathbb{J}_f)$$

The total internal conversion coefficient of a given (initial) level $\alpha^{\,(\mathrm{conversion})}(\alpha_i \mathbb{J}_i)$ is the sum of partial conversion coefficient associated with all possible ionization channels (lines) of the atom or ion.

## Further information:

- Internal conversion coefficients have been tabulated in a larger number of tables and compilations; in these tabulations, the screening of the nuclear electric field by the atomic electrons was often treated in the framework of either some statistical Thomas-Fermi-Dirac or Dirac-Fock-Slater models.
- For different $x_\alpha$ pre-factors in the Dirac-Fock-Slater (type) potentials, the differences in the calculated conversion coefficients are typically small $\sim 1$ % for $K$-shell electrons but may increase to $\sim 70$ % for outer electrons and even larger when the kinetic energy of the conversion electron is low $(\leq\ 1$ keV). The question of whether the hole should be incorporated into the potential or not has been explored previously and lead to a slight preference for noninclusion.

## 7.2.j. Electron capture with nuclear decay

## Process & notations:

- Electron capture of an atom or ion by nuclear decay: $A(Z+1) + e^- \quad \longrightarrow \quad A(Z) + \nu_e$
- Formal quantum notation: $E_\nu = Q^+ - E_f - E_b > 0$
- Here, the nucleus decays by capturing an atomic electron (often from the K-shell) and under the emission of an electron. $Q^+$ is the energy difference due to the rest masses of the parent and daughter nucleus, $E_f$ the energy of the final nuclear state of the daughter nucleus and $E_b$ the binding energy of the captured electron. The release energy $E_\nu$ will be shared between the emitted neutron and, possible, some bremsstrahlungs photon or some shaked valence electron.
- Using JAC: Perform an `Atomic.Computation(.., process=Jac.Conversion, processSettings=InternalConversion.Settings(..), ..)` or call directly functions from the module `InternalConversion`.

## Motivation:

- For allowed transitions, nearly all vacancies occur in the $ns$ shells, mainly for the K, $\mathrm{L}_1$ , $\mathrm{M}_1$ , etc.

## 7.3. Further processes, not yet considered in JAC

### 7.3.a. Electron-impact ionization (`ImpactIonization`)

#### Process & notations:

- Electron-impact ionization of an atom or ion: $e_s^- \,+\, A \quad\longrightarrow\quad A^* \,+\, e_s^{-'} \,+\, e^-$
- Formal quantum notation: $|\alpha_i \mathbb{J}_i\rangle + |\varepsilon_i\, \kappa_i\rangle \quad\longrightarrow\quad |\alpha_f \mathbb{J}_f\rangle + |\varepsilon_f\, \kappa_f\rangle + |\varepsilon_a\, \kappa_a\rangle$ where $|\varepsilon_c\, \kappa_c\rangle$ is the initially bound *atomic* electron.
- Using JAC: Perform an `Atomic.Computation(..., process = Jac.xxx, processSettings = ImpactIonization.Settings(), ...` or call directly functions from the module `ImpactIonization`.

#### Motivation:

- The electron-impact ionization process is important in all (high-temperature) plasma.
- We refer to the three *free* electrons, that are involved in this process, as incident, (final-) scattered and additional (-ly released) electron, and with the corresponding indices above.

#### Cross sections:

- Electron-impact ionization cross section: These cross sections are obtained similarly as the electron-impact excitation cross section but by allowing an ionizing transition between fine-structure levels $\alpha_i \mathbb{J}_i(N) \to \alpha_f \mathbb{J}_f(N-1)$ (Fontes *et al.* 2015)

$$\sigma\,(\text{ionization})(\alpha_i \mathbb{J}_i, \alpha_f \mathbb{J}_f) \;=\; \frac{8}{k_i^2\, g_i} \sum_{\mathbb{J}_s,\, \mathbb{J}_t} (2J_s + 1) \sum_{\kappa_i \kappa_f \kappa_e} \int_0^{\varepsilon_i \,-\, I_p} \varepsilon' \left| \left\langle (\alpha_f \mathbb{J}_f,\, \epsilon_a \kappa_a)\, \mathbb{J}_t \right\| \mathbb{V}^{\,(\text{e}-\text{e})} \left\| \alpha_i \mathbb{J}_i \right\rangle \right|^2$$

- This cross section contains a summation over all possible values $\mathbb{J}_t$ of the final ion and the (additionally) released electron due to the impact of the incident electron $\varepsilon_i \kappa_i$

## 7.3.b. Electron-impact multiple ionization

### Process & notations:

- ➢ Electron-impact multiple ionization of an atom or ion: $e_s^- \; + \; A \quad \longrightarrow \quad A^* \; + \; e_s^{-\prime} \; + \; e^- \; + \; ......$
- ➢ Formal quantum notation: $|\alpha_i \mathbb{J}_i\rangle \; + \; |\varepsilon_i \, \kappa_i\rangle \quad \longrightarrow \quad |\alpha_f \mathbb{J}_f\rangle \; + \; |\varepsilon_f \, \kappa_f\rangle \; + \; |\varepsilon_a \, \kappa_a\rangle \; + \; ......$ where $|\varepsilon_c \, \kappa_c\rangle$ is the initially bound *atomic* electron.
- ➢ Using JAC: Perform an ...

## 7.3.c. Coulomb ionization `(CoulombIonization)`

### Process & notations:

- ➢ Coulomb ionization by fast, heavy ions: $A^{(q+1)+} \; + \; Z_p \quad \longrightarrow \quad A^{(q+1)+\,(*)} \; + \; e^- \; + \; Z_p'$
- ➢ Formal quantum notation: $|\alpha_i \mathbb{J}_i\rangle \; + \; Z_p(...) \quad \longrightarrow \quad |\alpha_f \mathbb{J}_f\rangle \; + \; e^-$

### Motivation:

- ➢ The projectile ionization leads to a different charge state of ions in matter and determines, for example, the lifetime of ions in storage rings.
- ➢ At high projectile energies ($E \geq 10$ GeV/u), the ion velocity is essentially the speed of light, and the relevant parameter that describes the kinetic energy is $\gamma$. The ion energy per nucleon is given by $(\gamma - 1) M c^2$, where $M$ is the mass of the nucleus.
- ➢ If one of the projectile electrons is ionized, the projectile will be misbent by subsequent steering magnets, resulting in the loss of the ion from the ring.

### 7.3.d. Double-Auger decay (`DoubleAuger`)

#### Process & notations:

- ➢ Simultaneous double Auger (autoionization) of an atom or ion: $A^{q+*} \longrightarrow A^{(q+2)+(*)} + (e^-_{a_1} + e^-_{a_2})$

- ➢ Formal quantum notation: $|\alpha_i \mathbb{J}_i\rangle \longrightarrow |\alpha_f \mathbb{J}_f\rangle + |\varepsilon_1\, \kappa_1\rangle + |\varepsilon_2\, \kappa_2\rangle$

### 7.3.e. Radiative double electron capture

#### Process & notations:

- ➢ Radiative double electron capture (RDEC) of an ion:
- ➢ Formal quantum notation: $|\alpha_i \mathbb{J}_i\rangle + ... \longrightarrow$

#### Motivation:

- ➢ Double photoionization of atoms has attracted much interest during the last decades as the emission of a second electron is caused by the electron-electron interaction.

### 7.3.f. Interference of multi-photon ionization channels (`MultiPhotonInterference`)

#### Process & notations:

- ➢ Interference of non-resonant one-photon ($2\omega$) and resonant two-photon ($\omega$) ionization of an atom or ion:

- Formal quantum notation: $|\alpha_i \mathbb{J}_i\rangle \; + \; ... \quad \longrightarrow$

## Motivation:

- Two-pathway quantum interference process has been manipulated in order to obtain quantum control.
- Such quantum control studies were initially stimulated by the small fraction of the second harmonic that typically arise at XFEL and which is often difficult to be filtered out, though it can strongly influence the experimental from two-photon ionization experiments. Despite the rather small intensity of the second harmonic, the ionization by photons with frequency $2\,\omega$ (second harmonic, first-order process) can readily compete with, or even dominate, the two-photon ionization by photons with frequency $\omega$ .

## Interference of non-res. one-photon $(2\omega)$ and resonant two-photon $(\omega)$ ionization:

- For a linearly-polarized bichromatic beam, the interference due to different quantum pathes manifests itself in an asymmetry of the photoelectron angular distributions (PAD) with respect to the plane that is perpendicular to the electric field of the incident radiation; cf. Grum-Grzhimailo *et al.*(2015).
- Photoelectron angular distribution (PAD): In the dipole approximation and for an isotropic target, this angular distribution must be axially symmetric with regard to the polarization direction

$$\frac{dW}{d\Omega} \quad = \quad \frac{W_o}{4\pi} \left[ 1 \; + \; \sum_{k=1}^{K} \; \beta_k \; P_k(\cos\vartheta) \right]$$

  where $\vartheta$ is the angle of the photoelectron with regard to the polarization direction (E-field). The $\beta_k$ denote the anisotropy parameters, which can expressed in terms of the photoionization amplitudes.

- For a combination of one-photon and two-photon ionization paths, all terms with $k \;=\; 1, 2, 3, 4$ should be accounted for in the equation above. The odd polynomials appear due to coherent creation of photoelectron partial waves with opposite parities by the fundamental and the second harmonic of the radiation.

## 7.4. Other topics closely related to atomic processes

### 7.4.a. Atomic database from the literature

#### CHIANTI: A database for emission lines:

- ➢ CHIANTI is a database of assessed atomic parameters and transition rates needed for the calculation of the line and continuum emission of optically thin, collisionally-dominated plasma.
- ➢ CHIANTI was first released in 1996 and since then various new releases have been made available in order to expand the database and improve the quality of the data. Emphasis has been given especially to the line identifications and improvement of the reference wavelengths.
- ➢ For several ions, the wavelengths and identifications are different from and more accurate than those of the NIST database. Therefore, CHIANTI is now often used as a reference atomic database for ions and has been included in several other atomic codes and packages.
- ➢ In its last version (Del Zanna *et al.*, 2015), the CHIANTI database includes a large amount of new data and ions which improvement the soft X-ray, extreme UV (EUV) and UV spectral regions, which several space missions currently cover.

#### NIST-XCOM:

- ➢ The XCOM database provides photon scattering data and attenuation coefficients between 1 keV and 100 GeV for all the elements of the periodic table. It also lists total cross sections, attenuation coefficients and partial interaction coefficients for selected processes, such as Compton and Rayleigh scattering, photoelectric absorption as well as pair production (Amako *et al.*, 2005).

#### NIST-ESTAR:

- ➢ The ESTAR database provides stopping powers and ranges of electrons as a function of energy between 10 keV and 1 GeV, derived from the so-called ICRU Report (Amako *et al.*, 2005).

#### NIST-PSTAR:

- ➢ The PSTAR and ASTAR databases provide stopping powers and ranges of protons and in the energy intervals 1 keV – 10 GeV and 1 keV – 1 GeV, respectively, and were derived from the so-called ICRU Report 49.

### 7.4.b. Codes which require atomic data input

#### Codes from astro and plasma physics:

- Radiative-Collisional code based on FAC, RCF: This code has been used to simulate steady-state plasmas under non-local thermodynamic equilibrium condition, especially photoinization-dominated plasmas. RCF takes almost all of the radiative and collisional atomic processes into a rate equation to interpret the plasmas systematically. The Flexible Atomic Code (FAC) supplies all the atomic data needed for RCF, which insures calculating completeness and consistency of atomic data.
- RCF is a steady-state, collisionalradiative, optically thin model. Its rate-equation

  $$\frac{dN_{i,j}}{ddt} \;=\; \text{populating process} \;-\; \text{depopulating process} \;=\; 0$$

  where $N_{i,j}$ is the density of the j-th level of the i-th charge state. The processes included are the ionization and recombination between neighboring charge states as well as the excitation and de-excitation within the same charge state. Their inverse processes are typically taken into account by the detailed balance principle.

### 7.4.c. Radiative opacity

#### Motivation:

- The radiative opacity of a plasma is of great significance for various research fields, such as inertial confinement fusion, stellar physics as well as the development of x-ray lasers. The (so-called) Opacity Project calculated the atomic data for most astrophysically abundant elements and set a database of opacities.
- Knowing the opacity of a plasma, the fraction of transmitted radiation with regard to some incident radiation of given intensity can be expressed as:

  $$F(h\nu) \;=\; \exp\left(-\rho\, \eta'(h\nu)\, L\right)$$

  where $L$ is the path length of the light through the plasma, $\rho$ the mass density and $\eta'(h\nu)$ the radiative opacity. This fraction can be readily determined experimentally and can be obtained theoretically by taking the integral over a Gaussian function, and where the full width corresponds to the spectrometer resolution.

## Definition of detailed and mean radiative opacities:

- For a plasma in a local thermodynamic equilibirum at temperature T and mass density $\rho$, the radiative opacity $\eta(\hbar\omega)$ is given by (Cheng and Jiaolong, 2008)

$$\rho\,\eta(\hbar\omega)... \;=\; \left[\mu^{(\text{bound}-\text{bound})}(\hbar\omega) \,+\, \mu^{(\text{bound}-\text{free})}(\hbar\omega) \,+\, \mu^{(\text{free}-\text{free})}(\hbar\omega)\right] \left(1 \,-\, \exp\left(\frac{\hbar\omega}{k_B\,T}\right)\right) \,+\, \mu^{(\text{scattering})}(\hbar\omega)$$

  where $\mu^{(\text{bound}-\text{bound})}$, $\mu^{(\text{bound}-\text{free})}$, $\mu^{(\text{free}-\text{free})}$ and $\mu^{(\text{scattering})}$ are the absorption coefficients due to bound-boud, bound-free, free-free and well as scattering processes, respectively.

- The Rosseland and Planck mean opacities are required for many practical applications such as radiative transfer.
- Rosseland mean opacity: With $u \,=\, \frac{\hbar\omega}{k_B\,T}$, the Rosseland opacity is defined by

$$\frac{1}{K^{(\text{Rosseland})}} \;=\; \int_0^\infty du\, \frac{W^{(\text{Rosseland})}}{\eta(u)}\,; \qquad\qquad W^{(\text{Rosseland})} \;=\; \frac{15}{4\,\pi^4}\, \frac{u^4\, e^{-u}}{(1\,-\,e^{-u})^2}$$

- Planck mean opacity:

$$\frac{1}{K^{(\text{Planck})}} \;=\; \int_0^\infty du\, W^{(\text{Planck})}\left[\eta(u) \,-\, \eta^{(\text{scattering})}(u)\right]; \qquad\qquad W^{(\text{Planck})} \;=\; \frac{15}{\pi^4}\, \frac{u^3\, e^{-u}}{(1\,-\,e^{-u})}$$

### 7.4.d. Opacities for astrophysical matter clouds

## Neutron star mergers:

- Neutron stars: Neutron star have been postulated already short after the discovery of the neutron as the ultimate fate of massive stars, ending in supernova. The existence of neutron stars was later shown in the 1960s due to the observation of first pulsars.
- Today, the equation of state and the distribution of neutron star masses are believed to be known reasonably well.

- Modern simulations of neutron star mergers take into account both, the (elemental) composition of the ejecta as well as the neutrino wind along the poles.
- A current question is whether the mergers lead to a robust r-process environment that can produces heavy neutron-rich isotopes with mass $A \geq 130$, and in proportions similar to solar abundance (Thielemann *et al.*, 2017).

## Gravitational-wave astronomy:

- The discovery of gravitational waves (GW) from the inspiral and coalescence of binary black holes (BH) and/or neutron stars (NS) by the Laser Interferometer Gravitational Wave Observatory (LIGO) has opened a new window on the cosmos.
- In the neutron-rich ejecta from double neutron star (NS-NS) and BH-NS binaries, in particular, the so-called r-process nucleosynthesis (rapid neutron capture) is expected to proceed rapidly, leading to many heavy elements like gold, platinum and many others.
- Kilonova   Kilonovae are day to week-long thermal, supernova-like transients, which are powered by the radioactive decay of heavy, neutron-rich elements synthesized in the expanding merger ejecta. The radioactive decay of such unstable neutron-rich nuclei powers a rapid evolution of a supernova-like transition of stellar matter that is known as kilonova or macronov in the literature. These kilonovae can be understood also as roughly isotropic electromagnetic counterpart to the GW signal and, thusm provide a unique and direct probe of such r-process sites (Metzger 2017).
- In practice, however, it is not easy to precisely locate the sky positions of the GW sources which need to be determined by triangulating the arrival times of the GW signals by different detectors. At present, the uncertainties in this triangulation are quite large (initially $\approx 850\ \text{deg}^2$ for GW15091 and with a later improvement to $\approx 250\ \text{deg}^2$), though these uncertainties will be reduced to $\approx 10-100\ \text{deg}^2$, once Virgo in Italy and, eventually, KAGRA in Japan and LIGO-India will join the network (Metzger 2017).
- Nevertheless, even an localisation of the GW signals within $10-100\ \text{deg}^2$ greatly exceed the fields of view of most radio, optical and x-ray telescopes, and in particular those telescopes that are sensitive enough to detect the electro-magnetic counterparts of NS-NS and BH-NS mergers.
- The discovery of electromagnetic signals in coincidence with chirp at the graviational-wave detectors leads to a better location and a much richer picture about the merger process. This may allow to extract directly information on the binary formation channels, the age of the stellar population as well as the dynamics of binary mergers.

## r-process:

- ➢ Burbidge *et al.* (1957) and Cameron (1957) realized already more than 60 years ago that approximately half of the elements heavier than iron are synthesized via the capture of neutrons onto lighter seed nuclei like iron in a dense neutron-rich environment in which the timescale for neutron capture is shorter than the lifetimes for $\beta$-decay.

## Astrophysical opacities models:

- ➢ A new astrophysical opacity model (called OPAL) has been developed at the Lawrence Livermore National Laboratory (LLNL) with which it was shown that $\Delta n = 0$ transitions results in overlapping lines. This overlap significantly increase the opacity of the iron component of the mixture and which was suggested also by observation of stellar pulsations

## Opacities for ejecta from neutron-star mergers:

- ➢ In general, the merger of stellar mass BH-BH binaries is not expected to produce luminous electro-magnetic emission because there is not enough baryonic matter in these systems.
- ➢ Despite of a rather large number of the expected BH-BH mergers during the next few years, a better synthesis and analysis of GW and the associated electro-magnetic signals will probably come from NS-NS or BH-NS mergers, i.e. if neutron stars are involved.
- ➢ The ejecta from NS-NS binaries is hot immediately after the merger; however, this thermal energy can initially not escape so easily as radiation owing to its high optical depth just after the merger (Metzger 2017)

$$\tau \;=\; \rho\,\kappa\,R \;=\; \frac{3M\,\kappa}{4\pi\,R^2} \;\propto\; 70\,\left(\frac{M}{10^{-2}\,M_\odot}\right)\left(\frac{\kappa}{\mathrm{cm}^2\;\mathrm{g}^{-1}}\right)\left(\frac{v}{0.1\,c}\right)^{-2}\left(\frac{t}{\mathrm{day}}\right)^{-2}$$

where $\rho = 3M/(4\pi\,R^3)$ is the mean density and $\kappa$ the opacity, i.e. the cross section per unit mass. When the ejecta expands, the diffusion time of the photons decreases with $t^{\,(\mathrm{diffusion})} \propto 3M\,\kappa/4\pi\,c\,vt$ until the radiation can escape eventually, once we have $t^{\,(\mathrm{diffusion})} = t\,.$

## Opacity calculations:

- ➢ Radiative opacities are required for the modeling of astrophysically relevant plasmas under local thermodynamic equilibrium (LTE) conditions. For the computation of these opacities, the atomic structure calculations should be carried out for all fine-structure levels and by including configuration interactions.

- Three typical example applications for opacity calculations are: (i) iron opacities at conditions of the solar convection zone, (ii) nickel opacities for modeling various stellar envelopes and (iii) the samarium opacities for the modeling of light curves as produced by neutron star mergers.
- In recent work, the frequency-dependent LTE opacity of iron has been studied for the conditions of the base of the solar convection zone. These studied revealed rather large (30-400%) differences between experiment and theory for the monochromatic opacity of an neon-like iron plasma (or nearby charge states). Until the present, the source of this not yet understood and remains an active area of research.

## Opacity measurements for homogeneous plasma with uniform density:

- Uniform plasma density: For a uniform density, the transmisison of the sample

$$T(\omega) \;=\; \frac{I(\omega)}{I_o} \;=\; \exp\left(-\,\rho\, L\, \kappa(\omega)\right)$$

is measured where $I(\omega)$ is the attenuated intensity of the probe (backlighter) radiation and $I_o$ the reference intensity. This transmission is related also to opacity by the Beer-Lambert law if the reabsorption can be neglected in the homogeneous plasma. Here, $\rho$ is the density of the material and $L$ its thickness.

## 7.4.e. Absorption spectra of distinct astrophysical objects

## Identification of absorption spectra

- Sako *et al.* (2001) present first results from high-resolution X-ray observation of IRAS 13349+2438 with the XMM-Newton Observatory. The observed spectrum was obtained with the Reflection Grating Spectrometer (RGS) and shows a wealth of discrete spectral features, including the (first) astrophysical detection of an unresolved transition array (UTA) due to the $2p-3d$ inner-shell excitations of $M$-shell iron ions. These spectral features could be easily misidentified as an O VII edge when observed with moderate resolution spectrometers.
- Other prominent features in these spectra were $K$-shell absorption lines of hydrogen- and helium-like carbon, nitrogen, oxygen and neon, and L-shell lines of Fe XVII-XX.

### 7.4.f. Ionization equilibria in astrophysical sources

#### Astrophysical observation of EUV spectra:

- High-quality EUV spectra: The Solar EUV Rocket Telescope and Spectrograph (SERTS, 1992) and the Extreme Ultraviolet Explorer (EUVE, 1990) spectrometers provided high-quality EUV spectra and helped improve the diagnostics of high temperature plasmas.
- The ability to resolve a large number of individual emission lines and to measure accurate intensities over a wide wavelength range have allowed to analyze the temperatures, densities and abundances of elements in a variety of astrophysical sources (Brickhouse *et al.*, 1995).
- The fine structure of (line) multiplets nowadays allow to solve the full rate equations for several atoms in the plasma, including collisions among all levels and cascades. This enables one to calculate also the emissivities of weak lines that were previously omitted from the investigation.

### 7.4.g. Photoionized, steady-state plasma

#### Ion distributions:

-

### 7.4.h. Plasma light sources for nanolithography

#### EUV light sources:

- Ions with several open shells: The (correlated) electronic structure of medium and heavvy ions with several open shells is both, tedious and difficult to calculate, and their complex level structure often hampers a straightforward experimental assignment.
- EUV light at 13.5-nm wavelength: In order to generate extreme ultraviolet (EUV) light at 13.5-nm wavelength by laser-produced plasmas, the emission of multiply-charged tin ions have been found promising for nanolithographic applications. For these ions, the EUV light is generated by thousands of transitions that form so-called unresolved transition arrays (UTA) with rather little dependence on the particular charge state (Winderberger *et al.*, 2016).

- For multiply charged tin ions with a [Kr] $4d^m$ $m = 6..0$ configuration, the upper configurations for an EUV emission are [Kr] $(4p^6 4d^{m-1} 4f + 4p^6 4d^{m-1} 5p + 4p^5 4d^{m1})$ (Winderberger *et al.*, 2016).

## 7.4.i. Synthetic spectra for laser-induced breakdown spectroscopy (LIBS)

### Laser-induced breakdown spectroscopy:

- The laser-induced breakdown spectroscopy (LIBS) has been found a versatile analytical tool with various applications.
- In this technique, a high-power laser beam is typically focused onto the surface of a sample for analysis and, if the laser power exceeds a certain threshold, an optical breakdown occurs. In practice, the breakdown threshold depends on the wavelength and duration of the laser pulses as well as the analyzed media.
- For a nanosecond laser ablation, for example, the threshold varies from $1.9 \cdot 10^8$ W cm$^{-2}$ for copper up to $10^{10\,..\,11}$ W cm$^{-2}$ for aqueous solutions (Yaroshchyk *et al.* 2006).
- A plasma, i.e. a gas of highly-ionized atoms, is formed during the breakdown with an electron density of $10^{16\,..\,20}$ cm$^{-3}$ for typical Nd:YAG laser-induced plasmas.

### Computation of LIBS spectra:

- Ciucci *et al.* (1999) first estimated within a certain accuracy the composition of a laser-induced plasma by using computational methods instead of calibration standards. Their computation were based on the assumption that the plasma and sample compositions are the same and that the plasma is optically thin and in local thermal equilibrium (LTE) during the observation.
- The code by Yaroshchyk *et al.* (2006) is also based on the assumption of a LTE and a well-defined plasma temperature and electron density; it takes a number of characteristics atomic emission lines as input to create a synthesized theoretical emission spectrum of selected elements which are compared to the spectra of four separate compact spectrometers covering the spectral region 185–950 nm.

### 7.4.j. X-ray absorption of solid-state materials

**Motivation:**

- X-ray near-edge absorption (XANES): XANES as well as the related spectroscopies such as the resonant x-ray scattering (RXS) and x-ray magnetic circular dichroism (XMCD), are powerful spectroscopic techniques for probing the electronic structure around the absorbing atom (Bunau and Joly, 2009).
- In the near-edge region, one is very sensitive to the surroundings of the absorbing atom. This makes absorption spectroscopies a very useful tool to investigate geometric and electronic structure.
- In x-ray absorption spectroscopy, there has been a great need for codes that help reproduce the near-edge structure within a reasonable calculation time.
- These codes can be classified into two major categories: i) multi-electronic but monoatomic codes which are based on some multiplet theory and which give rise to a proper parametrized description of the localized electronic state, while the delocalized states can often not be decribed correctly. ii) multi-atomic but mono-electronic codes which provide correct description of the extended states but fail to account for the highly correlated state that interact with the core hole (for example, for the calculation of the L2 and L3 edges of the $3d$ elements).

### 7.4.k. X-ray quantum optics

**Motivation:**

-

### 7.4.l. Decay of medical radioisotopes

**Radioisotopes used in clinical therapy:**

- Most radioisotopes that are used in clinical therapy emit $\beta$ particles, i.e. ionizing radiation. The biological effect of this radiation is often characterized by the so-called linear energy transfer (LET) and measured in units of [keV/$\mu$m] for the deposited energy along the particle track.

- A new class of radionuclides including $^{149}$Tb, $^{213}$Bi, $^{211}$Po, $^{211}$A, $^{223}$Ra, $^{225}$Ac, $^{227}$Ac, $^{226}$Th and $^{230}$U, which all emit $\alpha$, have been considered for therapy. The LET for most therapeutic $\alpha$ emitters ranges from 25 to 230 [keV/$\mu$m].
- In addition, electrons and positrons emitted in the nuclear $\beta$ decay and the internal conversion processes have kinetic energies ranging from tens of keV to several MeV and their LET is much lower, typically 0.2 [keV/$\mu$m].

### 7.4.m. Configuration-averaged energies and cross sections

#### Configuration-averaged energies:

- Cowan (1981)provides a non-relativistic expression for the configuration-averaged energy as it often occurs in the computation of radiative and collisional rates (Peyrusse, 1999)

$$E_c = \sum_a N_a \, \langle a \rangle + \sum_{ab} N_a \, (N_b - \delta_{ab}) \, \langle a, b \rangle$$

$$\langle a \rangle = \varepsilon_a + \left\langle a \middle| - V^{\,(\mathrm{SCF})}(r) - \frac{2\,Z}{r} \middle| a \right\rangle, \qquad \langle a, b \rangle = \frac{1}{2} \, \frac{g_a}{g_a - \delta_{ab}} \left[ R^{(0)}(ab, ab) - \frac{1}{2} \sum_k \begin{pmatrix} \ell_a & k & \ell_b \\ 0 & 0 & 0 \end{pmatrix}^2 R^{(k)}(ab, ba) \right].$$

Here, $g_a = 2(2\ell_a + 1)$ is the degeneracy of subshell $a$, $V^{\,(\mathrm{SCF})}(r))$ is the self-consistent atomic potential and $R$ is the non-relativistic Slater integral.

#### Configuration-averaged cross sections:

- Peyrusse (1999) also provides non-relativistic expressions for the configuration-average radiative rates as well as for the configuration-average excitation strengths.

## 7.4.n. Mass attenuation coefficients

### Attenuation coefficients:

- The photon mass attenuation coefficient $\mu/\rho$ is calculated from the density $\rho$ of the target material and the thickness $d$ of the material in the direction of the incident photons as

$$\frac{\mu}{\rho} \;=\; -\frac{1}{\rho\, d}\, \ln\left(\frac{N}{N_o}\right),$$

and where $N_o$, $N$ are the numbers of incident and transversing photons, respectively.

### Theory:

-

# 8. Atomic cascades

## Cascades approaches

- Average singe-configuration approach (averageSCA): ... only one 'common set of orbitals' for all ionization stages of the atom and of 'configuration-averaged' data throughout the simulations.
- Singe-configuration approach (SCA): ... applies a common set of orbitals for each ionization stage of the atom.
- Multiple-configuration approach (MCA): ... incorporates also electron-electron correlations by configuration mixing contributions with closeby-lying configurations; it 'groups' the configurations together by using physical insight into the cascade process.

## 8.1. In JAC implemented cascade approximations

### Average singe-configuration approach (averageSCA):

- ... only partly implemented yet.
- This approach makes use of only one "common set of orbitals" for all ionization stages of the atom and of "configuration-averaged" data throughout the simulations; we here use the orbital set from the singly-charged ion to compute all necessary cross sections and rates.
- Approximate configuration averaged and decay rates are applied throughout by simply averaging over all fine-structure levels, rates and cross sections.
- For dealing with continuum electrons, we use approximate orbitals without exchange and without any relaxation of the electron density and by only using the first 3-4 (non-vanishing) partial waves in the computation of all photo- and autoionization amplitudes.

## 8.2. In JAC partly-implemented cascade approximations

### Singe-configuration approach (SCA):

- ... not yet implemented.
- This approach applies a common set of orbitals for each given ionization stage of the atom.
- However, all fine-structure (many-electron) transitions amplitudes are calculated explicitly for the selected atomic processes.

# 9. Field- and collision-induced atomic responses

## Atoms in intense laser pulses

- Atoms, which are irradiated by intense laser pulses, can emit radiation at multiples of the laser frequency, the (high) so-called harmonics.
- Such high-order harmonics, i.e. highly-energetic photons, can be produced by focusing either a high-frequency (excimer) laser or some low-frequency laser (Nd:glass, Ti:sapphire) into an atomic gas.
- Especially for low-frequency lasers, the harmonic spectrum is known to exhibit a characteristic behaviour: A rapid decrease of the yield for the first few harmonics, followed by a plateau and a rather abrupt cut-off.

## 9.1. Floquet theory

### Motivation:

- Many time-dependent problems in physics are periodic to a good approximation. For such physical systems, the (time) evolution can be solved either directly by numerical integration of the (time-dependent) Schrödinger, and making use of the time-dependent Hamiltonian.
- Floquet formalism: For a periodic evolution, time-dependent problems can be transformed also into a time-independent problem by applying the Floquet formalism, a very desirable transformation as iime-independent problems can often be solved more efficiently.
- While, in applying the Floquet formalism, often the Lindblad and Bloch-Redfield master equations are adapted, we note that these equations are derived for a time-independent Hamiltonian. In many cases, however, these standard master equations have still been found useful for solving time-dependent problems.

**Floquet ansatz:**

- Vector potential of a linearly-polarized electric field:

$$\mathbf{A}(t) \;=\; \boldsymbol{\epsilon}\, A_o \,\sin(\omega t); \qquad A_o \;=\; -\,\frac{c\,E_o}{\omega} \qquad \rightsquigarrow \qquad \mathbf{E}(t) \;=\; \boldsymbol{\epsilon}\, E_o \,\cos(\omega t).$$

- Floquet ansatz for the wave function:

$$\psi(t) \;=\; \exp(-i\,Et) \sum_{n=-\infty}^{\infty} \exp(-i\,n\,\omega t)\;\psi_n, \qquad E \;=\; \Re(E) \;-\; i\Gamma/2$$

where the functions $\psi_n$ are often called the harmonic components, while $E$ is the complex quasi-energy of the Siegert state $\psi(t)$ and $\Gamma$ the total ionization rate of this state.

## 9.2. In JAC implemented responses

None.

## 9.3. In JAC partly-implemented responses

None.

## 9.4. Further responses not yet considered in JAC

### 9.4.a. Collisional-radiative (CR) models

### Basic CR models:

- Collisional radiative models are sometimes called zero-dimensional plasma models. They are often applied in order to calculate atomic state distribution functions for one or more atomic species as function of the particle densities and temperatures. Most CR models assume that the radiative absorption and emission as well as electron-collision processes dominate the plasma and that all other (ion-atom, three-atom, ...) processes are negligible.
- A CR model can be used to calculate the effective emissivity or the effective ionization and recombination rates as function of electron temperature and density. These rates and results can then be applied in plasma transport model for determining local ionization, recombination and radiation effects.
- CR models help determine atomic level population densities of atoms in different plasma environments. Calculations are typically based on the CR recombination and ionization rate coefficients, radiative energy losses as well as on various individual rate coefficients.
- Different CR models can be distinguished due to the – analytic or numerical – treatment of the rate coefficients as well as the number and type of processes, for which such rate coefficients are taken into account.

### Approximations:

- CR models are typically built on the level densities $n(p)$ for a serious of levels $p_1,\, p_2,\, ...,\, p_N$. In general, the relation between the temporal and spatial distribution of the level density $n(p)$ is given by the diffusion equation

  $$\left( \frac{\partial\, n(p)}{\partial t} \right)_{\rm CR} \;=\; \frac{\partial\, n(p)}{\partial t} \;+\; \boldsymbol{\nabla} \cdot \left( n(p)\, \boldsymbol{\omega}(p) \right)$$

  Often, several atomic levels are simply combined into a single (effective) level $p_e$, and where an equal distribution is assumed for all of its physical levels: $n(p) \;=\; n(p_e)/g(p_e)$ with $g(p_e)$ being the statistical weight of the effective level $p_e$.
- If changes in the level density are dominated by radiative and collisional (de-) excitation processes, most CR models simply assume

  $$\left( \frac{\partial\, n(p)}{\partial t} \right)_{\rm CR} \;=\; 0 \;=\; P(p) \;-\; n(p)\, D(p)$$

and just solve a matrix equation. Here, $P(p)$ is the collisional and radiative production rate, and $D(p)$ the (so-called) *destructive* factor. The two functions $P(p)$, $D(p)$ can be written in terms of different rate coefficients for electron-impact excitation, ionization as well as for radiative and three-body recombination.

# 10. Time-evoluation of many-electron atomic state functions and density matrices

## 10.1. Time-dependent approximations of many-electron states

### Time-evolution of ASF:

- A reliable description of the time-dependent (TD) many-electron dynamics has attracted recent interest in order to theoretically support a real-time analysis and control of the ultrafast electronic and nuclear dynamics of atoms and molecules in intense laser pulses.
- A computational and conceptual simple approach to the many-electron dynamics is the TD configuration-interaction singles (TD-CIS) method in which only singly excited configurations, relative to the Hartree-Fock ground state, are taken into account in the configuration interaction expansion.
- Miyagi and Madsen (2013) make use of the TD-CIS method by performing an optimization of the orbitals as well as the expansion coefficients at each time step in the evolution. This separate optimization makes it possible to construct a reasonable accurate wave function with just a relatively small number of electronic configurations. For the optimization, Miyagi and Madsen (2013) utilized the Dirac-Frenkel-McLachlan TD variational principle.

## 10.2. Time-dependent statistical tensors

### Motivation:

- In physics, Liouville's theorem is known from classical statistical and Hamiltonian mechanics, and it asserts that the phase-space distribution function is constant along the trajectory of the system.

- Similarly, the quantum-mechanical analog of Liouville equation describes the time evolution of a mixed state. The quantum form can be obtained by the standard replacements of classical variables with quantum operators and Poisson brackets with commutators.
- The Liouville equation for the atomic density matrix $\rho$ reads

$$\frac{\partial \rho}{\partial t} \;=\; -\frac{i}{\hbar}\,[\mathbb{H},\, \rho\,] \;-\; \Gamma\,\rho, \qquad\qquad \mathbb{H} \;=\; \mathbb{H}^{\,(\mathrm{atom})} \;+\; \mathbb{H}^{\,(e-\gamma)}$$

where the first term in the Hamiltonian describes the (inner-) atomic and the atom-photon interactions, and the second term the relaxation matrix $\Gamma$. This relaxation matrix accounts for the atomic spontaneous decay due to either radiative or nonradiative (Auger) processes of the atom.

## 10.3. Time-integration of statistical tensors

### Motivation:

- Various methods can be applies to solve the coupled first-order odg's for the time-evolution of the statistical tensors. Apart from those methods which solve the equations with given accuracy (but typically require the evaluation of the rhs at any given time $t$), we are mainly interested in *shooting* or *predictor-corrector* methods which makes only use of previous solutions of $\rho$ and $d\rho/dt \;=\; f$ on a equidistant time grid.

### Numerical methods:

- If we use a step-size $h$ and define $\rho(t_j) \;=\; \rho_j$ , $\frac{d\rho}{dt}(t_j) \;=\; f_j$ , the following integration formulas can be applied.
- Euler's methods:

$$\rho_{j+1} \;=\; \rho_j \,+\, h\, f_j$$

- Adams-Bashford methods:

$$\rho_{j+1} = \rho_j + h \left[ \frac{3}{2} f_j - \frac{1}{2} f_{j-1} \right]$$

$$\rho_{j+1} = \rho_j + h \left[ \frac{23}{12} f_j - \frac{16}{12} f_{j-1} + \frac{5}{12} f_{j-2} \right]$$

$$\rho_{j+1} = \rho_j + h \left[ \frac{55}{24} f_j - \frac{59}{24} f_{j-1} + \frac{37}{24} f_{j-2} - \frac{9}{24} f_{j-3} \right]$$

# 10.4. Time evolution of statistical tensors. Formalism

## 10.4.a. Liouville equation for the atomic density matrix

### Vector potential and state multipoles:

- In the electron-photon interaction, the vector potential of the electromagnetic field is typically chosen to fulfill $\mathrm{div}\,\mathbf{A}(\mathbf{r}_i, t) = 0$.
- When the electron-photon interaction Hamiltonian $\mathbb{H}^{(e-\gamma)}$ is applied upon the density operator $\rho$, we shall consider only processes with one photon.
- Moreover, we assume a vector potential for a monochromatio field with frequency $\omega$ and wave vector $\mathbf{k} = (\vartheta_k, \varphi_k)$ $(|\mathbf{k}| = \frac{\omega}{c})$ with regard to the coordinates in the laboratory system.
- Envelope of the vector potential: For a pulse with (real) envelope $f(t)$, the vector potential then includes two terms

$$\mathbf{A}(\boldsymbol{r}, t) = \mathbf{A}(\mathbf{r})\, f(t)\, e^{-i\omega t} + \mathbf{A}^*(\mathbf{r})\, f^*(t)\, e^{i\omega t}.$$

## Liouville equation in the representation of well-defined angular momenta:

- ➢ Liouville equation: In an atomic basis with well-defined total angular momenta and parity, the Liouville equation can be re-written as

$$\begin{aligned}\frac{\partial}{\partial t}\,\langle \alpha \mathbb{J}_\alpha M_\alpha \,|\, \rho \,|\, \beta \mathbb{J}_\beta M_\beta \rangle \;&=\; -\frac{i}{\hbar}\,(E_\alpha \;-\; E_\beta)\;\langle \alpha \mathbb{J}_\alpha M_\alpha \,|\, \rho \,|\, \beta \mathbb{J}_\beta M_\beta \rangle \\ &\quad -\frac{i}{\hbar}\sum_{\nu \mathbb{J}_\nu M_\nu}\Big(\Big\langle \alpha \mathbb{J}_\alpha M_\alpha \Big|\, \mathbb{H}^{(\mathrm{e}-\gamma)} \Big|\, \nu \mathbb{J}_\nu M_\nu \Big\rangle\;\langle \nu \mathbb{J}_\nu M_\nu \,|\, \rho \,|\, \beta \mathbb{J}_\beta M_\beta \rangle \;-\; \langle \alpha \mathbb{J}_\alpha M_\alpha \,|\, \rho \,|\, \nu \mathbb{J}_\nu M_\nu \rangle\,\Big\langle \nu \mathbb{J}_\nu M_\nu \Big|\, \mathbb{H}^{(\mathrm{e}-\gamma)} \Big|\, \beta \mathbb{J}_\beta M_\beta \Big\rangle\Big) \\ &\quad -\sum_{\gamma \mathbb{J}_\gamma M_\gamma}\langle \alpha \mathbb{J}_\alpha M_\alpha \,|\, \Gamma \,|\, \gamma \mathbb{J}_\gamma M_\gamma \rangle\;\langle \gamma \mathbb{J}_\gamma M_\gamma \,|\, \rho \,|\, \beta \mathbb{J}_\beta M_\beta \rangle\end{aligned}$$

### 10.4.b. Time-dependent statistical tensors of atomic lines

## Time-dependent statistical tensors:

- ➢ Statistical tensors: With the substitutions of the statistical tensors from above and the notations $[ab...c] \equiv (2a+1)(2b+1)...(2c+1)$, the

Liouville equation can be written as Grum-Grzhimailo, 2012)

$$
\begin{aligned}
i\hbar\dot{\tilde{\rho}}_{kq}(\alpha\mathbb{J}_\alpha,\beta\mathbb{J}_\beta) \quad = \quad & -2\pi\sqrt{\frac{\hbar}{c\,k}}\sum_{\nu\mathbb{J}_\nu\,KQ} \\
& \Bigg[f(t)\,e^{-i(\omega-\omega_{\alpha\nu})t}\sum_{LM\lambda} g_\lambda(-1)^{J_\alpha+J_\beta+K+L}[LK]^{1/2}\ \langle KQ,\,LM\mid kq\rangle \begin{Bmatrix} J_\alpha & J_\beta & k \\ K & L & J_\nu \end{Bmatrix} D^L_{M\lambda}(\varphi_k,\vartheta_k,0)\ \left(\left\langle\alpha\mathbb{J}_\alpha\left\|\,\mathbb{T}^{(m)}_L\,\right\|\nu\mathbb{J}_\nu\right\rangle + i\lambda\left\langle\alpha\mathbb{J}_\alpha\left\|\,\mathbb{T}^{(e)}_L\,\right\|\nu\mathbb{J}_\nu\right\rangle\right)\ \tilde{\rho}_{KQ}(\nu\mathbb{J}_\nu,\beta\mathbb{J}_\beta) \\
& - f^*(t)\,e^{i(\omega-\omega_{\nu\alpha})t}\ \sum_{LM\lambda} g^*_\lambda(-1)^{J_\beta+k+J_\nu+L}[Lk]^{1/2}\ \langle kq,\,LM\mid KQ\rangle \begin{Bmatrix} J_\alpha & J_\beta & k \\ K & L & J_\nu \end{Bmatrix} D^{L\,*}_{M\lambda}(\varphi_k,\vartheta_k,0)\ \left(\left\langle\nu\mathbb{J}_\nu\left\|\,\mathbb{T}^{(m)}_L\,\right\|\alpha\mathbb{J}_\alpha\right\rangle - i\lambda\left\langle\nu\mathbb{J}_\nu\left\|\,\mathbb{T}^{(e)}_L\,\right\|\alpha\mathbb{J}_\alpha\right\rangle\right)\ \tilde{\rho}_{KQ}(\nu\mathbb{J}_\nu,\beta\mathbb{J}_\beta) \\
& + f(t)\,e^{-i(\omega-\omega_{\nu\beta})t}\ \sum_{LM\lambda} g_\lambda(-1)^{J_\alpha+J_\beta+K}[LK]^{1/2}\ \langle KQ,\,LM\mid kq\rangle \begin{Bmatrix} J_\alpha & J\_beta & k \\ L & K & J_\nu \end{Bmatrix} D^L_{M\lambda}(\varphi_k,\vartheta_k,0)\ \left(\left\langle\nu\mathbb{J}_\nu\left\|\,\mathbb{T}^{(m)}_L\,\right\|\beta\mathbb{J}_\beta\right\rangle + i\lambda\left\langle\nu\mathbb{J}_\nu\left\|\,\mathbb{T}^{(e)}_L\,\right\|\beta\mathbb{J}_\beta\right\rangle\right)\tilde{\rho}_{KQ}(\alpha\mathbb{J}_\alpha\,\nu\mathbb{J}_\nu) \\
& - f^*(t)\,e^{i(\omega-\omega_{\beta\nu})t}\ \sum_{LM\lambda} g^*_\lambda(-1)^{J_\alpha+K+J_\nu}[Lk]^{1/2}\ \langle kq,\,LM\mid KQ\rangle \begin{Bmatrix} J_\alpha & J_\beta & k \\ L & K & J_\nu \end{Bmatrix} D^{L\,*}_{M\lambda}(\varphi_k,\vartheta_k,0)\ \left(\left\langle\beta\mathbb{J}_\beta\left\|\,\mathbb{T}^{(m)}_L\,\right\|\nu\mathbb{J}_\nu\right\rangle - i\lambda\left\langle\beta\mathbb{J}_\beta\left\|\,\mathbb{T}^{(e)}_L\,\right\|\nu\mathbb{J}_\nu\right\rangle\right)\ \tilde{\rho}_{KQ}(\alpha\mathbb{J}_\alpha,\nu\mathbb{J}_\nu)\Bigg] \\
& - i\hbar\sum_{\gamma\mathbb{J}_\gamma} G^{KQ}_{kq}(\alpha\mathbb{J}_\alpha,\beta\mathbb{J}_\beta,\gamma\mathbb{J}_\gamma)\,e^{i\omega_{\alpha\gamma}t}\ \tilde{\rho}_{KQ}(\gamma\mathbb{J}\gamma,\beta\mathbb{J}_\beta)
\end{aligned}
$$

## 10.5. Observables to be derived from time-dependent statistical tensors

### Motivation:

- ➢ If we solve the set of time-dependent (Liouville) equations for the state multipoles, we can obtain the atomic statistical tensors for (a) discrete atomic states $\rho_{kq}(\alpha\mathbb{J}_\alpha;\beta\mathbb{J}_\beta)$ (b) for atomic states with one electron in continuum $\rho_{kq}(\alpha_f\mathbb{J}_f,\varepsilon\kappa:\alpha\mathbb{J}_\alpha,\alpha'_f\mathbb{J}'_f,\varepsilon'\kappa':\alpha\mathbb{J}_\alpha)$, (c) *nondiagonal* elements $\rho_{kq}(\alpha_f\mathbb{J}_f,\varepsilon\kappa:\alpha\mathbb{J}_\alpha,\ \beta\mathbb{J}_\beta)$ and $\rho_{kq}(\alpha_f\mathbb{J}_f,\varepsilon\kappa:\alpha\mathbb{J}_\alpha,\alpha'_f\mathbb{J}'_f,\varepsilon'\kappa':\beta\mathbb{J}_\beta)$.

# 11. Semiempirical estimates

## 11.1. In JAC implemented estimates for atomic properties and data

None.

## 11.2. In JAC partly-implemented estimates for atomic properties and data

### 11.2.a. Ionization energies

- Their are numerous tabulations for the first and second ionization potentials of (almost) all elements from the periodic table.
- A simple parametrization for the ionization of inner-shell electrons has been worked out by Thayer Watkins for elements from the $n\ell$-shell, although it seems not to be very reliable

$$E_b \;=\; 10.42924\,\left[(Z/n)^2 \,+\, 1.371650145\right]^2 \,-\, 16.76869944 \;=\; -11.0053 \,+\, 10.31048\,(Z/n)^2 \,+\, 28.83251\,(Z/n) \,-\, 2.88439\,\ell$$

- In JAC, an estimate for the binding energy of an $n\ell$-electron in the neutral atom can be obtained from `JAC.estimate("ionization potential: inner-shell", shell::Shell, Z::Int64)`.

## 11.2.b. Weak-field ionization of effective one-electron atoms

### Property & notations:

- Field ionization: by a quasi-static external field: $A^{(*)} + F\,\mathbf{e}_z \quad \longrightarrow \quad A^+ * e^-$ .
- Formal quantum notation: $|\alpha \mathbb{J}\rangle \quad \longrightarrow \quad ...$
- Not yet implemented.
- In JAC, all estimates on the field-ionization rates of atoms are always based on a non-relativistic, single-electron approach. No attempt has (yet) been made to generalize this approximation towards real many-electron atoms and ions with their fine-structure.

### Motivation:

- Ionization of atoms by an external electric field is a fundamental atomic process that plays an important role, for instance, in the formation of charge-state distributions in (dilute) plasma under strong fields.
- Vice versa: The observations of temporal variations in the line intensities of ions, that are produced by field ionization, can help determine spectroscopically the macroscopic-field distribution in plasma.
- Since the field-ionization probability grows (very) rapidly with the electric field strength $F$, the field strength can be derived from accurate measurements of the ionization probabilities.

### Further information:

- Ionization probabilities are often calculated within the WKB approximation, i.e. in the weak-field limit. In general, field ionization probability depends critically on the projection of the total orbital angular momentum upon the direction of the field.
- In most field-ionization probability computations, a quasi-static and homogeneous electric field is assumed as it occurs, for example, for macroscopic-scale fields in plasma. This assumption is in contrast to many local fields that may occur at the atomic scale.

- For the case of a single electron with binding energy $E$ in the valence shell $(n\,\ell)$ and outside of closed shells otherwise, the quasi-classical escape rate is given by (Fisher *et al.*, 1998)

$$\Gamma(E, \ell, m) \;=\; B_{n\ell}^2 \, \frac{(2\ell+1)\,(\ell+m)!}{2^{m+1}\, k^m\, m!\,(\ell-m)!} \, \left( \frac{2\,k^2}{F} \right)^{2Z/k \,-\, m \,-\, 1} \quad \exp\left( -\frac{2\,k^3}{3\,F} \right)$$

  where $Z$ is the charge of the parent ion as seen by the electron are large $r$, $k = \sqrt{2\,|E|}$ is the modulus of the (electron's) wave vector and $B_{n\ell}$ is the amplitude that characterizes the outgoing electron wave.

### 11.2.c. Electron-impact ionization. Cross sections

#### Kolbenstvedt model for the electron-impact ionization:

- Haque and coworkers (2010) explored a so-called Kolbenstvedt model for the electron-impact ionization of the $K$-, $L$- and $M$-shells of neutral atoms and ions.

## 11.3. Further estimates on atomic properties, not yet considered in JAC

### 11.3.a. Electron and positron stopping powers (`StoppingPower`)

#### Property & notations:

- Stopping power: due to the penetration of electrons and positrons through matter: $A^{(*)}$ .. .

#### Motivation:

- Stopping powers of matter for electrons are important for many applications involving energy deposition. In radiation physics, chemistry, biology and medicine, it is important to have simple but accurate estimates about the stopping power of energetic electrons in various media for (Gümüs, 2005).

- Until the present, no simple and practical model exists for the stopping power of electrons with energies below 10 keV.

## Approximate stopping power formulas:

- The stopping power of materials arise from two types of processes, namely collisional and radiative processes. The collisions of the incident particles with the target material is most important and mainly arises from collisions between the incident particles and the atomic electrons.

$$\frac{dE}{dx} = \left(\frac{dE}{dx}\right)^{\text{(collision)}} + \left(\frac{dE}{dx}\right)^{\text{(radiative)}}$$

- For incoming electrons, a modified collisional stopping power formula for incoming electrons can be written as given by Sugiyama (1985) or Rohrlich and Carlson (1954)
- Full Bethe-Bloch formula:

$$-\frac{dE}{dx} = \left(\frac{e^2}{4\pi\,\epsilon_o}\right) \frac{4\pi\, z^2\, N_A\, Z\, \rho}{mc^2\, \beta^2\, A} \left[\ln\left(\frac{2mc^2\,\beta^2}{I}\right) - \ln(1-\beta^2) - \beta^2\right]$$

### 11.3.b. Stark broadening of spectral lines in plasma

## Motivation:

- Stark broadening of spectral lines: This broadening has been found very important in (so-called) DA and DB white dwarf atmospheres.
- Apart from white dwarfs, Stark broadening of spectra is also an important pressure-broadening mechanism for arious types of other stars.
- Various semi-empirical calculations of the Stark widths and shifts have been performed in the impact approximation by using Griems (1968) formula.
- For selected lines, it was shown that Stark broadening can change the observed widths by 10-45 %.

## Semi-empirical approximations:

- Lorentzian profile of isolated lines: For isolated lines $|\alpha_i \mathbb{J}_i\rangle \rightarrow |\alpha_f \mathbb{J}_f\rangle$ with level energies $E_i$ and $E_f$, the line profile is often assumed to be Lorentzian, shifted by the energy $d$ and with the (total) line widths $\Gamma$ due to the (plasma) Stark broadening.

$$F(\omega) \;=\; \frac{(\Gamma/2\pi)}{(\omega \,-\, \omega_{if} \,-\, d)^2 \,+\, (\Gamma/2)^2}, \qquad\qquad \omega_{if} \;=\; \frac{E_i \,-\, E_f}{\hbar} \,.$$

where

- Energy shift and (total) widths of the Stard-broadened line: Both, the energy shift $d$ as well as the (total) widths $\Gamma$ can be expressed in terms of the velocity distribution $f(v)$ of the electrons in the plasma, its density $N^{\,(\mathrm{elec})}$, the impact parameter $b$ of the incident electrons as well as the elastic and inelastic (electron-impact excitation) cross sections for excitations of the initial and final levels to neighboured levels.

$$\Gamma \;=\; N^{\,(\mathrm{elec})} \int dv\, v\, f(v) \;\left(\sigma^{\,(\mathrm{elastic}} \,+\, \sigma^{\,(\mathrm{inelastic}}\right); \qquad\qquad d \;=\; N^{\,(\mathrm{elec})} \int dv\, v\, f(v) \;\int_{R_1}^{R_{\mathrm{Debye}}} db\, 2\pi\, b\, \sin(\phi_p)$$

and where $\phi_p$ is a plasma-specific phase shift. Further details on the Stark broadening of spectral lines are given by Dimitrijevich and Sahel-Brechot (1996).

- In 1968, Griem suggested simple semiempirical formulas for the Stark line shift and widths in impact approximation which is based on some original formular by Baranger (1958) as well as an effective Gaunt factor by Seaton (1962) and Regemorter (1962). With these formulas, the Stark linewidths and Stark line shifts can be obtained by:

$$\frac{\Gamma}{[a.u.]} \;=\; 8 \left(\frac{\pi}{3}\right)^{3/2} \frac{\hbar}{m\, a_o}\, N_e \left(\frac{E_H}{k\,T}\right)^{1/2} \left[ \sum_{i'} |\,\langle i'\,|\mathrm{r}|\, i\rangle\,|^2\, g_{se} \left(\frac{E}{\Delta\, E_{i'i}}\right) \,+\, \sum_{f'} |\,\langle f'\,|\mathrm{r}|\, f\rangle\,|^2\, g_{se} \left(\frac{E}{\Delta\, E_{f'f}}\right) \right]$$

$$\frac{d}{[a.u.]} \;=\; -8 \left(\frac{\pi}{3}\right)^{3/2} \frac{\hbar}{m\, a_o}\, N_e \left(\frac{E_H}{k\,T}\right)^{1/2} \left[ \sum_{i'} \left(\frac{\Delta\, E_{i'i}}{|\Delta\, E_{i'i}|}\right) |\,\langle i'\,|\mathrm{r}|\, i\rangle\,|^2\, g_{sh} \left(\frac{E}{\Delta\, E_{i'i}}\right) \,+\, \sum_{f'} \left(\frac{\Delta\, E_{f'f}}{|\Delta\, E_{f'f}|}\right) |\,\langle f'\,|\mathrm{r}|\, f\rangle\,|^2\, g_{sh} \left(\frac{E}{\Delta\, E_{f'f}}\right) \right]$$

In these formulae, $E_H$ is the hydrogen ionization energy, $N_e$ is the free-electron density of the perturber levels, $T$ is the electron temperature, $E \;=\; 3/2\, kT$ the mean energy of the perturbing electron and $g_{se}$, $g_{sh}$ are the effective Gaunt factors which are calculated and tabulated by Griem. These Gaunt factors are slowly varying functions of $x_{j'j}$ where $x_{j'j} = E/\Delta E_{j'j}$ is the energy difference between a perturbing level $j'$ and the perturbed initial/upper (final/lower) level $j$.

- The atomic matrix elements need often to be obtained from *ab-initio* Hartree-Dirac-Fock computations, and the summation over the levels is obtained by making use of the table by Moore (1958).

## 11.3.c. Atomic electron-momentum densities

### Definition & notations:

- For a given atomic level $|\alpha\mathbb{J}\rangle$ , the (radial electron) momentum density $I(p;\, \alpha\mathbb{J})$ and the one-electron momentum density $\Pi_{n\kappa}(p;\, \alpha\mathbb{J})$ and is given by (Koga and Thakkar, 1996)

$$I(p;\, \alpha\mathbb{J}) \;=\; 4\pi\, p^2\, \Pi(p;\, \alpha\mathbb{J}), \qquad\qquad \Pi(p;\, \alpha\mathbb{J}) \;=\; \frac{1}{4\pi\, p^2} \sum_{i=1}^{N} \langle \psi_\alpha \,|\, \delta(p \;-\; p_i |\, \psi_\alpha \rangle \,.$$

- The radial one-electron momentum density $I$ is used to calculate the corresponding moments of the momentum density

$$\left\langle p^k \right\rangle \;=\; \int_0^\infty dp\, p^k\, I(p;\, \alpha\mathbb{J}), \qquad\qquad -2 \;\leq\; k \;\leq\; 4$$

- These moments are often applied in:
  - density functional theory: since $\langle p \rangle \,/\, \pi$ is close to the Dirac-Slater exchange energy;
  - x-ray cristallography: since $\langle p^3 \rangle$ is roughly proportional to the initial value of the so-called Patterson function
  - Compton profiles: since $J(q) \;=\; \frac{1}{2} \int_{|q|}^{\infty} dp\, p^{-1}\, I(p)$ is twice the peak height of the isotropic Compton profile.

# 12. Beams of light and particles

## 12.1. Helmholtz wave equation

### Propagation of light in free space:

- Helmholtz wave equation: If we consider the propagation of light in free space, the Maxwell equations simplify and the spatial structure of their solution satisfy the well-known Helmholtz wave equation, an elliptic partial differential equation

  $$\nabla^2 u(\mathbf{r}) + k^2 u(\mathbf{r}) = 0 .$$

  This equation follows from the (full) time-dependent wave equations due to the separation of variables.

- Harmonic solution of the Helmholtz equation:

  $$u(\mathbf{r}) = C_1 e^{i \mathbf{k} \cdot \mathbf{r}} + C_2 e^{-i \mathbf{k} \cdot \mathbf{r}}, \qquad k = |\mathbf{k}| = \frac{\omega}{c} .$$

- The solution in time is a linear combination of sine and cosine functions with angular frequency $\omega$, while the form of the spatial solution of the Helmholtz equation depends rather sensitively on the given boundary conditions.

- Vector potential of optical beams: There exist various expressions to represent the vector potential of optical beams of different kind and spatial structure, and which are solutions of the Helmholtz equation. These vector potentials represent different spatial structures and phases.

- Below, several of these solution are provided for different beams in terms of the (scalar) amplitudes of the corresponding light fields.

- Synonym notions of vortex beams: helically phased light beams; optical vortex beams with a field dependence $e^{im\varphi}$ , ... .

## Paraxial approximation to the Helmholtz equation:

- Paraxial approximation: The Helmholtz equation still represents a complicated partial differential equation; in the science of optics, one often has well-defined paraboloidal waves or Gaussian beams in which the field change along the propagation direction is small compared to the change in perpendicular direction; $\partial u / \partial z \ll \partial u / \partial x, \partial u / \partial y$.
- For these conditions, the Helmholtz equation simplifies to

$$\nabla_{\perp}^{2} \, u(\mathbf{r}) \; + \; 2ik \, \frac{\partial u}{\partial z}(\mathbf{r}) \;\; = \;\; 0 \, .$$

- Conditions for the paraxial approximation: The restrictions upon the variation of the amplitude function $u$ is often also written in the form

$$\left| \frac{\partial u}{\partial z} \right| \; \ll \; |k \, u| \qquad\qquad \text{and} \qquad\qquad \left| \frac{\partial^{2} u}{\partial z^{2}} \right| \; \ll \; |k^{2} \, u| \, .$$

- The paraxial approximation is obtained if the ansatz $\psi(\mathbf{r}) \; = \; u(\mathbf{r}) \; e^{ikz}$ is used in the Helmholtz equation and if the term $\sim \frac{\partial^{2} u}{\partial^{2} z}$ is neglected, when compared with $\sim \frac{\partial \psi}{\partial z}$ .

# 12.2. Light beams

## Light beams:

- Characterization and properties of beams: In studying light-matter interactions, light beams play a major practical role and, hence, their characterization and properties are very important in order to understand the details of the interaction.
- Beams from applications: Light beams are usually formed when the em field from a given source is projected by filters and blends into a beam. In some lighting devices, lamps or parabolic reflector are used to produce an artificially light beam with a more or less large divergence (for example, car headlights, spotlights, ect.).
- Experimental beam parameters: The geometry and behavior of a Gaussian beam are governed by a set of beam parameters which are defined slightly different for different kinds of beams but which are often used to characterize the beams. These beam parameters include:

- Beam width: There are over five definitions of beam width.
- Beam quality: Quantified by the beam quality parameter, M2.
- Beam divergence: This is a measure of how the beam spreads with distance with regard to the focus plane.
- Beam profile: A beam profile is the 2D intensity plot of a beam at a given location along the beam path. A Gaussian or flat-top profile is often desired for many applications. The beam profile indicates nuisance due to high-order spatial modes in a laser cavity as well as hot spots in the beam.
- Beam astigmatism: A beam is called astigmatic when the vertical and horizontal focus of the beam is placed at different locations along the beam path.
- Beam wander or jitter: The amount by which the centroid or peak value of the beam profile moves with time.

### Twisted (vortex) light beams:

- ➢ Charles Darwin (1932; 1887-1962) was one of the first who worked on light with a spatial structure of the phase.
- ➢ For circularly-polarized plane-wave light, the photons carry a projection of the angular momentum $\Delta L_z = \pm\hbar$ upon the propagation direction.
- ➢ Polarization state of a light beam: In 1892, Poincare showed that the state of polarization of a light beam can be described as a point on the surface of a unit sphere now known as the Poincare sphere.

## 12.2.a. Gaussian beams

### Characerization and use:

- ➢ Gaussian beam: In optics, a Gaussian beam is a beam of electromagnetic radiation whose transverse electric field amplitude and, hence, its intensity distributions are approximately described by some Gaussian distribution.
- ➢ Both, planes waves and Gaussian beams are solutions of the Maxwell equation *and* the homogenous wave equation they both generally possess a **polarization** but can be readily described in terms of complex amplitudes.

- Complex-valued electric field amplitude $u(\mathbf{r})$: In a Gaussian beam, the electric field amplitude

$$u(\rho, z) = u_0 \frac{w_0}{w(z)} \exp\left(\frac{-\rho^2}{w^2(z)}\right) \exp\left(-ikz - ik\frac{\rho^2}{2R(z)} + i\zeta(z)\right)$$

obeys the paraxial Helmholtz equation. This amplitude is sufficient in order to describe the properties of the beam since the electric field and magnetic field propagate together and obey the same wave equation.

- Characteristic parameters: In the definition of the electric-field amplitude above, we have
  - $\rho$ ... radial distance from the center axis of the beam;
  - $z$ ... the axial distance from the beam's narrowest point (the beam waist),
  - $k = \frac{2\pi}{\lambda}$ ... the wave number (in radians per meter), $E0 = |E(0,0)|$
  - $w_0 = w(0)$ ... the waist size,
  - $w(z)$ ... the radius at which the field amplitude drop to $1/e$ and, hence, the intensity to $1/e^2$ at axis with regard to $w_0 = w(0)$,
  - $R(z)$ ... the radius of curvature of the beam's wavefronts,
  - $\zeta(z)$ ... the Gouy phase shift, an extra contribution to the phase that is seen in Gaussian beams.

- In fact, many laser emit beams with roughly a Gaussian profile; these beams are often called the $\mathrm{TEM}_{00}$ fundamental modes of the laser's optical resonator. Gaussian beams form a widespread model in laser physics.

### 12.2.b. Vortex beams. Characterization and properties

#### General remarks:

- ➢ The recent years have seen a tremendous effort in generating and manipulating vortex beams together with a good number of new or promising applications, including the capture, manipulation and transport of nanoscopic particles (optical tweezer), high-resolution microsocopy or for data transmission.

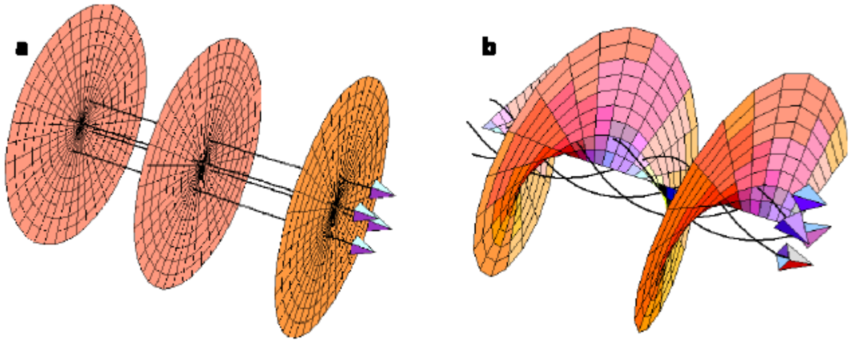

Figure 12.1.: Laser beams usually have planar wavefronts with wavevectors parallel to the beam axis. Beams with helical wavefronts have wavevectors which spiral around the beam axis and give rise to an orbital angular momentum; from Padgett and Allen (2000).

- ➢ Twisted photons carry both, spin angular momentum (SAM) as well as orbital angular momentum (OAM) along their propagation direction.
- ➢ Topological charge The $z$-projection of the OAM, $m$, is often called the topological charge or the winding number of the beam. This charge describes the number of the $2\pi$ windings of the helical phase around the vortex in one wavelength.
- ➢ Synonym notions of vortex beams: helically phased light beams; optical vortices with a field dependence $e^{im\varphi}$.
- ➢ Optical vortex beams are well-known and have been routinely used for the last 20 years; a first demonstration dates back to Durnin *et al.* (1987).
- ➢ For optical vortices, charge values of $m \leq 5000$ have been realized (Shen *et al.*, 2013).
- ➢ Reviews on optical vortex beams are given by Allen *et al.* (1999); Franke-Arnold *et al.* (2008), Zhan (2009) and Yao and Padgett (2011).

## Characterization of vortex beams:

- A vortex state of light carries a well-defined projection of the orbital angular momentum (OAM) with respect to the beam axis.
- Wave functions: $\sim e^{im\varphi}$ are eigenfunctions of $\ell_z = \frac{\partial}{\partial \varphi}$ .
- Photon field: For a quantized radiation field, each particle also carries a projection $m\,\hbar$ of the OAM, that is part of the total angular momentum. In general, the spin and orbital angular momentum cannot be separated.
- In the paraxial approximation, the spin and OAM longitudinal components of the vortex state can be separated from each other. Beyond the paraxial limit, however, the spin-orbit interaction does not allow a simple separation of the spin and orbital angular momentum.

## Properties of vortex beams:

- For all points in the beam, the ratio between the azimuthal and $z$-components of the momentum is found to be $\ell/kr$ .
- The linear momentum of each photon is given by $\hbar k$ ; since the azimuthal component of the wavevector is $m/r$ and is independent of the wavelength, the orbital angular momentum per photon is

$$p = \hbar k \qquad \longrightarrow \qquad p_\varphi = \hbar k \phi \qquad \longrightarrow \qquad \ell = r \times p_\varphi = r \times \frac{\cdot\cdot}{r} = m\hbar$$

- However, OAM $\neq$ SAM, despite the rather similar illustrations in the literatur; in particular, there exist also vortex states for spin-less waves, such as acoustic vortex waves.

## 12.2.c. Vortex beams. Generation

### Generation of vortex beams with different photon energies:

- For intense, short-wavelength FEL radiation, optical methods can often not be applied due to strong limitations and difficulties in the fabrications of optical surfaces (Terhalle *et al.* 2011, Peele *et al.* 2002).
- Twisted EUV beams: Ribic and coworkers (2014) proposed an efficient scheme in order to generate intense coherent and twisted OAM beams in the EUV region. These beams can be realized by means of a seeded FEL, i.e. by using a (seeding) laser pulse with a transverse, staircaselike phase. For this phase pattern, in particular, the diffraction and mode selection drive the radiation profile towards a dominant OAM mode at saturation.
- Twisted x-ray beams: Hemsing an coworkers proposed two clever approaches for generating FEL vortex beams within the x-ray region:
  (i) By using the interaction of an electron beam with a seeded laser within a helical undulator (Hemsing *et al.*, 2011);
  (ii) by using a so-called echo-enabled harmonic generation (EEHG) scheme, in which two seed lasers and two magnetic chicanes are utilized in order to produce harmonic microbunches of an electron beam with a corkscrew distribution.

### Generation of vortex beams by pitch-fork holograms:

- The superposition of a regular phase profile with some proper grating already results in a fork hologram that help generate vortex beams.
- Fork-like or pitch-fork holograms are known to diffract the light and to generate beams with OAM. Such holograms can be generated also dynamically by using a spatial light modulator and readily controlled by a computer.
- A pitchfork hologram is obtained adding a twisting and an oblique phase. The width of six $2\pi$ phase ramps is highlighted.

### Generation of vortex beams by spiral phase plates:

- A (plane-wave) light beam can acquire a non-zero OAM by crossing a spiral phase plate with an inhomogeneous thickness.
- Spiral phase plates (SPP): Such a SPP is a transparent dielectric plate with a thickness that varies as a smooth ramp; this variation in the thickness adds a phase shift to an incident field that increases linear with the azimuthal angle $\varphi$.
- Light field: If a SPP is placed into the waist of a Laguerre-Gaussian beam with well-defined quantum numbers, $u_{\ell p}^{\rm LG}$ , the complex light amplitude just behind the plate can be described by means of a phase-plate operator $S(m_s, \alpha)$

$$\langle r, \varphi \, | S(m_s, \alpha = 0) | \, l, p \rangle \;=\; u_{lp}^{\rm LG}(r, \varphi) \, e^{i m_s \varphi},$$

and where $m_s$ is the phase shift per unit angle of the given SPP.

- SPP help explore high-dimensional entanglement with just two detector, while 6 detectors are required by other popular methods in order to prove the entanglement of the OAM degree of freedom for two entangled photons (Oemrawsingh *et al.*, 2004).
- The figure below shows the transformation of a $\text{TEM}_{00}$ mode into a helical beam.

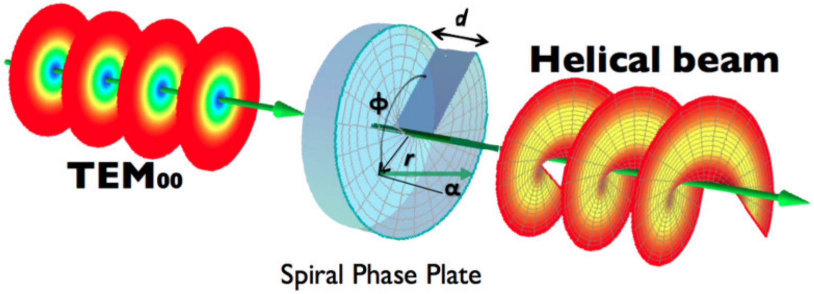

Figure 12.2.: Experimental scheme for generating light orbital angular momentum with spiral phase plates. Taken from Beijersbergen *et al.* (1994).

## Generation of vortex beams by q-plates:

- q-plate: A (so-called) q-plate is a device that is realized by means of liquid crystals, polymers or sub-wavelength gratings; this device exploits a change of sign if the polarization of the incoming light is modified.

## Generation of vortex beams by spatial light modulators:

- xxxxx A spatial light modulator (SLM) is an object that imposes some form of spatially varying modulation on a beam of light. A simple example is an overhead projector transparency. Usually when the phrase SLM is used, it means that the transparency can be controlled by a computer. In the 1980s, large SLMs were placed on overhead projectors to project computer monitor contents to the screen. Since then more modern projectors have been developed where the SLM is built inside the projector. These are commonly used in meetings of all kinds for presentations.

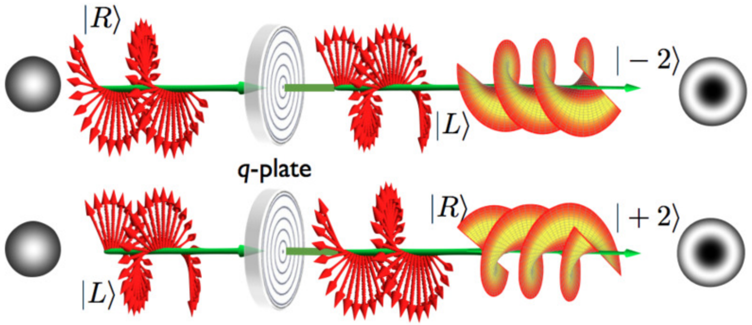

Figure 12.3.: The q-plate effect for left and right-hand circular polarizations.

### Generation of vortex beams by cylcindrical mode converters:

- A Hermite-Gaussian beam can be converted into a Laguerre-Gaussian beam with well-defined OAM by using an astigmatic system with two well-aligned cylindrical lenses. In this scheme, these lenses are placed at some specific distance in order to introduce a well-defined relative phase between the horizontal and the vertical Hermite-Gaussian beams.

### Generation of vortex beams by helical undulators:

- X-ray vortex beams with photon energies $\hbar\omega \approx 100$ eV have been generated in a helical undulator by Bahrdt *et al.* (2013) and Hemsing *et al.* (2013).
- Another interesting approach has been suggested by Ribic and coworkers (2014). These authors proposed to modify he phase mask and to manipulate directly the seeding laser in order to change the transverse properties of the FEL light.

## 12.2.d. Hermite-Gaussian beams

### Characterization and use:

- Hermite-Gaussian modes $HG_{mn}$ : have a rectangular symmetry and are described by means of two mode indices $m$ and $n$; these mode indices give the number of nodes in the $x$ and $y$ directions respectively.

- Hermite-Gaussian modes: These modes are a convenient description for the output of lasers whose cavity design is not radially symmetric but asymmetric in horizontal and vertical directions.

## 12.2.e. Laguere-Gauss beams

### Characterization and use:

- The Laguerre-Gaussian (LG) beams carry an intrinsic OAM like the intrinsic SAM for beams with a circular polarization (Allen *et al.* 1992, 2003). This appeared originally rather surprising as the OAM of LG beams arise from the helical phase distribution about the beam axis, and which coincides also with a phase singularity (Nye and Berry, 1974).
- Laguerre-Gaussian modes $u_{\ell p}^{\rm LG}$ : For a Laguerre-Gaussian beam with well-defined magnetic and radial quantum numbers $(m,p)$ , the complex amplitude of the light field in the waist of the beam is defined as in the polar represenation

$$u_{\ell p}^{\rm LG}(r,\varphi) \;=\; \langle r,\varphi\,|\,m,p\rangle \;=\; R_{mp}(r)\,\Phi_m(\varphi) \qquad \text{with} \qquad \Phi_m(\varphi) \;=\; \frac{e^{im\,\varphi}}{\sqrt{2\pi}}$$

- Laguerre-Gaussian modes $u_{\ell p}^{\rm LG}$ : If the problem is cylindrically symmetric, these modes are the natural solution of the paraxial wave equation. They are often written in cylindrical coordinates by using Laguerre polynomials.

## 12.2.f. Bessel beams

### Characterization and use:

- Bessel beams: A Bessel beam refers generally to an electromagnetic field whose amplitude is given by a Bessel function of the first kind. 5
- Although these beams are an idealization, true Bessel beam are monochromatic and non-diffractive and, hence, do not not diffract and spread out when they propagate. This behaviour is quite in contrast to other typical optical (or sound) waves if they are focused at some spot.
- Bessel beams are known to be self-healing if they are obstructed at some point, i.e. they reform to a Bessel beam again further down the beam axis.

- Pure Bessel modes generally carry a well-defined OAM; in particular, they typically include three components of the topological charge since only the (projection of the) total angular momentum is conserved for these beams. For this reason, the $z$-projections of the orbital and spin angular momentum are not defined independently.

- Bessel modes $|\kappa, m\rangle$ : Bessel beams can be written also as a superposition over plane waves with well-defined (fixed) transverse momentum , longitudinal momentum as well as circular polarization

$$\psi(\mathbf{r}) \;=\; e^{-i\,\omega t \,+\, i\, k_z\, z}\; |\kappa, m\rangle \;, \qquad\qquad |\kappa, m\rangle \;\propto\; e^{i\, m\varphi}\, J_m(\kappa\, \rho)$$

- Vector potential: The vector potential of the Bessel beams is often written as Fourierintegral over Bessel states of different projections of the orbital angular momentum $a_{\kappa\, m}(\mathbf{k}_\perp)$ ,

$$\mathbf{A} \;=\; e^{-i\,\omega t}\, \frac{1}{(2\pi)^2} \int d\mathbf{k}_\perp\, e^{-i\,\mathbf{k}\cdot\mathbf{r}}\, a_{\kappa\, m}(\mathbf{k}_\perp)\, \mathbf{e}_{\mathbf{k},\lambda}, \qquad\qquad a_{\kappa\, m}(\mathbf{k}_\perp) \;=\; \sqrt{\frac{2\pi}{\kappa}}\, (-i)^m\, e^{-i\, m\, \varphi_{\mathbf{k}}}\, \delta(k_\perp \,-\, \kappa)$$

$$\mathbf{e}_{\mathbf{k},\lambda} \;=\; \frac{1}{\sqrt{2}} \begin{pmatrix} \cos\vartheta_k\, \cos\varphi_k \;-\; i\lambda\, \sin\varphi_k \\ \cos\vartheta_k\, \sin\varphi_k \;+\; i\lambda\, \cos\varphi_k \\ -\, \sin\vartheta_k \end{pmatrix} \qquad\qquad \tan\vartheta_k \;=\; \frac{\kappa}{k_z}$$

and where $\mathbf{e}_{\mathbf{k},\lambda}$ are known as polarization (unit) vector and $\vartheta_k$ as the opening angle of the Bessel beam.

- Plane-wave expansion: Of course, every monochromatic plane-waves can be expanded also in terms of Bessel waves as they are both just two different bases in order to describe wave packets

$$e^{i\,(\mathbf{k}\cdot\mathbf{r} \,-\, \omega t)} \;=\; \sum_{m=-\infty}^{\infty} e^{-i\,\omega t \,+\, i\, k_z\, z}\; i^m\; e^{-i\, m\, \varphi_{\mathbf{k}}}\; |\kappa,\, m\rangle$$

- Electron-photon interaction operator for Bessel beams: For (a Bessel beam of) twisted photons, the transition operator reads as:

$$V^{\,\mathrm{(tw)}} \;=\; \alpha\, \mathbf{A}_{\varkappa m_\gamma k_z \lambda}(\mathbf{r})\, \mathbf{p}\,.$$

$$\mathbf{A}_{\varkappa m_\gamma k_z \lambda}(\mathbf{r}) \;=\; \int \mathbf{e}_{\mathbf{k}\lambda}\, e^{i\mathbf{k}\mathbf{r}}\, a_{\varkappa m_\gamma}(\mathbf{k}_\perp)\, e^{-i\mathbf{k}_\perp \mathbf{b}}\, \frac{d^2 k_\perp}{(2\pi)^2}, \qquad\qquad a_{\varkappa m_\gamma}(\mathbf{k}_\perp) \;=\; (-i)^{m_\gamma}\, e^{i m_\gamma \varphi_k} \sqrt{\frac{2\pi}{k_\perp}}\, \delta(k_\perp - \varkappa)\,.$$

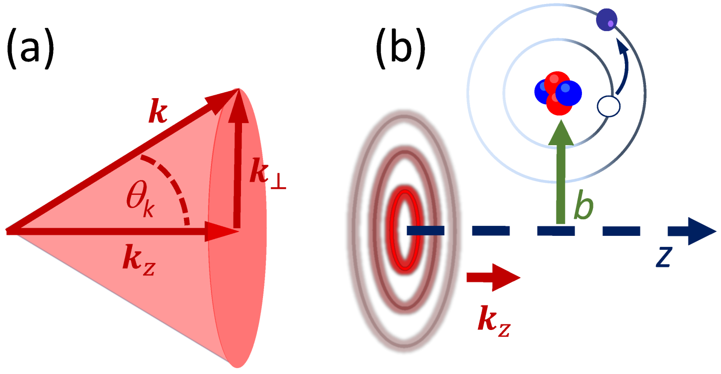

Figure 12.4.: (a) In momentum representation, the twisted light can be seen as a coherent superposition of plane waves. These plane waves with wavevectors $\mathbf{k}$ are all lying on a cone with (polar) opening angle $\vartheta_k = \arctan(|\mathbf{k}_\perp|/k_z)$ and with polarization vectors $\mathbf{e}_{\mathbf{k},\lambda}$ which are perpendicular to $\mathbf{k}$. (b) For a given atom, the absorption amplitude depends on the position of the atom in a plane perpendicular to the propagation direction. The position of the target atom with regard to the beam axis is specified by the impact parameter (vector) $\mathbf{b}$ (c-05-photobeam-interaction.eps).

In this expression, the factor $e^{-i\mathbf{k}_\perp \mathbf{b}}$ specifies the position of a target atom within the incident wave-front, and which refers to the complex spatial structure of the Bessel beam.

### 12.2.g. Airy beams

#### Characterization and use:

- Airy beams: Similar to Bessel beams, the cross section of an ideal Airy beam has an area of principal intensity and with a series of adjacent, less luminous areas up to infinity. Airy beams can be derived from the Airy integral that was first developed by George Biddell Airy in the 180s in order to explain the optical caustics in a rainbow and elsewhere.
- An Airy beam preserves its shape of intensity during propagation and forms a parabolic curve, quite analogue to the trajectory of a free projectile as seen in a plane perpendicular to the propagation.
- Airy beam are freely accelerating, i.e. they bend to form a parabolic arc as they propagate (Berry and Balazs, 1979; Siviloglou *et al.*, 2007), although the linear momentum remains conserved for these beams since the intensity centroid of an Airy beam forms a straight line.

- Airy beam do also not diffract, i.e. they do not spread out after focussing.

### 12.2.h. Necklace ring beams

**Characterization and use:**

- Necklace ring beams: These beams refer to optical vector solitons that consist of incoherently coupled self-trapped ‘necklace’ beams; these beams can carry zero, integer or even some fractional angular momentum.
- Necklace ring beams exhibit a self-stabilizing mutual attraction between different beam components and a quasistable propagation for much larger distances than the corresponding scalar vortex solitons

### 12.2.i. Light beams with non-integer OAM

**Characterization and use:**

- Beams with non-integer OAM: These beams refer to structurally propagation invariant light beams carrying non-integer orbital angular momentum (OAM) using Hermite-Laguerre-Gaussian (HLG) modes.

### 12.2.j. Vector beams

**Characterization and use:**

- Vector beams: The vector beams need to be described in the product space of the optical SAM and OAM subspaces and are characterized by higher-order Stokes parameters.
- Vector beams exhibit a spatially variant polarization.
- Cylindrical vector beams are axially symmetric solution to the full electromagnetic (vector) wave equation.
- Generation of vector beams: These beams can be generated via different active and passive methods.

### 12.2.k. Traktor beams

## Characterization and use:

- Tractor beam: These beams refer to optical fields that help attract one object to another from a distance.
- The concept of tractor beams originates from the novel Spacehounds of IPC by E. E. Smith (1931) and by re-coining an earlier ‘attractor beam’, in contrast to other, ’repulser beams’.
- Tractor beam are defined to use (a negative) nonconservative radiation pressure, that differs from a gradient force, and which is directed towards the source. This generally requires a continuous redirection of momentum flux (Sukhov and Dogariu, 2010, 2011; Chen *et al.* 2011).
- Traktor beams are based on the maximization of forward scattering of light due to interference of different radiation multipoles. It was shown especially that an simultaneous excitation of multipoles is necessary in the particle in order to realize a negative (pulling) optical force.

### 12.2.l. Polarization radiation

## Characterization and use:

- In electrodynamics, one generally distinguishes two classes of emitted radiation: bremsstrahlung and polarization radiation. While bremsstrahlung is produced by accelerated charges, polarization radiation can be emitted by a uniformly moving charge, although only in the presence of a medium.
- In dependence on the given medium or target geometry, one distinguishes various forms of polarization radiation: Cherenkov radiation, transition radiation, diffraction radiation as well as Smith-Purcell radiation.
- Polarization radiation: Electromagnetic radiation can be emitted not only by accelerated charges but also due to the motion of magnetic moments and higher multipoles. Until the present, however, this (so-called) polarization radiation has never been verified experimentally for any frequency of light.
- The main experimental difficulty for approving this radiation refers to the (very) small current of a magnetic moment that is suppressed by $\sim 10^{-5}$ w.r.t. a corresponding charge current.
- A pure quasi-classical treatment of the polarization radiation is inconsistent since quantum corrections are of the same order for this type of radiation phenomena.

### 12.2.m. Manipulation of optical beams

## Optical elements:

- Dove prism: This is a (type of) reflective prism that can be used to invert a given image. These prisms are often shaped from a truncated right-angle prism.
- If a beam enters the prims at one of the sloped faces and parallel to the longitudinal axis, it undergoes total internal reflection at the inside of the longest (bottom) face, and then leaves the prism at the opposite sloped face. Therefore, any image that passes through the prism is flipped (mirrored) and also also inverted but not laterally transposed.
- Hologram: A holgram usually refers to a three-dimensional image of an object that is created by holography, i.e. an optical technique for recording and reconstructing the amplitude and phase distributions of a coherent wave. Holography is often used to produce three-dimensional images or holograms.
- Half-wave plate: A wave plate, sometimes known as a retarder, designates an optical device that alters the polarization state of a light wave. While a half-wave plate shifts the polarization direction of linearly polarized light, a quarter-wave plate converts linearly-polarized light into circularly-polarized light and vice versa. Quarter-wave plate can be used also in order to produce elliptically-polarized light.

## Mach-Zehnder interferometers:

- These interferometers make use of two separate beam splitters in order to split and recombine an input beam but from which the beam can emerge and detected at two outputs. The optical path lengths in the two arms of the interferometer may be nearly identical or may be different in order to introduce an extra delay path.
- If a beam is sent through the interferometer, the optical powers at the two outputs depends on in practice sensitively on the the precise difference in optical arm lengths as well as on the wavelength of the light.
- The Mach-Zehnder interferometer was first developed by Ludwig Mach and Ludwig Zehnder.

### 12.2.n. Optical forces of vortex beams

#### Optical forces:

- :
- A positive radiation force is relatively intuitive and occurs in the backscattering or absorption of the forward-directed momentum of a beam; it was first reported already by Nichols and Hull (1903).

### 12.2.o. Application of optical (vortex) beams

#### Remarks:

- Different applications of optical vortex beams and the angular momentum of light have been envisaged and are currently explored in research laboratories, although no real commercial application are yet known.
- Fields of applications: Cold atoms, trapped nanoparticles, micro manipulation and detection of spinning objects, remote measurement of the rotation of mesoscopic particles, entanglement and quantum information, optical data transmission, interaction with matter, microscopy and astrophysics.
- X-ray magnetic circular dichromism By using different OAM states in the measurements, the dipole and quadrupole contributions to the circular dichroism signal can be separated from each other.

#### Optical tweezer:

- Optical tweezer: These tweezers usually refer to single-beam gradient force trap that are realized by some highly focused laser beam. These focused beams provide an attractive or repulsive force on nano- or mesoscopic dielectric objects.
- Optical tweezers have been utilized to manipulate the orientation of particles or particle aggregates.
- In optical tweezers, the forces are typically on the order of piconewtons; they depends on the refractive index of the object.

### Optical phasors:

- Phasor: A complex constant in complex wave notation that encapsulates the amplitude; sometimes known also as sinor or complexor.

### Applications in quantum information theory:

- The orbital-angular momentum (OAM) of light has recently emerged as a promising candidate for quantum and classical information systems.
- In OAM beams, the spatial degrees of freedom provide a high-dimensional alphabet to quantum information processing which enables one to use qunits instead of qubits.
- Quantum information encoding, Higher-dimensional quantum information encoding has been discussed in the literature for possible future applications in quantum cryptography or quantum computations. The discrete, unbounded state-space of OAM promises in particular vastly enhanced data rates as well as an increased tolerance to eavesdropping in quantum communication.

## 12.3. Electron beams

### Electron beams:

- Electron beams are quite frequently applied in physics; such beams may refer, for instance, to some stream of electrons as obtained from a betatron. Electron beams are generally generated either by heat (thermionic emission), bombardment of surfaces with charged atoms or particles (secondary electron emission), or by means of strong electric fields (field emission).
- Electrons may be collimated by holes and slits. Because they are electrically charged, they can also be deflected, focused or accelerated by electric and magnetic fields.

### Twisted electron beams:

- Apart from twisted (vortex) solutions of the Dirac equation, a quais-relativistic wave equation for twisted relativistic electron in arbitrary electric and magnetic fields can be derived by using a Foldy-Wouthuysen transformation.

- ➢ The interaction of twisted (vortex) electrons with electric and magnetic fields can be described quite readily, based on Lorentz transformations.

## 12.3.a. Gaussian electron beams

### Characterization and use:

- ➢ It has been demonstrated experimentally that a Gaussian-profile model better describes the (equilibrium) electron beam than a beam with a uniform-profile model.

## 12.3.b. Vortex electron beams

### General remarks:

- ➢ Electron vortex beams were first realized experimentally by Uchida and Tonomura (2010), Verbeeck, Tian and Schattschneider (2010) and McMorran *et al.* (2011). Uchida and Tonomura, in particular, generated an electron vortex beams with (electron) energy $E = 300$ keV, a projection of the OAM with $m \lesssim 100$ and by focusing the electron beam to a spot size of 1.2 Å.
- ➢ Vortex electrons can generally carry a rather large intrinsic projection of the orbital angular momentum (OAM) $m \sim 100$ with respect to their propagation direction. Therefore, the magnetic moment of vortex electrons $\mu \approx m\,\mu_B$ is similarly large, when compared with the Bohr magneton $\mu_B$ due to the spin motion of the electron.
- ➢ The magnetic moment of twisted electrons due to their OAM comes in addition to the known magnetic moment due to the spin motion.
- ➢ Since Vortex electrons are sensitive to external magnetic fields, they can be utilized to probe atomic magnetism and, thus, open novel opportunities for electron microscopy.
- ➢ While vortex photon beams have been created and routinely used for several decades already, the vortex states of electrons and charged particles is a presently emerging field.

### 12.3.c. Generation of vortex electron beams

#### Generation of vortex electron beams with different energies:

➢ Indeed, several new ideas were proposed in the literature in order to create electron vortex beams experimentally.

#### Generation of vortex electron beams by undulators:

➢ Electrons in a helical modulator: cf. Figure 12.3.c

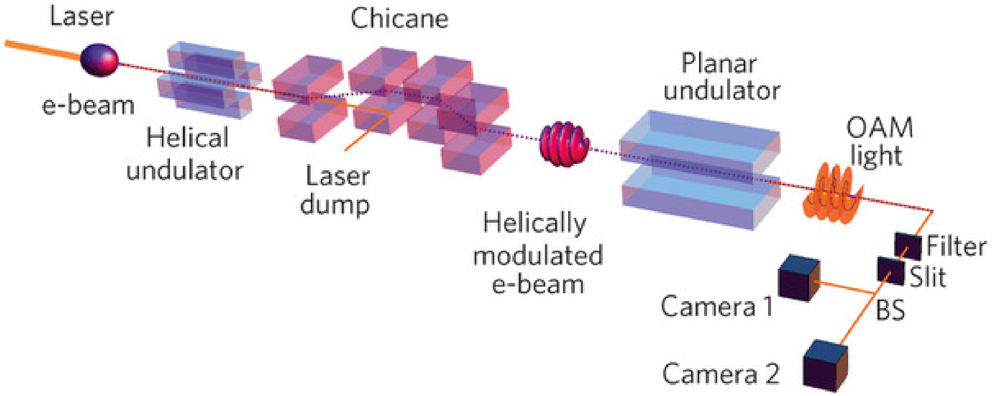

Figure 12.5.: An unmodulated relativistic electron beam interacts with a linearly polarized laser in a helical undulator, which gives the electrons an energy kick that depends on their position in the focused laser beam.

#### Generation of vortex electron beams by transmission electron microscopes:

➢ Voloch-Bloch *et al.* (2013) generated Airy electron beams by using a holographic technique within a transmission electron microscope. Both, self-bending and self-healing features were observed in the experiments if the beam was obstructed by a small object during its propagation.

## Generation of vortex electron beams by holograms:

- Grillo *et al.* (2014) generated an electron Bessel beam by the diffraction of electrons at a nanoscale phase hologram. This hologram imposed a conical phase structure upon the electron wave-packet. The so obtained beams propagated for 0.6 m without measurable spreading and could reconstruct also its intensity distributions, if these beams where partly obstructed by an obstacle.

## 12.3.d. Bessel electron beams

## Characterization and use:

- Quasi-Bessel beams can be obtained within a good approximation, while it is not possible to generate an ideal Bessel beam because they are not normalizable in their total intensity,
- Wave function of a Bessel electron: In cylindrical coordinates $r, \varphi, z$, the wave function of electrons in a Bessel beam is given by

$$\psi(r, \varphi, z; t) \quad = \quad J_m(\kappa\, r)\, e^{i\, m\varphi}\, e^{-i\,(\omega t \,-\, k_z z)},$$

  where $J_m(x)$ is the $m$-th order Bessel function of the first kind and $\kappa$ and $k_z$ denote the transverse and longitudinal components of the wave vector, respectively.

- Probability-density distribution of Bessel electron beams: This wave function give rise to a probability-density distribution $\mathcal{P} \;=\; \psi\, \psi^+$ that is independent of $z$ and $t$:

$$\mathcal{P}(r, \varphi, z;\, t) \quad = \quad \mathcal{P}(r, \varphi, 0; 0) \;=\; [\, J_m(\kappa\, r)\, ]^2\, .$$

- This shows that the probability-density distribution is stationary in the transverse plane and independent of where this plane is taken.
- The energy of the electron $E \;=\; \hbar\,\omega$ defines the de Broglie wave length and the modulus of the wave vector by

$$k^2 \;=\; k_r^2 \,+\, k_z^2 \;=\; \frac{2m\omega}{\hbar} \;=\; \left(\frac{2\pi}{\lambda_{dB}}\right)^2 .$$

- For Bessel beams with a nonzero $m$ value, the electrons possess a non-uniform helical phase front with $m$ dislocations in the phase, and where the handedness of the phase front is defined by the sign of $m$.
- Current density of electron Bessel beam: This current density circulates azimuthally in the transverse plane and introduces an (projection of the total) orbital angular momentum of $m\hbar$ per electron.
- An Bessel electron beam with a nonzero $m$ value possess exhibit a shape with multiple rings and with a null probability density at the origin.
- Bessel electron beams can be represented also as a coherent superposition of conical plane waves along a closed ring (circle).

## 12.3.e. Airy electron beams

### Characterization and use:

- Airy electron beams can be generated by diffraction of electrons through a nanoscale hologram, which imprints a cubic phase modulation on wavefunction of the electrons in the transverse plane.

## 12.3.f. Application of twisted electron beams

### Remarks:

- The scattering of twisted electrons can provide insights into the magnetic structure of the target materials.
- Beams with non-zero OAM helped explore the vacuum Faraday effect as well as Larmor and Gouy rotations.
- Bessel electron beams have been used in electron microscopy.

# 13. References

1992 *Phys. Rev.*

**Åberg T and Howat G** 1982 in *Corpuscles and Radiation in Matter I*, ed Mehlhorn W (in: Encyclopedia of Physics, vol XXXI; Springer, Berlin, p 469) *Theory of the Auger Effect*

**Agostinelli S and Geant 4 collaboration** 2003 *Nuc. Instr. Meth.* **A506** 250 *Geant 4 – A simulation toolkit*

**Allen L, Beijersbergen M W, Spreeuw R J C and Woerdman J P** 1992 *Phys. Rev.* **A45** 8185 *Orbital angular momentum of light and the transformation of Laguerre-Gaussian laser modes*

**Allen L, Barnett S M and Padgett M J** 2003 *Optical Angular Momentum* (Institute of Physics Publishing, Bristol)

**Allen L, Padgett M J and Babiker M** 1999 *Progress in Optics* **39** 291 *The orbital angular momentum of light*

**Ashkin A, Dziedzic J M, Bjorkholm J E and Chu S** 1986 *Opt. Lett.* **11** 288 *Observation of a single-beam gradient force optical trap for dielectric particles*

**Astropy Collaboration** 2013 *Astronomy & Astrophys.* **558** A33 *Astropy: A community Python package for astronomy*

**Avgoustoglou E, Johnson W R, Plante D R, Sapirstein J, Sheinerman S and Blundell S A** 1992 *Phys. Rev.* **A46** 5478 *Many-body perturbation theory formulas for the energy levels of excited states of closed-shell atoms*

**Avgoustoglou E, Johnson W R, Liu Z W und Sapirstein J** 1995 *Phys. Rev.* **A51** 1196 *Relativistic many-body calculations of* $[2p^5 3s]$ *excited state energy levels for neon-like ions*

**Badnell N R** 2011 *Comp. Phys. Commun.* **182** 1528 *A Breit-Pauli distorted wave implementation for* AUTOSTRUCTURE

**Bahrdt J, Holldack K, Kuske P, Müller R, Scheer M and Schmid P** 2013 *Phys. Rev. Lett.* **111** 034801 *First observation of photons carrying orbital angular momentum in undulator radiation*

**Balashov V V, Grum-Grzhimailo A N and Kabachnik N M** 2000 *Polarization and Correlation Phenomena in Atomic Collisions* (Kluwer Academic Plenum Publishers, New York)

**Band I M, Trzhaskovskaya M B, Nestor Jr N W, Tikkanen P O and Raman S** 2002 *Atom. Data Nucl. Data Tables* **81** 1 *DiracFock internal conversion coefficients*

**Bazhenov V Y, Vasnetsov M V and Soskin M S** 1990 *JETP Lett.* **52** 429 *Laser-beams with screw dislocations in their wave-fronts*

**Beijersbergen M W, Coerwinkel R P C, Kristensen M and Woerdman J P** 1994 *Opt. Comm.* **12** 321 *Helical-wavefront laser beams produced with a spiral phase plate*

**Bethe H A and Salpeter E E** 1957 *Quantum Mechanics of One- and Two-Electron Systems* (Springer-Verlag, Berlin, Gttingen, Heidelberg)

**Bezanson J, Edelman A, Karpinski S and Shah V B** 2017 *SIAM Review* **59** 65 *Julia: A fresh approach to numerical computing*

**Bezanson J, Chen J, Chung B, Karpinski S, Shah V B, Vitek J and Zoubritzky J** 2018 *Proceedings of the ACM on Programming Languages* **2** 120 *Julia: Dynamism and performance reconciled by design*

**Bliokh K Y, Bliokh Y P, Savelev S and Bliokh F N** 2007 *Phys. Rev. Lett.* **99** 190404 *Semiclassical dynamics of electron wave packet states with phase vortices*

**Bliokh K Y, Dennis M R and Franco Nori** 2011 *Phys. Rev. Lett.* **107** 174802 *Relativistic electron vortex beams: angular momentum and spin-orbit interaction*

**Bozinovic N, Yue Y, Ren Y, Tur M, Kristensen P, Huang H, Willner A E, Ramachandran S** 2013 *Science* **340** 1545 *Terabit-scale orbital angular momentum mode division multiplexing in fibers*

**Cai X, Wang J, Strain M J, Johnson-Morris B, Zhu J, Sorel M, O'Brien J L, Thompson M G, Yu S** 2012 *Science* **338** 363 *Integrated compact optical vortex beam emitters*

**Canton-Rogan S E, Wills A A, Gorczyca T W, Wiedenhoeft M, Nayandin O, Liu C-N and Berrah N** 2000 *Phys. Rev. Lett.* **85** 3113 *Mirroring doubly excited resonances in argon*

**Chen J, Ng J, Lin Z and Chan C T** 2011 *Nat. Photonics* **5** 531 *Optical pulling force*

**Cheng G and Jiaolong Z** 2008 *Phys. Rev.* **E78** 046407 *Spectrally resolved and Rosseland and Planck mean opacities of iron plasmas at temperatures above 100 eV: A systematic study*

**Cowan R D** 1981 *The Theory of Atomic Structure and Spectra* (University of California Press, 1981, 731 pages)

**Da Pieve F, Fritzsche S, Stefani G and Kabachnik N M** 2007 *J. Phys.* **B40** 329 *Linear magnetic and alignment dichroism in Auger-photoelectron coincidence spectroscopy*

**Darwin C G** 1932 *Proc. R. Soc. Lond.* **A 136** 36 *Notes on the theory of radiation*

**Derevianko A, Johnson W R, Safronova M S and Babb J F** 1999 Phys. Rev. Lett. **82** 3589 *High-precision calculations of dispersion coefficients, static dipole polarizabilities and atom-wall interaction constants for alkali-metal atoms*

**Dzuba V A, Flambaum V V and Porsev S G** 2009 *Phys. Rev.* **80** 032120 *Calculation of $(P, T)$-odd electric dipole moments for the diamagnetic atoms $^{129}$Xe, $^{171}$Yb, $^{199}$Hg, $^{211}$Rn, and $^{225}$Ra*

**Eichler J and Meyerhof W** 1995 *Relativistic Atomic Collisions* (Academic Press, San Diego)

**Fisher D, Maron Y and Pitaevskii L P** 1998 *Phys. Rev.* **A58** 2214 *Ionization of many-electron atoms by a quasistatic electric field*

**Flambaum V V and Ginges J S M** 2005 *Phys. Rev.* **A72** 052115 *Radiative potential and calculations of QED radiative corrections to energy levels and electromagnetic amplitudes in many-electron atoms*

**Fontes C J, Zhang H L, Abdallah Jr J, Clark R E H, Kilcrease D P, Colgan J, Cunningham R T, Hakel P, Magee N H and Sherrill M E** 2015 *J. Phys.* **B48** 144014 *The Los Alamos suite of relativistic atomic physics codes*

**Franke-Arnold S, Allen L, Padgett M J** 2008 *Laser and Photonics Reviews* **2** 299 *Advances in optical angular momentum*

**Freiburghaus C, Rosswog S and Thielemann F-K** 1999 *Astrophys. J.* **525** L121 *r-Process in neutron star mergers*

**Fritzsche S** 2001 *J. Electron Spectrosc. Relat. Phenom.* **114-116** 1155 *A toolbox for studying the properties of openshell atoms and ions*

**Fritzsche S** 2002 *Phys. Scr.* **T100** 37 *Largescale accurate structure calculations for openshell atoms and ions*

**Fritzsche S, Nikkinen J, Huttula S-M, Aksela H, Huttula M and Aksela S** 2007 *Phys. Rev.* **A75** 012501 *Interferences in the* $3p^4nl$ *satellite emission following the excitation of argon across the* $2p^5_{1/2}4s$ *and* $2p^5_{3/2}3d$ $J = 1$ *resonances*

**Fritzsche S, Fricke B and Sepp W-D** 1992 *Phys. Rev.* **A45** 1465 *Reduced* $L_1$ *level-width and Coster-Kronig yields by relaxation and continuum interactions in atomic zinc*

**Furukawa H and Nishihara K** 1992 *Phys. Rev.* **A46** 6596 *Fermi-degeneracy and discrete-ion effects in the spherical-cell model and electron-electron correlation effects in hot dense plasma*

**Gaidamauskas E, Naze C, Rynkun P, Gaigalas G, Jönsson P and Godefroid M** 2011 *J. Phys.* **B44** 175003 *Tensorial form and matrix elements of the relativistic nuclear recoil operator*

**Gaigalas G, Froese Fischer C, Rynkun P and Jönsson P** 2017 *atoms* **5** 6 *JJ2LSJ: Transformation and unique Labeling for energy levels*

**Gaigalas G, Zalandauskas T and Fritzsche S** 2004 *Comp. Phys. Commun.* **157** 239 *Spectroscopic LSJ notation for atomic levels obtained from relativistic calculations*

**Gaunt** 1929 *Proc. R. Soc.* **A122** 513 *IV. The triplets of helium*

**Ginzburg V L and Tsytovich V N** 1979 *Phys. Rep.* **49** 1 *Transition radiation and transition scattering*

**Goldman S P and Drake G W F** 1992 *Phys. Rev. Lett.* **68** 1683 *Asymptotic Lamb shifts for helium Rydberg states*

**Gordon R G and Kim Y S** 1972 *J. Chem. Phys.* **56** 3122 *Theory for the forces between closed-shell atoms and molecules*

**Grant I P** 1988 *in: Methods in Computational Chemistry* ed Wilson S, vol 2 (Plenum, New York, p 1) *Relativistic effects in atoms and molecules*

**Grant I P and Pyper N C** 1976 *J. Phys.* **B9** 761 *Breit interaction in multiconfiguration relativistic atomic calculations*

**Grant I P and Quiney H M** 1988 *in: Advances in Atomic and Molecular Physics* **23** eds D Bates and B Bederson (Academic, New York, p 37) *Foundation of Relativistic Theory of Atomic and Molecular Structure*

**Griem H** 1974 *Spectral Line Broadening by Plasmas* (Academic Press, New York, London)

**Grier D G** 2003 *Nature* **424** 810 *A revolution in optical manipulation*

**Grillo V, Gazzadi G-C, Mafakheri E, Frabboni S, Karimi E and Boyd R W** 2015 *Phys. Rev. Lett.* **114** 034801 *Holographic generation of highly twisted electron beams*

**Grum-Grzhimailo A N, Gryzlova E V, Staroselskaya E I, Venzke J and Bartschat K** 2015 *Phys. Rev.* **A91** 063418 *Interfering one-photon and two-photon ionization by femtosecond VUV pulses in the region of an intermediate resonance*

**Guo D-S, Åberg T and Crasemann B** 1989 *Phys. Rev* **A40** 4997 *Scattering theory of multiphoton ionization in strong fields*

**Guo D-S and Drake G W F** 1992 *Phys. Rev* **A45** 6622 *Multiphoton ionization in circularly polarized standing waves*

**Haque A K F, Shahjahan M, Uddin M A, Patoary M A R, Basak A K, Saha B C and Malik F B** 2010 *Phys. Scr.* **81** 045301 *Generalized Kolbenstvedt model for electron impact ionization of the K-, L- and M-shell ions*

**Hartgers A, van Dijk J, Jonkers J, van der Mullen J A M** 2001 *Comp. Phys. Commun.* **135** 199 *CR-Model: A general collisional radiative modeling code*

**He H, Friese M E J, Heckenberg N R and Rubinsztein-Dunlop H** 1995 *Phys. Rev. Lett.* **75** 826 *Direct observation of transfer of angular momentum to absorptive particles from a laser beam with a phase singularity*

**Hemsing E, Marinelli A Rosenzweig J B** 2011 *Phys. Rev. Lett.* **106** 164803 *Generating optical orbital angular momentum in a high-gain free-electron laser at the first harmonic*

**Hemsing E and Marinelli A** 2012 *Phys. Rev. Lett.* **109** 224801 *Echo-enabled x-ray vortex generation*

**Hemsing E, Knyazik A, Dunning M, Xiang D, Marinelli A, Hast D and Rosenzweig J B** 2013 *Nature Phys.* **9** 549 *Coherent optical vortices from relativistic electron beams*

**Hubbell J H, Veigele W J, Briggs E A, Brown R T, Cromer D T and Howerton R J** 1992 *J. Phys. Chem. Ref. Data* **4** 471 *Atomic form factors, incoherent scattering functions, and photon scattering cross sections*

**Huntemann N, Sanner C, Lipphardt B, Tamm C and Peik E** 2016 *Phys. Rev. Lett.* **116** 063001 *Single-ion atomic clock with* $3 \times 10^{18}$ *systematic uncertainty*

**Inal M K, Surzhykov A and Fritzsche S** 2005 *Phys. Rev.* **A72** 042720 *Linear polarization of the* $2p^5 3s \to 2p^6$ *lines following the inner-shell photoionization of sodiumlike ions*

**Inhester L, Burmeister C F, Groenhof G and Grubmüller H** 1992 *J. Chem. Phys.* **136** 144304 *Auger spectrum of a water molecule after single and double core ionization*

**Ivanov I P and Karlovets D V** 2013 *Phys. Rev. Lett.* **110** 264801 *Detecting transition radiation from a magnetic moment*

**Jahrsetz T, Fritzsche S and Surzhykov A** 2015 *Phys. Rev.* **A89** 042501 *Inelastic Raman scattering of light by hydrogenlike ions*

**Johnson W R** 1995 *in: Physics with Multiply Charged Ions* ed D Liesen (NATO ASI Series 348, Plenum Press, New York London, p 1 *Correlation and QED for highly-charged ions*

**Johnson W R** 2007 *Atomic Structure Theory: Lectures on Atomic Physics* (Springer)

**Johnson W R, Guo D S, Idrees M and Sapirstein J** 1985 *Phys. Rev.* **A32** 2093 *Weak-interaction effects in heavy atomic systems*

**Jönsson P, Gaigalas G, Bieron J, Froese Fischer C and Grant I P** 2013 *Comp. Phys. Commun.* **184** 2197 *New version: Grasp2K relativistic atomic structure package*

**Kabachnik N M** 1981 *J. Phys.* **B14** L337

**Kabachnik N M, Fritzsche S, Grum-Grzhimailo A N, Meyer M and Ueda K** 2007 *Phys. Rep.* **451** 155 *Coherence and correlations in photoinduced Auger and fluorescence cascades in atoms*

**Kassimi N E and Thakkar A J** 1994 *Phys. Rev.* **A50** 2948 *Static hyperpolarixability of atomic lithium*

**Kibeedia T, Burrows T W, Trzhaskovskayac M B, Davidsona P M and Nestor Jr C W** 2008 *Nucl. Instr. Meth.* **A589** 202 *Evaluation of theoretical conversion coefficients using BrIcc*

**Kim Y S and Gordon R G** 1974 *Phys. Rev.* **B9** 3548 *Theory of binding of ionic crystals: Application to alkali-halide and alkane-earth-dihalide crystals*

**Klar H** 1980 *J. Phys.* **B13** 4741

**Krause M O** 1979 *J. Phys. Chem. Ref. Data* **8** 329 *Atomic radiative and radiationless yields for K and L shells*

**Koga T and Thakkar A J** 1996 J. Phys. **B 29** 2973 *Moments and expansion coefficients of atomic electron momentum densities: numerical Hartree-Fock calculations for hydrogen to lawrencium*

**Libermann D A** 1979 *Phys. Rev.* **B20** 4981 *Self-consistent field model for condensed matter*

**Lindgren I and Rosen A** 1974 *Case Studies in Atomic Physics* **5** *Relativistic self-consistent-field calculations with application to atomic hyperfine interaction. Part I: Relativistic self-consistent fields*

**Liu C-N and Starace A F** 1999 *Phys. Rev. A***59** 1731(R) *Mirroring behavior of partial photodetachment and photoionization cross sections in the neighborhood of a resonance*

**Liu P F, Liu Y P, Zeng J L and Yuan J M** 2014 *Phys. Rev.* **A89** 042704 *Electron-impact excitation and single- and multiple-ionization cross sections of heavy ions:* $Sn^{13+}$ *as an example*

**Liu Z, Lee H, Xiong Y, Sun C and Zhang X** 2007 *Science* **315** 1686 *Far-field optical hyper lens magnifying sub-diffraction-limited objects*

**Marxer H** 1991 *Phys. Rev. A* **44** 1543 *Exact correspondence relationship for the expectation values of* $r^{-k}$ *for hydrogenlike states*

**Marxer H** 1995 *J. Phys.* **B28** 341 *Off-diagonal matrix elements* $\langle n\ell \,|\, r^k \,|\, n\ell' \rangle$ *for hydrogen-like states: an exact correspondence relationship in terms of orthogonal polynomials and the WKB approximation*

**Matula O, Hayrapetyan A G, Serbo V G, Surzhykov A and Fritzsche S** 2013 *J. Phys.* **B46** 205002 *Atomic ionization of hydrogen-like ions by twisted photons: angular distribution of emitted electrons*

**Matula O, Hayrapetyan A G, Serbo V G, Surzhykov A and Fritzsche S** 2014 *New J. Phys.* **16** 053016 *Radiative capture of twisted electrons by bare ions*

**Mazevet S and Abdallah Jr J** 2006 *J. Phys.* **B39** 3419 *Mixed UTA and detailed line treatment for mid-Z opacity and spectral calculations*

**McGloin D and Dholakia K** 2005 *Contemp. Phys.* **64** 15 *Bessel Beams: Diffraction in a New Light*

**McMorran B J, Agrawal A, Anderson I M, Herzing A A, Lezec H J, McClelland J J and Unguris J** 2011 *Science* **331** 192 *Electron vortex beams with high quanta of orbital angular momentum*

**Metzger B D** 2017 *Living Rev. Relativ.* **20** 3 *Kilonovae*

**Milione G, Sztul H I, Nolan D A and Alfano R R** 2011 *Phys. Rev. Lett.* **107** 053601 *Higher-order Poincare sphere, Stokes parameters and the angular momentum of light*

**Miyagi H and Madsen L B** 1992 *Phys. Rev.* **A87** 062511 *Time-dependent restricted-active-space self-consistent-field theory for laser-driven many-electron dynamics*

**Nye J F and Berry M V** 1974 *Proc. R. Soc. London Ser.* **A336** 165 *Dislocations in wave trains*

**Oemrawsingh S S R, Aiello A, Eliel E R, Nienhuis G and Woerdman J P** 2014 *Phys. Rev. Lett.* **92** 217901 *How to observe high-dimensional two-photon entanglement with only two detectors*

**Pan L, Taylor K T and Clark C W** 1988 *Phys. Rev. Lett.* **61** 2673 *Computation of the ac Stark effect in the ground state of atomic hydrogen*

**Parpia F, Froese Fischer C and Grant I P** 1996 *Comput. Phys. Commun.* **94** 249 *GRASP92: A package for large-scale relativistic atomic structure calculations*

**Peele A G, McMahon P J, Paterson D, Tran C Q, Mancuso A P, Nugent K A, Hayes J P, Harvey E, Lai B and McNulty I** 2002 *Opt. Lett.* **27** 1752 *Observation of an x-ray vortex*

**Picon A, Mompart J, Vaizquez de Aldana J A, Plaja L, Calvo G F and Roso L** 2007 *Opt. Express* **18** 3660 *Photoionization with orbital angular momentum beams*

**Porsev S G, Kozlov M G and Reimers D** 2009 *Phys. Rev.* **A79** 032519 *Transition frequency shifts with fine-structure constant variation for Fe I and isotope-shift calculations in Fe I and Fe II*

**Porsev S G and Derevianko A** 2006 *J. Exp. Theo. Phys.* **102** 195 *High-accuracy calculations of dipole, quadrupole and octupole electric-dynamic polarizabilities and van-der-Waals coefficients $C_6$, $C_8$ and $C_{10}$ for alkaline-earth dimers*

**Post D E and Kendall R P** 2004 *Int. J. HPC Applications* **18** 399 *Software project management and quality engineering practices for complex, coupled ...*

**Potvliege R M** 1998 *Comput. Phys. Commun.* **114** 42 *STRFLO: A program for time-independent calculations of multiphoton processes in one-electron atomic systems: I. Quasi-energy spectra and angular distributions*

**Poynting J H** 1909 *Proc. R. Soc.* **A82** 560 *The wave motion of a revolving shaft, and asuggestion as to the angular momentum in abeam of circularly polarised light*

**Radice D, Perego A, Hotokezaka K, Fromm S A, Bernuzzi S and Roberts L F** 1992 *Astrophys. J.* **869** 130 *Binary neutron star mergers: mass ejection, electromagnetic counterparts, and nucleosynthesis*

**Radtke T, Fritzsche S and Surzhykov A** 2006 *Phys. Rev. A* **74** 032709 *Density-matrix formalism for the photoion-electron entanglement in atomic photoionization*

**Ribic P R, Guathier D and De Ninno G** 2014 *Phys. Rev. Lett.* **112** 203602 *Generation of coherent extreme-ultraviolet radiation carrying orbital angular momentum*

**Rohrlich F and Carlson B C** 1954 *Phys. Rev.* **93** 38 *Positron-electron differences in energy loss and multiple scattering*

**Rose S J, van Hoof P M M, Jonauskas V, Keenan F P, Kisielius R, Ramsbottom C, Foord M E, Heeter R F and Springer P T** 1992 *J. Phys.* **37** L337 *Calculation of photoionized plasmas with an average-atom model*

**Safronova M S, Porsev S G, Sanner C and Ye J** 2018 *Phys. Rev. Lett.* **120** 173001 *Two clock transitions in neutral Yb for the highest sensitivity to variations of the fine-structure constant*

**Saha B and Fritzsche S** 2006 *Phys. Rev. E***73** 036405 *Be I isoelectronic ions embedded in hot plasma*

**Saha B and Fritzsche S** 2007 *J. Phys. B***40** 259 *Influence of dense plasma on the low-lying transitions in Be-like ions: relativistic multiconfiguration DiracFock calculation*

**Scholz-Marggraf H M, Fritzsche S, Serbo V G, Afanasev A and Surzhykov A** 2014 *Phys. Rev.* **A90** 013425 *Absorption of twisted light by hydrogen-like atoms*

**Sapirstein** 1987 *Phys. Scr.* **36** 801 *Quantum-electrodynamics of many-electron atoms*

**Sasaki S and McNulty I** 2008 *Phys. Rev. Lett.* **100** 124801 *Proposal for generating brilliant x-ray beams carrying orbital angular momentum*

**Shabaev V M, Tupitsyn I I and Yerokhin V A** 2013 *Phys. Rev.* **A88** 012513 *Model operator approach to the Lamb shift calculations in relativistic many-electron atoms*

**Sharma L, Surzhykov A, Inal M K and Fritzsche S** 2010 *Phys. Rev.* **A81** 023419 *Polarization transfer in the innershell photoionization of sodiumlike ions*

**Shen Y, Campbell G T, Hage B, Zou H, Buchler B C and Shen P K L et al.** 2013 *J. Opt.* **15** 044005 *Generation and interferometric analysis of high charge optical vortices*

**Simon A, Warczak A, ElKafrawy T and Tanis J A** 2010 *Phys. Rev. Lett.* **104** 123001 *Radiative double electron capture in collisions of $O^{8+}$ ions with carbon*

**Stone N J** 2005 *Atomic Data and Nuclear Data Tables* **90** 175 *Table of nuclear magnetic dipole and electric quadrupole moments*

**Sukhov S and Dogariu A** 2010 *Opt. Lett.* **35** 3847 *On the concept of tractor beams*

**Sukhov S and Dogariu A** 2011 *Phys. Rev. Lett.* **107** 203602 *Negative nonconservative forces: optical tractor beams for arbitrary objects*

**Surzhykov A, Radtke T, Indelicato P and Fritzsche S** 2009 *Eur. J. Phys. Spec. Topics* **169** 129 *Photon polarization in the two-photon decay of heavy hydrogenlike ions*

**Surzhykov A, Volotka A, Fratini F, Santos J P, Indelicato P, Plunien G, Stoöhlker and Fritzsche S** 2008 *Phys. Rev.* **A81** 042510 *Angular correlations in the twophoton decay of heliumlike heavy ions*

**Surzhykov A, Jentschura U D, Stöhlker T and Fritzsche S** 2006 *Phys. Rev.* **A73** 032716 *Radiative electron capture into high-Z few-electron ions: Alignment of the excited ionic states*

**Tchang-Brillet W L, Wyart J-F, Meftah A and Mammar S A** 2018 *atoms* **6** 52 *Parametric calculations of radiative decay rates for magnetic dipole and electric quadrupole transitions in Tm IV, Yb V, and Er IV*

**Torres and Torner (eds)** 2011 *Twisted photons* (Wiley-VCH, Weinheim)

**Tupitsyn I I, Shabaev V M, Lopez-Urrutia J R C, Draganic I, Orts R S and Ullrich J** 2003 *Phys. Rev.* **A68** 022511 *Relativistic calculations of isotope shifts in highly charged ions*

**Tupitsyn I I, Kozlov M G, Safronova M S, Shabaev V M and Dzuba V A** 2016 *Phys. Rev. Lett.* **117** 253001 *Quantum electro-dynamical shifts in multivalent heavy ions*

**Uchida M and Tonomura A** 2010 *Nature* **467** 737 *Generation of electron beams carrying orbital angular momentum*

**van Veenendaal M and McNulty I** 2007 *Phys. Rev. Lett.* **98** 157401 *Prediction of strong dichroism induced by x rays carrying orbital momentum*

**Verbeeck J, Tian H and Schattschneider P** 2010 *Nature* **467** 301 *Production and application of electron vortex beams*

**Voloch-Bloch N, Lereah Y, Lilach Y, Gover A and Arie A** 2013 *Nature* **494** 331 *Generation of Electron Airy Beams*

**Volotka A V, Yerokhin V A, Surzhykov A, Stöhlker T and Fritzsche S** 2016 *Phys. Rev.* **A93** 023418 *Many-electron effects on x-ray Rayleigh scattering by highly charged He-like ions*

**von der Wense, Seiferle B, Stellmer S, Weitenberg J, Kazakov G, Palffy A and Thirolf P G** 2017 *Phys. Rev. Lett.* **119** 132503 *A laser excitation* *scheme for* $^{229m}$ *Th*

**Yao A M and Padgett M J** 2011 *Adv. Opt. Photon.* **3** 161 *Orbital angular momentum: origins, behavior and applications*

**Yudin V Y, Taichenachev A V and Derevianko A** 2014 *Phys. Rev. Lett.* **113** 233003 *Magnetic-dipole transitions in highly charged ions as a basis of ultraprecise optical clocks*

**Yutsis A P, Levinson I B und Vanagas V V** 1962 *Mathematical apparatus of the theory of angular momentum.* Israel Program for Scientific Translation, Jerusalem 1962

**Zaitsevskii A V und Heully J-L** 1992 *J. Phys.* **B25** 603 *Rayleigh-Schrödinger QDPT for hermitian intermediate Hamiltonians by the shift technique*

**Zambrini R and Barnett S** 2006 *Phys. Rev. Lett.* **96** 113901 *Quasi-intrinsic angular momentum and the measurement of its spectrum*

**Zarrabian S, Laidig W D und Bartlett R J** 1990 *Phys. Rev.* **A41** 4711 *Convergence properties of multireference many-body perturbation theory*

**Zhan Q W** 2009 *Adv. Opt. Photon.* **1** 1 *Cylindrical vector beams: from mathematical concepts to applications*

**Zhu X-M and Pu Y-K** 2010 *J. Phys.* **D43** 015204 *A simple collisionalradiative model for low-temperature argon discharges with pressure ranging from 1 Pa to atmospheric pressure: kinetics of Paschen* 1*s and* 2*p levels*

# Index